

REQUIREMENTS OF MOVING DATA HOSTS TO BE

UNCLASSIFIED

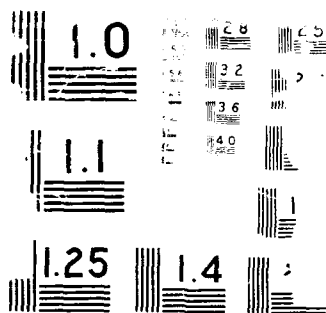
WRIGHT-PATTERSON AFB OH SCHOOL OF ENGI N R SCHORE

DEC 89 AFIT/GE/ENG/89D-46

N. R. SCHORE

F/G 22/2

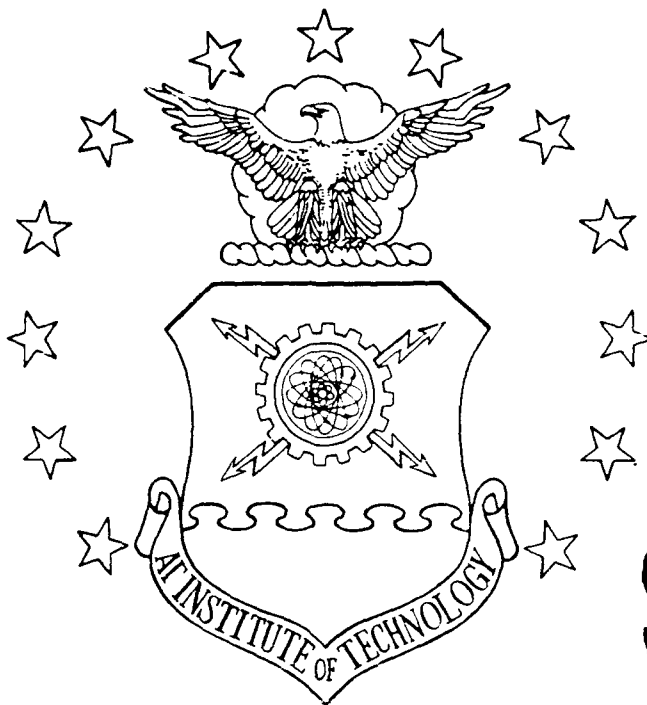
MI



FILE COPY

①

AD-A215 670



DTIC
ELECTE
DEC 19 1989
S B D

ROBUSTNESS OF A MOVING-BANK
MULTIPLE MODEL ADAPTIVE CONTROLLER
FOR A LARGE SPACE STRUCTURE

THESIS

Michael Roger Schore
Captain, USAF

AFIT/GE/ENG/89D-46

F

DEPARTMENT OF THE AIR FORCE
AIR UNIVERSITY
AIR FORCE INSTITUTE OF TECHNOLOGY

Wright-Patterson Air Force Base, Ohio

DISTRIBUTION STATEMENT A

Approved for public release;
Distribution Unlimited

89 12 18 091

AFTT/GE/ENG/89D-46

ROBUSTNESS OF A MOVING-BANK
MULTIPLE MODEL ADAPTIVE CONTROLLER
FOR A LARGE SPACE STRUCTURE

THESIS

Presented to the Faculty of the School of Engineering
of the Air Force Institute of Technology
Air University
In Partial Fulfillment of the
Requirements for the Degree of
Master of Science in Electrical Engineering

Michael Roger Schore, B.S.E.E.
Captain, USAF

December 1989

Approved for public release; distribution unlimited

Preface

The purpose of this thesis was to determine the robustness of the moving bank multiple model adaptive estimation and control algorithms in the face of order mismatched filters and truth model. The use of moving bank multiple model adaptive estimation and control is an attempt to reduce the computational loading that would be required for full-scale implementation of the multiple model adaptive estimator or controller. The results of this thesis showed that the mismatch had negligible effects compared to the additional computational burden that additional filter model states would require. The thesis also demonstrated the need for adaptive control in the face of filter/parameter location mismatch.

I would like to thank Dr. Peter Maybeck for his encouragement, guidance, and (most importantly) enthusiasm during this thesis effort. I would like to thank my lovely children, Elizabeth and Pamela, for living through this with me. Mostly, I would like to thank my wife Sharon, for holding us together and for helping me maintain a sane view on life through this ordeal.

Michael Roger Schore

| | |
|---------------------------|--|
| Accession For | |
| NTIS GRA&I | <input checked="checked" type="checkbox"/> |
| DTIC TAB | <input type="checkbox"/> |
| Unannounced | <input type="checkbox"/> |
| Justification | |
| By _____ | |
| Distribution/ | |
| Availability Codes | |
| Dist | Avail and/or Special |
| A-1 | |

Table of Contents

| | Page |
|---|---------|
| Preface | ii |
| Table of Contents | iii |
| List of Figures | vii |
| List of Tables | xii |
| Abstract | xiii |
| I. Introduction | 1-1 |
| 1.1 Background | 1-2 |
| 1.1.1 Kalman Filter | 1-2 |
| 1.1.2 System Model | 1-6 |
| 1.1.3 Multiple Model Adaptive Estimation - MMAE | 1-9 |
| 1.1.4 Multiple Model Adaptive Control - MMAC | 1-13 |
| 1.1.5 Moving-Bank MMAE/MMAC | 1-13 |
| 1.2 Problem | 1-19 |
| 1.3 Scope | 1-20 |
| 1.4 Approach | 1-21 |
| 1.5 Summary | 1-24 |
| II. Algorithm Development | 2-1 |
| 2.1 Introduction | 2-1 |
| 2.2 Bayesian Multiple Model Adaptive Estimation Algorithm Development | 2-1 |
| 2.3 Moving-Bank Algorithm Development | 2-8 |
| 2.3.1 Moving the Bank. | 2-8 |
| 2.3.2 Contraction and Expansion of the Bank. | 2-10 |

| | Page |
|--|------|
| 2.3.3 Initialization of New Elemental Filters. | 2-11 |
| 2.4 Stochastic Controller Design | 2-12 |
| 2.5 Summary | 2-14 |
| III. Rotating Two-Bay Truss Model | 3-1 |
| 3.1 Introduction | 3-1 |
| 3.2 Models: Second Order and State Space | 3-1 |
| 3.3 Modal Decomposition | 3-5 |
| 3.4 Two-Bay Truss | 3-7 |
| 3.4.1 Background. | 3-8 |
| 3.4.2 Two-Bay Truss Construction. | 3-8 |
| 3.4.3 Sensors and Actuators. | 3-9 |
| 3.4.4 Physical System Parameter Uncertainty. | 3-9 |
| 3.5 State Reduction | 3-10 |
| 3.5.1 Development. | 3-10 |
| 3.5.2 Order Reduction Selection. | 3-12 |
| 3.6 Summary | 3-13 |
| IV. Simulation | 4-1 |
| 4.1 Introduction | 4-1 |
| 4.2 Monte Carlo Analysis | 4-1 |
| 4.3 Software | 4-4 |
| 4.3.1 Introduction. | 4-4 |
| 4.3.2 The Preprocessor: SETUP.S.F. | 4-5 |
| 4.3.3 The Processor: 6BNK.F. | 4-6 |
| 4.3.4 The Postprocessor: RESULT.F. | 4-6 |
| 4.4 Simulation Plan | 4-6 |
| 4.4.1 The Dither Signal. | 4-7 |

| | Page |
|---|------|
| 4.4.2 MMAE Study. | 4-8 |
| 4.4.3 MMAC Study. | 4-9 |
| 4.4.4 Disturbance Rejection. | 4-10 |
| 4.5 Software Modifications | 4-10 |
| 4.6 Summary | 4-11 |
| V. Results | 5-1 |
| 5.1 Introduction | 5-1 |
| 5.2 Multiple Model Adaptive Estimation Study | 5-1 |
| 5.2.1 Duplication of Past Work. | 5-1 |
| 5.2.2 MMAE Benchmark. | 5-2 |
| 5.2.3 Non-Adaptive Single-Filter Analysis with Variable λ | 5-3 |
| 5.2.4 Non-Adaptive Single-Filter Worst Case Analysis. | 5-3 |
| 5.2.5 Moving-Bank MMAE Analysis. | 5-4 |
| 5.3 Multiple Model Adaptive Controller Study | 5-36 |
| 5.3.1 Duplication of Past Work. | 5-36 |
| 5.3.2 MMAC Benchmark. | 5-36 |
| 5.3.3 Non-Adaptive Single-Controller Analysis with Variable λ | 5-37 |
| 5.3.4 Non-Adaptive Single Controller Worst Case Analysis. | 5-37 |
| 5.3.5 Moving-Bank MMAC Analysis. | 5-37 |
| 5.4 MMAC Disturbance Rejection Study | 5-38 |
| 5.5 Number of Monte Carlo Analysis Runs | 5-39 |
| 5.6 Summary | 5-40 |
| VI. Conclusions and Recommendations | 6-1 |
| 6.1 Introduction | 6-1 |
| 6.2 Conclusions | 6-1 |
| 6.3 Recommendations | 6-2 |

| | Page |
|------------------------|--------|
| Bibliography | BIB-1 |
| Vita | VITA-1 |

List of Figures

| Figure | Page |
|---|------|
| 1.1. Rotating Two-Bay Truss Model | 1-7 |
| 1.2. Diagram of Feedback Control System | 1-10 |
| 1.3. Diagram of Multiple Model Adaptive Estimator | 1-11 |
| 1.4. Diagram of Multiple Model Adaptive Controller | 1-11 |
| 1.5. Diagram of MMAE/MMAC | 1-15 |
| 1.6. Moving-bank MMAE/MMAC - Fine Discretization | 1-16 |
| 1.7. Moving-bank MMAE/MMAC - Coarse Discretization | 1-16 |
| 3.1. Annotated Rotating Two-Bay Truss Model | 3-2 |
| 4.1. System Estimator Simulation | 4-3 |
| 4.2. System Controller Simulation | 4-5 |
| 5.1. Benchmark Estimation Errors, $\lambda = 0$, Node 1 | 5-6 |
| 5.2. Benchmark Estimation Errors, $\lambda = 0$, Node 2 | 5-7 |
| 5.3. Benchmark Estimation Errors, $\lambda = 0$, Node 3 | 5-8 |
| 5.4. Single-Filter Estimation Errors, $\lambda = 0.5$, Node 1 | 5-9 |
| 5.5. Single-Filter Estimation Errors, $\lambda = 0.5$, Node 2 | 5-10 |
| 5.6. Single-Filter Estimation Errors, $\lambda = 0.5$, Node 3 | 5-11 |
| 5.7. Single-Filter Estimation Errors, $\lambda = 1$, Node 1 | 5-12 |
| 5.8. Single-Filter Estimation Errors, $\lambda = 1$, Node 2 | 5-13 |
| 5.9. Single-Filter Estimation Errors, $\lambda = 1$, Node 3 | 5-14 |
| 5.10. "Worst Case" Single-Filter Estimation Errors with Parameter/Filter Location Mismatch, Node 1, $\lambda = 0.0$ | 5-15 |
| 5.11. "Worst Case" Single-Filter Estimation Errors with Parameter/Filter Location Mismatch, Node 2, $\lambda = 0.0$ | 5-16 |

| Figure | Page |
|---|------|
| 5.12. "Worst Case" Single-Filter Estimation Errors with Parameter/Filter Location Mismatch, Node 3, $\lambda = 0.0$ | 5-17 |
| 5.13. "Worst Case" Single-Filter Estimation Errors with Parameter/Filter Location Mismatch, Node 1, $\lambda = 0.5$ | 5-18 |
| 5.14. "Worst Case" Single-Filter Estimation Errors with Parameter/Filter Location Mismatch, Node 2, $\lambda = 0.5$ | 5-19 |
| 5.15. "Worst Case" Single-Filter Estimation Errors with Parameter/Filter Location Mismatch, Node 3, $\lambda = 0.5$ | 5-20 |
| 5.16. Position Estimation Means and Standard Deviations for MMAE, Node 1 | 5-22 |
| 5.17. Position Estimation Means and Standard Deviations for MMAE, Node 1 | 5-23 |
| 5.18. Position Estimation Means and Standard Deviations for MMAE, Node 2 | 5-24 |
| 5.19. Position Estimation Means and Standard Deviations for MMAE with "Worst Case" Analysis, Node 2 | 5-25 |
| 5.20. Position Estimation Means and Standard Deviations for MMAE, Node 3 | 5-26 |
| 5.21. Position Estimation Means and Standard Deviations for MMAE with "Worst Case" Analysis, Node 3 | 5-27 |
| 5.22. Moving-Bank Estimation Errors with Parameter/Filter Location Mismatch and Movement of the Bank, Node 1, $\lambda = 0.0$ | 5-28 |
| 5.23. Moving-Bank Estimation Errors with Parameter/Filter Location Mismatch and Movement of the Bank, Node 2, $\lambda = 0.0$ | 5-29 |
| 5.24. Moving-Bank Estimation Errors with Parameter/Filter Location Mismatch and Movement of the Bank, Node 3, $\lambda = 0.0$ | 5-30 |
| 5.25. Parameter Estimation and Actual Filter Bank Location, $\lambda = 0.0$ | 5-31 |
| 5.26. Mean Structure Positions | 5-31 |
| 5.27. Moving-Bank Estimation Errors with Parameter/Filter Location Mismatch and Movement of the Bank, Node 1, $\lambda = 0.5$ | 5-32 |
| 5.28. Moving-Bank Estimation Errors with Parameter/Filter Location Mismatch and Movement of the Bank, Node 2, $\lambda = 0.5$ | 5-33 |
| 5.29. Moving-Bank Estimation Errors with Parameter/Filter Location Mismatch and Movement of the Bank, Node 3, $\lambda = 0.5$ | 5-34 |

| Figure | Page |
|--|------|
| 5.30. Parameter Estimation and Actual Filter Bank Location, $\lambda = 0.5$ | 5-25 |
| 5.31. Benchmark Estimation Errors with Single-LQG-Controller, $\lambda = 0$, Node 1 | 5-41 |
| 5.32. Benchmark Estimation Errors with Single-LQG-Controller, $\lambda = 0$, Node 2 | 5-42 |
| 5.33. Benchmark Estimation Errors with Single-LQG-Controller, $\lambda = 0$, Node 3 | 5-43 |
| 5.34. Control Inputs for the MMAC Benchmark | 5-44 |
| 5.35. Structure Positions with MMAC and $\lambda = 0.0$ | 5-45 |
| 5.36. Estimation Errors with Single-LQG-Controller, $\lambda = 0.5$, Node 1 | 5-46 |
| 5.37. Estimation Errors with Single-LQG-Controller, $\lambda = 0.5$, Node 2 | 5-47 |
| 5.38. Estimation Errors with Single-LQG-Controller, $\lambda = 0.5$, Node 3 | 5-48 |
| 5.39. Control Inputs for MMAC with $\lambda = 0.5$ | 5-49 |
| 5.40. Structure Positions with MMAC and $\lambda = 0.5$ | 5-50 |
| 5.41. Estimation Errors with Single-LQG-Controller, $\lambda = 1.0$, Node 1 | 5-51 |
| 5.42. Estimation Errors with Single-LQG-Controller, $\lambda = 1.0$, Node 2 | 5-52 |
| 5.43. Estimation Errors with Single-LQG-Controller, $\lambda = 1.0$, Node 3 | 5-53 |
| 5.44. Control Inputs for MMAC with $\lambda = 1.0$ | 5-54 |
| 5.45. Structure Positions with MMAC and $\lambda = 1.0$ | 5-55 |
| 5.46. "Worst Case" Estimation Errors with Single-LQG-Controller, $\lambda = 0$, Node 1 | 5-56 |
| 5.47. "Worst Case" Estimation Errors with Single-LQG-Controller, $\lambda = 0$, Node 2 | 5-57 |
| 5.48. "Worst Case" Estimation Errors with Single-LQG-Controller, $\lambda = 0$, Node 3 | 5-58 |
| 5.49. Control Inputs for Worst Case Analysis | 5-59 |
| 5.50. "Worst Case" Estimation Errors with Single-LQG-Controller, $\lambda = 0.5$, Node 1 | 5-61 |
| 5.51. "Worst Case" Estimation Errors with Single-LQG-Controller, $\lambda = 0.5$, Node 2 | 5-62 |
| 5.52. "Worst Case" Estimation Errors with Single-LQG-Controller, $\lambda = 0.5$, Node 3 | 5-63 |
| 5.53. Control Inputs for the "Worst Case" Analysis | 5-64 |
| 5.54. Position Estimation Means and Standard Deviations for Single-LQG-Controller Case, Node 1 | 5-65 |
| 5.55. Position Estimation Means and Standard Deviations for Single-LQG-Controller Case with "Worst Case" Analysis, Node 1 | 5-66 |

| Figure | Page |
|---|------|
| 5.56. Position Estimation Means and Standard Deviations for Single-LQG-Controller Case, Node 2 | 5-67 |
| 5.57. Position Estimation Means and Standard Deviations for Single-LQG-Controller Case with "Worst Case" Analysis, Node 2 | 5-68 |
| 5.58. Position Estimation Means and Standard Deviations for Single-LQG-Controller Case, Node 3 | 5-69 |
| 5.59. Position Estimation Means and Standard Deviations for Single-LQG-Controller Case with "Worst Case" Analysis, Node 3 | 5-70 |
| 5.60. Estimation Errors with Parameter/Filter Location Mismatch and Movement of the Bank with MMAC, Node 1, $\lambda = 0.0$ | 5-71 |
| 5.61. Estimation Errors with Parameter/Filter Location Mismatch and Movement of the Bank with MMAC, Node 2, $\lambda = 0.0$ | 5-72 |
| 5.62. Estimation Errors with Parameter/Filter Location Mismatch and Movement of the Bank with MMAC, Node 3, $\lambda = 0.0$ | 5-73 |
| 5.63. Control Inputs for the Single-LQG-Controller Case Bank Movement Analysis, $\lambda = 0$ | 5-74 |
| 5.64. Parameter Estimation and Actual Filter Bank Location, $\lambda = 0.0$ | 5-75 |
| 5.65. Mean Structure Positions | 5-75 |
| 5.66. Estimation Errors with Parameter/Filter Location Mismatch and Movement of the Bank MMAC, Node 1, $\lambda = 0.25$ | 5-76 |
| 5.67. Estimation Errors with Parameter/Filter Location Mismatch and Movement of the Bank MMAC, Node 2, $\lambda = 0.25$ | 5-77 |
| 5.68. Estimation Errors with Parameter/Filter Location Mismatch and Movement of the Bank MMAC, Node 3, $\lambda = 0.25$ | 5-78 |
| 5.69. Control Inputs for the MMAC Bank Movement Analysis, $\lambda = 0.25$ | 5-79 |
| 5.70. Parameter Estimation and Actual Filter Bank Location, $\lambda = 0.25$ | 5-80 |
| 5.71. Mean Structure Positions | 5-80 |
| 5.72. Estimation Errors with Parameter/Filter Location Mismatch and Movement of the Bank with MMAC, Node 1, $\lambda = 0.5$ | 5-81 |
| 5.73. Estimation Errors with Parameter/Filter Location Mismatch and Movement of the Bank with MMAC, Node 2, $\lambda = 0.5$ | 5-82 |

| Figure | Page |
|--|------|
| 5.74. Estimation Errors with Parameter/Filter Location Mismatch and Movement of the Bank with MMAC, Node 3, $\lambda = 0.5$ | 5-83 |
| 5.75. Control Inputs for the MMAC Bank Movement Analysis, $\lambda = 0.5$ | 5-84 |
| 5.76. Parameter Estimation and Actual Filter Bank Location, $\lambda = 0.5$ | 5-85 |
| 5.77. Mean Structure Position | 5-85 |
| 5.78. Estimation Errors with Parameter/Filter Location Mismatch and Movement of the Bank with Control, Node 1, $\lambda = 1.0$ | 5-86 |
| 5.79. Estimation Errors with Parameter/Filter Location Mismatch and Movement of the Bank, Node 2, $\lambda = 1.0$ | 5-87 |
| 5.80. Estimation Errors with Parameter/Filter Location Mismatch and Movement of the Bank, Node 3, $\lambda = 1.0$ | 5-88 |
| 5.81. Control Inputs for the MMAC Bank Movement Analysis, $\lambda = 1.0$ | 5-89 |
| 5.82. Parameter Estimation and Actual Filter Bank Location, $\lambda = 1.0$ | 5-90 |
| 5.83. Mean Structure Positions | 5-90 |
| 5.84. Estimation Errors with Control and Disturbance, $\lambda = 0$, Node 1 | 5-91 |
| 5.85. Estimation Errors with Control and Disturbance, $\lambda = 0$, Node 2 | 5-92 |
| 5.86. Estimation Errors with Control and Disturbance, $\lambda = 0$, Node 3 | 5-93 |
| 5.87. Control Inputs for the MMAC with Disturbance | 5-94 |
| 5.88. Parameter Estimation and Actual Filter Bank Location for Disturbed System | 5-95 |
| 5.89. Mean Structure Positions for Disturbed System | 5-96 |
| 5.90. 100 Run Monte Carlo Analysis for Movement of the Bank with Control, Node 1 | 5-97 |

List of Tables

| Table | Page |
|---|------|
| 3.1. Structural Member's Cross-Sectional Areas | 3-8 |
| 3.2. Average Damping Factors and Natural Frequencies | 3-13 |
| 5.1. Position Estimation Means and Standard Deviations for MMAE | 5-24 |
| 5.2. Velocity Estimation Means and Standard Deviations for MMAE | 5-24 |
| 5.3. Position Estimation Means and Standard Deviations for MMAC (Single-LQG- Controller) | 5-30 |
| 5.4. Velocity Estimation Means and Standard Deviations for Single-LQG-Controller Case | 5-30 |

Abstract

The robustness of moving-bank multiple model adaptive estimation (MMAE) and control (MMAC) algorithms is analyzed in this thesis. The mismatch of a 24-state truth model and a 6-state filter model are evaluated on the basis of MMAE/MMAC performance.

A model developed using finite element analysis is used to approximate a large space structure which has a large central hub with appendages radiating out from it. The mass of the hub is considered to be much larger than the mass of the flexible structure. The model is developed in physical coordinates and then transformed into modal coordinates. To obtain a reduced order filter model, the method of singular perturbations is used. The actual positions and velocities of various physical points on the structure are used in the evaluation of the MMAE/MMAC algorithm performance.

The results of this study of model mismatching indicates that the MMAE provides accurate position and velocity estimates even in the face of a 6-state to 24-state model mismatch. When a non-adaptive filter is used with a mismatched parameter location, the performance suffers slightly. The use of an adaptive estimator does provide improved performance in the face of uncertain parameter location. Stable control was obtained with the use of MMAC. For the case of non-adaptive filter and mismatched parameter location, the control algorithm behaved in a possibly destructive manner. By allowing the filter to adapt to the initial parameter location, the MMAC algorithm provided stable control of the structure, even in the face of large disturbances.

ROBUSTNESS OF A MOVING-BANK MULTIPLE MODEL ADAPTIVE CONTROLLER FOR A LARGE SPACE STRUCTURE

1. Introduction

A situation exists in estimation and control design problems where the parameters describing the system are not known with certainty. Additionally, the parameters may be varying as a function of time, such as due to the depletion of a fuel cell or the jettisoning of external stores on an aircraft. Another possibility is that the system parameters may undergo a jump change (a radical change from one value to another) due to a hostile environment affecting the physical structure or structural failure due to an imperfection or structural fatigue. Due to these possible parameter value changes, adaptive estimation of the system states and adaptive control might be used in controlling the system's performance. Another problem is that using a complete mathematical (or "truth") model would create an unbearable computational load due to the high order of the model. Therefore, one usually chooses to use a reduced-order model for the basis of synthesizing a filter and/or controller, and so robustness of the adaptation process to unmodelled effects becomes an important issue.

This thesis uses Kalman filters for the estimation of the system states of a large flexible space structure. The technique of estimating the system states is referred to as Multiple Model Adaptive Estimation (MMAE), having the structure of a bank of Kalman filters (each based upon a single discrete value of the parameters) and then forming the final state estimate as a probabilistically weighted sum of the individual filter state estimates. The concept of a "moving-bank" MMAE algorithm is that not all possible elemental Kalman filters are maintained in the bank at all times, but only a dynamically redeclared subset, such as those corresponding to discrete parameter values *closest* to the current parameter estimate. The estimated states are, in turn, used as inputs to

a controller. This control process is referred to as Multiple Model Adaptive Control (MMAC). The MMAE/MMAC algorithms developed in this research are used to control a large flexible space structure. The algorithms have evolved over a five year period with research performed by Hentz [8], Filios [6], Karnick [11], Lashlee [15], and Van Der Werken [24]. In particular, the work performed in the last thesis [24] will be continued, concentrating on the effects of unmodelled states on the overall performance and robustness of the estimation and control system. This thesis uses the Kalman filters in a bank configuration where each filter has been optimized for a given combination of the parameters of interest. Due to computational loading concerns, the parameters have been limited to two. The reasoning behind this will be developed in Chapter 2. The robustness analysis of the controller provides insight into the effects of using a reduced-order state filter model.

1.1 Background

The original feasibility study using a moving-bank multiple-model estimator/controller was performed by Hentz [8] and subsequently presented by Maybeck and Hentz [22]. The Kalman filter, a recursive optimal filter, is the primary building block of the MMAE technique, and so it is now described. The development of the Kalman filter in this section is not intended to be complete. For detailed discussions of the Kalman filter and related topics see [18]-[20]. The notation used in this thesis follows [18] such that a stochastic process is denoted by $\underline{\mathbf{x}}$ while a deterministic process is denoted by \mathbf{x} .

1.1.1 Kalman Filter: The Kalman filter is the foundation of the MMAE/MMAC control design. To use the Kalman filter approach to state estimation, viewed here as a specific form of Bayesian estimation [19:129-136], the system of interest is assumed to be adequately defined by a linear stochastic state model [18:163-170]. The equation representing this system is given by:

$$\dot{\underline{\mathbf{x}}}(t) = \mathbf{F}(t)\underline{\mathbf{x}}(t) + \mathbf{B}(t)\mathbf{u}(t) + \mathbf{G}(t)\underline{\mathbf{w}}(t) \quad (1.1)$$

where $\underline{x}(\cdot)$ represents an n -vector state process, $\underline{u}(\cdot)$ is an r -vector deterministic control input, $\mathbf{F}(\cdot)$ is an n -by- n system dynamics matrix (which contains the parameters of interest in this effort), $\mathbf{B}(\cdot)$ is an n -by- r deterministic input matrix, and $\mathbf{G}(\cdot)$ is an n -by- s noise input matrix. The characteristics of the white Gaussian noise \underline{w} is of particular importance.

The statistics of $\underline{w}(\cdot)$ are given by:

$$E\{\underline{w}(t)\} = 0 \quad (1.2)$$

$$E\{\underline{w}(t)\underline{w}(t')^T\} = \mathbf{Q}\delta(t - t') \quad (1.3)$$

where $\mathbf{Q}(\cdot)$ is an s -by- s matrix that is symmetric and positive semidefinite. $\delta(t)$ is the Dirac delta function. \mathbf{Q} represents the dynamics noise strength being put into the system. The selection of \mathbf{Q} is often left to the engineering intuition of the designer [4:100] and therefore will be a challenge in the estimator/controller design.

Another important statistical property is related to the state process vector \underline{x} . The initial condition of \underline{x} and the certainty with which this value is known is required. The initial condition mean value of the state is given by:

$$E\{\underline{x}(t_0)\} = \hat{\mathbf{x}}_0 \quad (1.4)$$

The right hand side of Equation (1.4) is the mean of \underline{x} at the initial time t_0 . The degree to which the initial condition is known is given by the covariance which is denoted by \mathbf{P}_0 and given in Equation (1.5).

$$E\{[\underline{x}(t_0) - \hat{\mathbf{x}}_0][\underline{x}(t_0) - \hat{\mathbf{x}}_0]^T\} = \mathbf{P}_0 \quad (1.5)$$

To implement the Kalman filters, the discrete forms of the above equations are used. Equation (1.1) contains the matrices \mathbf{F} , \mathbf{B} , and \mathbf{G} . This same system representation may be expressed in a discrete time formulation [18:170-172]. The state transition matrix, Φ , is derived using the system

dynamics matrix \mathbf{F} :

$$\Phi(t, t_0) = \Phi(t - t_0) = \mathcal{L}^{-1}\{[s\mathbf{I} - \mathbf{F}]^{-1}\} \quad (1.6)$$

if \mathbf{F} is a constant matrix. Φ defines how the state vector changes over the specified time period.

Additionally, the deterministic input matrix \mathbf{B} may be expressed in a discrete-time form using Φ .

$$\mathbf{B}_d(t_i) = \int_{t_i}^{t_{i+1}} \Phi(t_{i+1}, \tau) \mathbf{B}(\tau) d\tau \quad (1.7)$$

The discrete-time white Gaussian system dynamics noise vector \mathbf{w}_d has a covariance \mathbf{Q}_d that is a function of the state transition matrix, the noise input matrix, and the strength of the continuous-time \mathbf{w} :

$$\mathbf{Q}_d(t_i) = \int_{t_i}^{t_{i+1}} \Phi(t_{i+1}, \tau) \mathbf{G}(\tau) \mathbf{Q}(\tau) \mathbf{G}^T(\tau) \Phi^T(t_{i+1}, \tau) d\tau \quad (1.8)$$

In terms of these discrete-time matrices, equation (1.1) is rewritten as:

$$\mathbf{x}(t_i) = \Phi(t_i, t_{i-1}) \mathbf{x}(t_{i-1}) + \mathbf{B}_d(t_{i-1}) \mathbf{u}(t_{i-1}) + \mathbf{w}_d(t_{i-1}) \quad (1.9)$$

and the time propagation equations for the conditional mean state estimate of \mathbf{x} and the covariance are given by [18:174-175]:

$$\hat{\mathbf{x}}(t_i^-) = \Phi(t_i, t_{i-1}) \hat{\mathbf{x}}(t_{i-1}^+) + \mathbf{B}_d(t_{i-1}) \mathbf{u}(t_{i-1}) \quad (1.10)$$

$$\mathbf{P}(t_i^-) = \Phi(t_i, t_{i-1}) \mathbf{P}(t_{i-1}^+) \Phi^T(t_i, t_{i-1}) + \mathbf{Q}_d(t_{i-1}) \quad (1.11)$$

These equations give the relationship between two consecutive state estimates and covariances at the times t_i^- and t_{i-1}^+ . Note that, in order to carry out the above calculations, the estimate $\hat{\mathbf{x}}(t_{i-1}^+)$ and the covariance $\mathbf{P}(t_{i-1}^+)$ must be known. For these to be determined, a measurement from the system must be taken and the entire system of equations updated. The "+" and "-" superscripts indicate

that the variable of interest is evaluated just after or just before a measurement is incorporated, respectively.

The discrete-time (or sample-data) measurement \underline{z} is determined by a measurement model:

$$\underline{z}(t_i) = \mathbf{H}(t_i)\underline{x}(t_i) + \underline{v}(t_i) \quad (1.12)$$

The variable \underline{v} is the measurement noise accounting for the uncertainty with which the measurements are obtained. The measurement noise is generally considered to be a Gaussian discrete-time process with zero mean and a covariance of \mathbf{R} . The system model developed assumes that the system dynamics noise \underline{w} and the measurement noise \underline{v} are independent. In addition, the noises are independent of the initial condition $\underline{x}(t_0)$. Once \underline{z} has been measured, the entire system of equations are updated using the following three equations (in addition to the equations already given in (1.10) and (1.11) for the filter's propagation cycle):

$$\mathbf{K}(t_i) = \mathbf{P}(t_i^-)\mathbf{H}^T(t_i) [\mathbf{H}(t_i)\mathbf{P}(t_i^-)\mathbf{H}^T(t_i) + \mathbf{R}(t_i)]^{-1} \quad (1.13)$$

$$\hat{\mathbf{x}}(t_i^+) = \hat{\mathbf{x}}(t_i^-) + \mathbf{K}(t_i) [\underline{z}(t_i) - \mathbf{H}(t_i)\hat{\mathbf{x}}(t_i^-)] \quad (1.14)$$

$$\mathbf{P}(t_i^+) = \mathbf{P}(t_i^-) - \mathbf{K}(t_i)\mathbf{H}(t_i)\mathbf{P}(t_i^-) \quad (1.15)$$

The bracketed term in Equation (1.14) is called the residual (or in some literature, innovations [4, 14]) and denoted by $\mathbf{r}(t_i)$. The residual of the Kalman filter indicates how much error correction is required in the filter, since it is the difference between the most recent measurement and the best prediction of that measurement based on estimates prior to that sample time. The residual is weighted by \mathbf{K} and added to the previous estimate of the state to arrive at the new estimate of the state.

The discrete-time Kalman filter stochastic difference equation and propagation equations have

been presented as a review. Several important numbers in the scalar case, or matrices in the vector case, are involved in these equations. They are derived from the model of the system developed by the designer.

1.1.2 System Model The integration of control system design and structural considerations during the design phase of a system is becoming both commonplace and necessary [25:1768]. While this research effort does not develop the actual system model, it is important to understand some basic concepts that underlie the models. The large space structure considered is modelled by linear equations.

The thesis research performed over the last five years has involved different types of investigations. Hentz performed a feasibility study on using a moving-bank MMAE/MMAC approach to solve the control problem. Filios continued to look at the problem of applying this same technique to a more realistic spacecraft model; however, online adaptation was not really required for that particular spacecraft. Karnick was given the basic two-bay truss model, added modifications, and used the new model to perform his research. Lashlee used the same model to perform his research. Van Der Werken used the same filter model but included higher order modes in the truth model, 24 states versus 6 states.

One of the primary concerns in control design is disturbance rejection. The ability to withstand outside interference from natural and man-made phenomena as well as disturbances from the system itself is essential.

In large space structures the disturbances are the result of slewing/pointing maneuvers, thermal transients, and mechanical machinery such as coolers, generators, etc. Control of the dynamic response is essential for maintaining the ride quality and performance requirements, as well as for the safety of the structure [25:1768].

The parameters that affect the performance of the system may be categorized as (1) the physical composition of the structure, (2) the sources of disturbances, and (3) the control system itself.

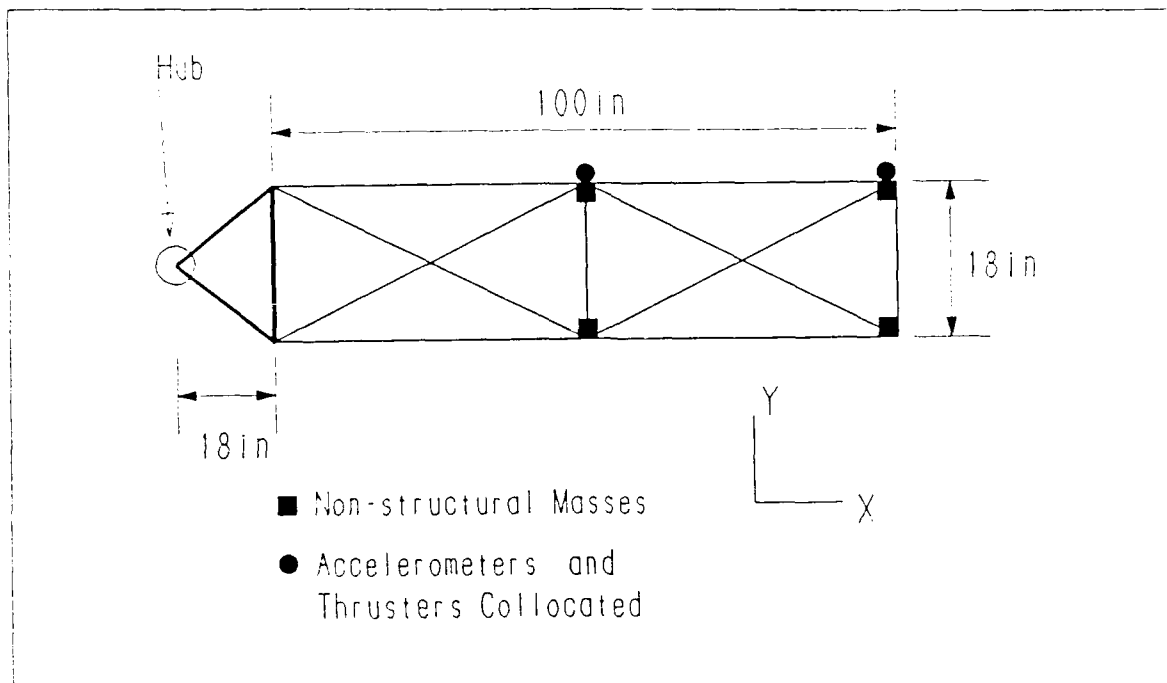


Figure 1.1. Rotating Two-Bay Truss Model

The physical composition of the structure is shown in Figure 1.1. The structure has co-located accelerometers and thrusters, which simplifies some of the calculations. The hub has gyroscopes to determine angular displacement and velocity and a co-located inertia wheel as an actuator. The sensor and actuator locations and functions will be explained in detail in Chapter 3.

Karnick presents a very thorough description of the components of the two-bay truss model that represents an appendage of a larger space structure (such as a manned space station) [11:39-58]. The aluminum rods that make up the two-bay truss are assumed to be of a certain cross-sectional area and elasticity. The mass and stiffness matrices that describe the model were calculated using finite element analysis [11, 26]. Chapter 3 presents the results of the finite element analysis and the development of the matrices that describe the system. The matrices are considered to be the nominal values for design purposes. During this research the parameters that are considered to vary, namely the damping factor and natural frequency of the structure, are the result of changes in the mass and stiffness matrices. The truth model is developed by using twelve modes, the rigid

body and eleven bending modes, which are represented by twenty-four states.

In efforts prior to those that addressed the rotating two-bay truss, the MMAE and MMAC algorithms were used to control models of various complexities. Hentz used a simple two-state model of the structure [8:16]. The control ratio of the structure dynamics is

$$\frac{C(s)}{R(s)} = \frac{\omega_n^2}{s^2 + 2\zeta\omega_n s + \omega_n^2} \quad (1.16)$$

or in state variable form (standard controllable form) the structure dynamics are described by:

$$\dot{\mathbf{x}}(t) = \begin{bmatrix} 0 & 1 \\ -\omega_n^2 & -2\zeta\omega_n \end{bmatrix} \mathbf{x}(t) + \begin{bmatrix} 0 \\ \omega_n^2 \end{bmatrix} u(t) \quad (1.17)$$

$$c(t) = \begin{bmatrix} 1 & 0 \end{bmatrix} \mathbf{x}(t) \quad (1.18)$$

The state vector \mathbf{x} is composed of two components: $\mathbf{x}_1(t)$, which represents a position variable, and $\mathbf{x}_2(t)$, which represents a velocity variable.

The work performed by Filios [6:38-41] used a more complex model. Filios evaluated the MMAE and MMAC algorithms against the Draper Laboratory/Rocket Propulsion Laboratory Configuration model, which consists of four cantilevered appendages attached to a central hub. This model more closely represents a satellite with four "whip" antennas than the structure developed by Karnick. A six state model was used by Filios.

The work performed by Karnick [11] used a two-bay truss model attached to a hub. Karnick used a six-state model accounting for the rigid body mode and two bending modes of the structure; a reduced order model derived from an analysis using the method of singular perturbations [13]. Lashlee's research [15] used the same model. Both the truth and filter models used six states for Karnick's and Lashlee's research, and thus there were no unmodelled state effects. Being concerned about the effect of unmodelled states (a robustness concern), Van Der Werken used a 24-state truth

model and a 6-state filter model [24]. The full development of the truth model is presented in Chapter 3.

The number of states describing a model used in control analysis cannot be predetermined solely on the basis of *mathematical insight or engineering intuition*. The computational loading requirements of a specific implementation may preclude the use of more than a few states. This limitation may have implications on the robustness of the control system and is the concern of this thesis effort. By increasing the number of states used in the truth model, Van Der Werken observed changes in the system performance as compared to that portrayed by Lashlee. These observations indicate that the filter model state size may require modifications for proper performance from the MMAE/MMAC algorithms.

1.1.3 Multiple Model Adaptive Estimation - MMAE The use of full state feedback is the normal initial approach for optimal control. Full state feedback provides the control system stability and robustness to external and internal disturbances. However, perfect access to all states is seldom attainable and so a state estimator is used to provide best estimates of plant states to the controller that was designed as though full state access were actually available. The controller for this research is an LQG controller.

Using LQG control assumes that the system model is **L**inear, there is a **Q**uadratic cost criterion associated with the control problem, and the noises used in the dynamics and measurement equations are taken to be **G**aussian. "The LQG optimal controller has the *certainty equivalence property*" [20:17]. The certainty equivalence property is a special case of the separation property. The LQG controller is equivalent to the optimal deterministic controller "but with the state replaced with the conditional mean of the state given the observed measurements..." [20:17]. Figure 1.2 shows the flow of the signals from the system to the estimator. The estimator provides the current state estimation to the controller, which in turn provides a control signal to the system.

The usual problems encountered in a real world system, as is the case with the flexible space

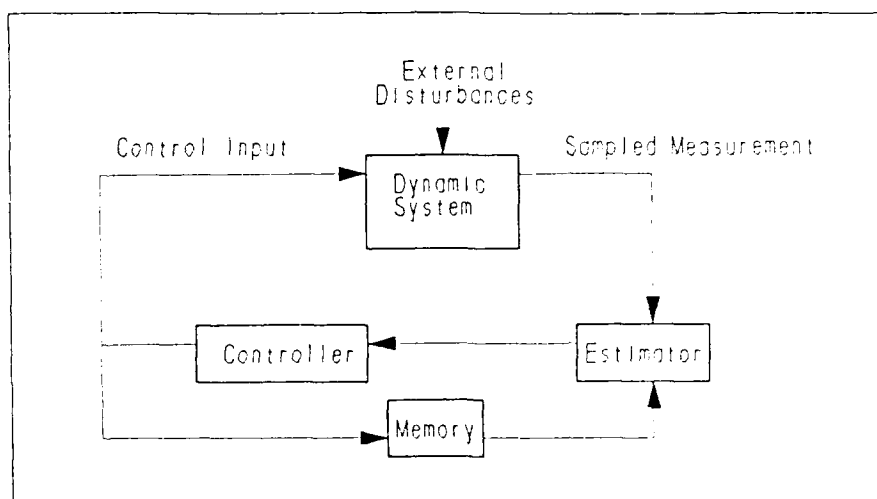


Figure 1.2. Diagram of Feedback Control System [20]

structure, are that the states themselves may not be directly measurable or the system parameters may vary from the original design as discussed earlier. The approach that MMAE uses is to design each Kalman filter for a discrete point of interest in the parameter space. The real parameters may actually be *continuous in the region of interest*. The number of values that a parameter could attain would therefore be infinite and the resulting combinations of parameters would also be infinite. Since the use of infinite (or even very large) computers is not realistic or practical for this research, the parameter space is viewed as a discretized version of this continuum. For example, if the system had two parameters of interest that could take on two discrete values each, then the parameter space would be comprised of four discrete points. If, however, the parameters could take on 100 values each, the parameter space would be composed of 10,000 discrete points, each requiring a Kalman filter and eventually an LQG controller, which would be an unbearable computational load for any real-time control system. The work performed in previous research [11, 15, 24] uses a two-parameter, 10-value-per-parameter approximation of the actual continuous parameter space. The parameter space employs 100 points. Figure 1.3 shows the block diagram of the MMAE algorithm. A full-scale MMAE algorithm would require a bank of 100 Kalman filters for this application.

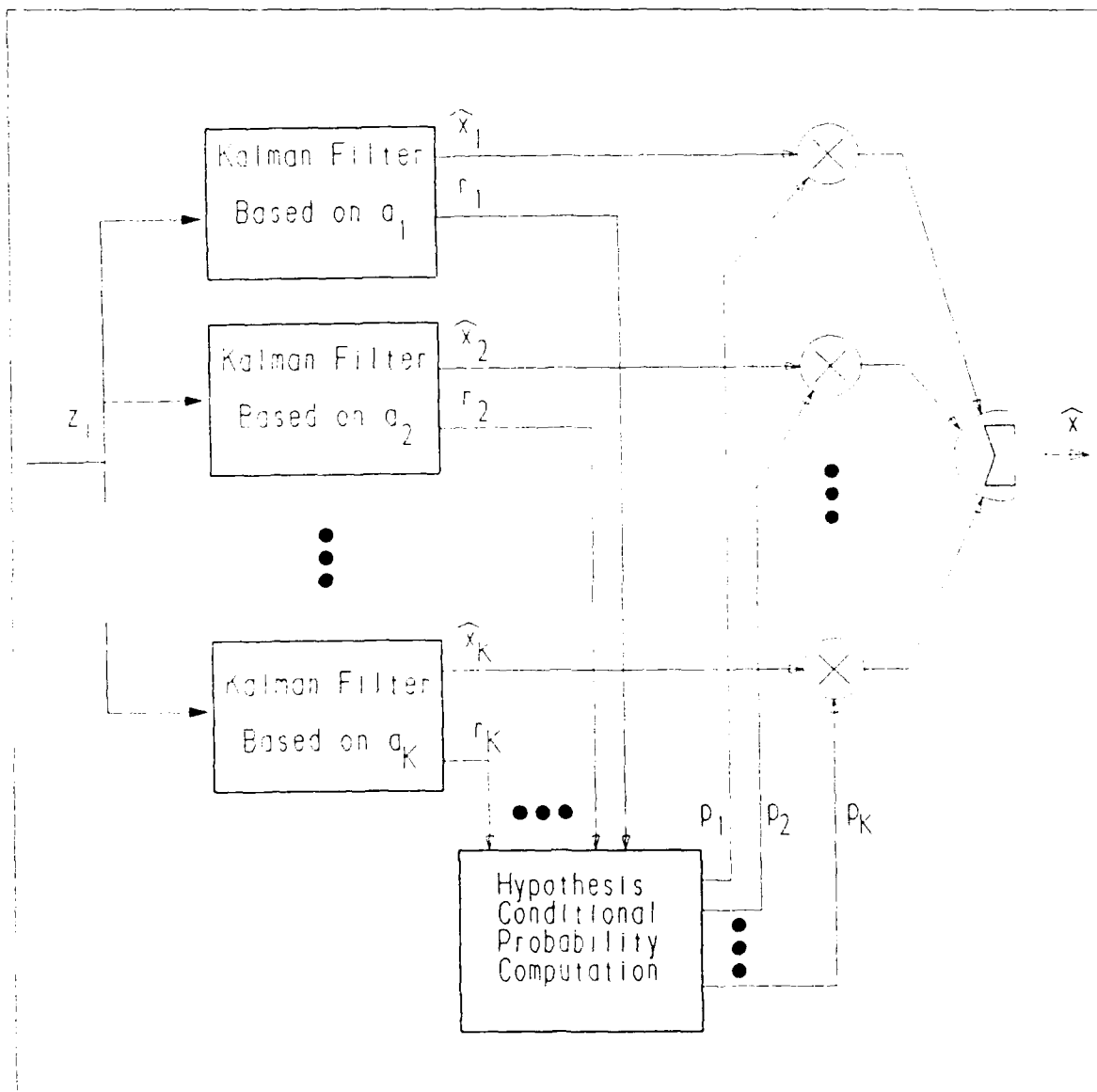


Figure 1.3. Diagram of Multiple Model Adaptive Estimator [21]

The adaptive estimation occurs due to the multiplication of the probabilities generated based on the residuals from each Kalman filter. The state estimate of each filter is multiplied by the probability that the assumed value of parameter for that particular filter is the best parameter value to use. The probability from each Kalman filter is a function of the conditional probability densities related by

$$p_k(t_i) = \frac{f_{\mathbf{Z}(t_i)|\mathbf{a}, \mathbf{Z}(t_{i-1})}(\mathbf{z}_i | \mathbf{a}_k, \mathbf{Z}_{i-1})p_k(t_{i-1})}{\sum_{j=1}^K f_{\mathbf{Z}(t_i)|\mathbf{a}, \mathbf{Z}(t_{i-1})}(\mathbf{z}_i | \mathbf{a}_j, \mathbf{Z}_{i-1})p_j(t_{i-1})} \quad (1.19)$$

where K is the number of filters. The first numerator term represents the probability density of the current measurement based on the assumed \mathbf{a}_k parameter and given the previous measurement history through time t_{i-1} , \mathbf{Z}_{i-1} . The second numerator term is the previous p_k value, and thus (1.19) is an iterative relation. The probability density function is formed by:

$$\begin{aligned} f_{\mathbf{Z}(t_i)|\mathbf{a}, \mathbf{Z}(t_{i-1})}(\mathbf{z}_i | \mathbf{a}_k, \mathbf{Z}_{i-1}) &= \frac{1}{(2\pi)^{\frac{m}{2}} |\mathbf{A}_k(t_i)|^{\frac{1}{2}}} \exp\{\cdot\} \\ \{\cdot\} &= \left\{-\frac{1}{2} \mathbf{r}_k^T(t_i) \mathbf{A}_k^{-1}(t_i) \mathbf{r}_k(t_i)\right\} \end{aligned} \quad (1.20)$$

where $\mathbf{A}_k(t_i)$ is a function of the measurement matrix $\mathbf{H}_k(t_i)$, the covariance matrix $\mathbf{P}_k(t_i^-)$, and the noise covariance matrix $\mathbf{R}_k(t_i)$, namely $\mathbf{A}_k(t_i) = [\mathbf{H}_k(t_i)\mathbf{P}_k(t_i^-)\mathbf{H}_k^T(t_i) + \mathbf{R}_k(t_i)]$. The denominator is the sum of all numerator terms for $j = 1, \dots, K$, so that the sum of all p_k is unity. Another way of stating this is that the conditional probability $p_k(t_i)$ is the probability that the discrete random process, \mathbf{a} , equals some specific value, \mathbf{a}_k , given that the measurement $\mathbf{Z}(t_i)$ has taken a specific realization \mathbf{Z}_i [19:130-131]. The weighted estimates are then summed to provide the *best* probabilistically weighted estimate of the current state. The computed probabilities have the characteristic that:

$$\sum_{k=1}^K p_k = 1 \quad (1.21)$$

This property does not let any one filter control the estimation process unless one of the estimator's

probability goes to one and all the others go to zero. The possibility that this case could occur has been considered by several research efforts [8, 22, 6, 11, 15, 24, 14]. Steps must be taken to prevent any probabilities from going to zero, since any such probability would become permanently locked onto zero by the iteration performed by (1.19) even if changing conditions were to cause that particular parameter value to become the best value. One way to prevent the probabilities from going to zero is to set some lower and upper limits that the p_k may take on. Once this is accomplished, a viable adaptive state estimate is available for use by a control system as shown in Figure 1.2 or 1.4.

1.1.4 Multiple Model Adaptive Control - MMAC Karnick developed the LQG controller for the two-bay truss model [11:97-98], that has been used by other research efforts [15, 24]. The MMAC algorithm uses the MMAE algorithm to develop estimates of the states. Each of the state estimates is then fed into a controller optimized for the parameter value corresponding to its estimate input. Figure 1.4 shows the signal flow. The blocks denoted by $-G_r^*(a_k)$ are optimal controller gains specifically established for each discrete parameter value a_k . Slight mistuning of the filter and/or controller parameters can cause poor performance of an individual LQG controller. The MMAC controller provides some relief from this parameter mismatch problem since it uses a weighted sum of control inputs based on the hypothesis conditional probabilities computed on the basis of the residuals generated by the Kalman filters. The MMAC approach to a control solution suffers from the same computational loading problem as MMAE. An alternative to full-scale MMAE/MMAC is the use of moving-bank MMAE/MMAC to provide a very close approximation to full-scale MMAE/MMAC optimal control with reduced computational loading.

1.1.5 Moving-Bank MMAE/MMAC The theory behind the moving-bank MMAE/MMAC is that the estimate, and in turn the proper control input to the system, may be approximated by a reduced number of discretized parameter values that take on the values of appropriate (dynamically redeclared) locations used for the basis of the full bank. Figure 1.5 shows how the full

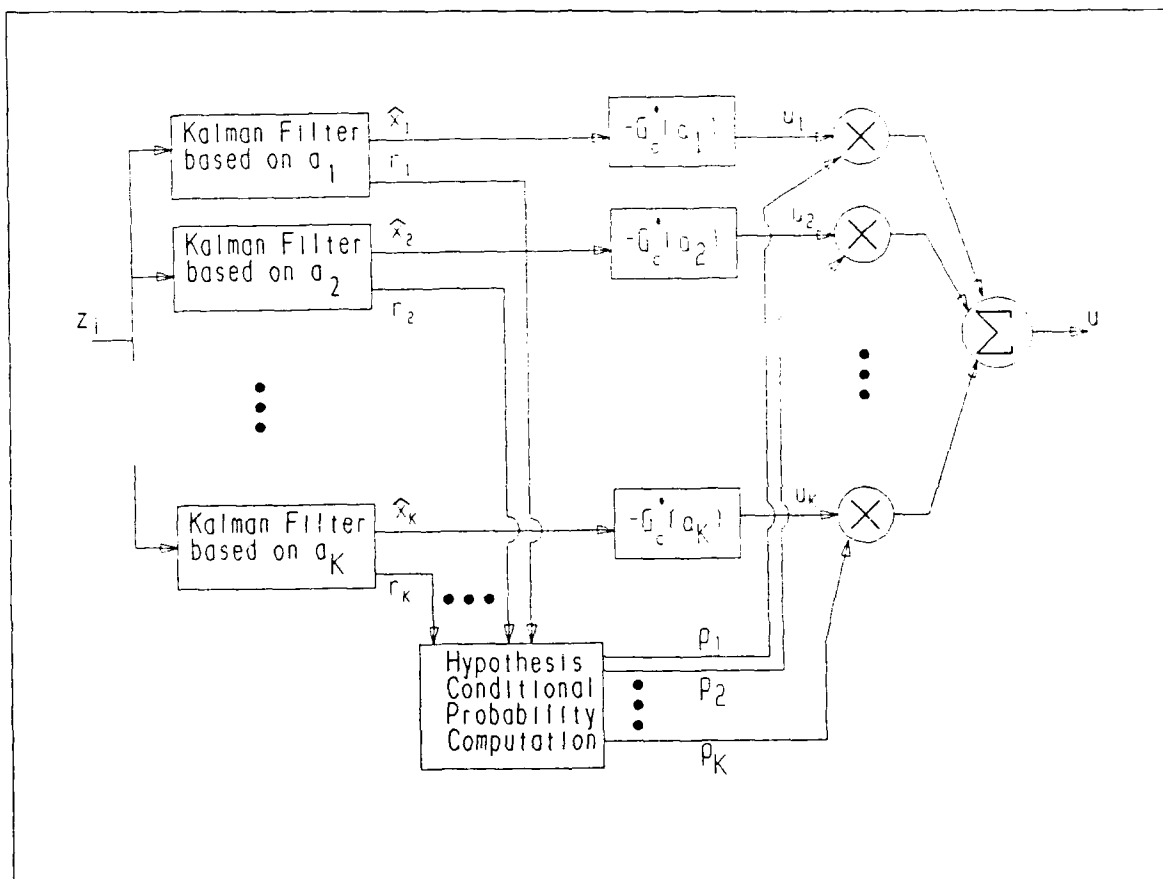


Figure 1.4. Diagram of Multiple Model Adaptive Controller [21]

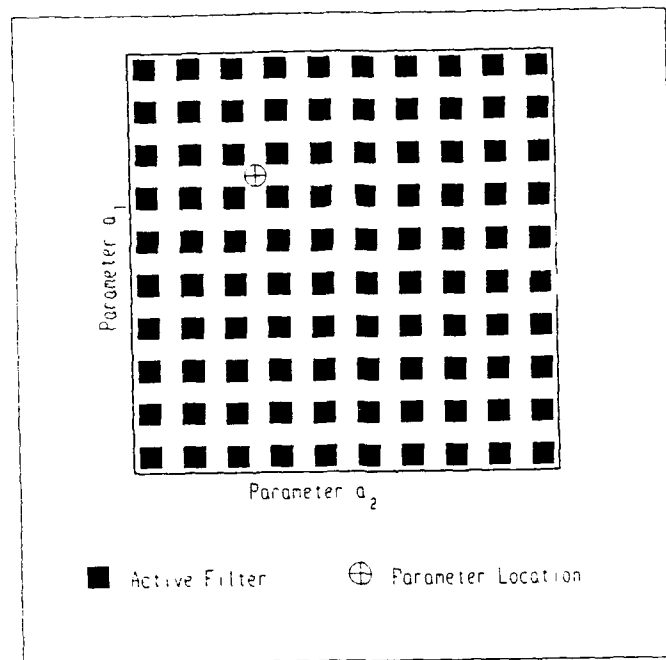


Figure 1.5. Diagram of MMAE/MMAC

MMAE/MMAC system would look if all the filters were used. Each of the blocks represent a discrete parameter point used as the basis for a Kalman filter and/or a control gain. Figure 1.6 shows how a moving 3-by-3 bank might appear surrounding the current (estimated) parameter value. The moving bank is composed of nine solid blocks. The "discarded filter" points correspond to a 3-by-3 bank at an earlier time instant when that set of nine points most closely surrounded the estimated parameter location at that time.

The problem of how to move the bank has been discussed and evaluated [8, 22, 6, 11, 15, 24]. There are five basic techniques for deciding to move the bank or perform a coarser discretization of the active bank of filters as shown in Figure 1.7. The techniques are:

- Residual monitoring
- Parameter position estimate monitoring
- Parameter position and "velocity" estimate monitoring
- Probability monitoring

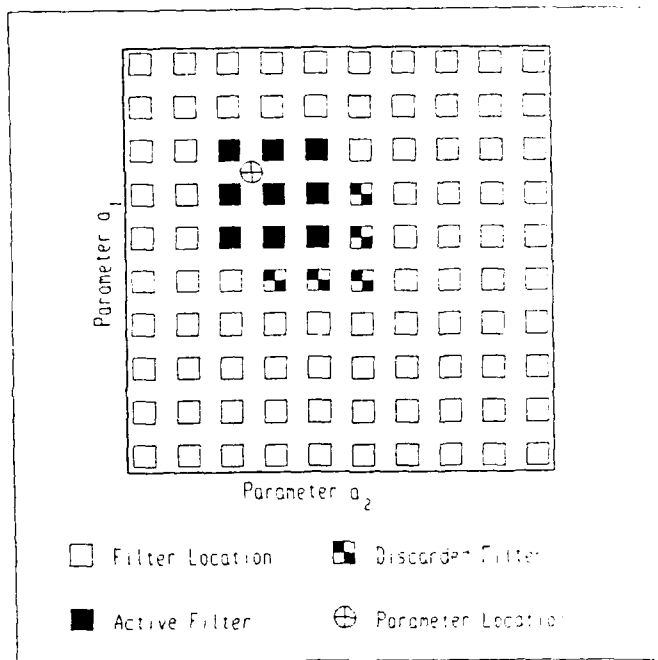


Figure 1.6. Moving-bank MMAE/MMAC - Fine Discretization

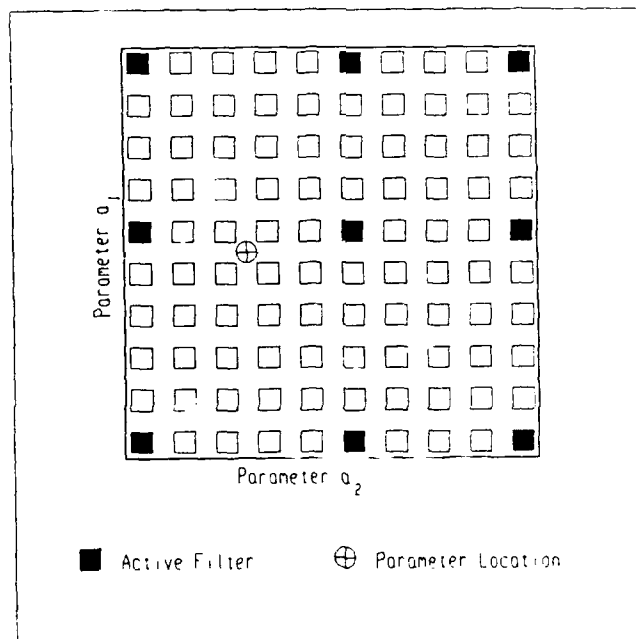


Figure 1.7. Moving-bank MMAE/MMAC - Coarse Discretization

- Parameter estimation error covariance monitoring

Residual monitoring uses a likelihood quotient defined as:

$$L_k(t_i) = \mathbf{r}_k^T(t_i) \mathbf{A}_k^{-1} \mathbf{r}_k(t_i) \quad (1.22)$$

to determine whether a move of the bank is required, where \mathbf{A}_k^{-1} is the inverse matrix appearing in Equation (1.13) (the bracketed inverse). If all the L_k are above a preset bound, the bank is moved. Further, the filter with the smallest likelihood quotient should be the filter nearest the true parameter value. Residual monitoring is susceptible to single large samples of measurement noise and may give false alarms [22:92], i.e., the bank may be moved even though the move is unnecessary.

Parameter Position Estimate Monitoring attempts to keep the bank centered on the current estimate of the true parameter. The estimated true parameter is given by:

$$\hat{\mathbf{a}}(t_i) = E\{\mathbf{a} \mid \mathbf{Z}(t_i)\} = \sum_{k=1}^K \mathbf{a}_k \cdot p_k(t_i) \quad (1.23)$$

When the "distance" between the center of the bank and the estimated parameter location becomes larger than a preset value, the filter bank is moved. Since the calculation depends on the time history of measurements, this technique is less susceptible to false alarms than the residual monitoring method [22:29].

Parameter Position and "Velocity" Estimate Monitoring is an extension of the previous method. By tracking the "velocity" of the parameter estimate through the most recent parameter position estimates, the next position of the parameter may be predicted. If the distance between the predicted location and the current center of the filter bank exceed a preset limit, the bank is moved.

Probability Monitoring via the equations already presented also provides an indication of

the most likely location of the parameter. The computed probabilities are compared to a preset threshold or simply the largest probability to determine if the center of the filter bank should be moved to the filter that is producing the probability exceeding the threshold.

Parameter Estimation Error Covariance Monitoring provides a means for determining whether the bank should be contracted from a coarser discretization, as shown in Figure 1.7. The parameter estimation error covariance, given by Equation (1.24), is monitored. The parameter covariance can be readily computed as:

$$\begin{aligned} \mathbf{P}_a(t_i) &= E\{[\mathbf{a} - \hat{\mathbf{a}}(t_i)][\mathbf{a} - \hat{\mathbf{a}}(t_i)]^T \mid \mathbf{Z}(t_i) = \mathbf{Z}_i\} \\ &= \sum_{k=1}^K [\mathbf{a} - \hat{\mathbf{a}}(t_i)][\mathbf{a} - \hat{\mathbf{a}}(t_i)]^T \cdot p_k(t_i) \end{aligned} \quad (1.24)$$

within the MMAE or MMAC algorithm. When the norm of the vector \mathbf{P}_a falls below some preset threshold, the bank may then be contracted. Monitoring the parameter estimation error covariance is not effective for expansion decision making, however, since Equation (1.24) depends on the current choice of $\hat{\mathbf{a}}_k$ and is "artificially bounded from above by the current size of the bank" [22].

When the parameter undergoes a jump change or is changing rapidly, the closely spaced filter bank may not be able to track the parameter adequately. By expanding the filter bank, the parameter is reacquired and a decision to contract the bank around the new parameter location can be made. Returning to Equation (1.22), it is seen that this equation is dependent on the residuals, \mathbf{r}_k . If all the likelihood quotients are large and close in value, then a good estimate of the parameter location in the parameter space is not possible. Since the estimator does not "know" where the parameter is located with any certainty, it is more appropriate to expand the bank rather than move it [22].

Hentz found that probability monitoring is the method of choice [22:95]. Lashlee used the same technique and observed the effects of varying the parameter space discretization on the ability

of the filter to track the true parameter location [15]. Both of these efforts present an extensive discussion of the decision logic.

The parameter estimate of the moving bank MMAE/MMAC algorithm should be as nearly as good as the full bank estimate, provided that the vast majority of the full-scale MMAE algorithm parameter probability weight is contained within the moving bank, but problems have been seen in five years of thesis research [8, 22, 6, 11, 15, 24]. The tuning of the noise matrices, \mathbf{Q} and \mathbf{R} , the discretization strategy used to generate the discrete parameter points, as well as the tuning of the other parameters in the filter algorithm, apparently affect the system rather substantially. Van Der Werken's thesis shows that the number of states used in the state space representation of the truth model may be a very important cause of poor tracking performance of the MMAE/MMAC used to control the space structure model, and so this robustness issue warrants further study.

1.2 Problem

The computational burden of a fixed-bank MMAE/MMAC implementation is higher than a moving-bank estimator/controller, and so the moving-bank algorithms are preferable for implementation. The problem remains to determine the robustness of the estimator and/or controller to unmodelled effects, whether it be a moving-bank algorithm or a fixed-bank algorithm using a necessarily coarser parameter discretization to maintain computational feasibility. Therefore, the mismatch of the 24-state truth model and the 6-state filter model is investigated. The selected truth model is assumed to model the real world adequately. This thesis research will provide insight into the effects of the mismatch and determine the number of filter states required to track the states and control the space structure adequately.

1.3 Scope

The research performed investigates the control of a large space structure represented by a rotating two-bay truss as developed by Karnick [11]. The truss is allowed to move only in the x-y plane of Figure 1.1. Restricting the motion to this plane allows for the investigation of the MMAE/MMAC algorithm without overly complicating the model with motion out of this plane, i.e. without coupling of x-y plane, x-z plane, and torsional motions. Masses attached to the structure were added by Karnick to allow changes in the mass matrices to obtain a more realistic space structure model. This situation represents the effects of depletion of fuel tanks on the structure. The model developed by Karnick is described in terms of mass and stiffness matrices obtained from a finite element analysis [26].

The parameters of interest for this thesis are the mass and stiffness matrices that appear in the system dynamics equations through modal analysis [25, 11]. Tuning of the \mathbf{Q} matrix describing the uncertainties associated with these dynamics model matrices is continued from the efforts of Karnick [11], Lashlee [15], and Van Der Werken [24]. Additional tuning effects due to the measurement noise covariance matrix \mathbf{R} are also considered. The measurement noise covariance matrix was considered to be diagonal in previous theses [15, 24:94,77]. A diagonal matrix indicates that the measurement noises are independent, i.e. the measurement of the velocity at node 1 is not affected by the measurement of the velocity at node 2. \mathbf{R} will be modified to include non-zero off-diagonal values that are chosen in a physically motivated manner.

1.4 Approach

Previous thesis efforts concentrated on observing the estimation and control of the filter-modeled states. The filter-model states used in the previous research effort are defined by:

$$\mathbf{x}_f = \begin{bmatrix} x_1 \\ x_2 \\ x_3 \\ x_4 \\ x_5 \\ x_6 \end{bmatrix} = \begin{bmatrix} \text{Rigid body mode position} \\ \text{First bending mode position} \\ \text{Second bending mode position} \\ \text{Rigid body mode velocity} \\ \text{First bending mode velocity} \\ \text{Second bending mode velocity} \end{bmatrix} \quad (1.25)$$

The truth model vector is correspondingly assumed to be composed of the rigid body and first eleven bending mode position states, followed by the corresponding twelve velocity states:

$$\mathbf{x}_t = \begin{bmatrix} x_1 \\ x_2 \\ \vdots \\ x_{12} \\ x_{13} \\ x_{14} \\ \vdots \\ x_{24} \end{bmatrix} = \begin{bmatrix} \text{Rigid body mode position} \\ \text{First bending mode position} \\ \vdots \\ \text{Eleventh bending mode position} \\ \text{Rigid body mode velocity} \\ \text{First bending mode velocity} \\ \vdots \\ \text{Eleventh bending mode velocity} \end{bmatrix} \quad (1.26)$$

An error vector, \mathbf{e} , was used by Van Der Werken [24] for evaluating estimator performance, given by:

$$\mathbf{e} = \mathbf{T}\mathbf{x}_t - \mathbf{x}_f \quad (1.27)$$

The subscripts indicate whether the variable is a filter variable, f , or the truth model variable, t . The matrix \mathbf{T} is a 6-by-24 transformation matrix which moves the states representing the velocity of the rigid body mode and the first two bending modes to the fourth, fifth, and sixth vector positions. Van Der Werken compared the truth and filter states (an estimate in the filter case) directly, thus asking whether the filter estimated the truth model states associated only with the first three modes. This thesis effort will instead ask if the reduced order filter can estimate (or if the reduced-order regulator can control) the true total shape of the truss (due to all modes' effects). Furthermore, it will attempt to answer robustness questions, i.e. will the controller work with a reduced state filter model, by gradually increasing the higher order state effects into the system.

The new error term will be defined as the difference between true and estimated positions and velocities at the accelerometer and thruster (used as control elements) locations on the truss, and at the hub, of Figure 1.1:

$$\mathbf{e} = \mathbf{H}_t \mathbf{x}_t - \mathbf{H}_f \hat{\mathbf{x}}_f \quad (1.28)$$

where

$$\mathbf{H}_f = \begin{bmatrix} \mathbf{H}_{f13 \times 3} & \mathbf{0}_{3 \times 3} \\ \mathbf{0}_{3 \times 3} & \mathbf{H}_{f23 \times 3} \end{bmatrix}_{6 \times 6} \quad (1.29)$$

and

$$\mathbf{H}_t = \begin{bmatrix} \mathbf{H}_{t13 \times 3} & \lambda \mathbf{H}_{tp3 \times 9} & \mathbf{0} & \mathbf{0} \\ \mathbf{0} & \mathbf{0} & \mathbf{H}_{t23 \times 3} & \lambda \mathbf{H}_{tv3 \times 9} \end{bmatrix}_{6 \times 24} \quad (1.30)$$

where \mathbf{H}_{tp} corresponds to the effect of the upper nine modal position states, and \mathbf{H}_{tv} to the effect of the upper nine modal velocity states. \mathbf{H}_t will provide a means to observe the effects of the unmodelled states in the operation of the estimator/controller. The scalar multiplier λ will be varied from 0, the case where the truth model is of the same order as the filter model, to 1, the case where the full effect of all the states of the truth model are being incorporated. By gradually increasing λ , the effects of the unmodelled states should become apparent. The requirement for

adding more states to the filter model is determined by how large λ becomes for the controlled system to become unstable or exhibit other unacceptable behavior. After quantifying the effects of the unmodelled states, the \mathbf{H}_{tp} and \mathbf{H}_{tu} matrices may be further partitioned to determine which states are needed for a robust controller.

The robustness of the estimator/controller is the primary concern of this thesis. Robustness is the ability of the estimator/controller to function properly in the face of unmodelled effects due to reduced order filter models. Slowly varying parameters and jump changes in the parameters of interest will be explored as well as stationary parameters. If the addition of more states is indicated, the work performed by previous thesis efforts will be repeated with a new filter structure based on an appropriately higher dimensional state vector.

The \mathbf{Q}_f and \mathbf{R}_f matrices will be varied in such a way that a useful tuning strategy can be established. Previous efforts concluded that the tuning of these matrices are critical to the robustness of the controller [15, 24]. The previous research also concluded that the LQ regulator weighting matrices are also critical to the performance of the controller. The previous research used a tuning process that may not be practical in all cases. \mathbf{Q}_f was held fixed while \mathbf{R}_f was varied until best performance was obtained. Then \mathbf{R}_f was fixed and \mathbf{Q}_f was changed. Once the values were fixed in this manner, the remainder of the research was performed. Van Der Werken experienced difficulty in the tuning process: \mathbf{R}_f was appropriately established as \mathbf{R}_t plus additional terms to account for the impact of the 18 unmodelled states (this will be discussed in detail in the following chapters), but \mathbf{Q}_t was incorrectly equated to \mathbf{Q}_f as \mathbf{Q}_f was varied to accomplish tuning. A way to perform true tuning of \mathbf{Q}_f and \mathbf{R}_f shall be incorporated into the software, and the tuning philosophy of \mathbf{Q}_f and \mathbf{R}_f will be researched. In addition, once the noise matrices have been tuned, the process of tuning the LQ regulator weighting matrices will also be evaluated.

Investigation of the difficulties encountered by previous thesis research in tuning the weighting matrices will be continued. Once the weighting matrices have been tuned, the parameters will be

allowed to traverse the parameter space slowly to study the ability of the MMAE/MMAC algorithms to maintain control. Jump changes in the parameters will also be investigated. The parameter space discretization itself will be evaluated on the basis of Lashlee's recommendations [15].

Lashlee observed that the parameter identifying capability of the estimator was enhanced by proper discretization of the parameter space [15:115-117]. The choice of parameter discretization levels is determined by holding one parameter constant and varying the other parameter in the truth model. From the data gathered from a single filter from the bank matched against the changing truth model, rms error plots are used to determine the discretization levels that yield a given percentage degradation in the likelihood quotient given by Equation (1.22). Thus, the discretization is established such that the elemental filters (and controllers) in the bank are readily distinguishable from one another on the basis of their residual characteristics.

1.5 Summary

The remaining chapters of this thesis cover the following areas. Chapter 2 develops the algorithms used in the MMAE and MMAC portions of this research, including decision logic for moving and expanding/contracting the bank of filters/controllers. The modelling of the large space structure, the two-bay truss structure, is developed in Chapter 3. The simulations performed by this thesis will be explained in Chapter 4. Chapter 5 presents the results of the research, with corresponding conclusions and recommendations presented in Chapter 6.

II. Algorithm Development

2.1 Introduction

The algorithm development for the control of a large space structure using MMAE/ MMAC has not changed appreciably over the last three thesis efforts performed by Karnick [11:13-38], Lashlee [15:19-45], and Van Der Werken [24:23-43]. This chapter presents the development of the algorithms, with little modification from the previous efforts. New issues and/or issues critical to this thesis research will be stressed.

2.2 Bayesian Multiple Model Adaptive Estimation Algorithm Development

The basic development of the MMAE algorithm was presented in Chapter 1. The following material is presented for completeness. A thorough treatment of this subject is presented by Maybeck [19:129-136].

The system under investigation is considered to be adequately modelled by the linear stochastic difference equation

$$\underline{\mathbf{x}}(t_{i+1}) = \underline{\Phi}(t_{i+1}, t_i)\underline{\mathbf{x}}(t_i) + \underline{\mathbf{B}}_d(t_i)\underline{\mathbf{x}}(t_i) + \underline{\mathbf{G}}_d(t_i)\underline{\mathbf{w}}_d(t_i) \quad (2.1)$$

from which measurements are taken by sampling via the linear relationship

$$\underline{\mathbf{z}}(t_i) = \underline{\mathbf{H}}(t_i)\underline{\mathbf{x}}(t_i) + \underline{\mathbf{v}}(t_i) \quad (2.2)$$

As stated in Chapter 1, $\underline{\mathbf{w}}_d$ and $\underline{\mathbf{v}}$ are assumed to be independent of each other and zero-mean, white Gaussian discrete-time noise processes. The statistics of interest are:

$$E\{\underline{\mathbf{w}}_d(t_i)\underline{\mathbf{w}}_d^T(t_j)\} = \underline{\mathbf{Q}}_d(t_i)\delta_{ij}(t_i) \quad (2.3)$$

$$E\{\underline{\mathbf{v}}(t_i)\underline{\mathbf{v}}^T(t_j)\} = \mathbf{R}(t_i)\delta_{ij}(t_i) \quad (2.4)$$

where $\mathbf{Q}_d(t_i)$ is positive semidefinite and $\mathbf{R}(t_i)$ is positive definite for all t_i . The initial condition of the state is not generally known with absolute certainty and is described by means of a Gaussian random vector that is assumed to be independent of $\underline{\mathbf{w}}_d$ and $\underline{\mathbf{v}}$. The mean and covariance of the initial state condition are given by:

$$E\{\underline{\mathbf{x}}(t_0)\} = \hat{\mathbf{x}}_0 \quad (2.5)$$

$$E\{[\underline{\mathbf{x}}(t_0) - \hat{\mathbf{x}}_0][\underline{\mathbf{x}}(t_0) - \hat{\mathbf{x}}_0]^T\} = \mathbf{P}_0 \quad (2.6)$$

The above equations provide a starting point for observing the system of interest [19:70]. The above equations have been presented with little explanation of the actual variables. The variables of interest to this point are [15, 24]:

- $\underline{\mathbf{x}}(t_i)$ = n -dimensional state vector
- $\Phi(t_{i+1}, t_i)$ = state transition matrix which transitions the state from t_i to t_{i+1}
- $\mathbf{u}(t_i)$ = r -dimensional deterministic input vector
- $\mathbf{B}_d(t_i)$ = control input matrix
- $\underline{\mathbf{w}}_d(t_i)$ = s -dimensional white Gaussian dynamics driving noise vector
- $\mathbf{G}_d(t_i)$ = noise input matrix
- $\underline{\mathbf{z}}(t_i)$ = m -dimensional measurement vector
- $\mathbf{H}(t_i)$ = measurement matrix
- $\underline{\mathbf{v}}(t_i)$ = m -dimensional white Gaussian measurement noise vector

From Maybeck [19:129-133], let $\underline{\mathbf{a}}$ be the vector of uncertain parameters for the model under study. The uncertain parameters affect any or all of the matrices described above. The purpose of the Bayesian estimator is to compute the conditional density function:

$$f_{\underline{\mathbf{x}}(t_i), \underline{\mathbf{a}} | \underline{\mathbf{Z}}(t_i)}(\underline{\xi}, \underline{\alpha} | \underline{\mathbf{Z}}_i) = f_{\underline{\mathbf{x}}(t_i) | \underline{\mathbf{a}}, \underline{\mathbf{Z}}(t_i)}(\underline{\xi} | \underline{\alpha}, \underline{\mathbf{Z}}_i) f_{\underline{\mathbf{a}} | \underline{\mathbf{Z}}(t_i)}(\underline{\alpha} | \underline{\mathbf{Z}}_i) \quad (2.7)$$

which is the conditional density of $\underline{\mathbf{x}}$ and $\underline{\mathbf{a}}$ given the measurement history through the current time, \mathbf{Z}_i , where \mathbf{Z}_i is composed of partitions equal to the realizations of $\underline{\mathbf{z}}(t_1), \underline{\mathbf{z}}(t_2), \dots, \underline{\mathbf{z}}(t_i)$. Based on the assumed model, the first density on the right hand side of Equation (2.7) is Gaussian, with mean $\underline{\mathbf{x}}(t_i^+)$ and covariance $\mathbf{P}(t_i^+)$, for a specific value of the parameter vector $\underline{\mathbf{a}}$. These variables are computed by a Kalman filter for that particular parameter vector $\underline{\mathbf{a}}$.

The parameter vector $\underline{\mathbf{a}}$ can assume values in the continuous range defined by:

$$A \subset R^p \quad (2.8)$$

where R^p is real Euclidean p-dimensional space. The parameter vector may be "uncertain but constant, it may be slowly varying, or it may undergo jump changes" [15:21]. The nature of $\underline{\mathbf{a}}$ being continuous would cause a problem computationally since the calculations to solve Equation (2.7) would require an infinite number of separate Kalman filters and integrations that would make online usage of the Bayesian estimator prohibitive. To allow online computation, the parameter space is discretized. The uncertain parameter vector might be reasonably defined as taking one of the values in the finite set $\{\underline{\mathbf{a}}_1, \underline{\mathbf{a}}_2, \dots, \underline{\mathbf{a}}_K\}$, where each discrete value is chosen for optimal performance of the control system. The discretization of the parameter space is one of the subjects of this thesis effort. Each discrete value $\underline{\mathbf{a}}_k$ has an individual system model associated with it, requiring recomputation of Equations (2.1) and (2.2). Before the calculation of the conditional mean and covariance of the k -th system state is presented, the hypothesis conditional probability will be defined.

The hypothesis conditional probability is defined by

$$\begin{aligned} p_k(t_i) &\equiv \text{prob}\{\underline{\mathbf{a}} = \underline{\mathbf{a}}_k \mid \mathbf{Z}(t_i) = \mathbf{Z}_i\} \\ &= \frac{f_{\underline{\mathbf{z}}(t_i) \mid \underline{\mathbf{a}}, \mathbf{Z}(t_{i-1})}(\underline{\mathbf{z}}_i \mid \underline{\mathbf{a}}_k, \mathbf{Z}_{i-1}) p_k(t_{i-1})}{\sum_{j=1}^K f_{\underline{\mathbf{z}}(t_i) \mid \underline{\mathbf{a}}, \mathbf{Z}(t_{i-1})}(\underline{\mathbf{z}}_i \mid \underline{\mathbf{a}}_j, \mathbf{Z}_{i-1}) p_j(t_{i-1})} \end{aligned} \quad (2.9)$$

which shows that the conditional probability of the k -th filter being the most correct filter is the product of the probability density of the most recent measurement (for a given discrete assumed parameter value and the observed measurement history) and the previous conditional probability, divided by the sum of the K probability density and conditional probability products (thus forcing the $p_k(t_i)$'s to sum to one for all t_i).

The state estimate produced by the estimator based on the assumption that \underline{a}_k is the correct parameter vector is given by [19:131]:

$$\begin{aligned}\hat{\mathbf{x}}(t_i^+) &= E\{\underline{\mathbf{x}}(t_i) \mid \underline{\mathbf{Z}}(t_i) = \underline{\mathbf{Z}}_i\} \\ &= \int_{-\infty}^{\infty} \underline{\boldsymbol{\xi}} \left[\sum_{k=1}^K f_{\underline{\mathbf{x}}(t_i) \mid \underline{\mathbf{a}}_k, \underline{\mathbf{Z}}(t_i)}(\underline{\boldsymbol{\xi}} \mid \underline{\mathbf{a}}_k, \underline{\mathbf{Z}}_i) p_k(t_i) \right] d\underline{\boldsymbol{\xi}} \\ &= \sum_{k=1}^K \underline{\mathbf{x}}_k(t_i^+) p_k(t_i)\end{aligned}\quad (2.10)$$

The state estimate is the sum of all the probabilistically weighted estimates generated by the K Kalman filters, where the hypothesis conditional probabilities $p_k(t_i)$ are the weighting factors. The conditional covariance of the state is calculated in a similar fashion, again weighted by the hypothesis conditional probabilities, and is given by [19:131]:

$$\begin{aligned}\mathbf{P}(t_i^+) &= E\{[\underline{\mathbf{x}}(t_i) - \hat{\mathbf{x}}(t_i^+)] [\underline{\mathbf{x}}(t_i) - \hat{\mathbf{x}}(t_i^+)]^T \mid \underline{\mathbf{Z}}(t_i) = \underline{\mathbf{Z}}_i\} \\ &= \sum_{k=1}^K p_k(t_i) \{ \mathbf{P}_k(t_i^+) + [\hat{\mathbf{x}}_k(t_i^+) - \hat{\mathbf{x}}(t_i^+)] [\hat{\mathbf{x}}_k(t_i^+) - \hat{\mathbf{x}}(t_i^+)]^T \}\end{aligned}\quad (2.11)$$

The conditional covariance $\mathbf{P}_k(t_i^+)$ is the "state error covariance" associated with the Kalman filter based on the parameter $\underline{\mathbf{a}}_k$. The conditional covariance is dependent on the measurement history, as shown in Equation (2.11), and therefore is not precomputable. However, neither is it absolutely required for online use of the MMAE algorithm.

The *multiple model adaptive estimation algorithm* developed above is an adaptive filter and

the structure was shown in Figure 1.3. The discretization of the continuous parameter space into a limited number of points makes online use of this algorithm feasible. As each measurement z_i becomes available at time t_i , the Kalman filters generate residuals which are used to generate new hypothesis conditional probabilities. With this information available, $f_{\underline{z}(t_i), \underline{a}}(\underline{z}_i | \mathbf{a}_k, \mathbf{Z}_{i-1})$ needed in Equation (2.9) may be computed for all k as:

$$\begin{aligned} f_{\underline{z}(t_i), \underline{a}}(\underline{z}_i | \mathbf{a}_k, \mathbf{Z}_{i-1}) &= \frac{1}{(2\pi)^{\frac{m}{2}} |\mathbf{A}_k(t_i)|^{\frac{1}{2}}} \exp \{ \cdot \} \\ \{ \cdot \} &= \left\{ -\frac{1}{2} \mathbf{r}_k^T(t_i) \mathbf{A}_k^{-1}(t_i) \mathbf{r}_k(t_i) \right\} \end{aligned} \quad (2.12)$$

where the k th Kalman filter generates $\mathbf{A}_k(t_i)$ as

$$\mathbf{A}_k(t_i) = \mathbf{H}_k(t_i) \mathbf{P}_k(t_i^-) \mathbf{H}_k^T(t_i) + \mathbf{R}_k(t_i) \quad (2.13)$$

The K implemented filters thus provide the terms to evaluate the conditional probabilities required to determine the state of the system given the current measurement. Using the weighting technique seen in Equations (2.10) and (2.11), the state estimate $\hat{\mathbf{x}}(t_i^+)$ is generated.

The other estimate that may be desired or required is that of the parameter vector. The conditional mean of the parameter vector at time t_i is given by [19:132]:

$$\begin{aligned} \hat{\mathbf{a}}(t_i) &\equiv E\{\underline{\mathbf{a}}(t_i) | \underline{\mathbf{Z}}(t_i)\} = \underline{\mathbf{Z}}_i \\ &= \int_{-\infty}^{\infty} \underline{\alpha} f_{\underline{a}|\underline{\mathbf{Z}}(t_i)}(\underline{\alpha} | \underline{\mathbf{Z}}_i) d\underline{\alpha} \\ &= \sum_{k=1}^K \mathbf{a}_k p_k(t_i) \end{aligned} \quad (2.14)$$

The covariance of the estimated parameter vector gives an indication of the precision of the estimate,

and it can be estimated via [19:133]:

$$E\{\{\underline{a} - \hat{a}(t_i)\}[\underline{a} - \hat{a}(t_i)]^T \mid \underline{Z}(t_i) = \underline{Z}_i\} = \sum_{k=1}^K [\underline{a}_k - \hat{a}(t_i)][\underline{a}_k - \hat{a}(t_i)]^T p_k(t_i) \quad (2.15)$$

It should be noted that neither the calculations of the parameter estimate nor the covariance of the parameter estimate are required for the calculation of the state estimate.

For the case of non-varying parameters, the MMAE has been shown to be optimal and converge [7]. The situation examined by Hawkes and Moore showed that the MMAE converged to the filter that matched the actual parameter or was closest to the true parameter [7]. The previous theses did not develop theoretical results for the case of varying parameters [6, 8, 11, 15, 21]. One of the concerns presented by the previous theses is that the filter may converge to one parameter value and lock on to that value. If the real parameter remains at that location, the filter would perform correctly. However, if the parameter is likely to vary, the filter would be of little use in providing a state or parameter estimate. Dasgupta and Westphal showed that the algorithm may converge to the wrong parameter value for the case of unknown biases in the measurement process [5:614-615].

To prevent the problems discussed above, the addition of dynamics pseudonoise to the model is used. "Essentially, the dominant aspects of the dynamics are included in the model, and one accounts for the many neglected effects by introducing additional uncertainty into the model" [19:25]. The pseudonoise is added to each filter. The difficulty of using this approach is how much pseudonoise to add. If too much pseudonoise is added, as in the case where \underline{Q}_d is made artificially large to account for the inadequacy of the propagation model, then the propagation equations may not remain usable for online calculations. The addition of excessive driving noise to the model will mask the difference between a good and bad propagation model. The addition of too little dynamics driving noise will give an unrealistically "perfect" perspective of the dynamics model and cause the filter to use the model's characteristics above any real-world measurement inputs.

The MMAE algorithm has the additional burden of using this same dynamics noise throughout the filter space for the implementation used in this research. The tuning of Q_d may be difficult to achieve with a single-valued matrix.

The selection of adequate measurement noise is not new to the MMAE/MMAC algorithms, but is a Kalman filter problem in general. Consider Equation (1.13) which provides the Kalman filter gain. If R were set to too large a value, K (or at least many of its elements) would tend to go to zero, causing the state propagation equation to stop using the residual in changing the values of the states. Likewise, the state covariance would also remain relatively unchanged due to a very small Kalman filter gain value. The filter must "realize" that imperfections in the dynamics model exist without being made useless in the process, too.

If a particular filter is nearest to the true parameter location, the residual from that filter would be expected to be smallest in magnitude (relative to the filter-computed covariance A_k of Equations (2.12) and (2.13)) of the active bank of filters. Equation (2.12) would then provide the largest conditional density value for this filter and when applied to Equation (2.9), would ultimately yield the highest probability to the "best" filter. The two equations mentioned show that the filter's performance is dependent on the differences between the residuals of the filters in the bank. Thus, it is essential to ensure, by the manner of discretizing the parameter space and by the means of tuning each elemental filter, that the residuals of "good" versus "bad" filters have very distinguishing characteristics. The value of A_k would begin to dominate however if the residual values were of the same magnitude. Under this condition, the p_k 's are dominated by the A_k since the residual values are equal. The conditional density then becomes dominated by the filter with the lowest A_k and diverges. "Unfortunately, no rigorous general proofs are available concerning the asymptotic properties of the hypothesis conditional probabilities" [19:133].

Previous theses prevented filter lock by fixing a lower bound on the p_k [6, 8, 11, 15, 24]. The hypothesis conditional probabilities are monitored and when one or more probabilities fall below

the threshold, they are set to the minimum and the entire bank rescaled to maintain the unity sum of the probabilities.

2.3 Moving-Bank Algorithm Development

The MMAE filter algorithm presented in the previous section presents an immense computational burden if implemented in a full bank form, i.e., a filter for every discrete point in the parameter space. To lessen the computational loading, the technique of a moving bank of filters has been investigated in the previous theses. Maybeck and Hentz performed the original research that has direct application to this thesis research [22]. Their work showed that the full bank of filters could be replaced by a moving bank of filters that could follow the changes in the parameters of interest [15:27]. The techniques examined for moving this smaller bank were briefly discussed in Chapter 1 and are presented here in detail.

2.3.1 Moving the Bank. The moving-bank MMAE is a subset of the full-bank MMAE. Conceptually, the bank is centered around the best estimate of the parameter. The knowledge of the parameter may be uncertain a priori or the parameter location may change. The decision logic used to move the bank is critical in these realistic cases [8, 11, 15, 22].

2.3.1.1 Residual Monitoring. The effect of the residuals on the calculation of the probability density was seen in the exponential term of Equation (2.12). The exponential term contains a quadratic factor of the residual vector and \mathbf{A}_k , a function of \mathbf{H}_k , \mathbf{R}_k , and the covariance of the state estimate of the k -th filter. Let this term be defined as the likelihood quotient $L_k(t_i)$:

$$L_k(t_i) \equiv \mathbf{r}_k^T(t_i) \mathbf{A}_k^{-1}(t_i) \mathbf{r}_k(t_i) \quad (2.16)$$

Considered in the scalar case, the likelihood quotient is the ratio of the residual squared divided by the filter-computed variance for the residual [22:92]. Consider the effect of the parameter

being outside the area of the filter. The residual values would all become large and drive the K likelihood quotients high. A preset limit could be determined through performance evaluations such that, when the smallest L_k exceeds some value T , an appropriate filter movement action could be determined. Additionally, the filter closest to the true parameter should have the smallest likelihood quotient and thus provide an indication of where to move the bank.

The use of residual monitoring is limited however to situations where the system is not subject to "single large samples of measurement noise" [22:92]. Examination of Equation (2.16) shows that the values of $L_k(t_i)$ would all rise appreciably in the face of a sudden high value of $\mathbf{y}(t_i)$ which affects the residual directly through the realized measurement value.

2.3.1.2 Parameter Position Monitoring. Equation (2.14) gave an expression for the estimated parameter location based on the K discretized parameter locations and hypothesis conditional probabilities. The estimated parameter location is used in this technique for determining where the center of the bank should be. If the parameter location begins to move to the edge of the current bank or to move to some predetermined distance from the current center, then the decision to move the bank could be made.

Reviewing Equation (2.14) shows that the strength of this technique is that it relies on a history of measurements rather than just on the single current measurement. However, while this technique is not prone to the measurement noise problem of residual monitoring, it does require a priori knowledge of the parameter location or at least sufficient knowledge to place the range of the bank around the true parameter location. For the case where the parameter is not initially known, the bank may be set at a very coarse discretization that covers the entire admissible range of parameter values, and then changed to a finer discretization as information about the parameter is developed by the estimator.

2.3.1.3 Parameter Position and "Velocity" Estimate Monitoring. This technique is an extension of the previous parameter position monitoring technique. If the parameter is varying slowly, the position and "velocity" can both be monitored. The parameter velocity is the change in parameter location between sample periods or over an extended period of time. The velocity vector could be used to estimate where the parameter will be at the next sample period. If the predicted location is outside the current bank of filters or beyond a certain criterion distance from the current center, then a move of the bank is indicated in the direction of the velocity vector.

2.3.1.4 Probability Monitoring. Monitoring the hypothesis conditional probabilities generated by Equation (2.9) provides insight into which filter is located nearest the true parameter location. Using a preset threshold, the bank can be moved in the direction of the filter providing the most correct parameter \mathbf{a}_k , i.e., the one with the highest p_k value. The bank seeks to center itself on the filter which is based on the most correct assumed parameter value. As with parameter position monitoring, probability monitoring uses a time history of measurements and is less susceptible to radical changes due to individual large realizations of measurement noise.

2.3.2 Contraction and Expansion of the Bank. The size of the bank need not be fixed and the bank filters need not be at adjacent finely discretized points in the parameter space. If the active filters are not associated with adjacent discrete parameter values, the bank behaves as a coarsely discretized moving bank. A coarsely discretized bank was illustrated in Figure 1.7. The estimates provided by such a bank may not provide as accurate estimates as a bank where the active filters occupy adjacent discrete parameter locations. It does offer a higher probability that the true parameter location will be within the bank however. This is a good attribute for initialization of the moving bank since initial convergence has a higher probability of occurring. Maybeck and Hentz found that an initial coarse discretization of the bank improved parameter acquisition [22].

The bank may require expansion for the case of a jump change of the parameter location. Using residual monitoring, the jump change is detected and the bank expanded. The likelihood

ratios of the implemented filters are expected to be large, exceeding some threshold, using residual monitoring [11:29]. Once the bank has been expanded and a new parameter location estimate made, the bank may then be contracted around the new location and the algorithm proceeds with new estimations and control inputs as before. When the bank is coarsely discretized, monitoring the parameter estimation error conditional covariance, \mathbf{P}_a , provides an indication when to contract the bank. When the norm of this matrix falls below some chosen threshold, "the bank can be contracted about the parameter estimate" [22:92].

Karnick proposed an alternative method in which the probability of a side of the bank was monitored such that

$$p_{\text{side}}(t_i) = \frac{\sum_{\text{side}} f_j(\mathbf{z}(t_i))}{\sum_{4 \text{ sides}} f_j(\mathbf{z}(t_i))} \quad (2.17)$$

is the probability associated with each side [11:27-29]. The threshold logic for contracting and expanding the bank are also given. If the side probability falls below some threshold, then the side is contracted. "Conversely, if the probability associated with a side rises above some threshold, the remaining three sides are 'moved in'" [11:29]. The third possibility involves evaluating all four sides, and when the sum of the sides' probabilities fall below some threshold, the bank is contracted.

2.3.3 Initialization of New Elemental Filters. The issue of initialization of new elemental filters, after the bank has been expanded or contracted, has been studied by Hentz [8:26-30] and Karnick [11:29-32]. The techniques developed proved to be computationally intense. Since there appears to be no loss of performance from the equal redistribution of the discarded filters' probabilities among the new filters [15:36], this will be the method used in this thesis effort. For the case where all nine filters are new, the probability will be divided equally, i.e., $p_k = \frac{1}{9}$ for all k .

2.4 Stochastic Controller Design

Both the moving-bank and fixed-bank MMAE algorithms can be used with several stochastic controller designs [20:9-20], [22:93], [8:33-40]. The "assumed certainty equivalence design" methodology presented by Maybeck [20:241-245] will be used. As a form of feedback controller synthesis technique, this method separates the controller into the cascade of an estimator and a deterministic optimal control function. This method is also known "as the forced or heuristic certainty equivalence design technique" [20:241]. While this technique leads naturally to MMAE-based control (using the $\hat{\mathbf{x}}$ of Figure 1.3 premultiplied by a single gain $-\mathbf{G}_c^*(\hat{\mathbf{a}})$ evaluated on the basis of the estimated parameter), the implementation used in this thesis is MMAC control, which primarily differs in the implementation of the controller: the structure shown in Figure 1.4.

The estimator for this thesis is the moving-bank MMAE. The systems developed for each parameter location are assumed to be linear and time invariant with stationary noise. The estimate of the state is propagated with the previously developed equations (from Chapter 1, Equations (1.10) to (1.15), and in this chapter). Likewise, the system is updated using the update equations developed previously.

Each controller developed is a linear, quadratic cost, full-state feedback optimal deterministic controller based upon a specific assumed parameter value of \mathbf{a}_k . The cost weighting matrices in the quadratic cost are constant, and the error state space formulation is time invariant [18:29]. The output of the controller is desired to be the optimal control function, \mathbf{u}^* , such that the quadratic cost function

$$J = E \left\{ \sum_{i=0}^N \frac{1}{2} [\hat{\mathbf{x}}^T(t_i) \mathbf{X}(t_i) \hat{\mathbf{x}}(t_i) + \mathbf{u}^T(t_i) \mathbf{U}(t_i) \mathbf{u}(t_i)] + \frac{1}{2} \hat{\mathbf{x}}^T(t_{N+1}) \mathbf{X}_f \hat{\mathbf{x}}(t_{N+1}) \right\} \quad (2.18)$$

is minimized [20:10]. The variables in Equation (2.18) are:

- J = cost function to be minimized
- \mathbf{X} = state weighting matrix
- \mathbf{X}_f = final state weighting matrix
- \mathbf{U} = control weighting matrix
- N = number of sample periods from t_0 to t_N
- t_{N+1} = final time
- t_N = last time a control is applied and
held constant over the next sample period

If the assumption of a linear system driven by white Gaussian noise is used, with a quadratic cost function given by Equation (2.18), then the optimal constant-gain discrete linear feedback control law, assuming full-state access, is given by:

$$\mathbf{u}^*(t_i) = -\mathbf{G}_c^*(t_i)\mathbf{x}(t_i) \quad (2.19)$$

The full state access is replaced via assumed certainty equivalence by the state estimate provided by the MMAE elemental filter associated with the controller, each being based on a specific parameter value \mathbf{a}_k . The controller gain is given by [20:16]:

$$\mathbf{G}_c^*(t_i) = [\mathbf{U}(t_i) + \mathbf{B}_d^T(t_i)\mathbf{K}_c(t_{i+1})\mathbf{B}_d(t_i)]^{-1} [\mathbf{B}_d^T(t_i)\mathbf{K}_c(t_{i+1})\mathbf{\Phi}(t_{i+1}, t_i)] \quad (2.20)$$

which is also part of the solution of the backward Riccati equation solving for $\mathbf{K}_c(t_i)$ [20:15-16]:

$$\begin{aligned} \mathbf{K}_c(t_i) = & \mathbf{X}(t_i) + \mathbf{\Phi}^T(t_{i+1}, t_i)\mathbf{K}_c(t_{i+1})\mathbf{\Phi}(t_{i+1}, t_i) \\ & - [\mathbf{\Phi}^T(t_{i+1}, t_i)\mathbf{K}_c(t_{i+1})\mathbf{B}_d(t_i)][\mathbf{U}(t_i) + \mathbf{B}_d^T(t_i)\mathbf{K}_c(t_{i+1})\mathbf{B}_d(t_i)]^{-1} \\ & \times [\mathbf{B}_d^T(t_i)\mathbf{K}_c(t_{i+1})\mathbf{\Phi}(t_{i+1}, t_i)] \end{aligned} \quad (2.21)$$

as solved backward from the terminal condition:

$$\mathbf{K}_c(t_{n+1}) = \mathbf{X}_f \quad (2.22)$$

The selection of the weighting matrices found in Equation (2.18) is important in determining the performance of the controller. By choosing an appropriate \mathbf{X} , the importance of maintaining the structure's rigid body position may be stressed algorithmically. The use of a diagonal matrix with large values emphasizes the importance of maintaining the states near zero. The input weighting matrix must also be chosen with care since it influences the amount of control energy the controller is allowed to use in order to accomplish the purpose of proper state control. The degree that the individual states are allowed to vary during the sample period. Tuning of the control and state weighting matrices "is usually required, in analogy to tuning of $\mathbf{Q}_d(t_i)$ and $\mathbf{R}(t_i)$..." in the Kalman filter [20:10-11].

The relationship given in Equation (2.19) is also the solution for the deterministic LQ optimal control problem with no driving noise. Since we are assuming that the system is noise-corrupted and only noise corrupted measurements are accessible versus perfect knowledge of the state, the state used in Equation (2.19) is replaced by the state estimate $\hat{\mathbf{x}}(t_i^+)$ provided by the elemental filter based on the parameter value a_k . As seen in Figure 1.4, once the state estimation has been passed to the controllers and the hypothesis conditional probabilities computed, the control inputs are multiplied by their appropriate probabilities and then summed to provide a control input to the system.

2.5 Summary

The algorithms for the moving-bank MMAE and MMAC have been developed in this chapter. The moving-bank MMAE should provide a substantial computational savings compared to the full-bank implementation. This computational cost savings is carried through to the controller, since

not all the elemental control inputs need to be calculated. A primary assumption through this development was that the system of interest could be described in a linear manner. Without this assumption, the problem would become extremely difficult to address with an on-line controller. The next chapter develops the linear model used in this and previous theses.

III. Rotating Two-Bay Truss Model

3.1 Introduction

The control of a large flexible space structure is being investigated using a two bay truss model. The structure is allowed to rotate about a pivot point, the hub. The original structure model, investigated by Lynch and Banda [17:13-16], does not have this pivoting feature, but its dynamic characteristics are thoroughly understood. The use of the structure attached to a hub allows for the study of both rigid body rotation and bending mode dynamics [15:47]. The rotating model has not been changed since it was developed by Karnick [11:39-58], and used by Lashlee [15:47-69] and Van Der Werken [24:44-63], and it is shown in Figure 3.1. This chapter presents the material from the appropriate chapters of the last three theses.

3.2 Models: Second Order and State Space

A mathematical model is required to determine the feasibility of the MMAE/MMAC control technique for the large space structure. The second order differential equation "which governs the flexural vibrations of a structure" [17:3] is given by [11:39], [15:47], [24:44]:

$$M\ddot{\mathbf{r}}(t) + C\dot{\mathbf{r}}(t) + K\mathbf{r}(t) = \mathbf{F}(t) = \mathbf{F}_1(t) + \mathbf{F}_2(t) \quad (3.1)$$

where the left hand side is the sum of the products of mass and acceleration, damping and velocity, and stiffness and position. The right hand side of Equation (3.1) is actually composed of a deterministic component, $\mathbf{F}_1(\mathbf{u}, t)$, and a noise component, $\mathbf{F}_2(t)$. As noted in the above explanation, the capital letters on the left side of Equation (3.1) represent specific structure characteristics defined as:

$$\begin{aligned} M &= \text{constant } nxn \text{ mass matrix} \\ C &= \text{constant } nxn \text{ damping matrix} \end{aligned}$$

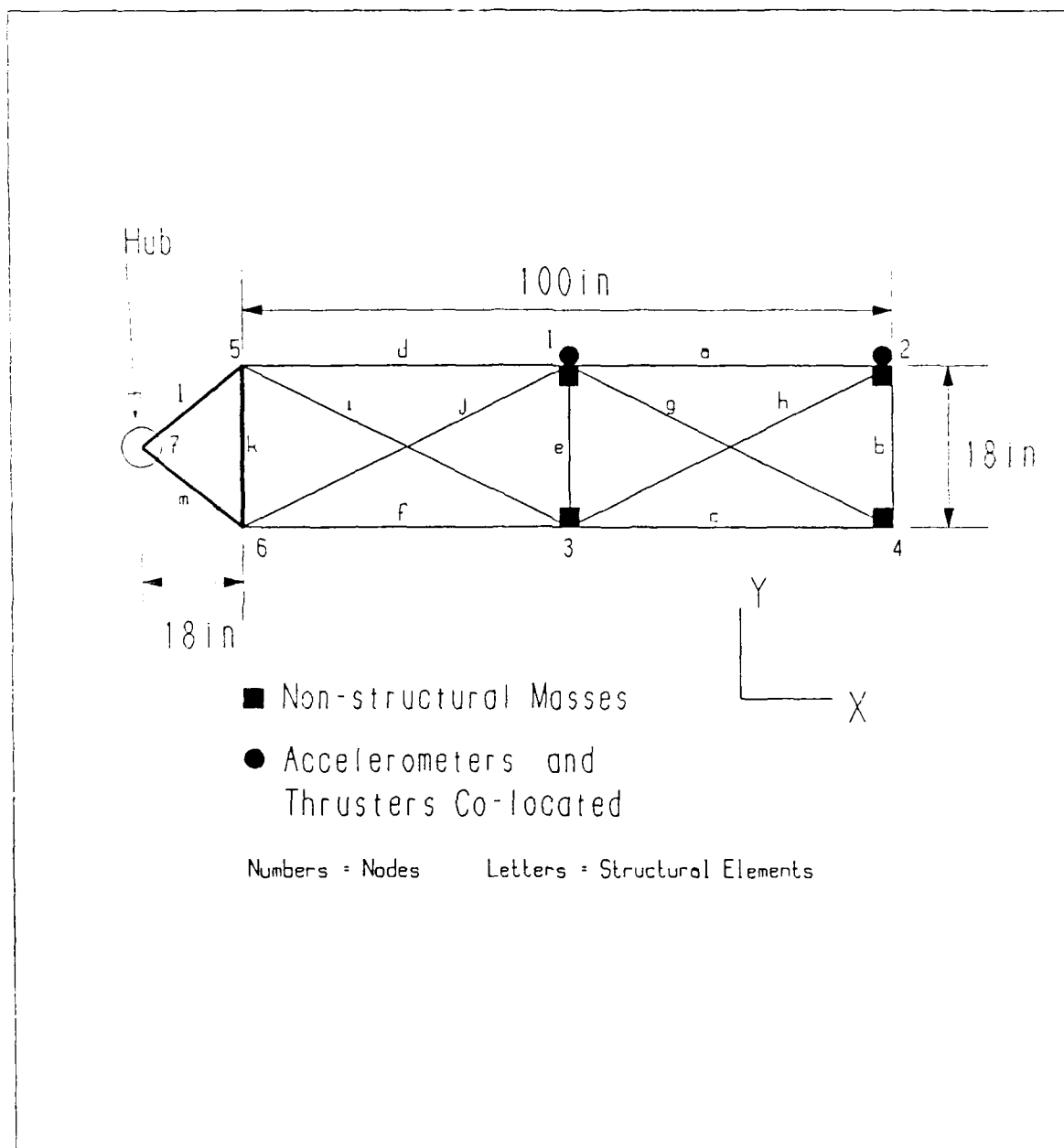


Figure 3.1. Annotated Rotating Two-Bay Truss Model

K = constant nxn stiffness matrix

The n -dimensional $\mathbf{r}(t)$ vector in Equation (3.1) represents the position or physical coordinates of the structure.

If the external disturbances are assumed to be white Gaussian noises, then Equation (3.1) is changed to:

$$M\ddot{\mathbf{r}}(t) + C\dot{\mathbf{r}}(t) + K\mathbf{r}(t) = -b\mathbf{u}(t) - g\mathbf{w} \quad (3.2)$$

where [15:48]

- $\mathbf{u}(t)$ = r -dimensional vector actuator inputs
- b = nxr matrix identifying position and velocity
relationship between actuators and controlled variables
- \mathbf{w} = s -dimensional vector representing the dynamics
driving noise, where s is the number of noise inputs
- g = $nx s$ matrix identifying position and relationships
between the dynamics driving noise and controlled variables

If the states of the system are taken to be composed of the position and velocity vectors, then Equation (3.2) may be written in state space form as [15:49]:

$$\dot{\mathbf{x}} = F\mathbf{x} + B\mathbf{u} + G\mathbf{w} \quad (3.3)$$

where the states are stochastic processes since they are driven by noise as well as a deterministic input. The state vector is given by [15:49]:

$$\mathbf{x} = \begin{bmatrix} \mathbf{r} \\ \dot{\mathbf{r}} \end{bmatrix}_{2n \times 1} \quad (3.4)$$

The uncertain parameters enter the mathematical model via the matrices in Equation (3.3). The

system matrices are given by:

$$F = \begin{bmatrix} \mathbf{0}_{n \times n} & \mathbf{I}_{n \times n} \\ -M^{-1}K_{n \times n} & -M^{-1}C_{n \times n} \end{bmatrix}_{2n \times 2n} \quad (3.5)$$

$$B = \begin{bmatrix} \mathbf{0}_{n \times r} \\ -M^{-1}b_{n \times r} \end{bmatrix}_{2n \times r} \quad (3.6)$$

$$G = \begin{bmatrix} \mathbf{0}_{n \times s} \\ -M^{-1}g_{n \times s} \end{bmatrix}_{2n \times s} \quad (3.7)$$

One of the assumptions taken in this thesis is that the measurement noise enters the system at the same location as the actuators (thrusters). This assumption causes the g and b matrices, and therefore G and B , to be equal and the dimensions r and s are equal, too. The locations of the actuators are shown in Figure 3.1 and are discussed in detail later in this chapter.

The states are position and velocity contributions of the various rigid body and bending modes to physical position and velocity variables at arbitrary points on the structure which are measured by accelerometers. The accelerometer outputs are integrated once for velocity and integrated again for position. Since the velocity and position measurements are derived in this manner, the position and velocity measurements are co-located. The co-location of these measurements would imply a highly correlated noise measurement matrix, \mathbf{R} , and corresponding non-zero off-diagonal elements. However, for purposes of simplicity, \mathbf{R} will be assumed to be diagonal. The actual measurement of these values would be transformed via an analog-to-digital conversion (ADC) so that the computer-implemented control algorithm can be used. The ADC process has inherent errors due to finite wordlength. For the purposes of this thesis, the ADC error is assumed to be small and will be accounted for by increasing the measurement noise matrix \mathbf{R} .

The model of the measurement of the states is given by [11:42], [15:50], [24:47]:

$$\underline{z} = \left\{ \begin{bmatrix} H_p & 0 \\ 0 & H_v \end{bmatrix}_{m \times 2n} \underline{x} \right\} + \underline{v} \quad (3.8)$$

where:

- m = number of measurements
- \underline{v} = an uncertain measurement disturbance of dimension m and modeled as a zero-mean white Gaussian noise of covariance \mathbf{R}
- H_p = position measurement matrix
- H_v = velocity measurement matrix

Since the position and velocity measurements are co-located, $H_p = H_v$. The equations are highly coupled, that is, the equations are not independent. This situation is not desirable and therefore modal decomposition is used to transform the sets of equations into independent modal equations.

3.3 Modal Decomposition

The equations just developed are transformed into a system of equations that are decoupled. "The general response of a complicated system can be broken down into the sum of n simple responses" [3:260]. The assumption that the matrices are constant allows the modal decomposition to be useful. If the matrices were variable, then the advantage of using modal decomposition would be lost [3:262].

Following the research performed by Lynch and Banda, the damping matrix is assumed to be a linear combination of the mass and stiffness matrix [17:4]:

$$C = \alpha M + \beta K \quad (3.9)$$

Due to the transformation from physical to modal coordinates, the actual determination of α and β are not required.

If the modal coordinates are denoted by Ω , the relationship between the modal and physical coordinates is given by [17:5], [11:42], [15:51], [24:48]:

$$\mathbf{r} = \mathcal{T} \Omega \quad (3.10)$$

where \mathcal{T} is the $n \times n$ transformation matrix composed of eigenvectors determined from the solution of [11:43], [15:51], [24:48], [17:5]:

$$\omega^2 M \mathcal{T} = K \mathcal{T} \quad (3.11)$$

Note that Equation (3.11) relates the modal frequency, ω , the mass matrix, and the stiffness matrix. The damping matrix is not involved in the solution of the eigenvectors. The solution of α and β are not explicitly found since they are not required for the modal decomposition. The values of ω that satisfy Equation (3.11) are called the natural or modal frequencies.

Substituting Equation (3.10) into Equation (3.3) yields the transformed state space equation to [11:43], [15:52], [24:48]:

$$\dot{\tilde{\mathbf{x}}} = \tilde{F} \tilde{\mathbf{x}} + \tilde{B} \mathbf{u} + \tilde{G} \mathbf{w} \quad (3.12)$$

where the state is now defined as [11:43]:

$$\tilde{\mathbf{x}} = \begin{bmatrix} \Omega \\ \dot{\Omega} \end{bmatrix} \quad (3.13)$$

The other matrices from Equation (3.3) are also transformed and calculated as [11:43]:

$$\tilde{F} = \begin{bmatrix} 0 & I \\ -\mathcal{T}^{-1} M^{-1} K \mathcal{T} & -\mathcal{T}^{-1} M^{-1} C \mathcal{T} \end{bmatrix}_{2n \times 2n} \quad (3.14)$$

$$\tilde{B} = \begin{bmatrix} 0 \\ -T^{-1}M^{-1}b \end{bmatrix}_{2n \times r} = \tilde{G} \quad (3.15)$$

The open loop plant matrix may also be written in terms of the undamped natural frequencies and the damping ratio of the i -th mode. \tilde{F} becomes [25:1769]:

$$\tilde{F} = \begin{bmatrix} 0 & I \\ -\omega_i^2 & -2\zeta_i\omega_i \end{bmatrix}_{2n \times 2n} \quad (3.16)$$

Finally, the equation describing the measurement process may be rewritten as [11:44]:

$$\underline{z} = \begin{bmatrix} H_p T & 0 \\ 0 & H_v T \end{bmatrix} \underline{\tilde{x}} + \underline{v} \quad (3.17)$$

The use of modal coordinates allows the following assumptions to be made [17], [11:44], [15:54]. The structural damping is assumed to be uniform throughout the structure. The damping coefficients selection does not play a role in the undamped natural frequencies and therefore may be selected based upon design requirements. The previous theses used a value of $\zeta = 0.005$ based on work performed by Lynch and Banda [17] and as representative of many space structures.

The mathematics of the model have been developed in this section. The parameters used in the equations of this section are derived from finite element analysis of the structure. The next section provides a detailed explanation of the structural model itself.

3.4 Two-Bay Truss

The two-bay truss has been discussed in general terms to this point. This section gives a physical description of the model used and describes the sensors and their locations. The original truss model was used to study the effects of structural optimization on optimal control. It consisted

Table 3.1. Structural Member's Cross-Sectional Areas

| Member | Area (in ²) | Member | Area (in ²) |
|--------|-------------------------|--------|-------------------------|
| a | 0.00321 | h | 0.00328 |
| b | 0.00100 | i | 0.00439 |
| c | 0.00321 | j | 0.00439 |
| d | 0.01049 | k | 0.20000 |
| e | 0.00100 | l | 0.20000 |
| f | 0.01049 | m | 0.20000 |
| g | 0.00328 | | |

of the two-bay truss attached to a fixed body [17:13].

3.4.1 Background. The model used by Lynch and Banda was modified by adding non-structural masses at nodes one through four to simulate a more realistic large space structure. The masses model various types of loads that might be found on a large space structure, such as fuel tanks and control jets. The model was further modified by attaching the structure to a hub with a mass much greater than the truss. This configuration approximates a large space platform with appendages extending from it. This configuration also allows for rigid body motion to be examined

The rigid body motion is established by letting the hub node remain fixed and the truss move around it in the x - y plane as shown in Figure 3.1 [11:47]. The rods connecting the truss to the hub are much larger in diameter than the truss members, causing this link to be very stiff compared to the truss rigidity. The addition of this physical link does introduce high frequency modes into the system but maintains the low frequency modes of the original fixed structure [15:57].

3.4.2 Two-Bay Truss Construction. The thirteen rods that make up the truss structure are listed in Table 3.1 with their cross-sectional areas. The members are made of aluminum which has a modulus of elasticity of 10 psi and weight density of 0.1 pounds per cubic inch. The sizes of rods k , l , and m were arbitrarily selected to obtain a stiff link between the truss and the hub.

The non-structural masses are indicated in Figure 3.1 and are masses of $1.294 \text{ lb} - \text{sec}^2$. This mass is very large compared to the member masses, which achieves the low frequencies associated

with large space structures [17:14]. The actual mass values were selected based on an optimizing technique that maintains the lowest undamped natural frequency (associated with the lowest mode) of 0.5 Hz [26].

Once the masses were determined, finite element analysis was performed to determine the mass and stiffness matrices describing the model [26]. The physical characteristics of the truss members, length, cross-sectional area, modulus of elasticity, and weight density, were evaluated to determine mass and stiffness matrices with dimensions equal to the number of degrees of freedom associated with the model [15:58]. Since node 7 is fixed, the elements of the matrices associated with this node are eliminated. With three degrees of freedom and 6 nodes, the full model is represented by 18 modes and 36 states. However, only motion in a plane is being considered so that the system may be fully represented by 12 modes and 24 states.

3.4.3 Sensors and Actuators. A combination of gyros and accelerometers is used to provide motion information to the control system. Accelerometers are located at nodes 1 and 2 as shown in Figure 3.1. The accelerometers are not located at the node of the bending modes being detected since the "displacement of the truss caused by the bending modes can not be detected" [15:59] under those conditions. As previously stated, the output of the accelerometers are integrated once to obtain velocity data and once again to obtain position data. Gyros are placed at the hub, node 7, to provide angular displacement and angular velocity information. Actuators are co-located with the accelerometers at nodes 1 and 2. The co-location is done to simplify the system model, specifically the measurement matrix H . The actuators at nodes 1 and 2 are assumed to be thrusters. The hub also contains an inertia wheel to act as an additional actuator.

3.4.4 Physical System Parameter Uncertainty. The goal of this thesis is to determine whether MMAC can control a physical system with uncertain physical parameters. The parameter space is composed of 100 discrete combinations of the parameters of interest. The non-structural masses and stiffness matrix are varied. The non-structural mass changes are motivated by relating this

action to the depletion of fuel tanks on the structure, refueling of the fuel tanks (where weight is being added), or weight being shifted from one part of the truss to another. The variations in stiffness of the truss members might be caused by structural fatigue in a rod or rods or, in the more extreme case, actual failure of one of the members.

3.5 State Reduction

The state reduction performed on the system of equations developed follows the work done by Kokotovic, et.al. [13:123-124]. The need to reduce the state dimension is due to the large computational load that a 24-state system would place on the MMAE/MMAC algorithm. Additionally, the actual effect of the higher order states may not play a major role in the dynamics of the system. This issue is addressed in this thesis by observing the effect of the higher order states in a gradual manner, as was explained in Chapter 2. The truth model contains all 24 states. The reduced order model is developed in this section.

3.5.1 Development. The general deterministic system is first reformulated as [11:52-57]:

$$\dot{\mathbf{x}} = \begin{bmatrix} \dot{\mathbf{x}}_1 \\ \dot{\mathbf{x}}_2 \end{bmatrix} = \begin{bmatrix} F_{11} & F_{12} \\ F_{21} & F_{22} \end{bmatrix} \begin{bmatrix} \mathbf{x}_1 \\ \mathbf{x}_2 \end{bmatrix} + \begin{bmatrix} B_1 \\ B_2 \end{bmatrix} \mathbf{u} \quad (3.18)$$

where \mathbf{x}_1 corresponds to "slower" modes to be maintained in the design model and \mathbf{x}_2 corresponds to "faster" modes to be ignored, and

$$\mathbf{z} = \begin{bmatrix} H_1 & H_2 \end{bmatrix} \mathbf{x} \quad (3.19)$$

If steady state is assumed to be reached instantaneously by the "fast" modes, the \mathbf{x}_2 modes are removed while maintaining the low frequency modes in \mathbf{x}_1 . F_{11} and F_{22} are square matrices and \mathbf{x}_2 can be expressed in terms of \mathbf{x}_1 assuming that F_{22}^{-1} exists. Then the higher order modes may

be expressed by [24:58], [15:62], [11:53]:

$$\dot{\mathbf{x}}_2 = F_{21}\mathbf{x}_1 + F_{22}\mathbf{x}_2 + B_2\mathbf{u} = 0 \quad (3.20)$$

$$\mathbf{x}_2 = -F_{22}^{-1}(F_{21}\mathbf{x}_1 + B_2\mathbf{u}) \quad (3.21)$$

Substituting these equations into Equations (3.18) and (3.19) yields [24:58], [15:62], [11:53]:

$$\dot{\mathbf{x}}_1 = (F_{11} - F_{12}F_{22}^{-1}F_{21})\mathbf{x}_1 + (B_1 - F_{12}F_{22}^{-1}B_2)\mathbf{u} \quad (3.22)$$

$$\mathbf{z} = (H_1 - H_2F_{22}^{-1}F_{21})\mathbf{x}_1 - H_2F_{22}^{-1}B_2\mathbf{u} \quad (3.23)$$

The term multiplying the input in Equation (3.23) is a direct feedforward term created by the order reduction [15:63].

Applying the above order reduction technique to the *original truth model system in modal coordinates* yields a new system dynamics matrix given by [11:54], [11:64], [24:59]:

$$F = \begin{bmatrix} 0 & I & \vdots & 0 & 0 \\ -\omega_1^2 & -2\zeta_1\omega_1 & \vdots & 0 & 0 \\ \dots & \dots & \dots & \dots & \dots \\ 0 & 0 & \vdots & 0 & I \\ 0 & 0 & \vdots & -\omega_2^2 & -2\zeta_2\omega_2 \end{bmatrix} \quad (3.24)$$

The matrix given by Equation (3.24) has obvious partitions. The upper left partition contains the low frequency modes to be retained while the lower right partition contains the high frequency modes assumed to reach steady state instantaneously. The partitions correspond to the F_{11} and F_{22} partitions observed in Equation (3.18). Additionally, the submatrices F_{12} and F_{21} are zero.

Substituting this information into Equations (3.18) and (3.19) yields [15:64]:

$$\dot{\mathbf{x}}_1 = F_{11}\mathbf{x}_1 + B_1\mathbf{u} = F_r\mathbf{x}_1 + B_r\mathbf{u} \quad (3.25)$$

$$\mathbf{z} = H_1\mathbf{x}_1 - H_2F_{22}^{-1}B_2\mathbf{u} = H_r\mathbf{x}_1 + D_r\mathbf{u} \quad (3.26)$$

where the subscript r denotes "reduced-order." The only term associated with the high frequency modes is the direct feedthrough term in Equation (3.26). The other matrices are found by truncating the states associated with \mathbf{x}_2 from the full state model.

Of the terms contained in Equations (3.25) and (3.26), D_r is the most complicated since the other terms are readily available. Previous theses have shown that [11:55-56], [15:65-66], [24:59-60]:

$$\begin{aligned} D_r &= -H_2F_{22}^{-1}B_2 \\ &= -\begin{bmatrix} H_c & 0 \\ 0 & H'_c \end{bmatrix} \begin{bmatrix} [-\omega_2^2][2\zeta_2\omega_2] & [-\omega_2^2]^{-1} \\ I & 0 \end{bmatrix} \begin{bmatrix} 0 \\ b' \end{bmatrix} \\ &= \begin{bmatrix} H_c[-\omega_2^2]^{-1}b' \\ 0 \end{bmatrix}_{m \times r} \end{aligned} \quad (3.27)$$

where "the unmodeled position and velocity states are represented by H_c and H'_c respectively" [24:60]. The terms seen in D_r show that it is dependent on the state terms that are assumed to reach steady state immediately.

3.5.2 Order Reduction Selection. For each location in the discretized parameter space, eigenvalues and eigenvectors of the unreduced system may be calculated from the system dynamics matrix F . Table 3.2 shows the average natural frequencies and damping factors associated with each of the 12 modes of the structure for the 100 filters that were developed for the discretized parameter space. The damping factors are all close to the 0.005 value used as an approximation in

Table 3.2. Average Damping Factors and Natural Frequencies

| Mode Number | Natural Frequency (Hz) | Damping Factor |
|-------------|------------------------|----------------|
| 1 | 0.000000 | 0.000000 |
| 2 | 1.415014 | 0.007617 |
| 3 | 2.941387 | 0.011020 |
| 4 | 4.953902 | 0.005000 |
| 5 | 5.440887 | 0.005790 |
| 6 | 7.078167 | 0.004720 |
| 7 | 9.119647 | 0.005000 |
| 8 | 9.872206 | 0.005559 |
| 9 | 155.113838 | 0.005116 |
| 10 | 1418.481250 | 0.005000 |
| 11 | 1811.221250 | 0.005004 |
| 12 | 3138.732500 | 0.005000 |

previous theses. The eigenvalues fall into closely spaced groups. For example, one group of three modes is seen in modes 4 through 6. The thesis by Van Der Werken [24] was the only previous work to use a 24-state truth model, and problems arose when comparing this to a reduced order filter model. On observation of the frequencies listed in Table 3.2, modes 2 through 8 are all in the same decade and therefore may all play a role in the performance of the control system, although the amount of energy in each mode must also be considered. Van Der Werken elected to use the first three modes in his filter model corresponding to a 6-state filter model as done previously by Karnick [11] and Lashlee [15] (versus a 24-state truth model). As explained in Chapter 1, one of the major goals of this thesis is to investigate this mismatch and to determine the number of states needed to provide adequate performance from the MMAE/MMAC for controlling a large space structure.

3.6 Summary

The 24-state truth model and the 6-state filter model that may be employed in a MMAC controller have been developed in this chapter. The degree that the filter model will require increased states to provide adequate performance is the purpose of this thesis and the simulation plan to determine this increase is presented in the next chapter.

IV. Simulation

4.1 Introduction

The space structure under investigation is simulated in order to study the robustness of the estimation and control capabilities of the MMAE and MMAC technique employed. To determine the statistical properties of the estimation/control process, Monte Carlo analysis is performed. The software used has been developed over a period of years and is outlined in this chapter. The simulation plan is presented at the end of this chapter.

4.2 Monte Carlo Analysis

The Monte Carlo analysis performed by the simulation software provides the statistical information about the performance of the MMAE and MMAC algorithms described in the previous chapters. If the system under investigation were fully linear, then covariance analysis could be used [18:329]. However, the adaptive nature of the MMAE/MMAC techniques used to control the large space structure requires the employment of Monte Carlo analysis to obtain many samples of the process and evaluate the statistics of the process. As with the work performed by Van Der Werken [24], the simulation involves two models: a 24-state "truth model" for accurate simulation and performance evaluation and a 6-state filter model for algorithm design purposes. The filter model is the same one used by Karnick [11], Lashlee [15], and Van Der Werken [24]. The 24-state truth model was developed in the last thesis by Van Der Werken [24].

Figure (4.1) shows a block diagram of the Monte Carlo analysis simulation which is a variation of that used by Van Der Werken [24:65-67]. The variables of interest are:

- $\mathbf{x}_t(t_i)$: the truth model states; 24-dimensional and in modal coordinates, representing the rigid body mode and eleven bending modes

- $\underline{\mathbf{x}}(t_i)$: estimates of the system states: 6-dimensional and in modal coordinates, representing the rigid body and the first five bending modes
- $\underline{\mathbf{a}}_t(t_i)$: the vector representing the structure mass and stiffness parameters
- $\underline{\mathbf{a}}(t_i)$: estimates of the uncertain parameter vector
- $\underline{\mathbf{e}}_a(t_i)$: the error in the parameter estimate defined as $\underline{\mathbf{e}}_a(t_i) = \underline{\mathbf{a}}_t(t_i) - \underline{\mathbf{a}}(t_i)$
- $\underline{\mathbf{e}}_x(t_i)$: the error in the system estimate defined in Equation (1.28) as:

$$\underline{\mathbf{e}}_x(t_i) = \mathbf{H}_t \underline{\mathbf{x}}_t(t_i) - \mathbf{H}_f \underline{\mathbf{x}}(t_i) \quad (1.1)$$

This is a six-dimensional vector, composed of positions and velocities of the structure at nodes 1 and 2, and at the hub, node 3, of Figure 3.1

- \mathbf{H}_t : the truth model measurement matrix modified by the variable λ as described in Equation (1.30)
- \mathbf{H}_f : the filter model measurement matrix

Note that the time arguments have been omitted from the figure for clarity.

The statistics of primary concern for the estimation error (and control) processes may be defined as the sample mean and covariance of the processes. The mean is determined by [24:67], [15:74]:

$$\mathbf{E}\{\underline{\mathbf{e}}_x(t_i)\} \approx \mathbf{M}_{e_x}(t_i) = \frac{1}{L} \sum_{k=1}^L \underline{\mathbf{e}}_{x_k}(t_i) \quad (4.2)$$

where L is the number of Monte Carlo analysis runs made and $\underline{\mathbf{e}}_{x_k}(t_i)$ is the value of the error signal during the k^{th} simulation run at run time t_i . The covariance may be calculated as [24:67], [15:74]:

$$\mathbf{P}_{e_x}(t_i) = \mathbf{E}\{[\underline{\mathbf{e}}_x(t_i) - \mathbf{M}_{e_x}(t_i)][\underline{\mathbf{e}}_x(t_i) - \mathbf{M}_{e_x}(t_i)]^T\}$$

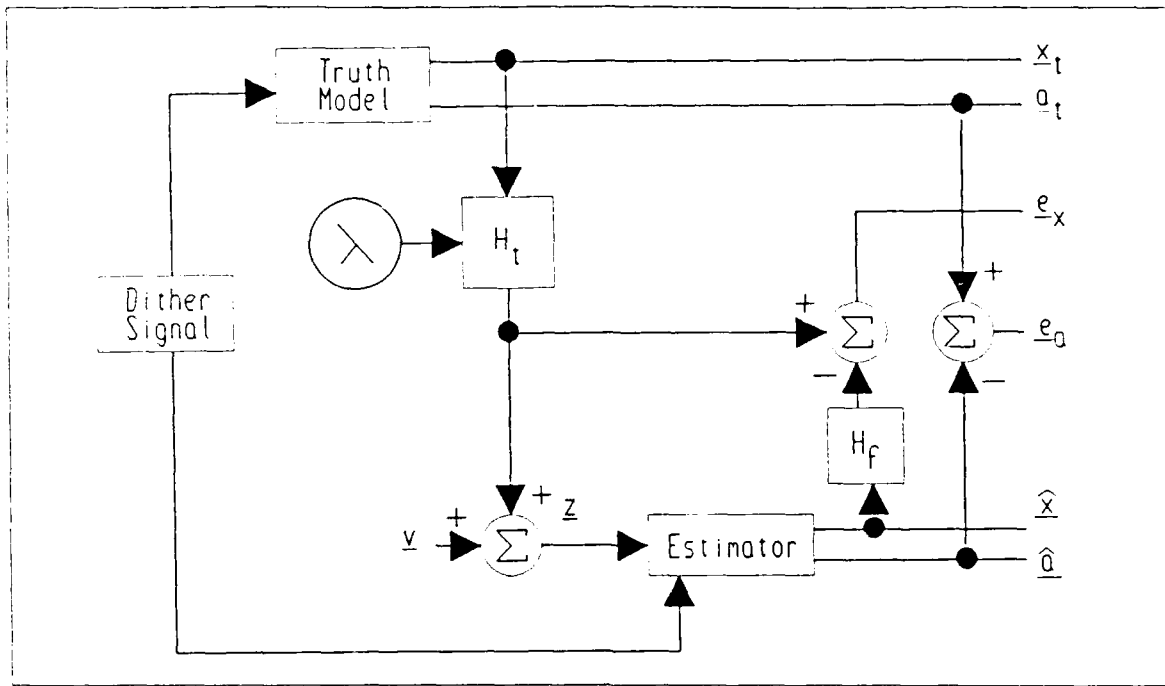


Figure 4.1. System Estimator Simulation

$$\approx \frac{1}{L-1} \sum_{k=1}^L \{e_{x_k}(t_i) e_{x_k}^T(t_i)\} - \frac{L}{L-1} M_{e_x}(t_i) M_{e_x}^T(t_i) \quad (4.3)$$

The statistics of the parameter estimation errors, e_a , or true states, x_t or Hx_t (for control evaluations), may also be obtained similarly with appropriate substitutions into Equations (4.2) and (4.3).

While previous thesis efforts ([11], [15], [24]) viewed the estimation of the states as the error signals, the goal of this research is to view physically meaningful quantities. The position and velocity estimates of the filter bank corresponding to nodes 1 and 2 and the hub of Figure 3.1 are compared to the truth-model-generated positions and velocities (taken to be "noiseless") via the manipulation of the truth model measurement matrix. The manipulation is of the form of varying λ to observe the effects of the higher order bending modes of the structure on the ability of the estimation technique to provide accurate position and velocity estimates. Van Der Werken [21,67-68] viewed the truth states associated with the rigid body mode and the first two bending

modes versus the filter states.

However, this thesis asks a more appropriate question: How well does the algorithm estimate (and also control) the true shape of the space structure? The simulation software was modified to allow the structure positions and velocities at nodes 1, 2, and 3 to be calculated from the truth model and estimated from the filter. A vector of error signals is then determined by subtracting the filter estimates from the true positions and velocities.

The other simulation performed is the same as the above open-loop estimator simulation, but with a controller implemented for closed-loop estimation and control. The control simulation is depicted in Figure (4.2). The error signals will be generated and evaluated statistically as for the estimation study. Again, the error signals are the actual differences of the positions of the structure as determined from the truth model versus the estimated position provided by the filter bank. This is significant since the goal of the controller is to quell the oscillations of the structure that may be induced by moving the structure, changes in structural characteristics, or changes in non-structural masses on the structure. Therefore, the primary quantities to be statistically evaluated are the actual positions of the structure. In particular, the position means and variances of nodes 1 and 2 will be determined using $\mathbf{H}_t \mathbf{\hat{x}}_t$.

4.3 Software

4.3.1 Introduction. The software used in this research was started by Hentz [8] and then modified and used by Filios [6], Karnick [11], Lashlee [15], and Van Der Werken [24]. The work performed through Lashlee was performed on a CDC Cyber computer (a non-AFIT resource). Van Der Werken [24:69-70] moved the FORTRAN programs to an Elxsi 6400 superminicomputer (in-house). During the beginning of this thesis effort, the programs were moved once again due to restructuring of computer resources. The programs now reside on two separate computer systems within AFIT: galaxy, an ELXSI 6400 superminicomputer, and blackbird, a DEC VAX-11/785

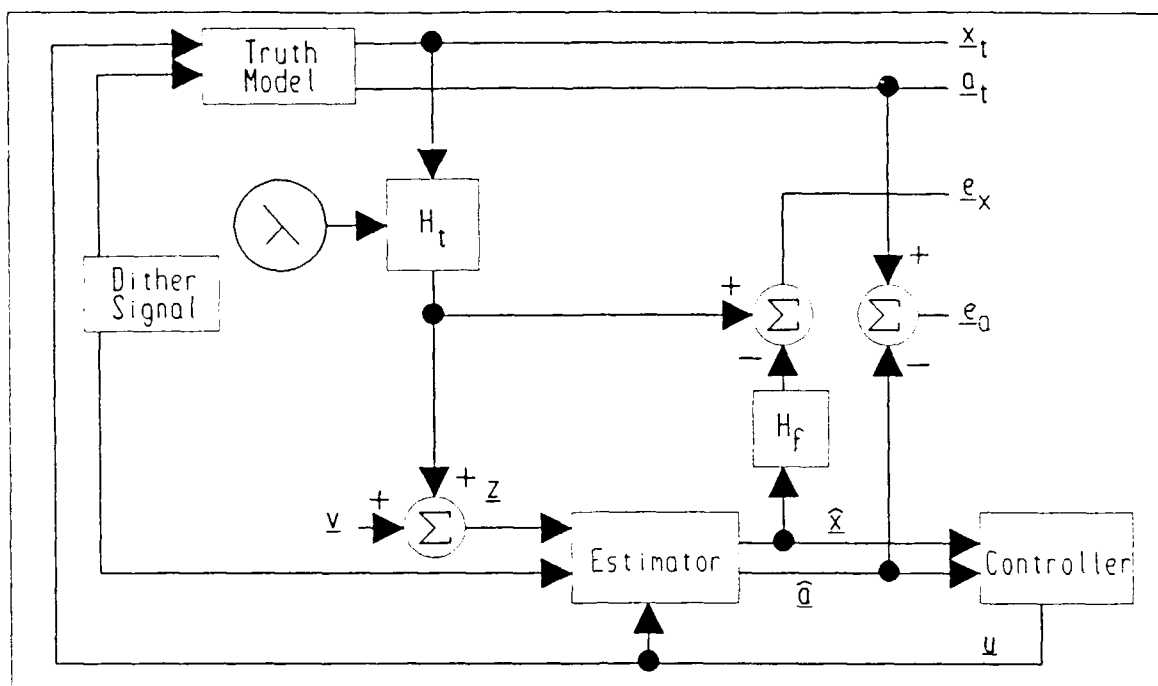


Figure 4.2. System Controller Simulation

superminicomputer. The programs used are a preprocessor, a processor, and a postprocessor.

4.3.2 The Preprocessor: *SETUPS.F*. The preprocessor generates the matrices used to describe the structure over a range of mass and stiffness parameter points. The matrices generated are Φ , B_d , G_d , and H for the system model; and D_r given by Equation (3.27); the Kalman filter gains; and the LQ controller gains for the 100-point parameter space. An input file is used to input the state and control weighting matrices, the measurement noise covariance matrix (R), the dynamic driving noise matrix (Q), and the time variables (start time, stop time, and time increment). The mass and stiffness matrices that describe the structure are also contained in this file. The parameter space is determined by multiplying both the mass and stiffness matrices by ten different scalar values, thus generating the 100 point space. The truth models and the reduced-state filter models are contained in two output files to be used by the processor.

4.3.3 The Processor: 6BNK.F. The primary processor uses the information generated by the preprocessor to perform the moving-bank simulation via Monte Carlo analysis. As Figures 4.1 and 4.2 indicate, the processor propagates the true system, which is a full 24-state model of the structure, and uses measurements of this system to update the estimator (and controller). At the measurement input to the estimator, noise is introduced in the form of a white Gaussian noise vector. The software has the capability to perform bank expansions, contractions, and movements according to the logic described in Section 2.3.1. These functions are used once the states of the filter bank have been updated and various internal parameters are compared to preset thresholds. At the end of each time increment, pertinent data is written to output files to be postprocessed.

4.3.4 The Postprocessor: RESULT.F. Once the simulation is completed, the data must be reduced and put into a presentable format, i.e. graphs of the mean \pm one standard deviation of quantities of interest. The most important values observed in this thesis effort are the errors in position and velocity estimation and the corresponding true positions and velocities for control evaluation.

4.4 Simulation Plan

The main objective of this thesis effort is to determine the robustness of MMAE and MMAC to the effects of the modelling mismatch caused by a 24-state truth model and a 6-state filter model. The difficulties encountered by Van Der Werken after he increased the model states to 24 may have been due to the mismatch between the 24-state truth model and the 6-state filter model. A means to observe the capability of the MMAE/MMAC algorithms to provide useful information (in the case of the estimator) and/or control (in the case of the controller) is to monitor the position and velocity estimation errors and true position and velocities of the structure. These values will be emphasized. The simulations performed dealt with the performance of the estimation of the structure shape and rigid body orientation, and the performance of the control algorithm, in the

presence of a higher order truth model. Additionally, the work of previous theses is attempted due to the changes made to the software and the computer systems on which the work is performed, in order to corroborate correct implementation of these software changes.

4.4.1 The Dither Signal. To view the effects of the different modes of the large space structure adequately, a dither signal is applied at the beginning of each 10 second Monte Carlo analysis run. The dither signal excites the system model and enhances parameter identification [15:74]. Karnick [11:81] and Lashlee stated that a $30 \frac{rad}{sec}$ square-wave dither signal was used with magnitudes of 100 and 300, respectively. Van Der Werken states that a "30 Hz" square-wave signal of magnitude 100 was used in his research. In reality, the software was written to provide a pseudo- $30 \frac{rad}{sec}$ dither signal generated by using the sign of $\sin(30t)$ times the dither magnitude, which creates a square wave whose polarity is determined by the sine function. The dither created in this manner, with the sample period of 0.05 seconds in use, did not provide a symmetric dither signal since this violates Shannon's sample theorem. The hub and attached structure had an initial (post-dither) velocity instead of remaining at the null or pre-dither position.

From the Nyquist criterion [23:334-336], the maximum frequency of the dither must be

$$f < \frac{1}{2T} \quad (4.4)$$

where f is the highest frequency contained in the signal of interest. The sample period used in this and previous thesis research is 0.05 seconds which corresponds to a maximum sample frequency of:

$$f = \frac{1}{2T} = \frac{1}{2 \times 0.05} = 10Hz \approx 63 \frac{rad}{sec} \quad (4.5)$$

From Table (3.2), the first eight average frequencies are all below this 10 Hz frequency and should be adequately excited by the dither signal used for this research. The square wave used does contain harmonics of the fundamental frequency with sufficient energy to excite the higher order modes of

the structure. The effect of the higher modes of the structure may well be negligible, but major software modifications would be required to change this limitation.

4.4.2 MMAE Study. Van Der Werken attempted to observe the effects of higher order modes by comparing the filter performance to the truth model via a transformation matrix. This thesis effort follows his recommendations to scale the partition of the truth model measurement matrix, \mathbf{H}_t , associated with the higher order mode states, to be scaled by a constant, λ . The value of λ will be increased gradually from zero to one, unless drastic effects are observed. This gradual introduction of the unmodeled states into the estimation process will allow for an investigation of whether more states need to be added to the estimator to provide robust state estimation of the space structure.

The actual formation of the modified \mathbf{H}_t is performed by forming a Λ matrix defined as

$$\Lambda = \begin{bmatrix} I_{6 \times 6} & \mathbf{0}_{6 \times 18} \\ \mathbf{0}_{18 \times 6} & \lambda \mathbf{I}_{18 \times 18} \end{bmatrix} \quad (4.6)$$

and the modified \mathbf{H}_t matrix is formed by

$$\tilde{\mathbf{H}}_t = \mathbf{H}_t \Lambda \quad (4.7)$$

The reason Λ is diagonally partitioned is due to the way Van Der Werken generated the system matrices in the preprocessor program [24:223]. Unlike the expression given in Equation (1.25), the truth states were modified by Van Der Werken so that the first six states represent the rigid body and first two bending modes for both position and velocity. Thus, the implemented $\tilde{\mathbf{H}}_t$ will appear as in Equation (1.30), but with the two inner column partitions interchanged.

Once $\tilde{\mathbf{H}}_t$ has been formed, the measurement of the true states will be modified by the λ value. A λ of 0 corresponds to a truth model and filter mode order match. A λ of 1 would be the

case where the truth model is a full 24-state model and thus a mismatch between model and filter will exist. A benchmark is run with the truth model and the filter bank at the same parameter location, (7,6). This position represents the nominal position in the filter space since the scalar multipliers are both one at this point and is used to maintain some comparability with previous thesis efforts. The first number of the position pair is the mass location while the second number represents the stiffness location in the filter space as generated by the preprocessor. Additionally, the initial probability of the center filter is set to 1. This arrangement gives an output that is comparable to a single Kalman filter with full artificial knowledge about the parameter condition. Additionally, the filter is not allowed to move by this arrangement. Once a benchmark has been established, other tests are performed to determine the effects of the truth model/filter mismatch.

To test the estimation performance, the true parameter is fixed at representative position (7,6), which corresponds to the mass and stiffness matrices being unmodified while generating the truth model system matrices. The center of the filter bank is placed at position (5,5). This corresponds to a mass matrix scaling of 0.8 and a stiffness matrix scaling of 0.9. The Monte Carlo runs are performed, with varying values of λ , with the filter fixed (a *worst case* analysis) and with the filter being able to move within the filter space. The ability of the algorithm to move the filter bank properly is essential for the cases of varying parameters and jump changes in the parameters.

4.4.3 MMAC Study. The MMAC study is performed by enabling the software to control the structure by applying control forces. As with the MMAE study, the goal is to determine the degree of influence of the higher states of the truth model on the performance of the 6-state filter and controller model.

The controller study is performed with both fixed and moving bank configurations. Additionally, the cases of the informed filter bank (the filter bank fixed at the true parameter location) and uninformed filter bank (the filter bank fixed at the same parameter location other than the true parameter location) will be performed to determine the performance characteristics of the MMAC

algorithm. For these studies and the MMAE studies, the values of the dynamics noise strength \mathbf{Q} and the measurement noise covariance \mathbf{R} will remain unchanged for the various elemental filter and controller models.

4.4.4 Disturbance Rejection. Once the estimation and control processes have been investigated, the robustness of the algorithms is to be determined in the event of a disturbance once the estimation and control process has reached an intermediate steady state condition (as determined from the MMAC study results). The disturbance is to be of the form of a dither signal applied in the same manner as the dither signal applied at the beginning of each simulation run.

4.5 Software Modifications

Several problems with the software were encountered during this research effort. The IMSL FORTRAN subroutines [10] used in the preprocessor had to be replaced with a newer version of the IMSL Mathematics Library. An N+1 problem was discovered in the postprocessor. Additionally, several poorly coded sections of various subroutines were modified to be readable. These modifications are now described in some detail.

One of the problems caused by the conversion from IMSL Version 9.3 to IMSL Version 10.0 is that the calculation of the Kalman filter gain matrices for the filter space is possibly numerically unstable. This problem asserts itself only for large values of \mathbf{Q} . In order to create a filter space with confidence, the value of \mathbf{Q} was reduced by an order of magnitude from that used by Lashlee [15:94]. The filter matrices were generated with

$$\mathbf{Q} = \begin{bmatrix} 8 & 0 & 0 \\ 0 & 8 & 0 \\ 0 & 0 & 5 \end{bmatrix} \quad (4.8)$$

The numerical instability did not prevent the generation of useful results but does deserve some future consideration.

The N+1 problem discovered in the postprocessor did not adversely affect the results of this thesis, since it was corrected, and most likely did not drastically affect the previous thesis efforts. When the processor writes data to the intermediate files, it writes at every time increment, including the first and last time points: 0 and 10 seconds respectively. This arrangement creates 200 intervals since the time increment is 0.05 seconds. However, the number of measurements is 201. The Monte Carlo analysis therefore writes 201 measurements for each run of the analysis, and not 200, as assumed by the previous thesis effort [24]. For a large number of analysis runs, the N+1 problem just described could be significant, especially if the beginning and ending magnitudes of each simulation run are greatly different. With the N+1 problem still in the software, the postprocessor reads in 200 measurements for each analysis. The 201st data point is then read in as the first data point in the next analysis run and so on. For a Monte Carlo analysis performed with 100 runs, the last set of measurements read from the intermediate files would be misindexed by 100 data points and possibly provide totally erroneous insights into the process being studied.

4.6 Summary

Section 4.2 explained the need for and the use of Monte Carlo analysis as it pertains to this thesis. Sections 4.3.2 through 4.3.4 described how the simulation of MMAE/MMAC of a large space structure is performed. Section 4.4 explained how the simulation would be used to investigate the mismatch between the truth model and the moving bank of Kalman filters or LQG controllers. Finally, Section 4.5 presented details on how the software was implemented and some of the problems encountered with the implementation. The next chapter describes the results derived from this simulation.

V. Results

5.1 Introduction

The results of the Monte Carlo analysis are presented in this chapter. The intent of this thesis is to show the robustness of the moving-bank MMAE/MMAC algorithm in the presence of unmodeled states in the truth model. Van Der Werken [24] modified the software to provide a 24-state truth model. The dimension of the filters remained at 6-state. This research demonstrates whether or not that six-state design model can yield adequate performance as the effect of unmodeled higher order true bending modes is gradually changed from nonexistent to fully present.

5.2 Multiple Model Adaptive Estimation Study

5.2.1 Duplication of Past Work. The duplication of past work was performed in a somewhat subjective manner. The results achieved by Van Der Werken were not repeatable [24:84-206]. The software problems described in Section 4.5 may have caused the problems his work displayed, but there is no direct evidence of this. Lashlee worked with a 6-state filter and truth model [15:80-81] and thus only the cases of $\lambda = 0.0$ are useful for comparison. Based on the results Lashlee presents, this work compares very favorably. Therefore, the intent of this work is to accept this duplication of Lashlee's work as a basis, and to extend beyond it to determine the robustness of the algorithms in the full presence of higher order modes contained in the truth model.

In the previous theses, the difference of the states were used in the Monte Carlo analysis. Lashlee used an error signal of [15:72-74]:

$$\mathbf{e}_r(t_i) = T\mathbf{\hat{x}}_t(t_i) - \mathbf{\hat{x}}(t_i) \quad (5.1)$$

where T is an $n \times n_t$ matrix "to make the dimensions compatible." For this thesis, the error signals will be physically significant values rather than the modal variables. The signals of interest within

the simulation diagram, Figure 4.1, are the noise-free measurement of the positions and velocities of nodes 1, 2, and 3. The plots that follow show the errors in position and velocity estimates of these nodes, as well as parameter estimates and filter movement plots.

5.2.2 MMAE Benchmark. To judge the robustness of the MMAE algorithm adequately, a benchmark is needed to compare to other results. The estimation benchmark is generated by setting λ to zero and placing the filter bank and parameter at location (7,6), i.e., the mass parameter is located at its seventh discrete value out of ten and the stiffness matrix is at its sixth discrete location out of ten. The benchmark analysis is shown in Figures 5.1 through 5.3. Additionally, the probability of filter five in the bank (the center of the finely discretized bank) is set to one. In essence, this is the case of an artificially informed (with correct parameter values), non-adaptive filter. The (7,6) location corresponds to no scaling of the mass and stiffness matrices, i.e., as determined by the finite element analysis. The 10 Hz square-wave dither is applied for the first 0.5 seconds in order to excite the system, and the actuator outputs are zeroed after this period. The dither should stimulate the first eight modes of the truth model (and probably stimulate the ninth through twelfth modes adequately as well) and provide an adequate means of performing parameter and state estimation.

Figure 5.1 shows the benchmark performance of the artificially informed, non-adaptive filter when the parameter location and filter location match. The order of the truth model and filter match, and thus the filter should provide optimal performance. After 10 seconds, the error in estimate of the position of node 1 is near zero and the standard deviation is approximately 0.006 inches or 0.006% of the structure length. The error in the velocity estimate of node 1 is comparatively steady, with the signal settling after the dither signal is removed. Figure 5.2 shows the same information for node 2 with similar results. Figure 5.3 shows the errors in the position and velocity estimation for node 3, the structure hub. It must be noted that, unlike the node 1 and node 2 estimation errors, the node 3 errors are in radians and radians per second, since the hub is fixed in

space and only rotates. Again, the small error signals and correspondingly small deviations would indicate that the estimation process is providing good information.

5.2.3 Non-Adaptive Single-Filter Analysis with Variable λ . Figures 5.4 through 5.9 show the results of the λ variation runs under the same conditions as the benchmark, i.e., for a single artificially informed filter. The position estimation errors for nodes 1 and 2 are essentially the same for λ 's of 0.5 and 1.0. Some high frequency effects are observable but are not significant in magnitude. The same cannot be said of the errors in the velocity estimates of nodes 1 and 2 and the error of the position estimate of the hub. The error signals dramatically show the high frequency effect of admitting some of the higher order modes into the measurement for the filter. The magnitude of the errors is an order of magnitude higher than the benchmark, which may cause a significant problem for the controller if the tuning process is not properly performed.

5.2.4 Non-Adaptive Single-Filter Worst Case Analysis. Figures 5.10 through 5.12 provide a worst case analysis. The single filter is set to the (5.5) parameter position and is made to be non-adaptive. The true parameter is located at (7.6). The same dither signal is used to excite the system. The plots show a dramatic loss in estimation capability with the deviations being an order of magnitude larger than those for the benchmark. This simulation clearly shows the need for an adaptive filter: mismatch of true and filter-assumed parameter values yields unacceptable degradation. The value of λ was also varied in this worst case analysis. The changes in λ showed no appreciable changes in performance. See Figures 5.13 through 5.15 for the case of $\lambda = 0.5$.

The position estimate error data from the above simulations are summarized in Table 5.1. The time averages of the data suggests that the higher order modes observed in the non-zero λ cases do not significantly affect the performance of the filter. The worst case analysis did show that there is a strong need for adaptive estimation in the case of mismatched filter-assumed and true parameters. The worst case analysis, i.e., the case where a fixed filter is not located at the true parameter location, is indicated by the " " in the λ column. The data presented for the worst

case analysis was generated with $\lambda = 0.0$. The velocity estimate errors, shown in Table 5.2, did not provide the same insights as the position estimate errors since the velocity estimates did not change considerably as a function of λ . The data from these tables are also presented in the bar charts of Figures 5.16 through 5.21 in order to enhance comparisons. The first three figures present the data for the cases of MMAE with varying λ while the last three present the same data with the “worst case” (mismatched filter/parameter and $\lambda = 0$) data included for direct comparison. The trends in the performance of the algorithms in the face of unmodeled modes is obvious in the velocity estimate errors. Additionally, the “worst case” analysis shows a definite degradation in the algorithm’s performance due to mismatch between filter-assumed and real parameter values.

5.2.5 Moving-Bank MMAE Analysis. The next performance analysis of the MMAE algorithm was to determine the ability of the bank to move within the filter space when the initial parameter estimate and filter location differ from the true parameter location. The simulation was initiated the same as for the worst case analysis except that the bank was allowed to move. The probabilities of all the filters in the bank were initialized to $\frac{1}{5}$ and the lower limit of the probabilities was set to 0.05. The value of 0.05 was used after it was determined to provide the best movement of the bank under the current software configuration. Residual monitoring was used for the movement logic and the move threshold set to 0.25, again determined in an ad hoc manner based on performance. The results of these simulations are shown in Figures 5.22 through 5.30.

The results are considerably different from those seen with no movement allowed, as in the worst case analysis. During the 10 second run time, the position estimates undergo considerable changes. The jumps seen in the position estimations are correlated with the actual position of the structure as expected. The true position of node 1 seen in Figure 5.26, the mid-structure point, shows the effect of the mixture of high and low frequency bending modes. At about 2.2, 4.0, 6.0, 7.6, and 9.6 seconds of the run time, the position “smooths” as the bending mode components go out of phase and tend to cancel each other. The changes in the position estimate error plot for

node 1 seem to correlate to these points. The changes in the node 2 position estimation errors are not *visibly* correlated to the node 2 position. As the structure bends and moves, and the positions are measured from the truth model via $\mathbf{z} = \mathbf{H}_t \mathbf{x}_t$, the new measurement information is passed to the filters and acted upon. The changes in the bank location are evident in Figure 5.25. The mass parameter estimate and the actual shifting of the bank performed well, lingering in the vicinity of the true mass parameter location (mass = 7). The stiffness parameter estimate performed less well, with the stiffness estimate and location remaining near the initial stiffness location (initial stiffness = 5 versus the true stiffness = 6), after drifting in the wrong direction initially. Again the changes in the parameter estimates and the movement of the bank can be correlated somewhat to changes in the actual position of the structure as with the correlation of the position estimation errors discussed above. Figures 5.27 through 5.30 show the results of this analysis performed with λ set to 0.5. The change in λ revealed the same types of response changes as seen with the artificially informed, non-adaptive filter. The results of the $\lambda = 0.5$ analysis makes this behavior less clear since the performance is reversed, i.e., the stiffness performs better than the mass estimation and movement process.

In both cases, $\lambda = 0.0$ and $\lambda = 0.5$, the visible pattern of the position and velocity estimation errors of nodes 1 and 2 were not evident in node 3, the hub. This is logical since the hub has much greater mass and would not be moved or otherwise change its position after the dither signal is removed.

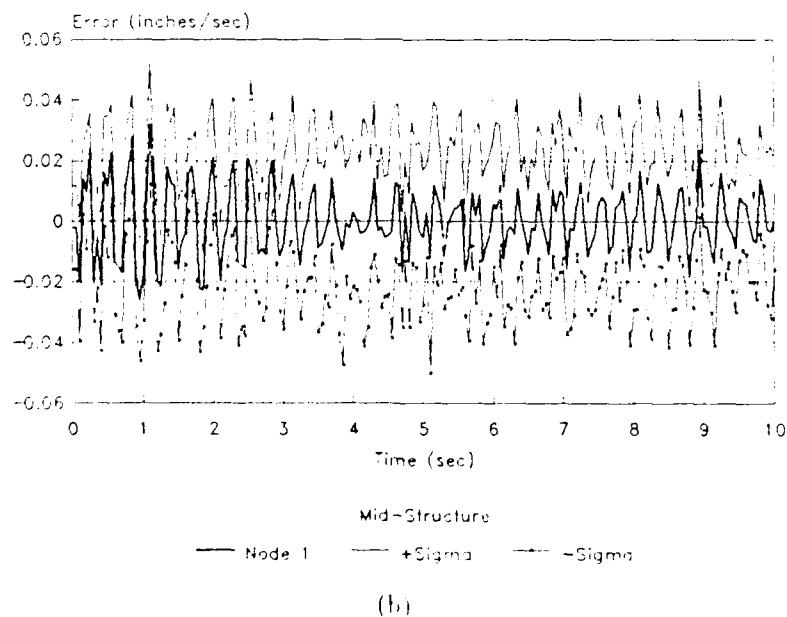
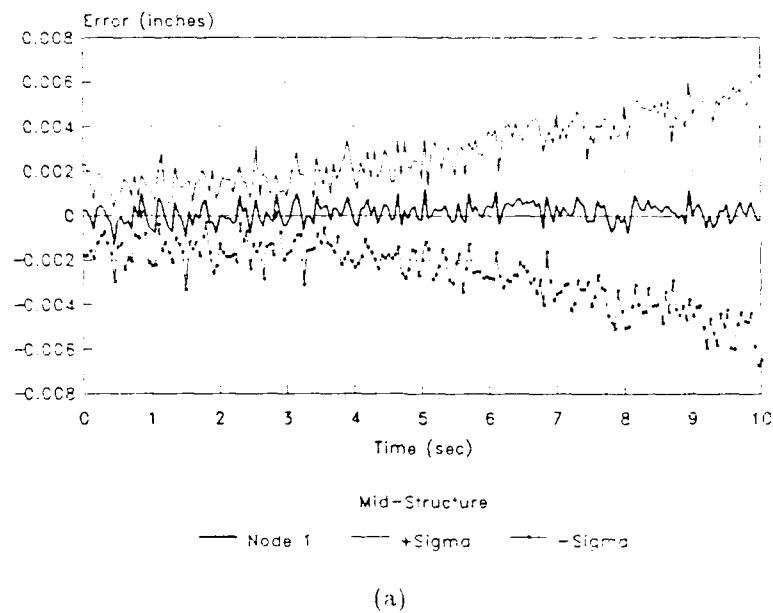
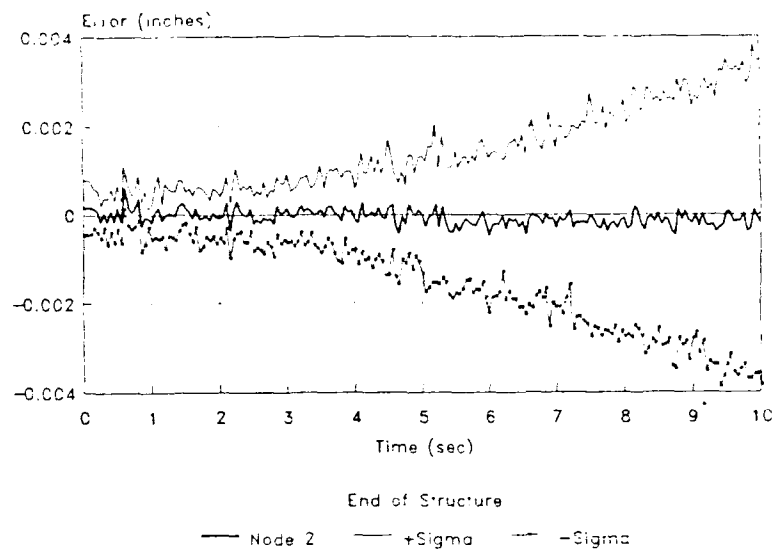
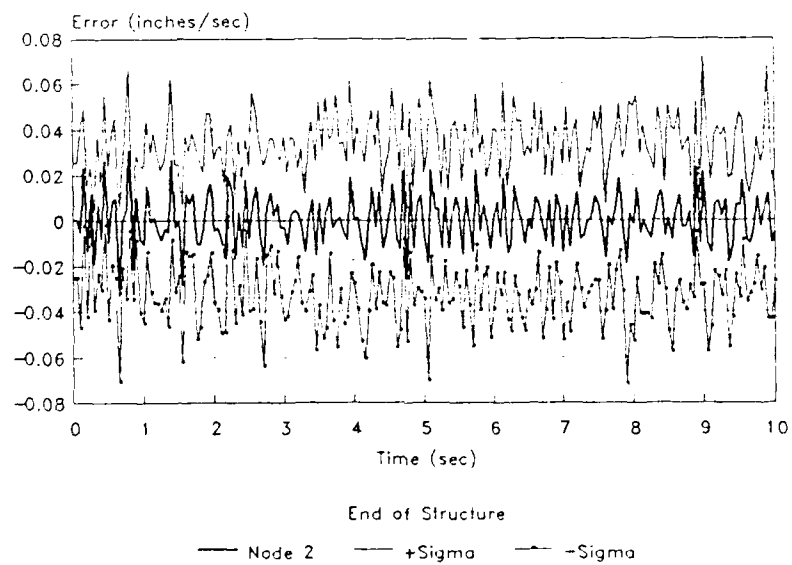


Figure 5.1. Benchmark Estimation Errors - True Parameter and Filter at Mass = 7 and Stiffness = 6. (a) Position and (b) Velocity Estimation Errors. $\lambda = 0$

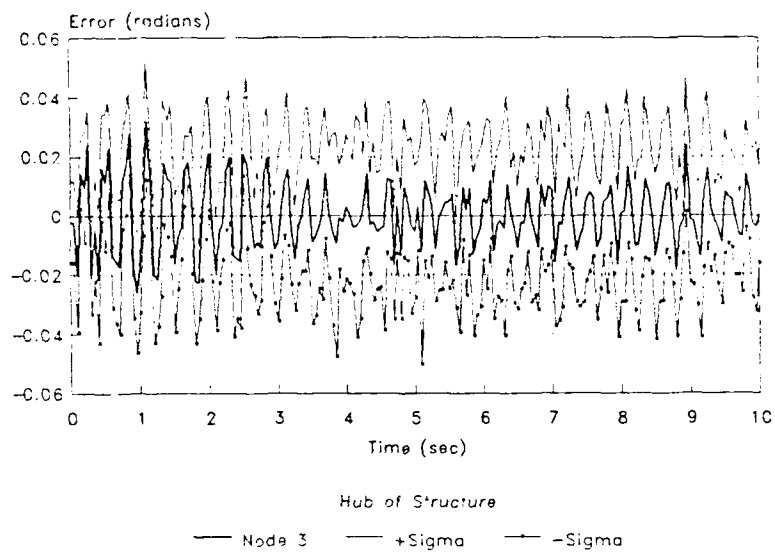


(a)

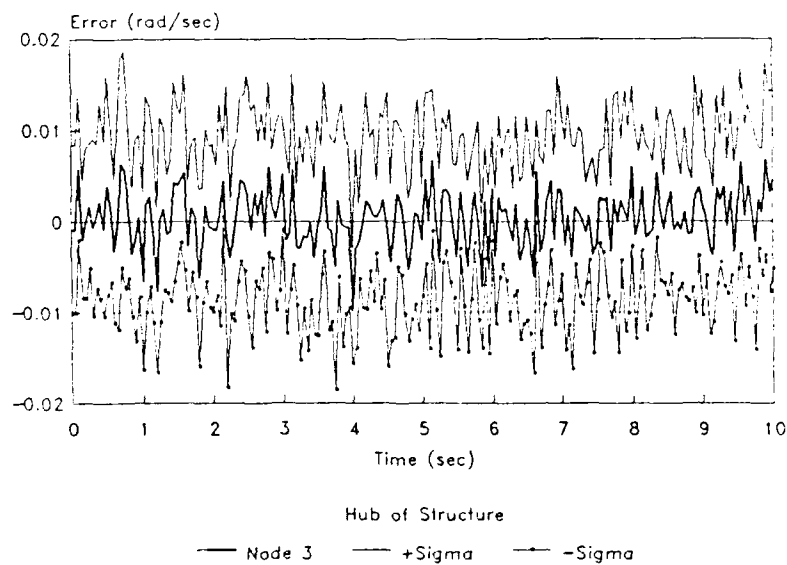


(b)

Figure 5.2. Benchmark Estimation Errors - True Parameter and Filter at Mass = 7 and Stiffness = 6. (a) Position and (b) Velocity Estimation Errors. $\lambda = 0$.

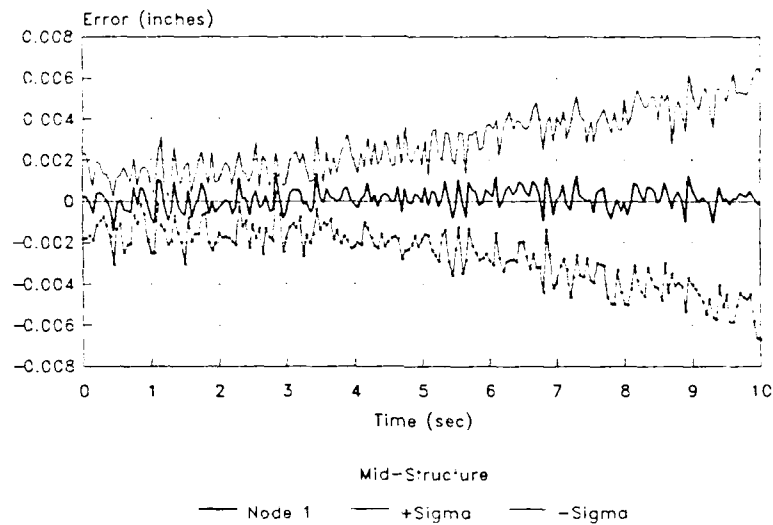


(a)

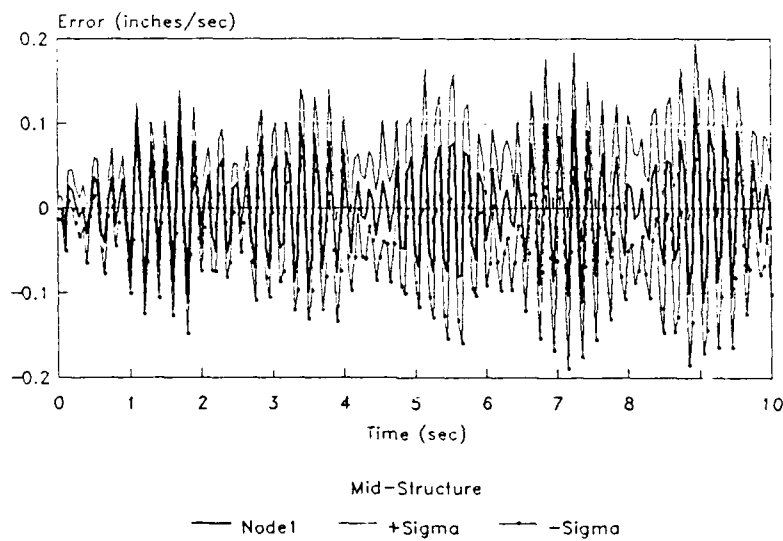


(b)

Figure 5.3. Benchmark Estimation Errors - True Parameter and Filter at Mass = 7 and Stiffness = 6. (a) Position and (b) Velocity Estimation Errors. $\lambda = 0$.

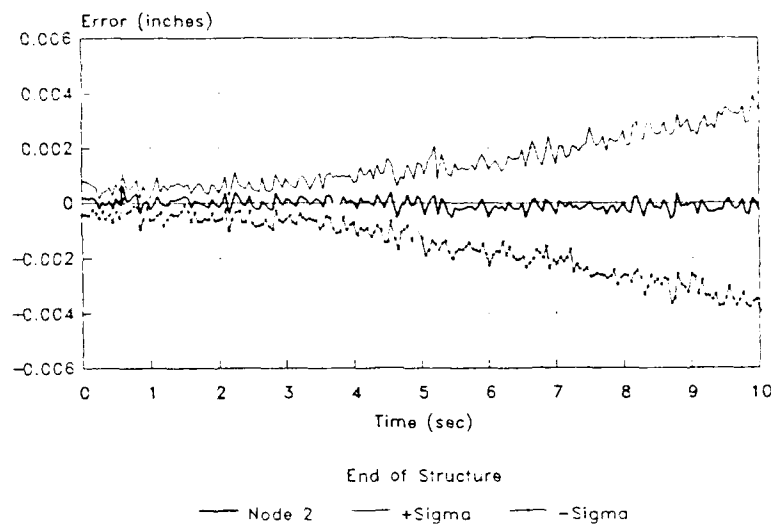


(a)

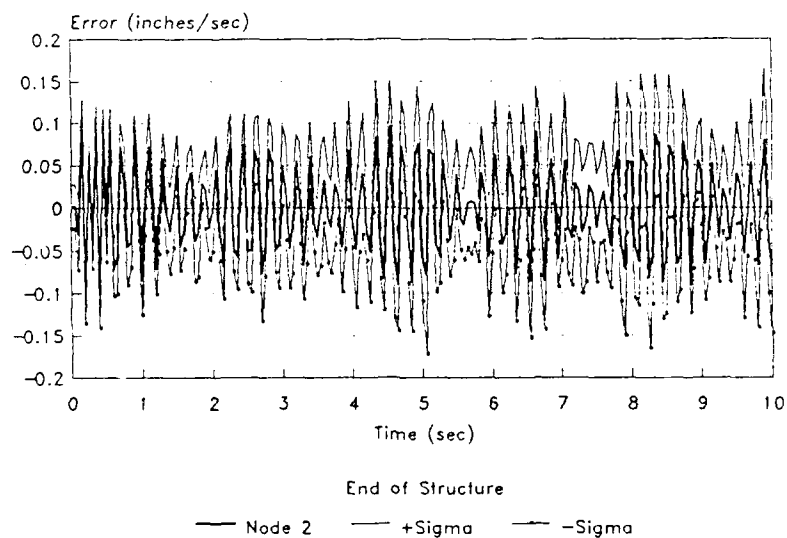


(b)

Figure 5.4. Single-Filter Estimation Errors - True Parameter and Filter at Mass = 7 and Stiffness = 6. (a) Position and (b) Velocity Estimation Errors. $\lambda = 0.5$.

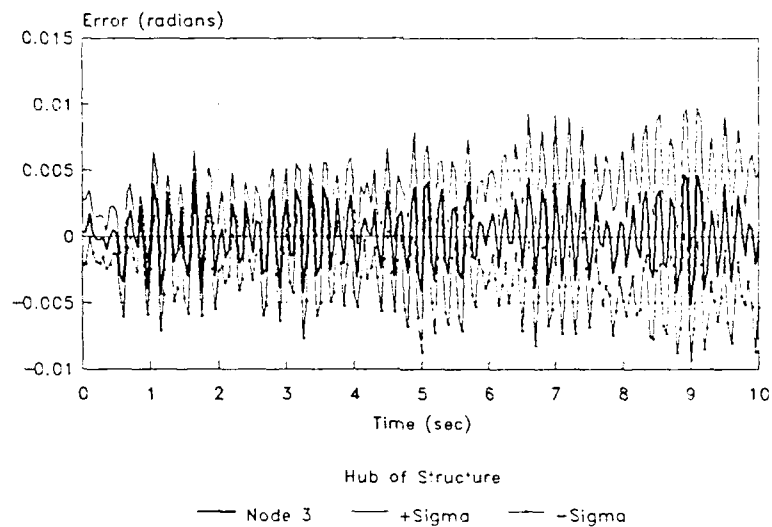


(a)

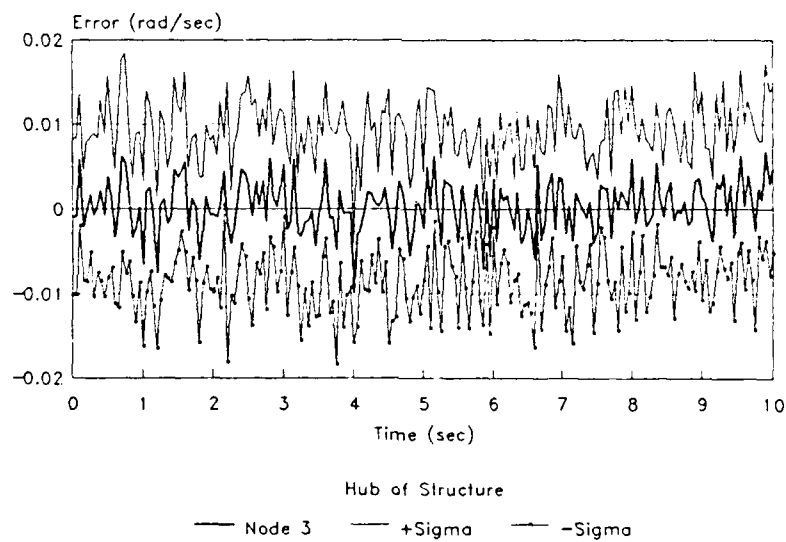


(b)

Figure 5.5. Single-Filter Estimation Errors - True Parameter and Filter at Mass = 7 and Stiffness = 6. (a) Position and (b) Velocity Estimation Errors. $\lambda = 0.5$.

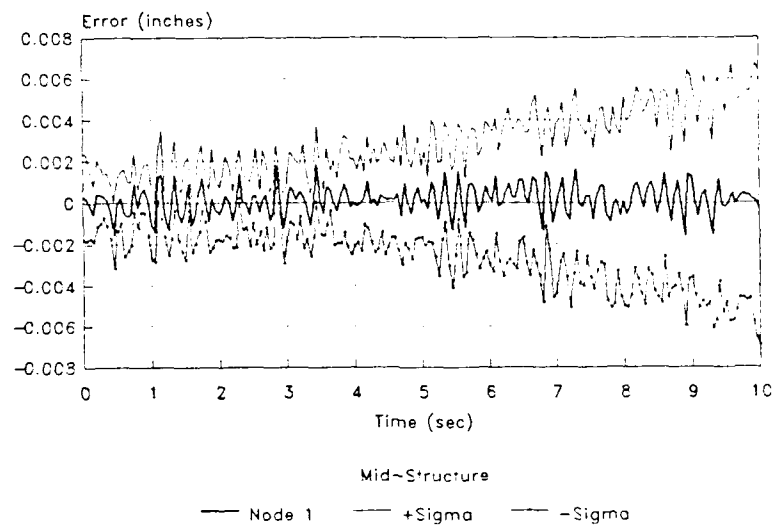


(a)

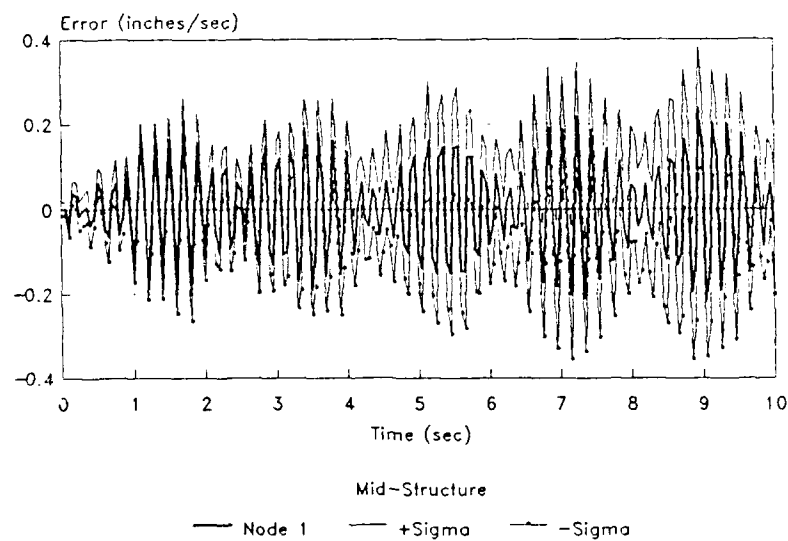


(b)

Figure 5.6. Single-Filter Estimation Errors - True Parameter and Filter at Mass = 7 and Stiffness = 6. (a) Position and (b) Velocity Estimation Errors. $\lambda = 0.5$.

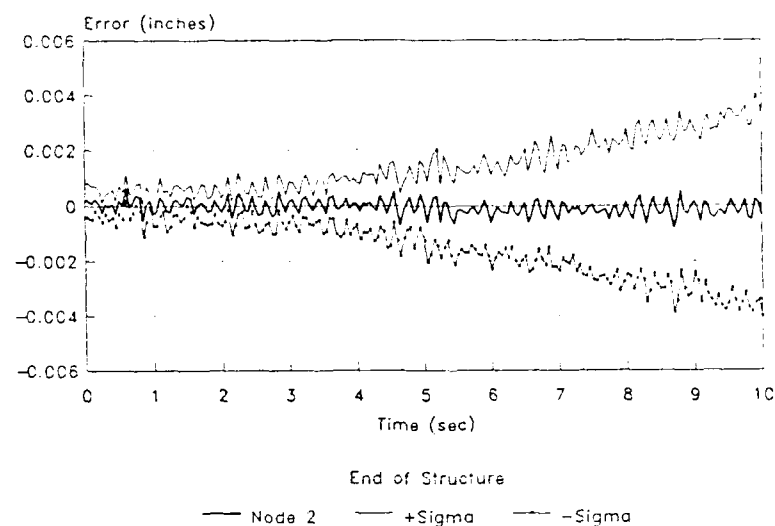


(a)

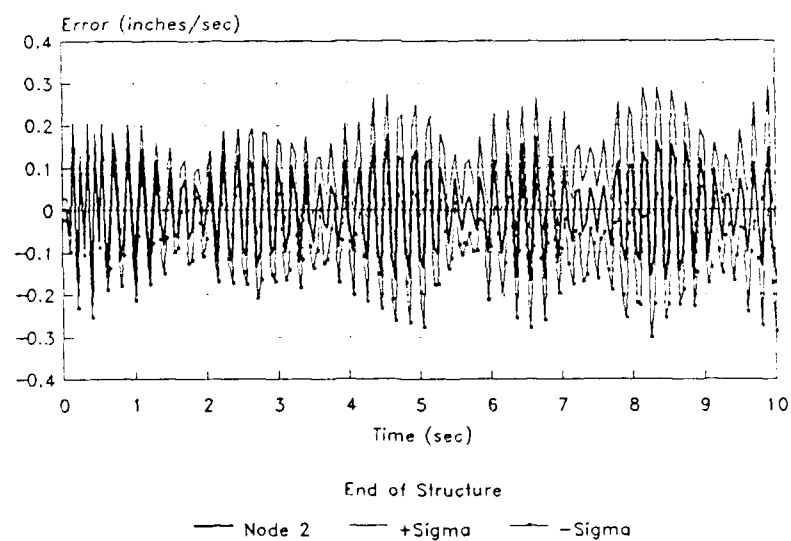


(b)

Figure 5.7. Single-Filter Estimation Errors - True Parameter and Filter at Mass = 7 and Stiffness = 6. (a) Position and (b) Velocity Estimation Errors. $\lambda = 1.0$.

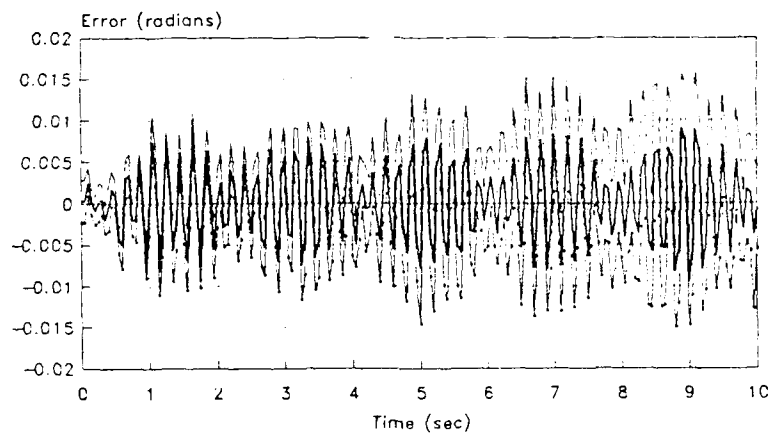


(a)



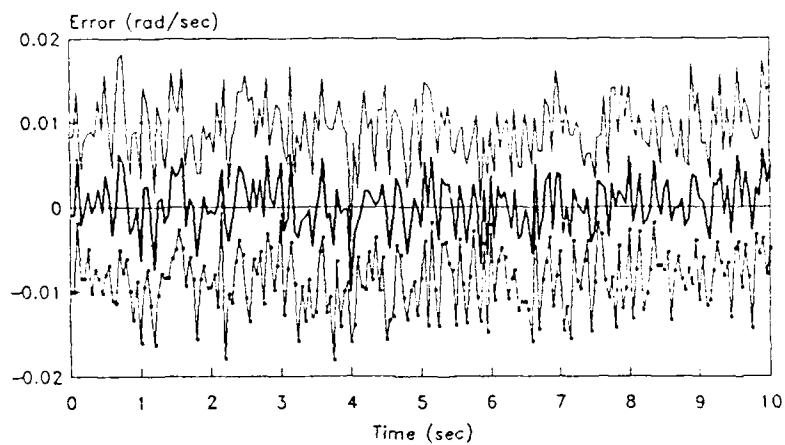
(b)

Figure 5.8. Single-Filter Estimation Errors - True Parameter and Filter at Mass = 7 and Stiffness ≈ 6 . (a) Position and (b) Velocity Estimation Errors. $\lambda = 1.0$.



Hub of Structure
 — Node 3 - - - +Sigma . . . -Sigma

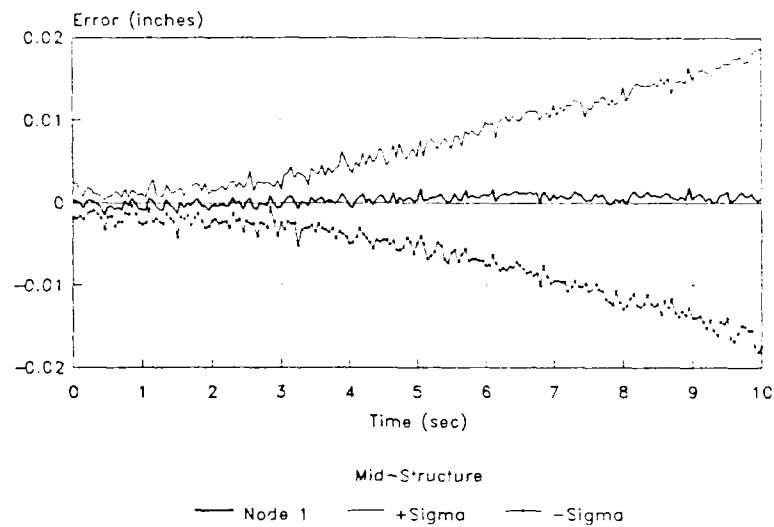
(a)



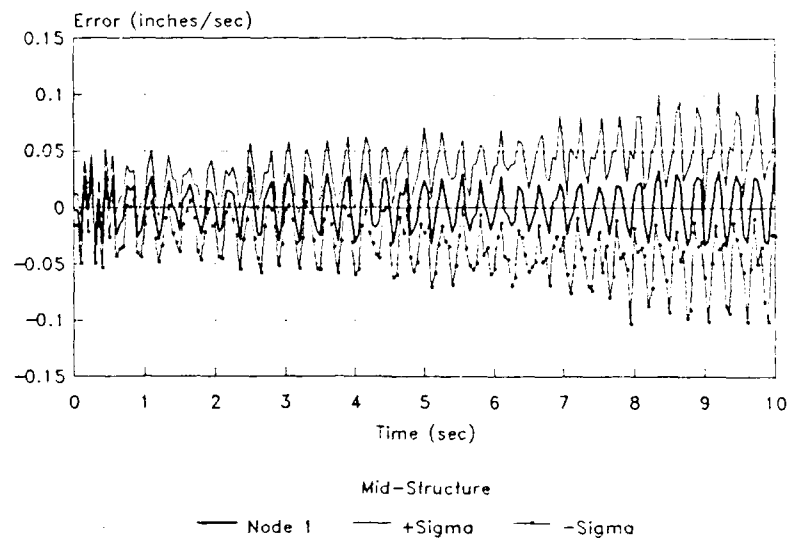
Hub of Structure
 — Node 3 - - - +Sigma . . . -Sigma

(b)

Figure 5.9. Single-Filter Estimation Errors - True Parameter and Filter at Mass = 7 and Stiffness = 6. (a) Position and (b) Velocity Estimation Errors. $\lambda = 1.0$.

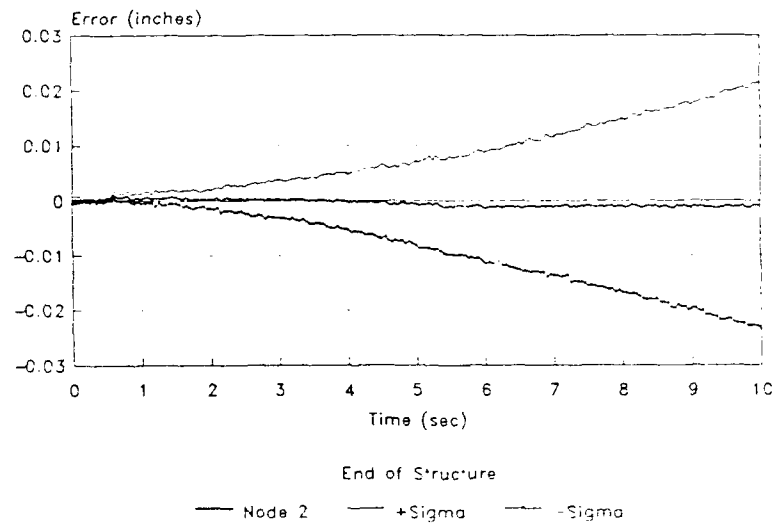


(a)

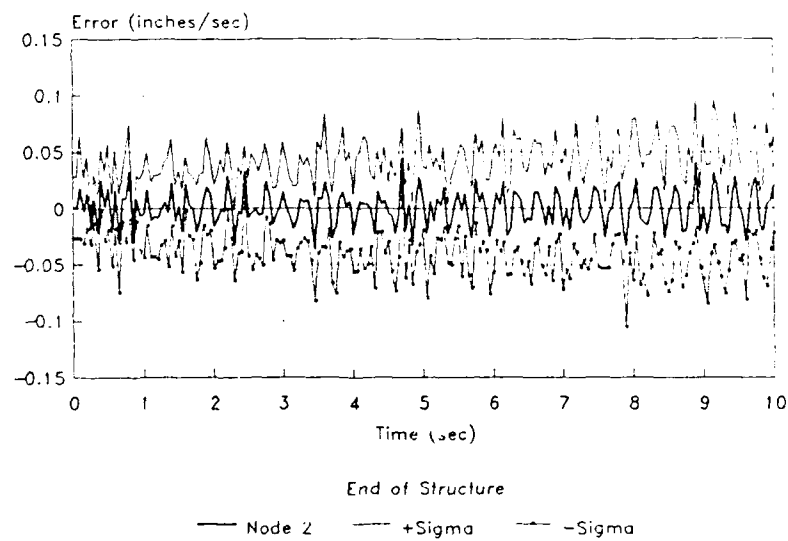


(b)

Figure 5.10. "Worst Case" Single-Filter Estimation Errors - True Parameter at (7.6) and Filter at (5.5). (a) Position and (b) Velocity Estimation Errors. $\lambda = 0.0$.

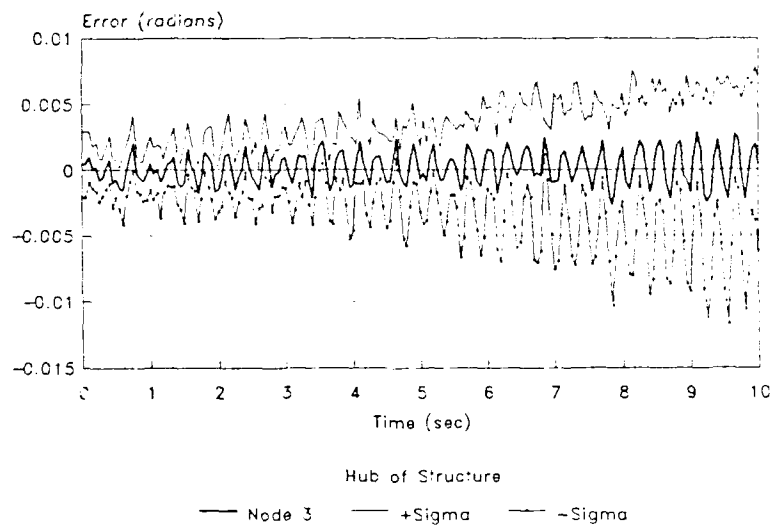


(a)

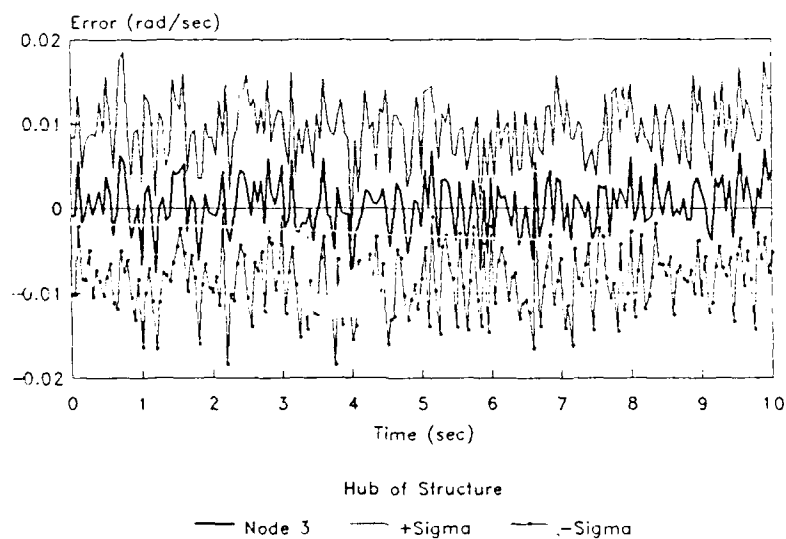


(b)

Figure 5.11. "Worst Case" Single-Filter Estimation Errors - True Parameter at (7,6) and Filter at (5,5). (a) Position and (b) Velocity Estimation Errors. $\lambda = 0.0$.

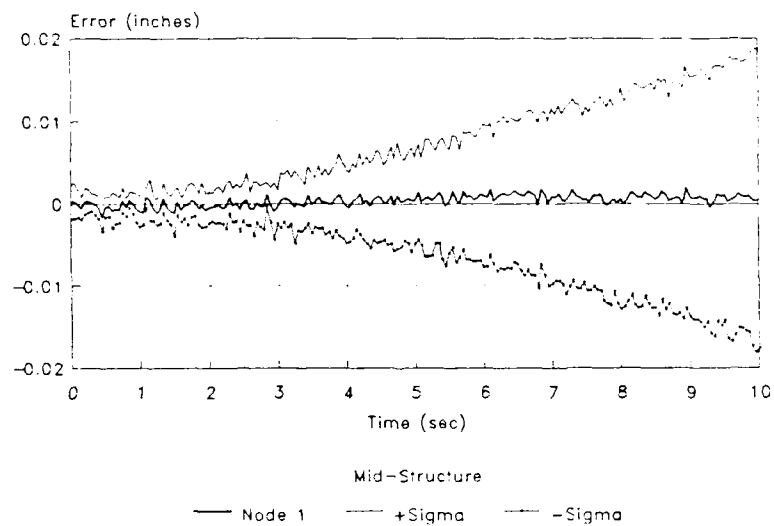


(a)

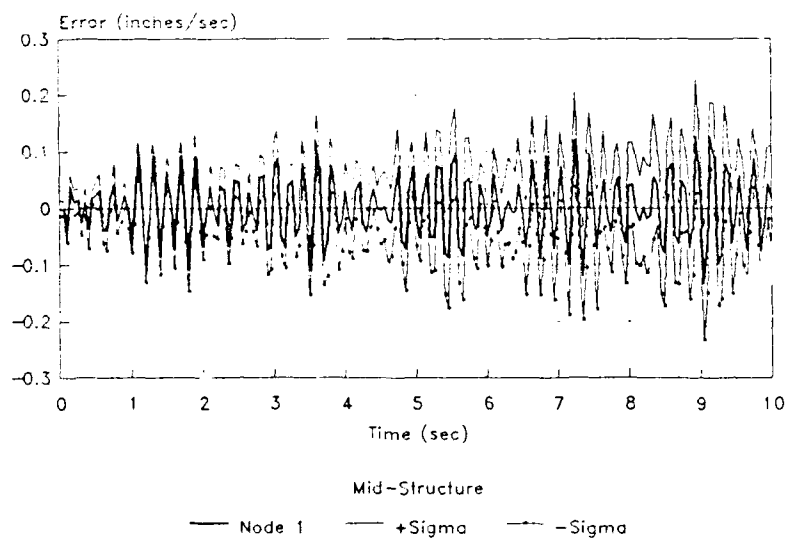


(b)

Figure 5.12. "Worst Case" Single-Filter Estimation Errors - True Parameter at (7,6) and Filter at (5,5). (a) Position and (b) Velocity Estimation Errors. $\lambda = 0.0$.

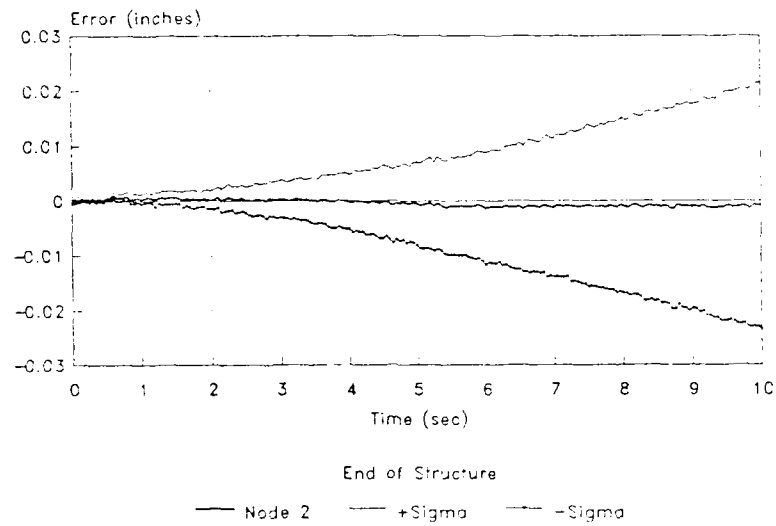


(a)

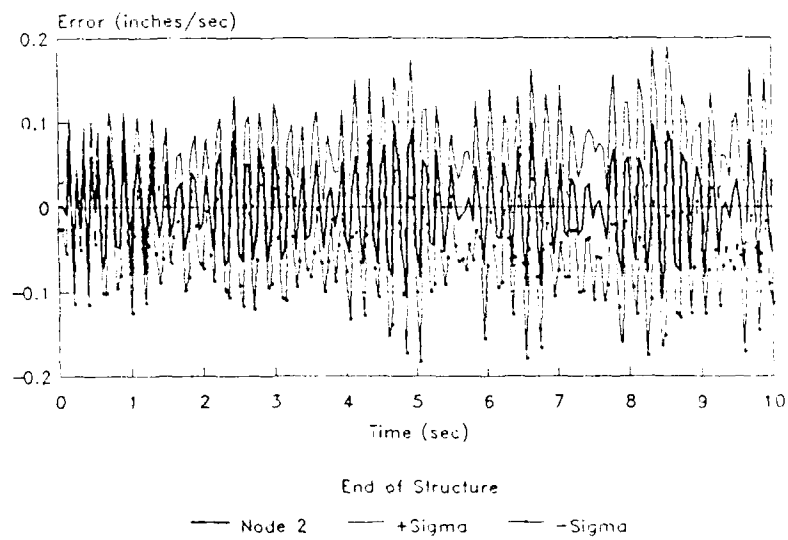


(b)

Figure 5-13. "Worst Case" Single-Filter Estimation Errors - True Parameter at (7.6) and Filter at (5.5). (a) Position and (b) Velocity Estimation Errors. $\lambda = 0.5$.



(a)



(b)

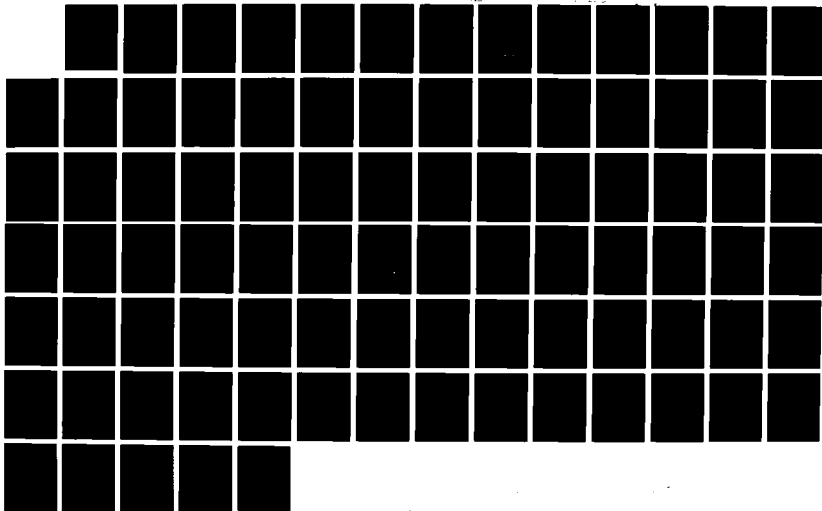
Figure 5.11. "Worst Case" Single-Filter Estimation Errors - True Parameter at (7.6) and Filter at (5.5). (a) Position and (b) Velocity Estimation Errors. $\lambda \approx 0.5$.

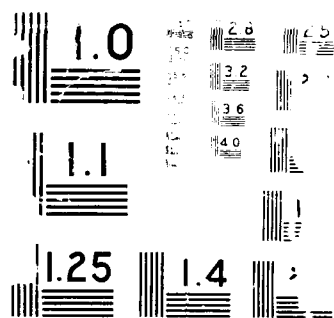
NO-A215 670

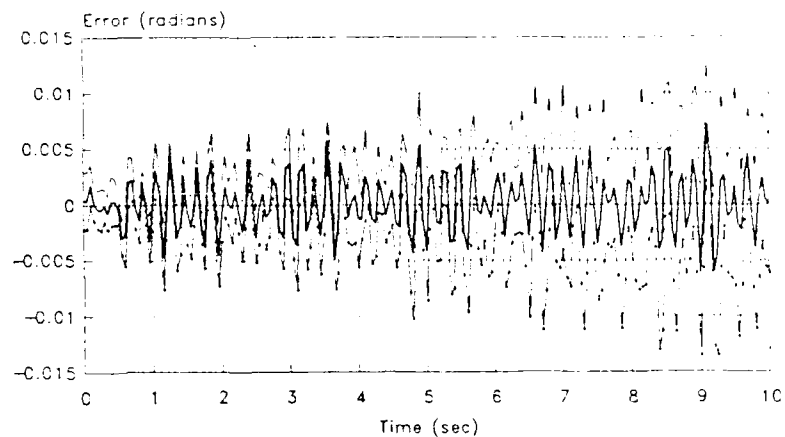
ROBUSTNESS OF A MOVING-SINK MULTIPLE MODEL ADAPTIVE
CONTROLLER FOR A LARG. (U) AIR FORCE INST OF TECH
WRIGHT-PATTERSON AFB OH SCHOOL OF ENGI. M R SCHORE
DEC 89 AFIT/GE/ENG/89D-46 F/G 22/2

UNCLASSIFIED

NL



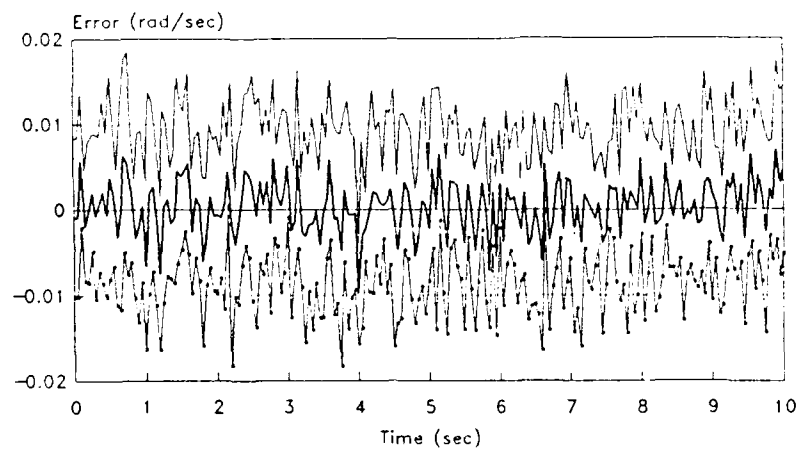




Hub of Structure

— Node 3 - - - +Sigma . . . -Sigma

(a)



Hub of Structure

— Node 3 - - - +Sigma . . . -Sigma

(b)

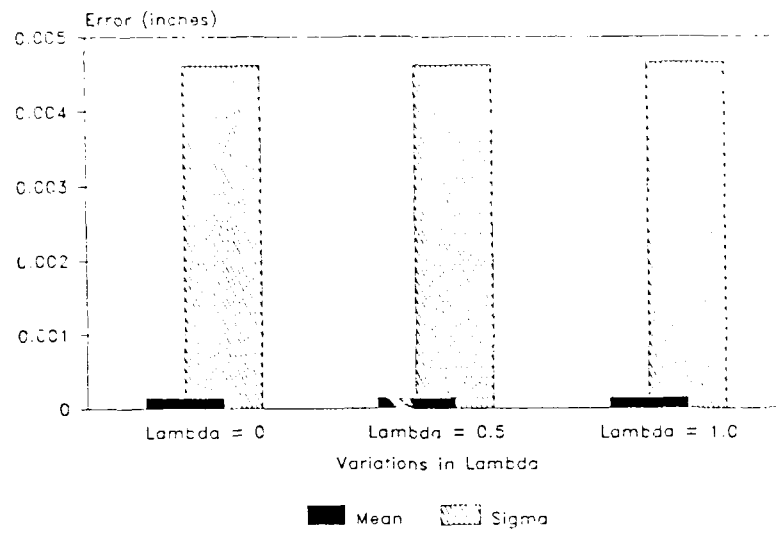
Figure 5.15. "Worst Case" Single-Filter Estimation Errors - True Parameter at (7.6) and Filter at (5.5). (a) Position and (b) Velocity Estimation Errors. $\lambda = 0.5$.

| Node | λ | Mean | σ |
|------|-----------|-----------|---------------|
| 1 | 0.0 | 0.000146 | 0.00461 (in) |
| 1 | 0.5 | 0.000145 | 0.00462 |
| 1 | 1.0 | 0.000145 | 0.00457 |
| 1 | — | 0.000714 | 0.01436 |
| 2 | 0.0 | -0.000153 | 0.00263 |
| 2 | 0.5 | -0.000153 | 0.00263 |
| 2 | 1.0 | -0.000154 | 0.00263 |
| 2 | — | -0.001050 | 0.01639 |
| 3 | 0.0 | 0.000060 | 0.00395 (rad) |
| 3 | 0.5 | 0.000095 | 0.00472 |
| 3 | 1.0 | 0.000114 | 0.00644 |
| 3 | — | 0.000158 | 0.00565 |

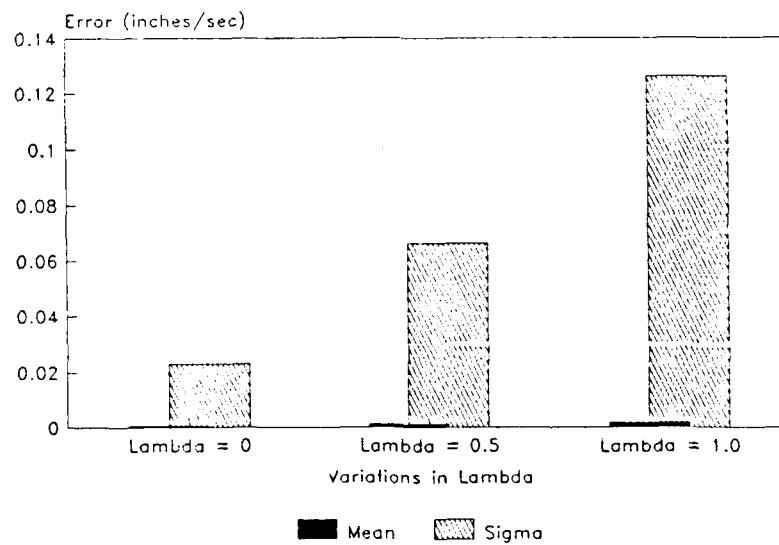
Table 5.1. Position Estimation Means and Standard Deviations for MMAE

| Node | λ | Mean | σ |
|------|-----------|-----------|---------------------------|
| 1 | 0.0 | 0.000345 | 0.02295 $\frac{m}{sec}$ |
| 1 | 0.5 | 0.001073 | 0.06638 |
| 1 | 1.0 | 0.001800 | 0.12617 |
| 1 | — | 0.000632 | 0.05166 |
| 2 | 0.0 | 0.000215 | 0.03425 |
| 2 | 0.5 | -0.000160 | 0.06018 |
| 2 | 1.0 | -0.000537 | 0.10590 |
| 2 | — | 0.000177 | 0.04922 |
| 3 | 0.0 | 0.000902 | 0.00986 $\frac{rad}{sec}$ |
| 3 | 0.5 | 0.000919 | 0.00984 |
| 3 | 1.0 | 0.000919 | 0.00985 |
| 3 | — | 0.000919 | 0.00985 |

Table 5.2. Velocity Estimation Means and Standard Deviations for MMAE

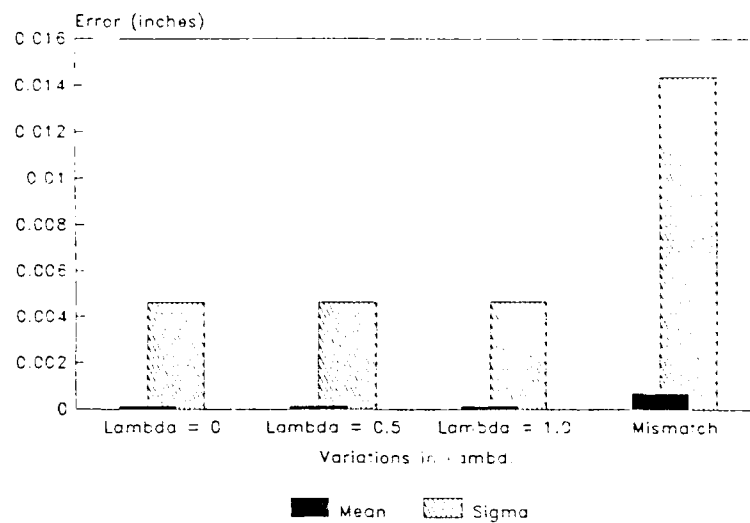


(a)

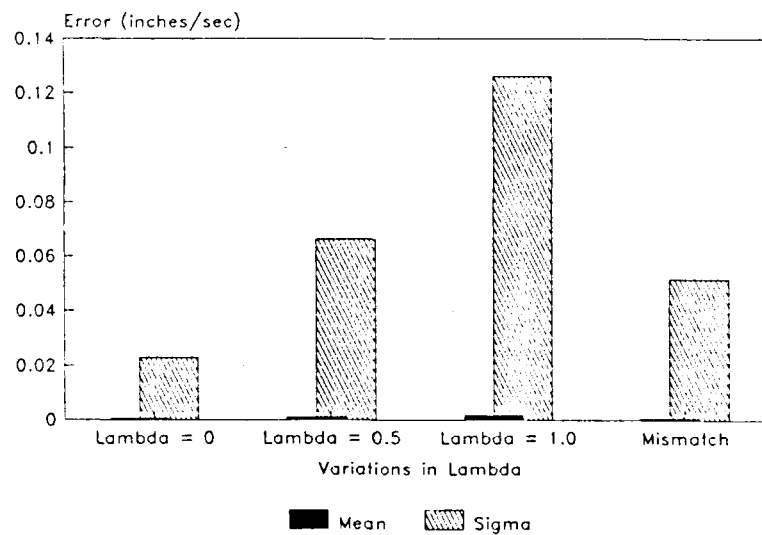


(b)

Figure 5.16. Position Estimation Means and Standard Deviations for MMAE, Node 1: (a) Position Estimates and (b) Velocity Estimates.

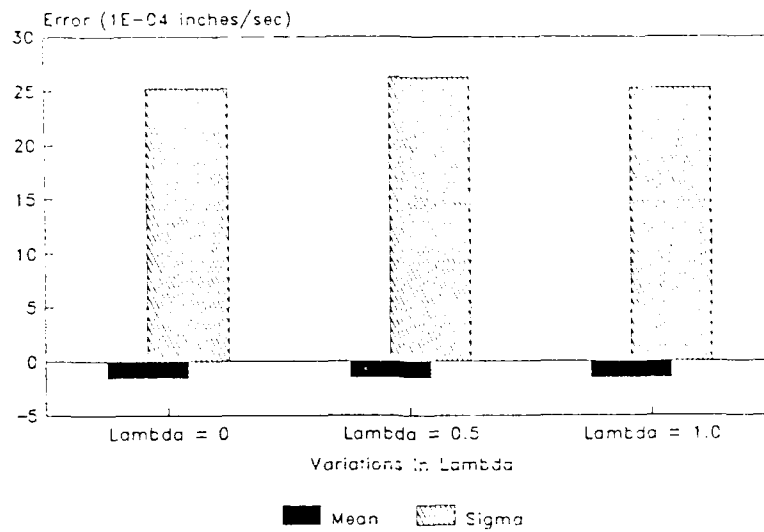


(a)

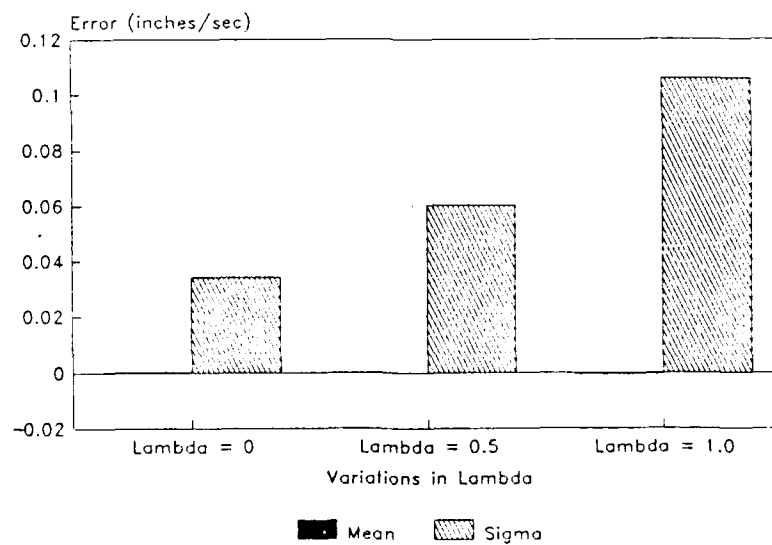


(b)

Figure 5.17. Position Estimation Means and Standard Deviations for MMAE, Node 1: (a) Position Estimates with Worst Case Analysis, (b) Velocity Estimates with "Worst Case" Analysis



(a)



(b)

Figure 5.18. Position Estimation Means and Standard Deviations for MMAE, Node 2: (a) Position Estimates and (b) Velocity Estimates.

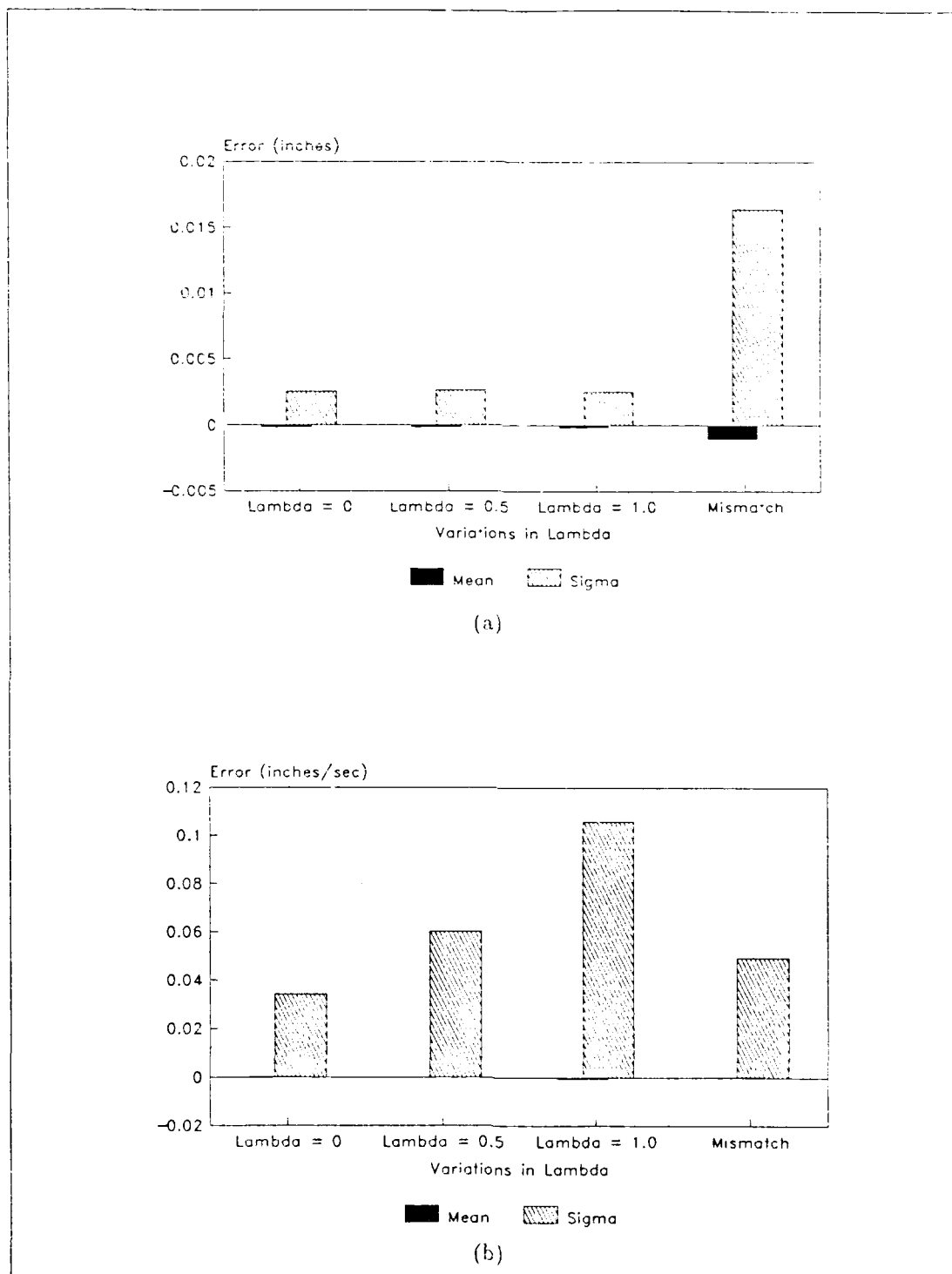
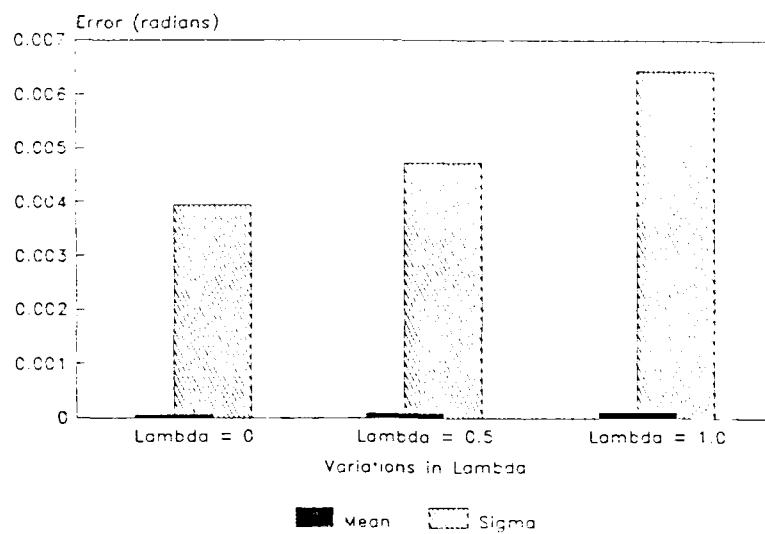
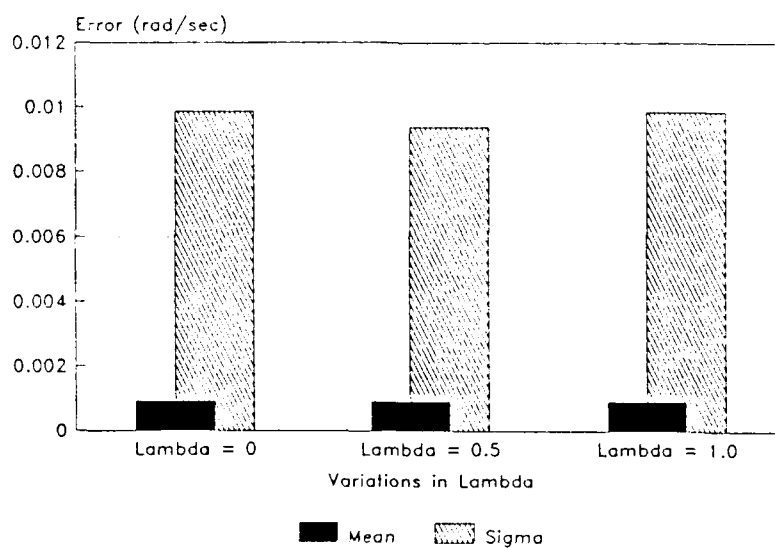


Figure 5.19. Position Estimation Means and Standard Deviations for MMAE, Node 2: (a) Position Estimates with Worst Case Analysis. (b) Velocity Estimates with "Worst Case" Analysis

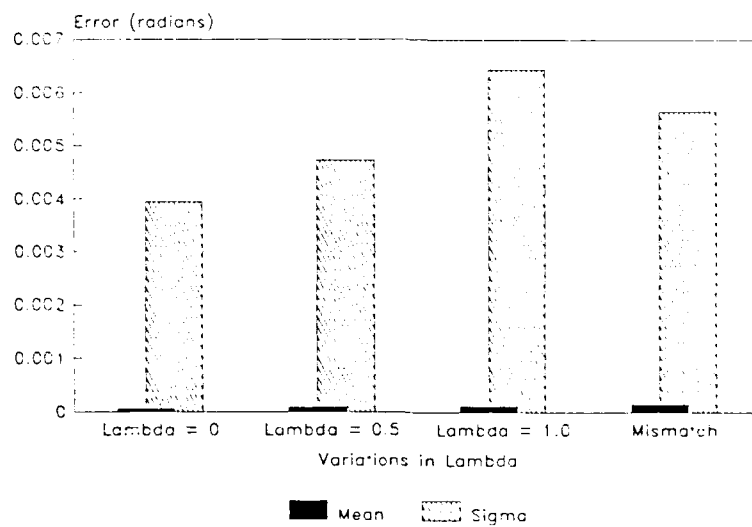


(a)

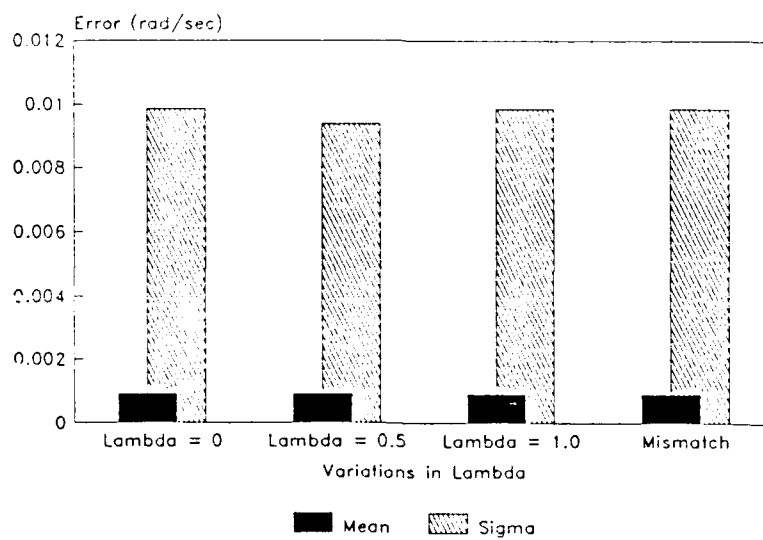


(b)

Figure 5.20. Position Estimation Means and Standard Deviations for MMAE, Node 3: (a) Position Estimates and (b) Velocity Estimates.



(a)



(b)

Figure 5.21. Position Estimation Means and Standard Deviations for MMAE, Node 3: (a) Position Estimates with Worst Case Analysis, (b) Velocity Estimates with "Worst Case" Analysis

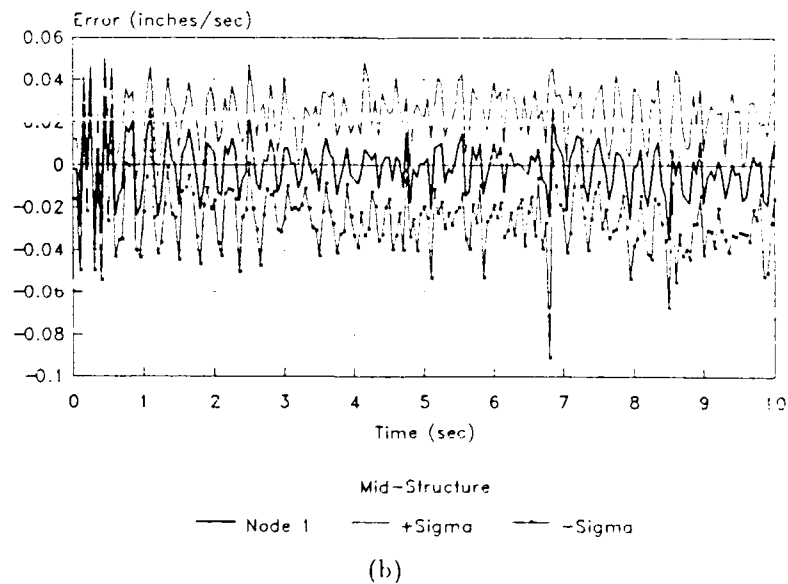
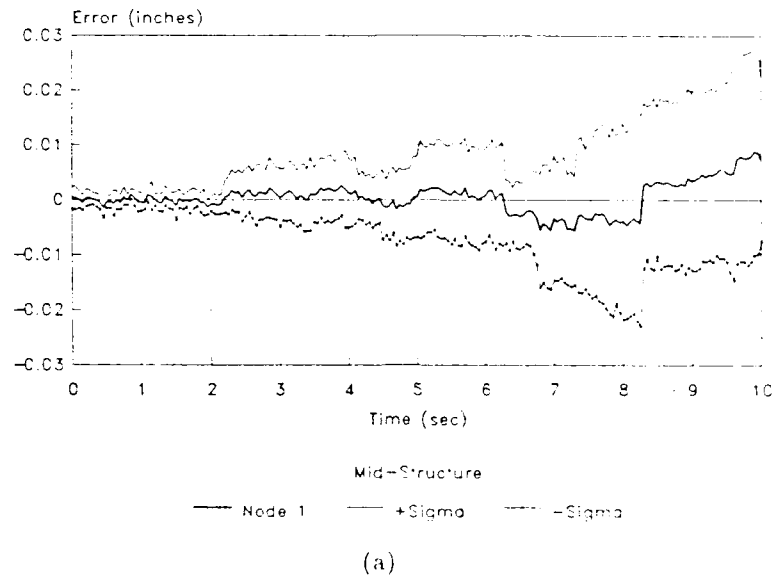


Figure 5.22 Moving-Bank Estimation Errors with Parameter/Filter Location Mismatch and Movement of the Bank. Node 1 - True Parameter at (7,6) and Filter Initially at (5,5). (a) Position and (b) Velocity Estimation Errors. $\lambda = 0.0$.

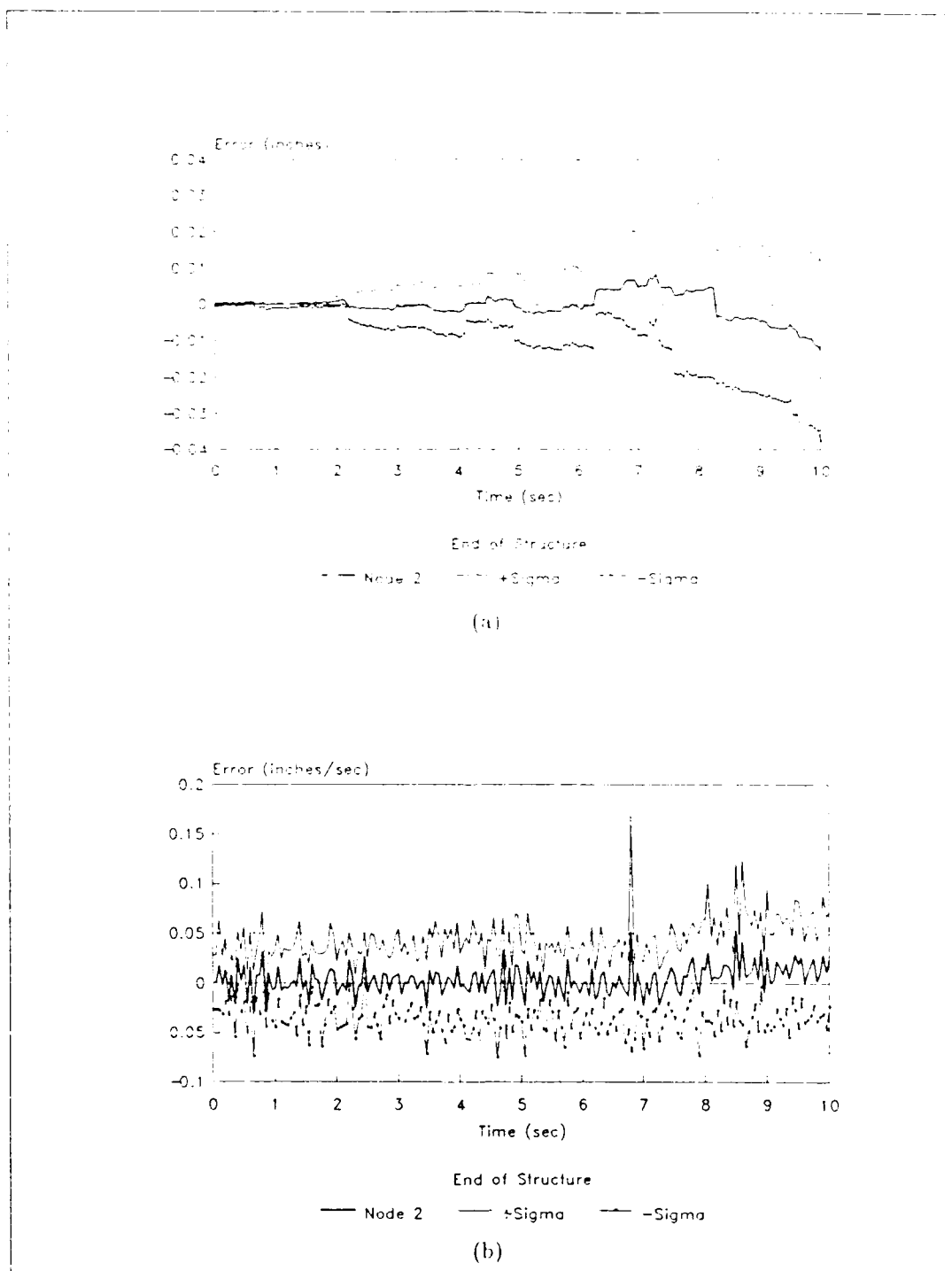
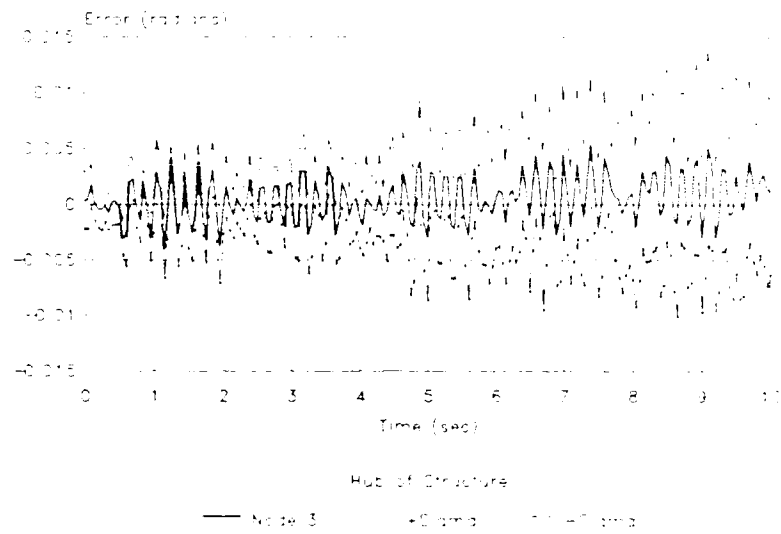
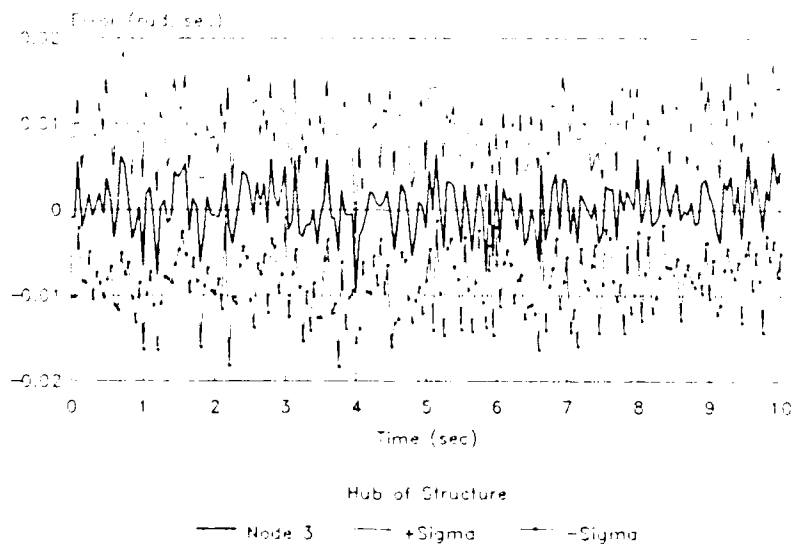


Figure 5.23. Moving-Bank Estimation Errors with Parameter/Filter Location Mismatch and Movement of the Bank, Node 2 - True Parameter at (7,6) and Filter Initially at (5,5). (a) Position and (b) Velocity Estimation Errors. $\lambda = 0.0$.



(a)



(b)

Figure 5.24. Moving-Bank Estimation Errors with Parameter/Filter Location Mismatch and Movement of the Bank. Node 3 - True Parameter at (7.6) and Filter Initially at (5.5). (a) Position and (b) Velocity Estimation Errors. $\lambda = 0.0$.

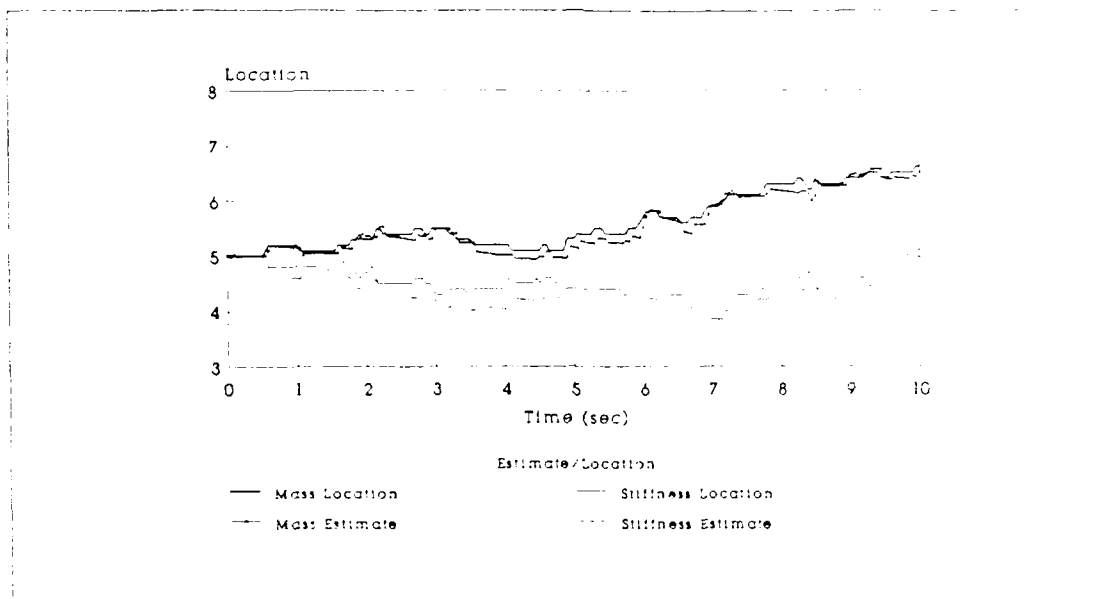


Figure 5.25. Parameter Estimation and Actual Filter Bank Location - True Parameter at (7.5) and Filter Initially at (5.5). $\lambda = 0.0$. Initial Probabilities $= \frac{1}{2}$.

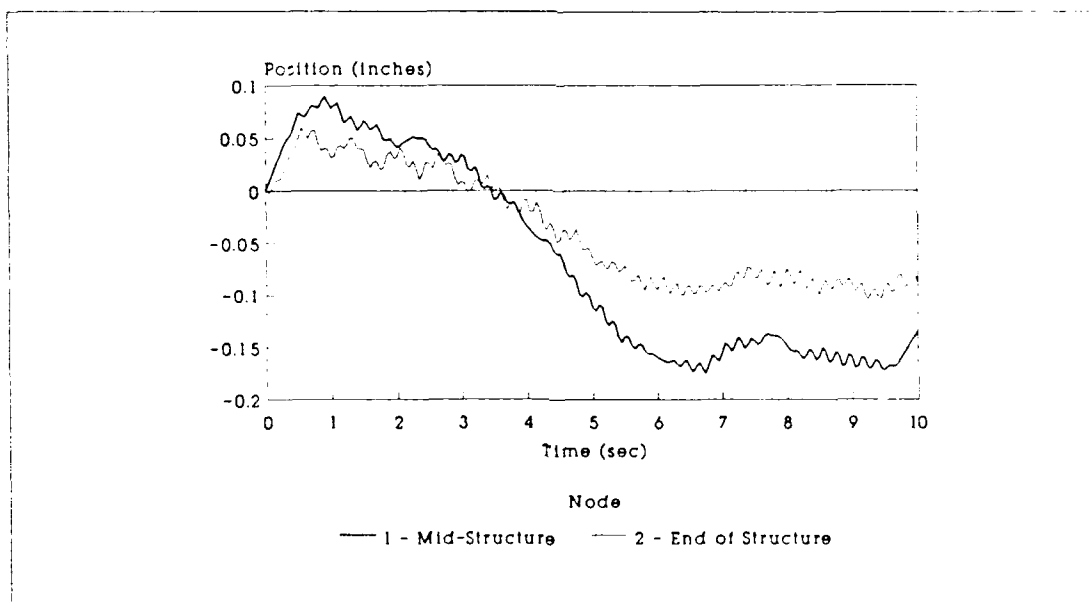


Figure 5.26. Mean Structure Positions

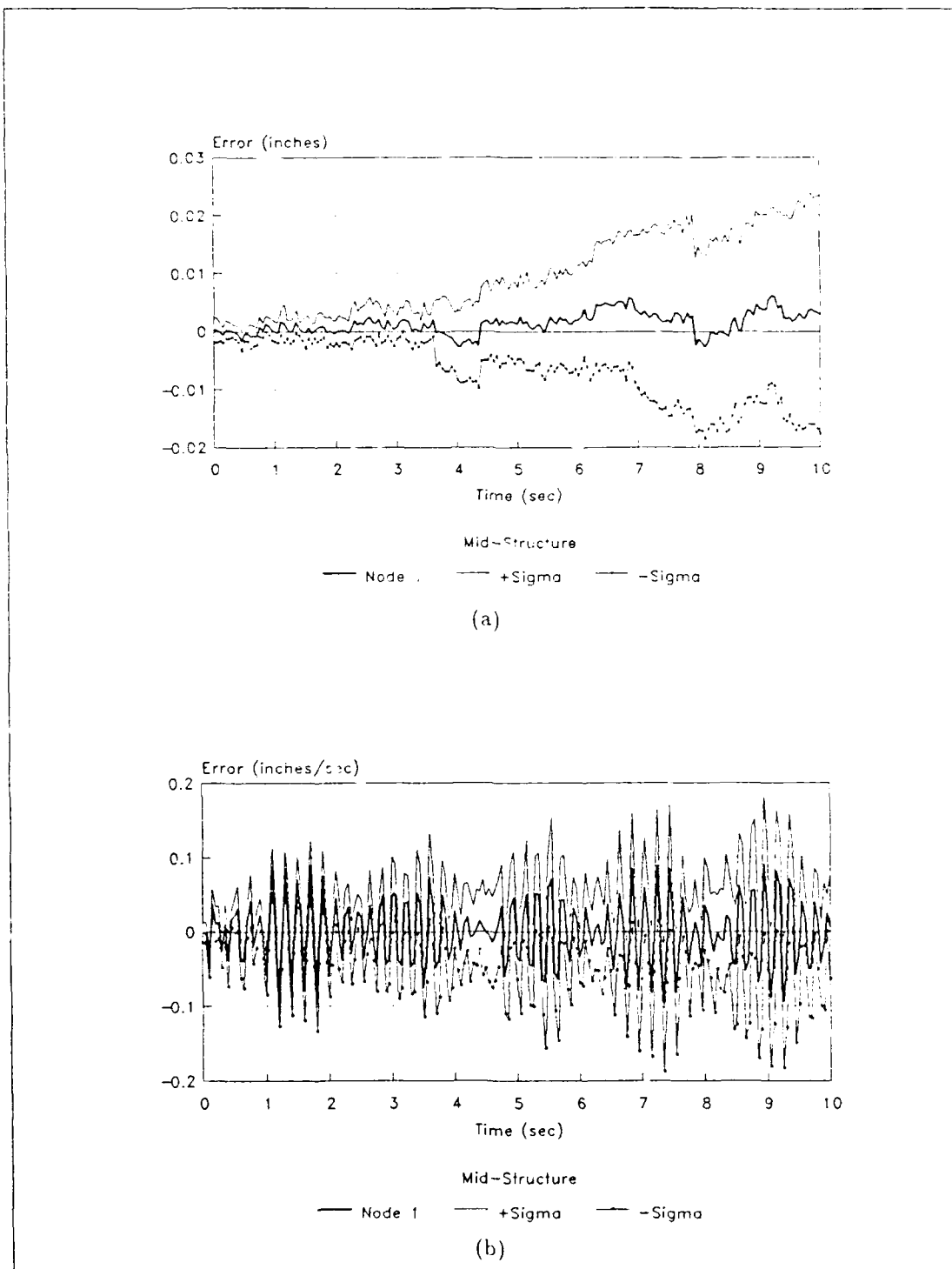


Figure 5.27. Moving-Bank Estimation Errors with Parameter/Filter Location Mismatch and Movement of the Bank, Node 1 - True Parameter at (7,6) and Filter Initially at (5,5). (a) Position and (b) Velocity Estimation Errors. $\lambda = 0.5$.

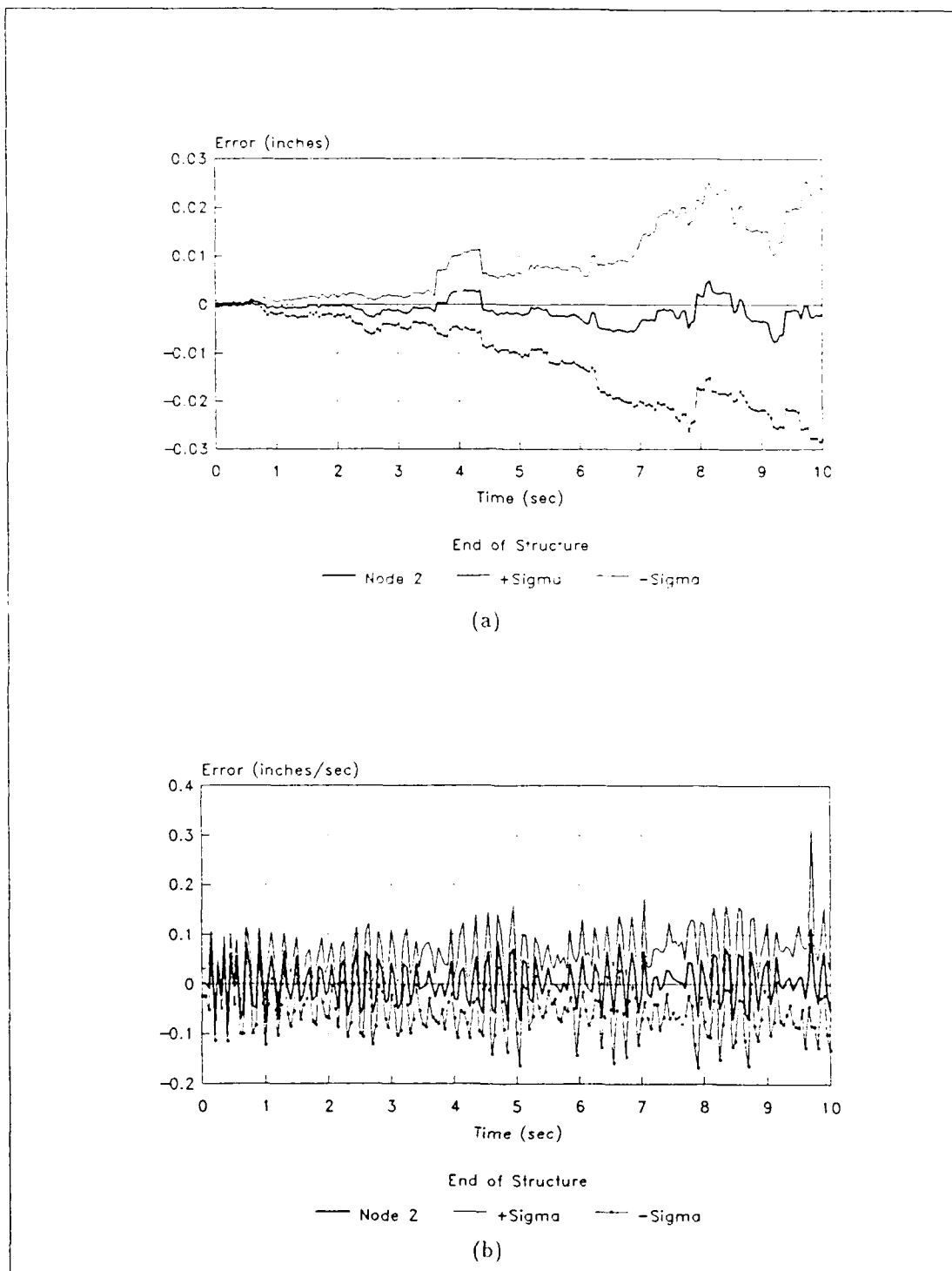


Figure 5.28. Moving-Bank Estimation Errors with Parameter/Filter Location Mismatch and Movement of the Bank, Node 2 - True Parameter at (7.6) and Filter Initially at (5.5). (a) Position and (b) Velocity Estimation Errors. $\lambda = 0.5$.

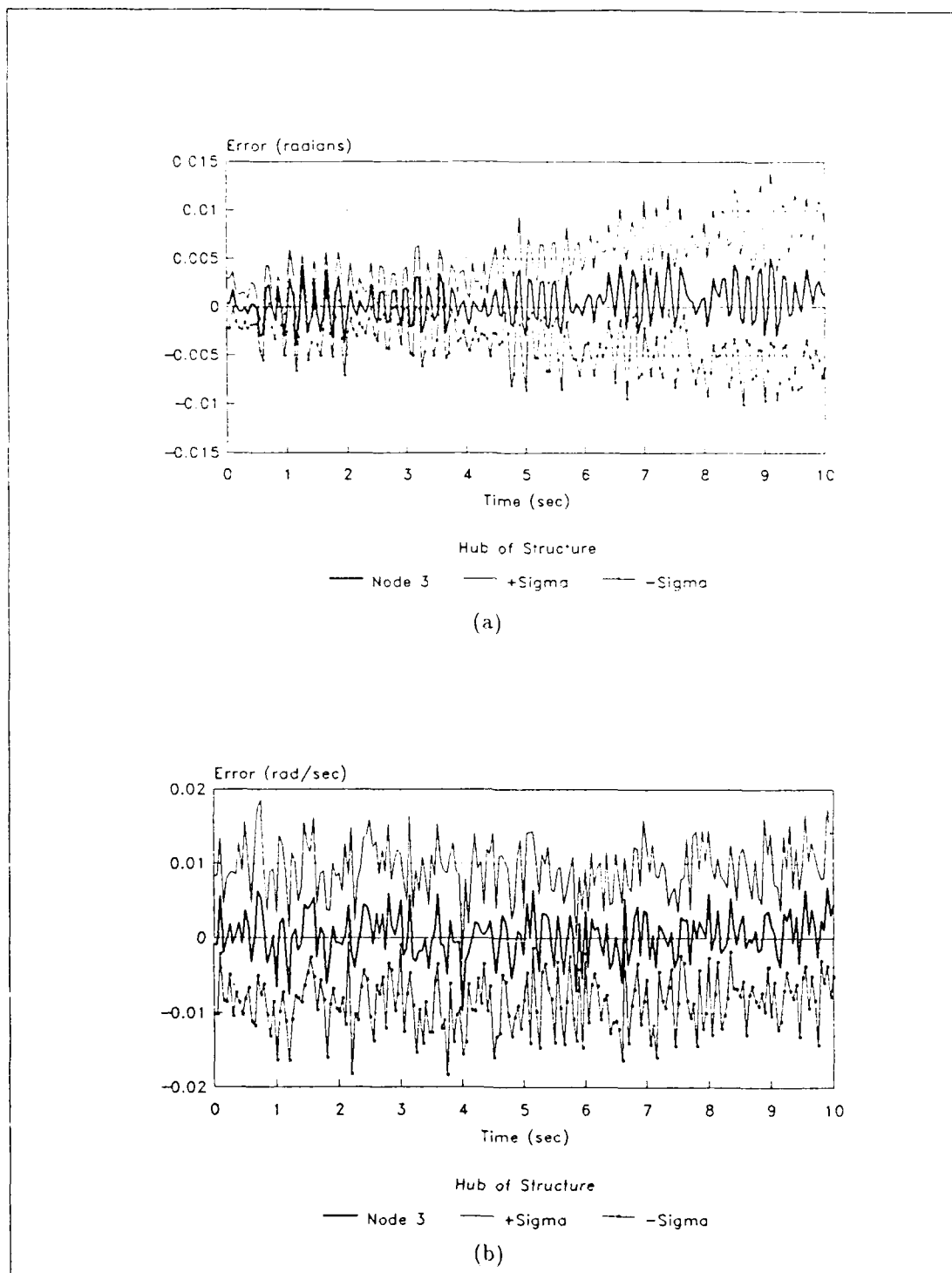


Figure 5.29. Moving-Bank Estimation Errors with Parameter/Filter Location Mismatch and Movement of the Bank, Node 3 - True Parameter at (7.6) and Filter Initially at (5.5). (a) Position and (b) Velocity Estimation Errors. $\lambda = 0.5$.

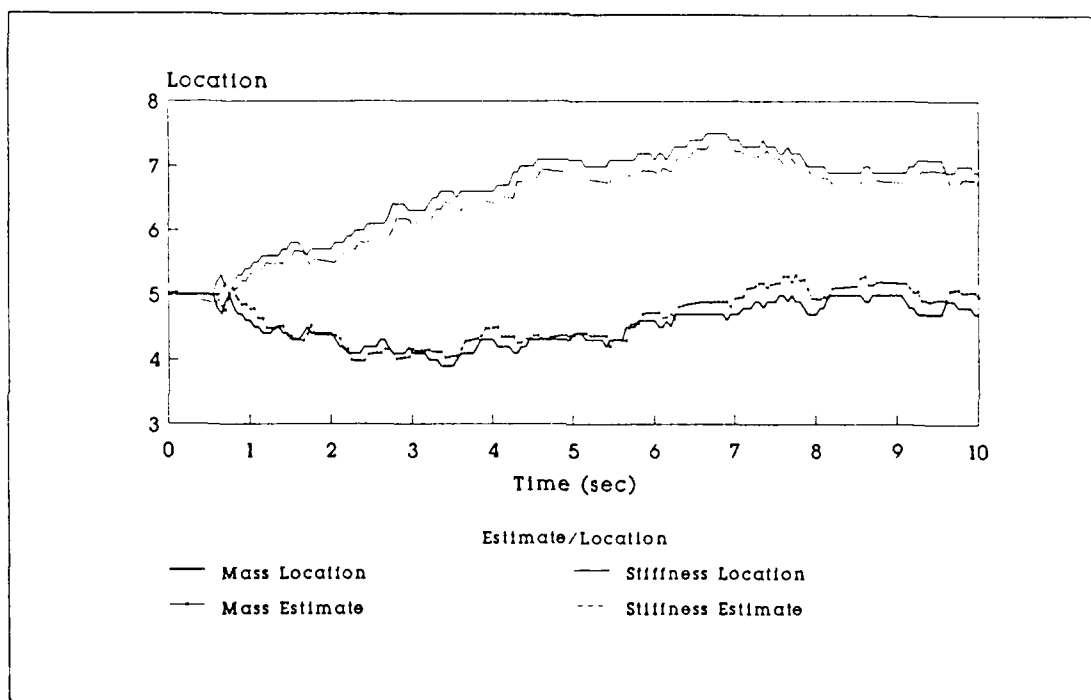


Figure 5.30. Parameter Estimation and Actual Filter Bank Location - True Parameter at (7,6) and Filter Initially at (5,5). $\lambda = 0.5$. Initial Probabilities = $\frac{1}{9}$.

5.3 Multiple Model Adaptive Controller Study

5.3.1 Duplication of Past Work. As with the MMAE study, the duplication of past work was performed in a somewhat subjective manner and the same limitations were observed. The same analysis was performed with the MMAC algorithm as with the MMAE algorithm and the following subsections present the MMAC study results.

5.3.2 MMAC Benchmark. The MMAC benchmark is determined the same way as for the MMAE benchmark and is equivalent to a single artificially informed LQG controller. The filter and parameter location are set to (7.6). The filter is an artificially informed, non-adaptive element of the moving-bank. The results of the benchmark are shown in Figures 5.31 through 5.35. Figure 5.35 shows the position of nodes 1 and 2 and contains the most critical information concerning the MMAC algorithm's ability to provide control of the structure. Also note that the hub actuator input, shown as the darker line in Figure 5.34, is zero after the initial dither during the first 0.5 seconds.

Figure 5.31 shows that the position estimate error is maintained below 0.002 inches for the period of the Monte Carlo analysis run. This is an improvement by a factor of three over the MMAE benchmark. The position estimate at node 2 is similarly improved. The velocity estimates and the node 3 position estimates do not show much change in their performance over the MMAE algorithm. Figure 5.34 shows the control inputs as determined by the MMAC algorithm.

The control signal is activated at the 0.5 second point of the run. The initial magnitudes are large but soon quell down as the controller gains control of the structure. As the process continues, the algorithm causes the control inputs to grow suddenly. This activity may be, in part, a phenomenon that is called bursting. By bursting the control inputs periodically, the controller is able to enhance parameter identification and thereby improve estimates of the states and the positions and velocities. The control input magnitudes remain at less than 5 lbs for most of the control run as shown in Figure 5.34.

5.3.3 Non-Adaptive Single-Controller Analysis with Variable λ . Figures 5.36 through 5.45 show the results of the control performance study with variations in λ . The only appreciable difference for the variations is in the initial control acquisition phase, between 0.5 and 1 second. The introduction of the higher frequencies obviously cause the control inputs to be considerably larger, thus causing a transient in the position and velocity estimate errors. Surprisingly, the state (shape) control for the case with $\lambda = 1$ is superior to the case where $\lambda = 0$.

5.3.4 Non-Adaptive Single Controller Worst Case Analysis. As with the MMAE study, a worst case MMAC analysis is performed with the bank in a misinformed, non-adaptive mode, i.e., the bank at position (5,5), the parameter at position (7,6), and the bank fixed. Figures 5.46 through 5.53 show the performance for this configuration. The MMAE worst case analysis showed that the estimation process suffered considerable degradation due to this configuration. The non-adaptive control worst case analysis shows that this configuration is a catastrophic one. The control input rises in an exponential manner from the initial control turn-on transient. The position and velocity estimation errors grow in the same fashion. If this were to be allowed to continue the structure would surely self-destruct. Adaptivity is thus seen to be critical for control of this system. An increase in λ does provide some improvement in performance but still leads to probable catastrophic behavior. The results of the benchmark, λ variations, and worst case analysis are summarized in Tables 5.3 and 5.4. Figures 5.54 through 5.59 present this data graphically with the first three illustrating the effect of λ variations. The last three figures present the same data with the "worst case" included and show temporal average results over the simulation time. The meaningful information contained in these latter graphs is the unstable behavior of the system under the "worst case" mismatched conditions.

5.3.5 Moving-Bank MMAC Analysis. The next performance analysis of the MMAC algorithm was to determine the ability of the bank to move within the filter space when the initial parameter estimation and filter location differ from the true parameter location, and to investigate

its capacity to maintain stable control of the structure. The simulation was initiated the same as for the worst case analysis, except that the bank was allowed to move. The probabilities of all the filters in the bank were initialized to $\frac{1}{9}$ and the lower limit of the probabilities was set to 0.05. Residual monitoring was used for the movement logic and the move threshold set to 0.25. The results of these simulations are shown in Figures 5.60 through 5.81. These figures represent four sets of figures for four different λ values: 0.0, 0.25, 0.5, and 1.0. The values of λ were chosen on an ad hoc basis. The value of 0.25, not used in the MMAE study, was chosen to assure that no performance indicator was missed. After performing numerous Monte Carlo runs, the decision to use plots such as Figure 5.35 to show only the mean position of the structure was made since the additional data of \pm standard deviation was not informative to the degree that necessitated their presentation, i.e., they were very small.

While the "worst case" study and the moving-bank study both started the filter at a parameter location different from the true parameter location, the ability of the bank to move and locate the true parameter proved to be essential. The moving-bank MMAC study showed that the filter bank could perform as well as the artificially informed non-adaptive single-filter controller. Conversely, the non-adaptive mismatched filter performed catastrophically, with the structure becoming unstable.

The performance seen in these plots indicates that there is no dramatic degradation in adaptive control as λ is increased from zero to one. Thus, there would be little benefit to be gained by increasing the number of states of the filter model beyond the current six.

5.4 MMAC Disturbance Rejection Study

With the data just presented available, a disturbance rejection study was performed. The intent of this study is to determine whether the controller can maintain control of the structure in the face of both the model mismatch and an unanticipated external disturbance. For this study,

note that $\lambda = 0.0$. The ability to reject a disturbance is essential for a control system operating in an environment perturbed by both man and nature. The MMAC study was reworked with a modification to the control inputs. At the 4-second point of each run, the dither was turned on again for 0.5 seconds with a magnitude of 50 versus 10 for the initial dither. Closed-loop control was maintained, as opposed to no control inputs being applied during the initial 0.5 second dither period. Figures 5.84 through 5.89 show the results of this study. The results of the disturbed system follow a pattern similar to that seen with the previous MMAC results. The velocities of nodes 1 and 2, and the position of the hub, node 3, are greatly affected by any disturbances, be they the initial dither or a disturbance during the control process. The control inputs in Figure 5.87 show that the structure is brought under control in less than 0.5 seconds after the disturbance is removed. In Figure 5.87(b), the controller has added its own control inputs to the disturbance signal and remains high for a short time after the disturbance ends. After the disturbance was applied, the controller continued to perform well and maintained control of the structure although the disturbance has increased the amount of "vibration" about the zero null position for both nodes 1 and 2. The position and velocity estimation errors returned back to their pre-disturbance levels after about 1.5 seconds after the disturbance was removed. The previous results for the moving-bank MMAC with $\lambda = 0$ should be compared to these results. The controller rejected the disturbance well, and this provides insights into its ability to handle system disturbances.

5.5 *Number of Monte Carlo Analysis Runs*

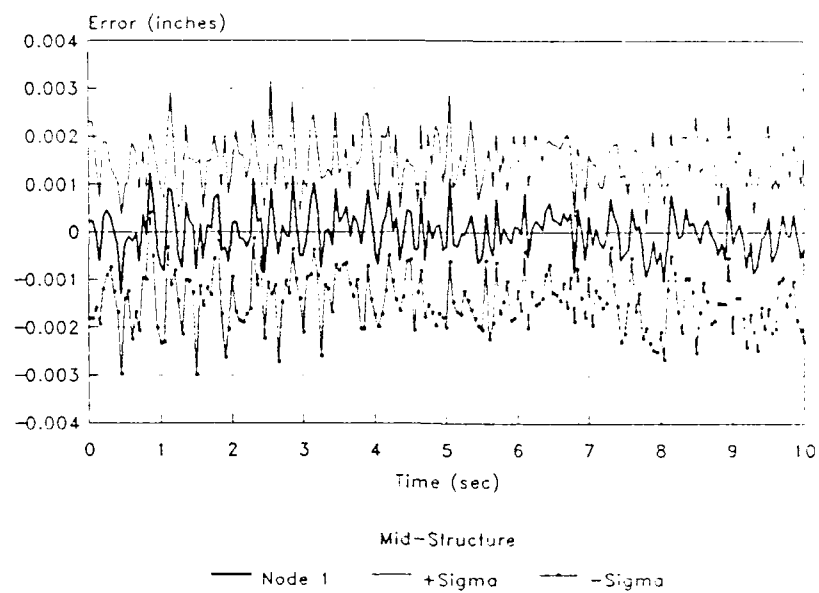
Several Monte Carlo analysis were performed in which the number of runs was significantly increased. The results did not justify the added expense of increased computation times. Figure 5.90 is an example of a 100-run Monte Carlo analysis. This is a repeat of the disturbance rejection study performed in the previous section. While the plots shown in Figure 5.84 and 5.90 are not identical, the general characteristics are similar and provide the same fundamental information. The velocity estimation error does show that the post-disturbance transient is somewhat longer

than for the 100-run Monte Carlo analysis. More significantly, the structure remains under control. Obviously, after 100 runs, the additional data smooths the means and variances. This comparison of 10 and 100-run Monte Carlo analyses provides corroboration of the validity of the results given in this chapter which were performed with 10-run Monte Carlo analysis.

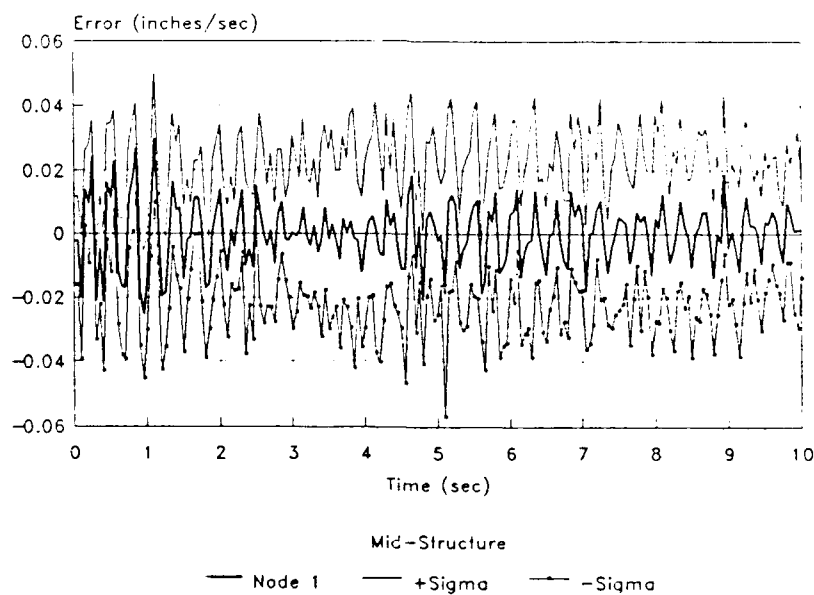
5.6 Summary

The results presented in this chapter covered the performance of two algorithms: the MMAE and MMAC algorithms. The estimation by the moving-bank MMAE of the positions and velocities of the nodes of interest was not drastically affected by the presence of higher order modes of the truth model. When faced with the lack of true parameter information, the single non-informed filter performed poorly. The problem of a non-adaptive fixed filter/controller was even more clearly demonstrated in the case of the MMAC study, in which the parameter mismatch caused instability of the closed loop system.

The performance of the MMAC to estimate the positions and velocities of the nodes was improved over the MMAE performance. The structure was also effectively brought back to the null position. The moving-bank MMAC preformed nearly as well as the benchmark and maintained adequate control of the structure. The disturbance rejection showed that the controller could maintain control of the structure in the face of a strong short duration disturbance signal.



(a)



(b)

Figure 5.31. Benchmark Estimation Errors with Single-LQG-Controller, Node 1 - True Parameter and Filter at Mass = 7 and Stiffness = 6. (a) Position and (b) Velocity Estimation Errors. $\lambda = 0$.

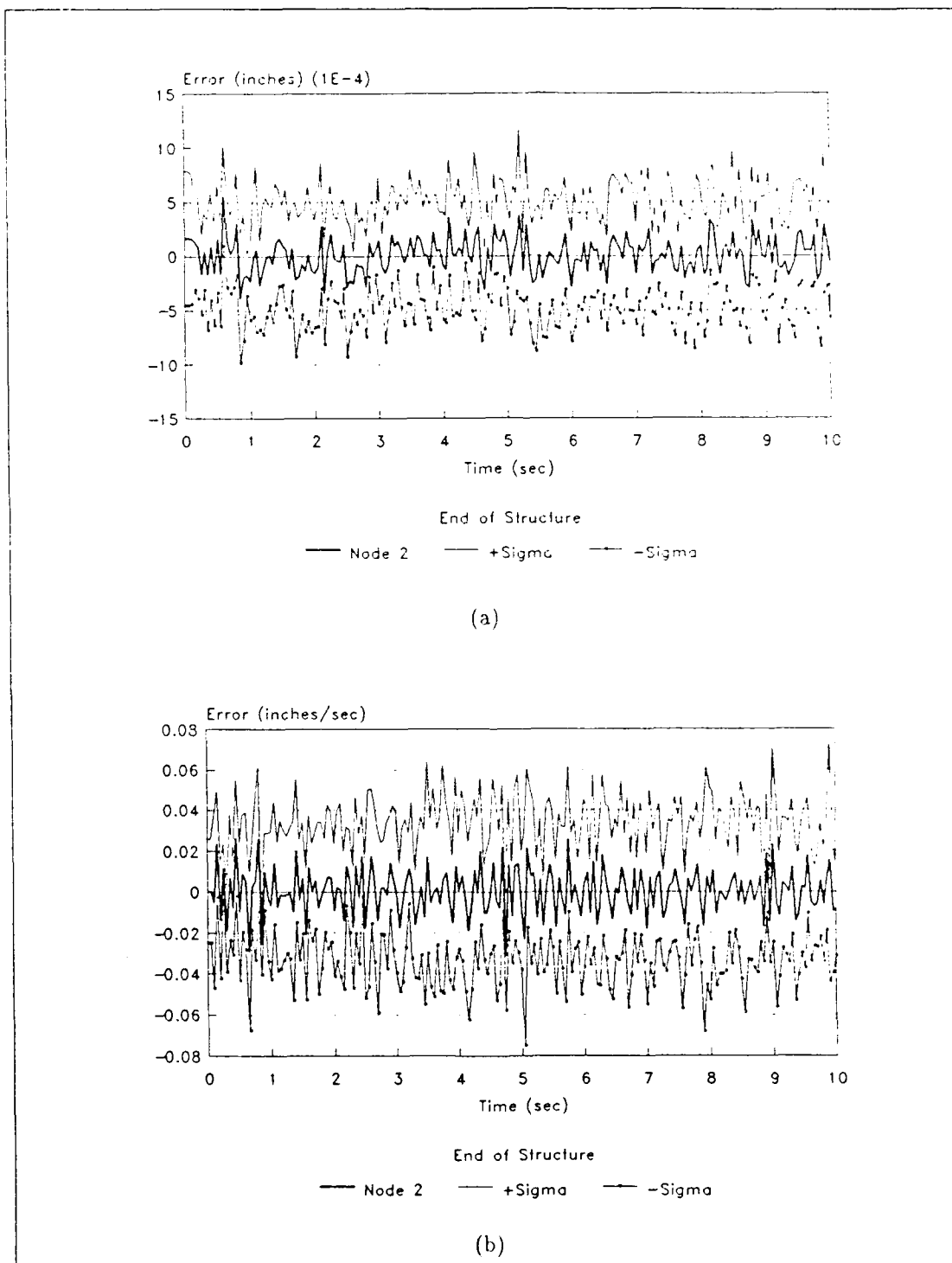
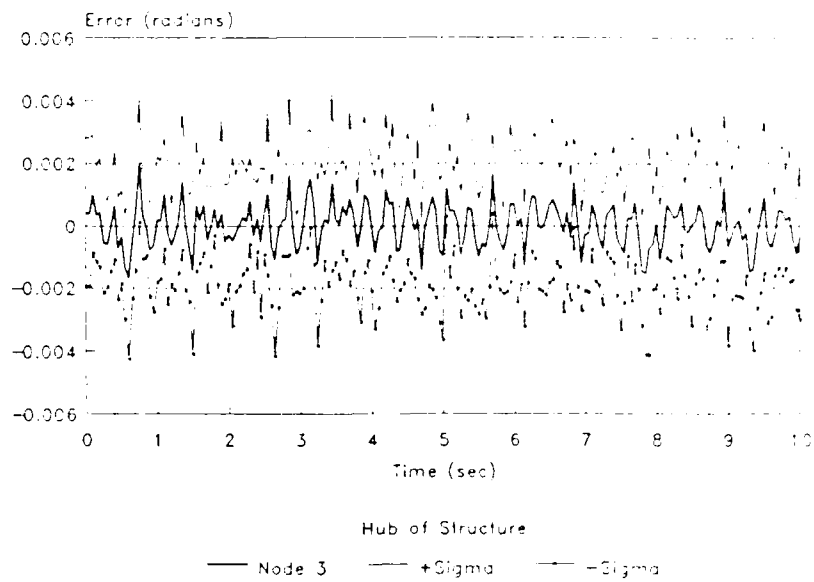
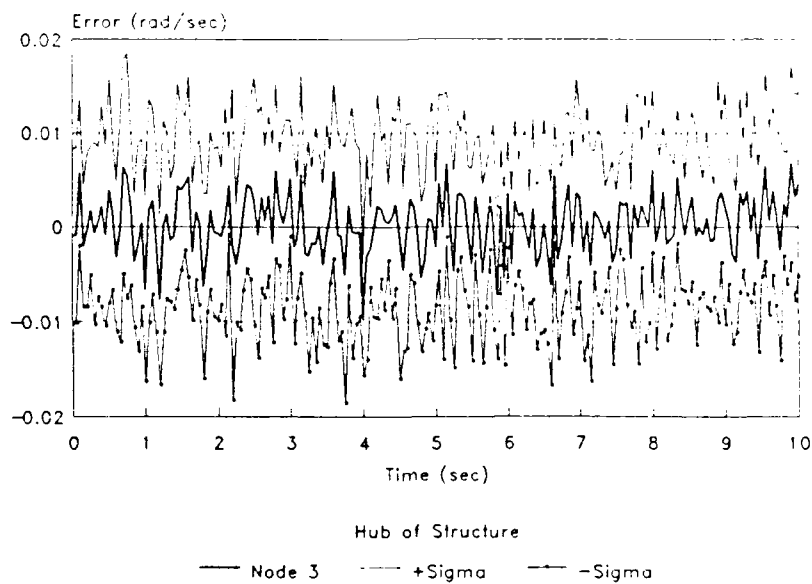


Figure 5.32. Benchmark Estimation Errors with Single-LQG-Controller, Node 2 - True Parameter and Filter at Mass = 7 and Stiffness = 6. (a) Position and (b) Velocity Estimation Errors. $\lambda = 0$.



(a)



(b)

Figure 5.33. Benchmark Estimation Errors with Single-LQG-Controller, Node 3 - True Parameter and Filter at Mass = 7 and Stiffness = 6. (a) Position and (b) Velocity Estimation Errors. $\lambda = 0$.

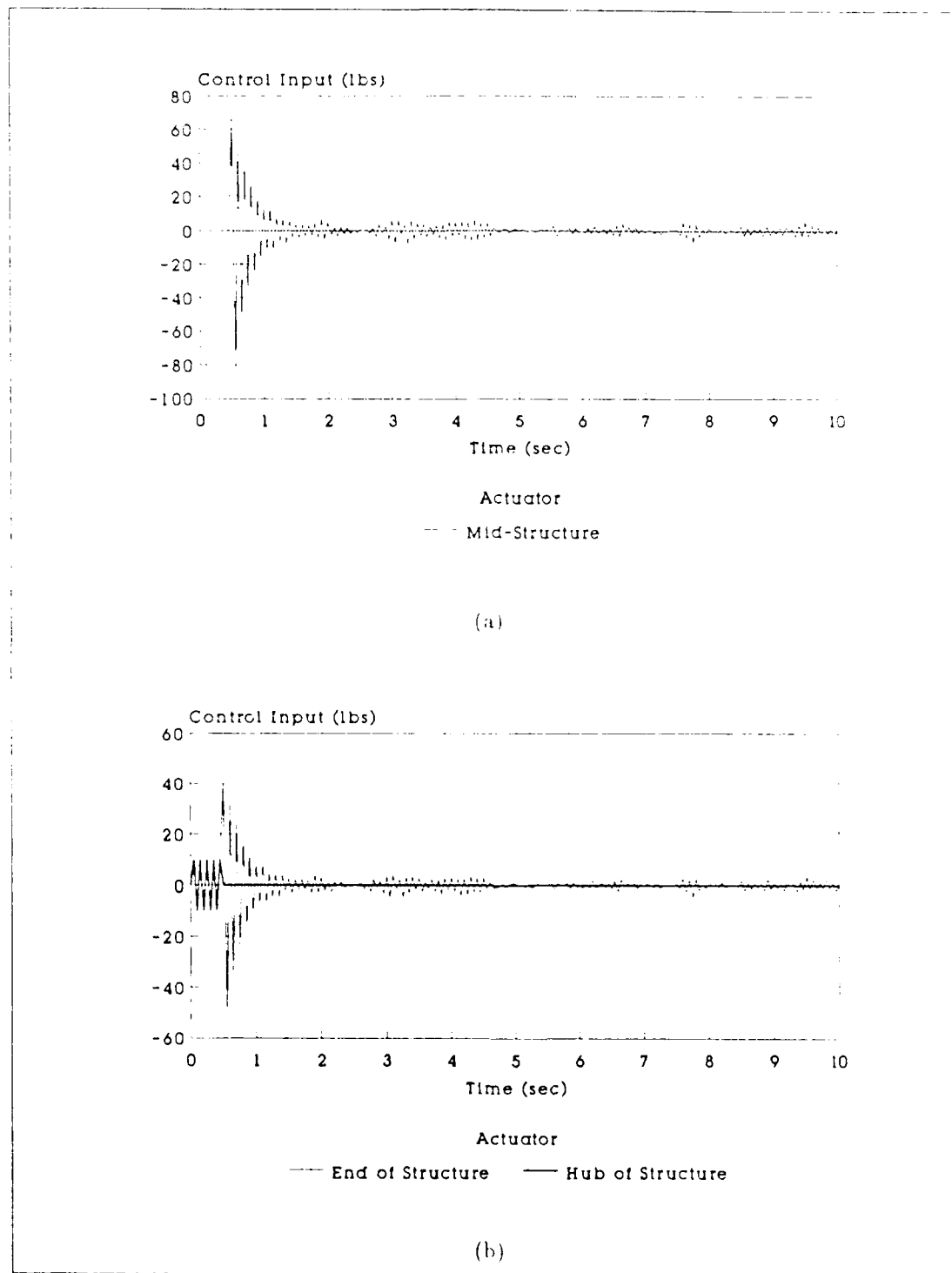
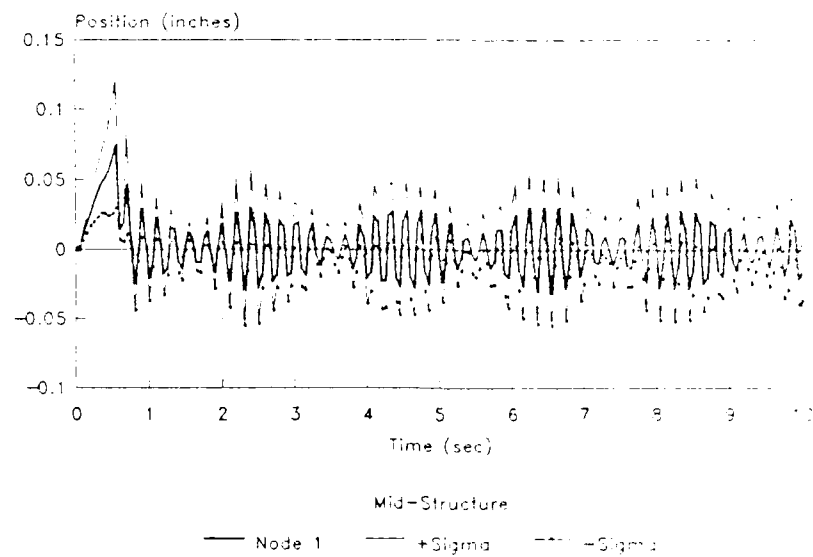
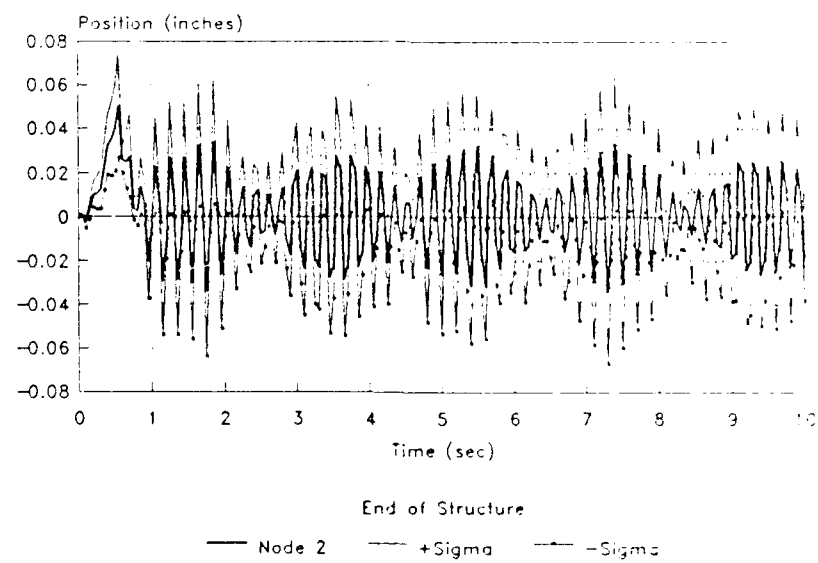


Figure 5.34. Control Inputs for the MMAC Benchmark. (a) Mid-structure actuator, (b) End of structure and hub of structure actuator.

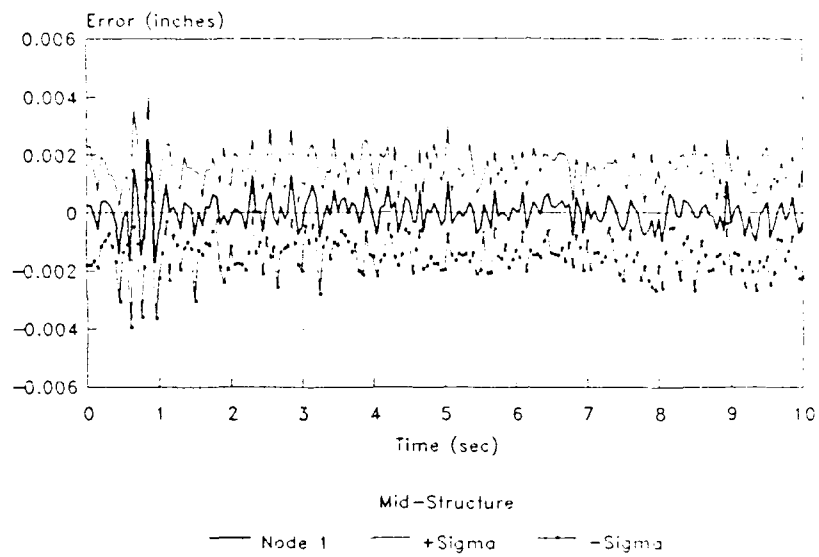


(a)

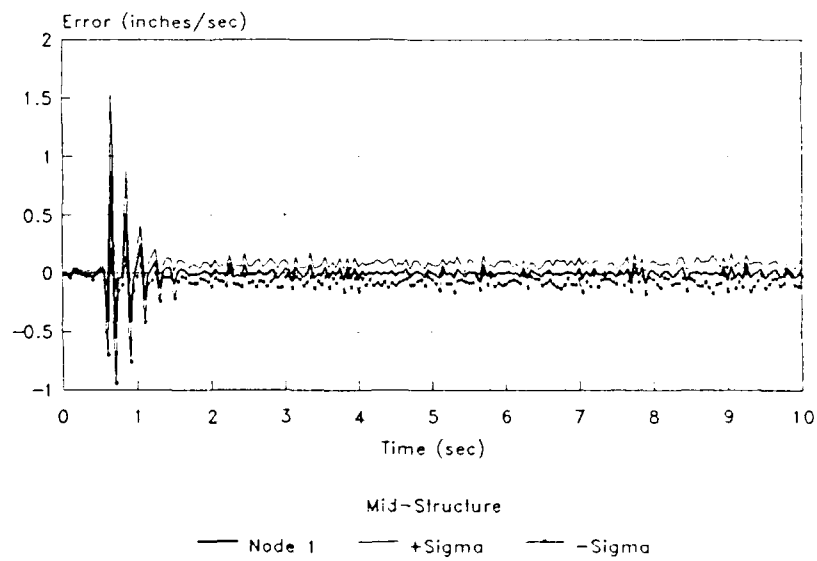


(b)

Figure 5.35. Structure Positions with MMAC and $\lambda = 0.0$. (a) Node 1 position mean and variances and (b) Node 2 position mean and variances.

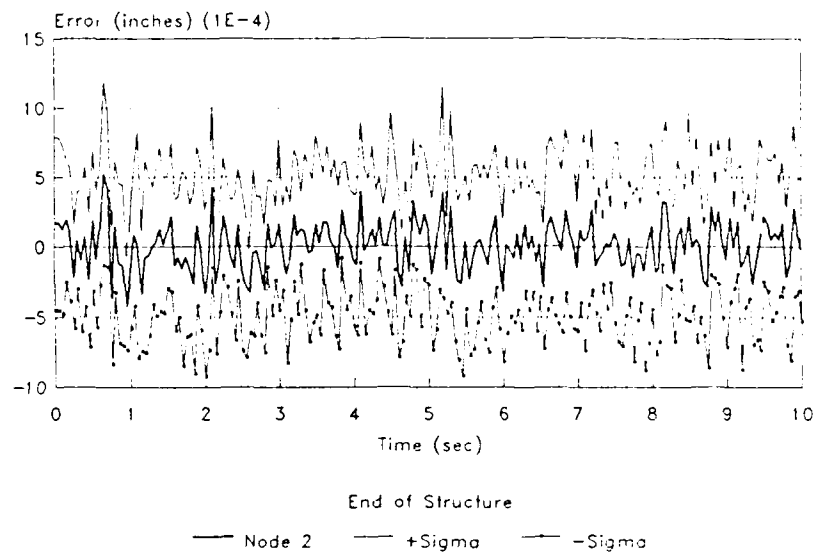


(a)

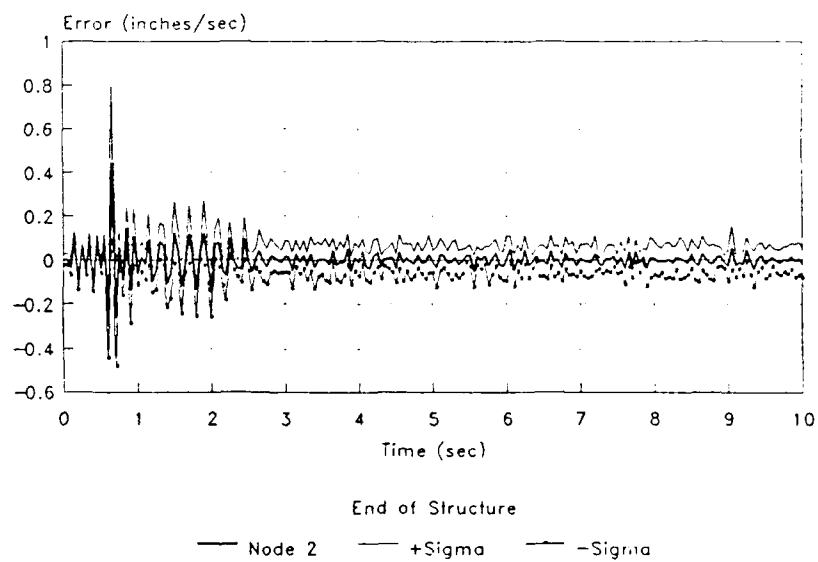


(b)

Figure 5.36. Estimation Errors with Single-LQG-Controller, Node 1 - True Parameter and Filter at Mass = 7 and Stiffness = 6. (a) Position and (b) Velocity Estimation Errors. $\lambda = 0.5$.

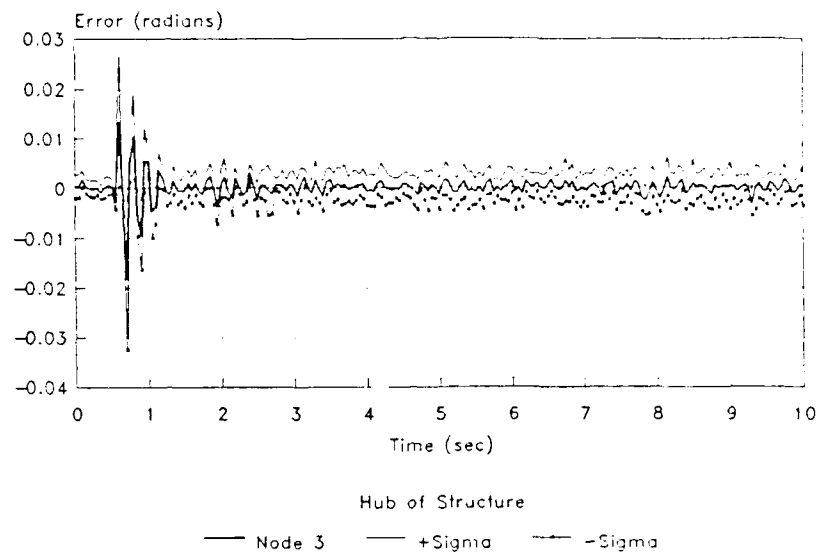


(a)

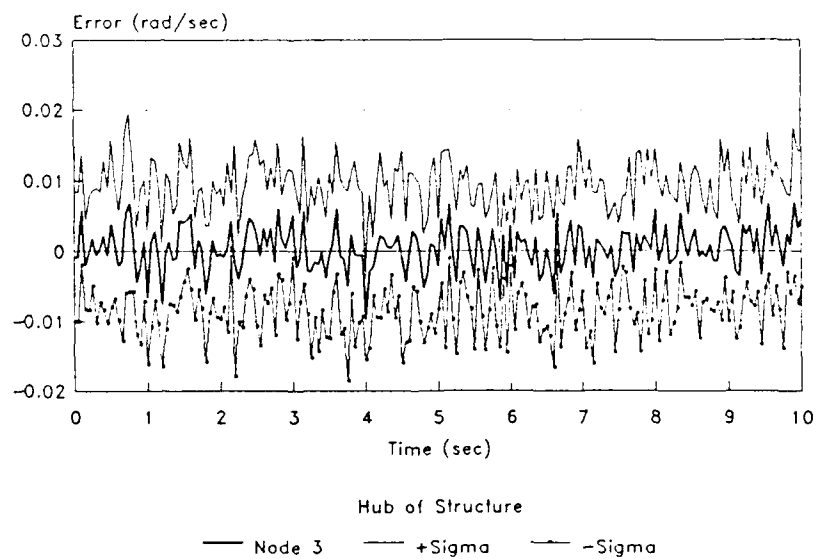


(b)

Figure 5.37. Estimation Errors with Single-LQG-Controller, Node 2 - True Parameter and Filter at Mass = 7 and Stiffness = 6. (a) Position and (b) Velocity Estimation Errors $\lambda = 0.5$.

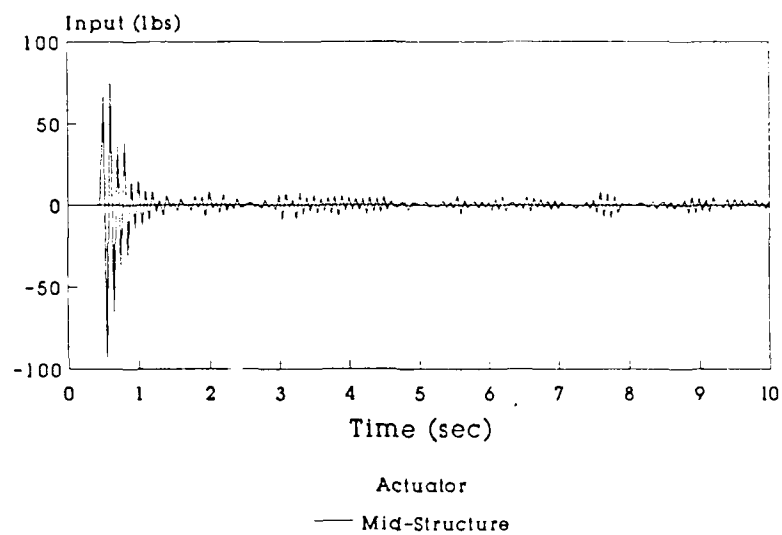


(a)

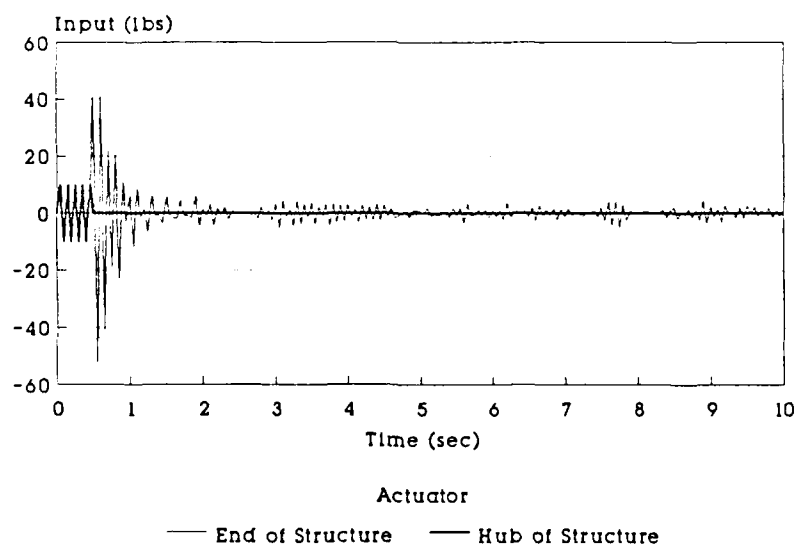


(b)

Figure 5.38. Estimation Errors with Single-LQG-Controller, Node 3 - True Parameter and Filter at Mass = 7 and Stiffness = 6. (a) Position and (b) Velocity Estimation Errors. $\lambda = 0.5$.

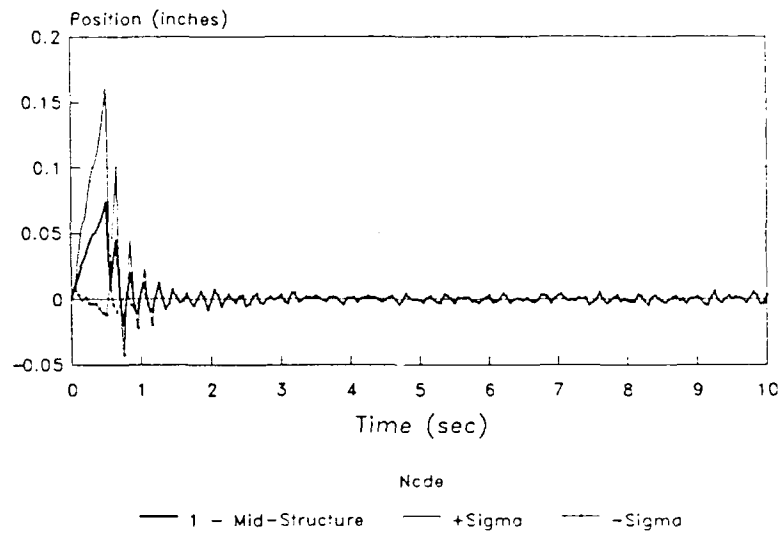


(a)

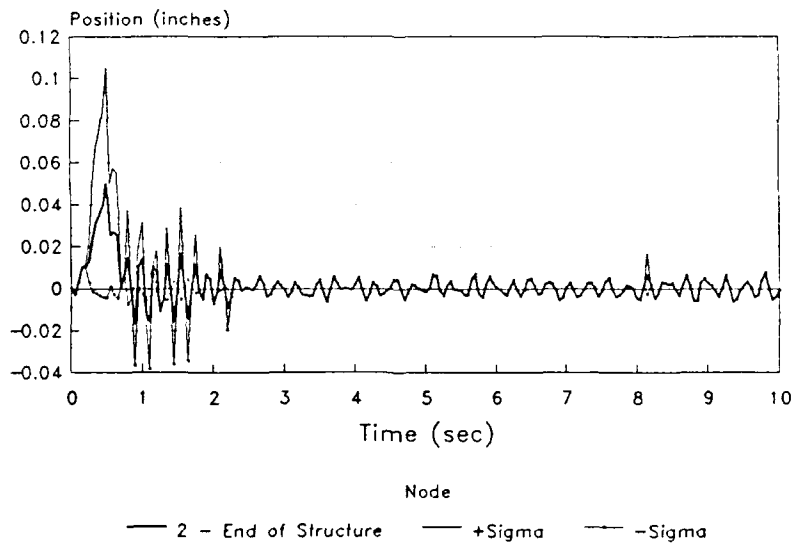


(b)

Figure 5.39. Control Inputs for MMAC with $\lambda = 0.5$. (a) Mid-structure actuator, (b) End of structure and hub of structure actuators.

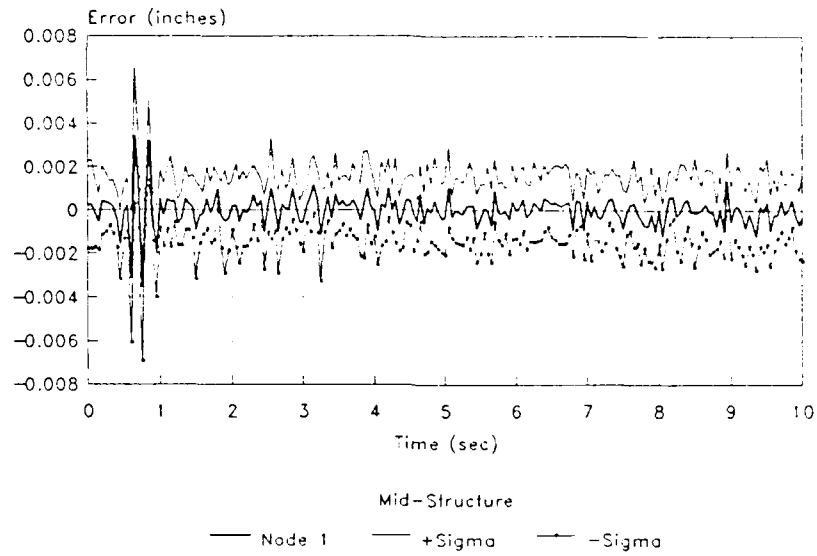


(a)

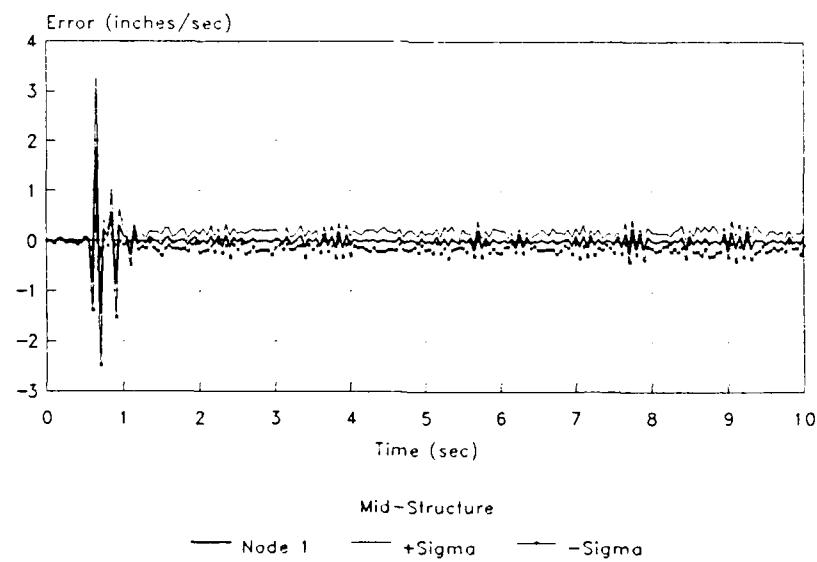


(b)

Figure 5.40. Structure Positions with MMAC and $\lambda = 0.5$. (a) Node 1 position mean and variances and (b) Node 2 position mean and variances.

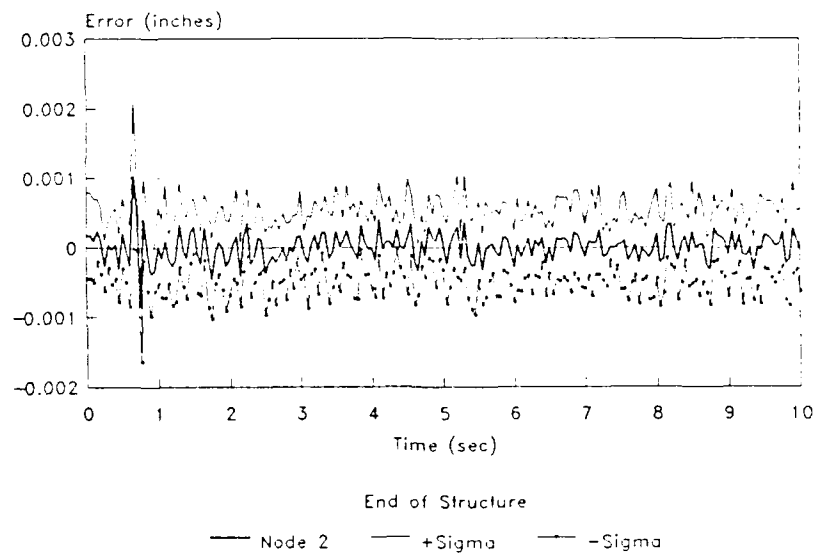


(a)

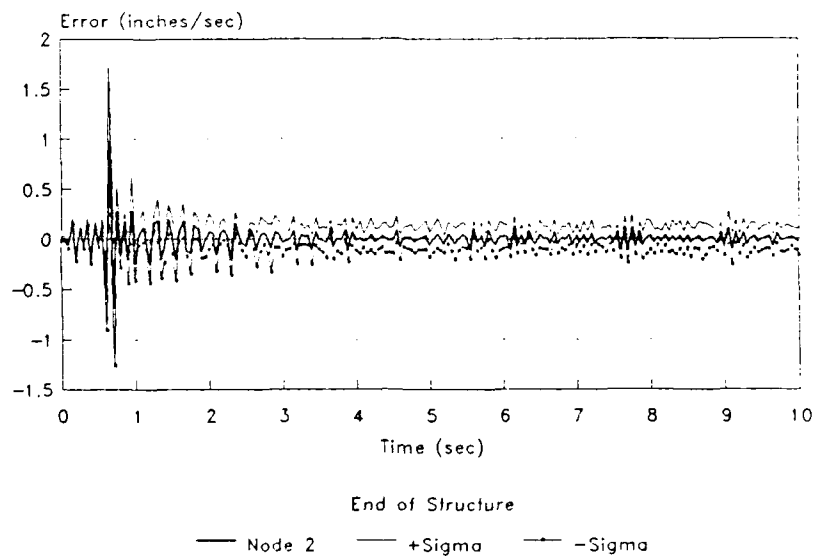


(b)

Figure 5.41. Estimation Errors with Single-LQG-Controller, Node 1 - True Parameter and Filter at Mass = 7 and Stiffness = 6. (a) Position and (b) Velocity Estimation Errors. $\lambda = 1.0$.

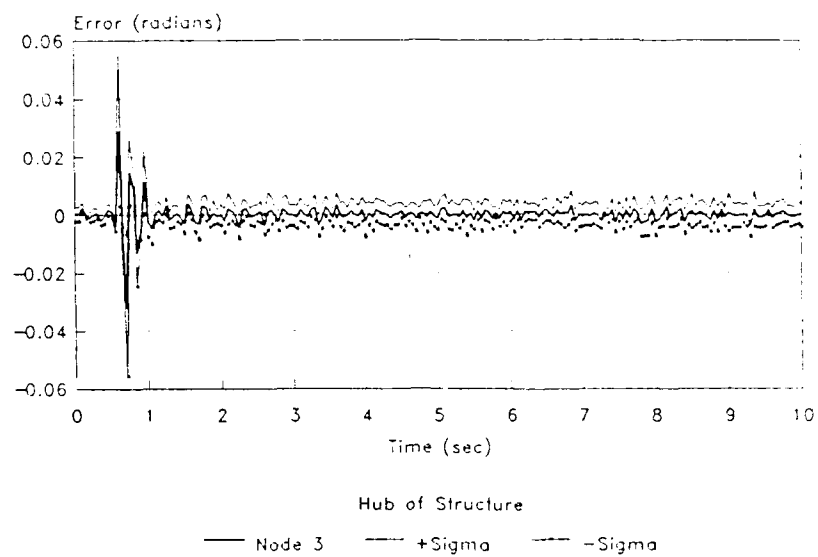


(a)

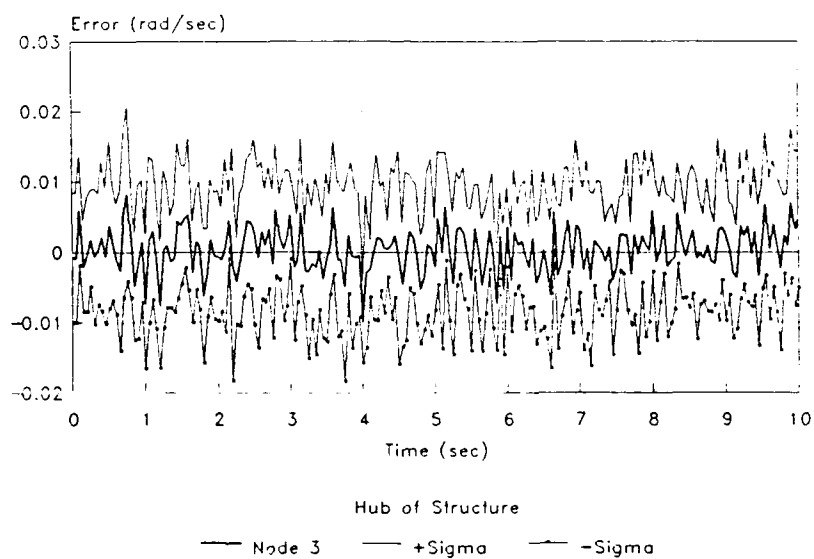


(b)

Figure 5.42. Estimation Errors with Single-LQG-Controller, Node 2 - True Parameter and Filter at Mass = 7 and Stiffness = 6. (a) Position and (b) Velocity Estimation Errors. $\lambda = 1.0$.

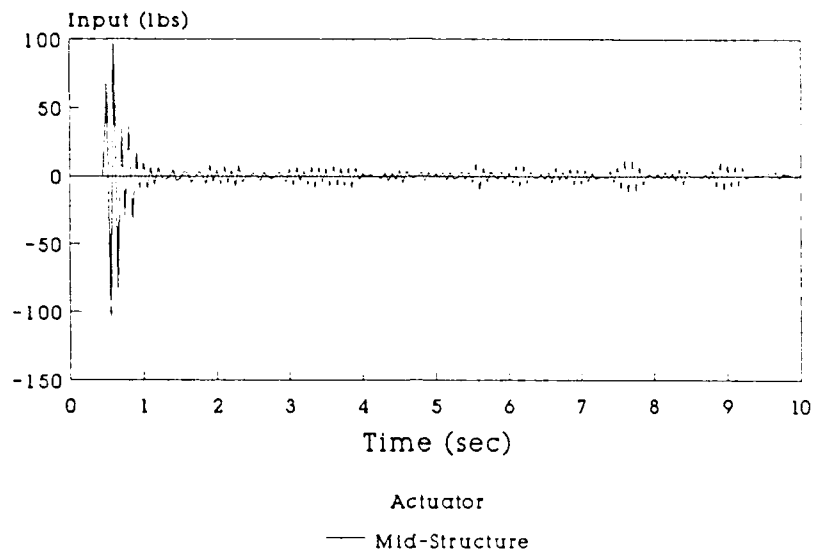


(a)

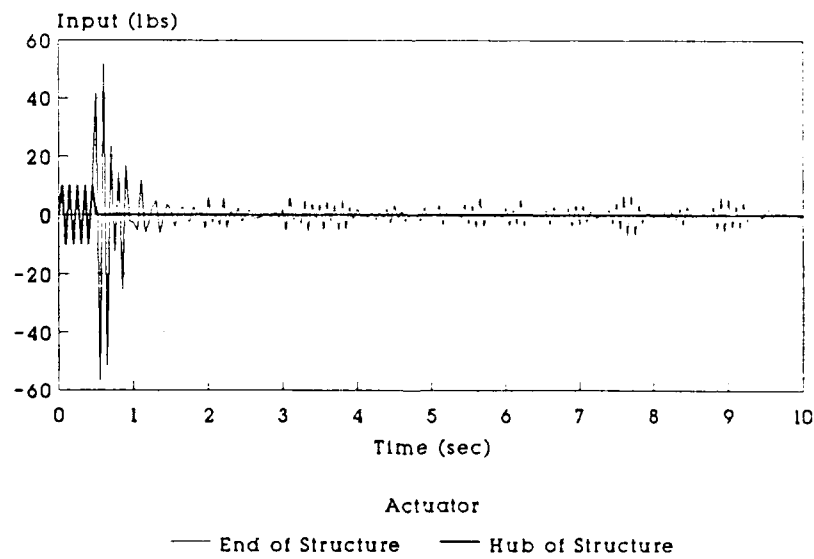


(b)

Figure 5.43. Estimation Errors with Single-LQG-Controller, Node 3 - True Parameter and Filter at Mass = 7 and Stiffness = 6. (a) Position and (b) Velocity Estimation Errors. $\lambda = 1.0$.

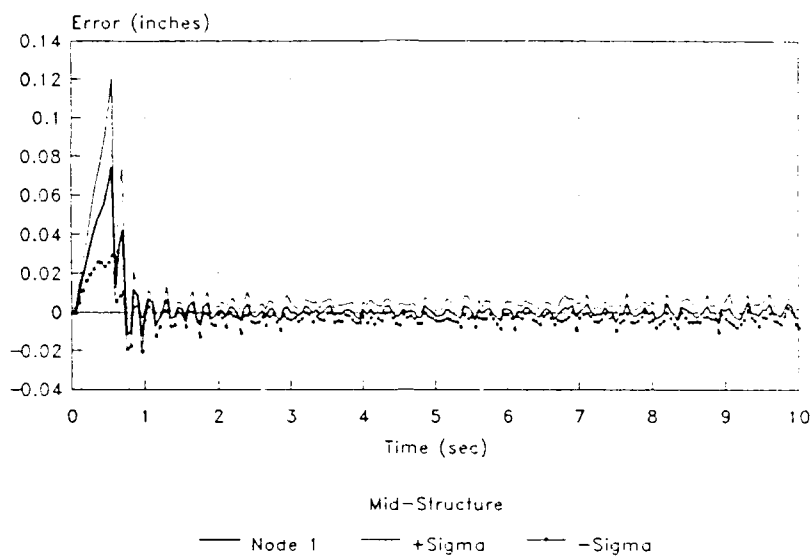


(a)

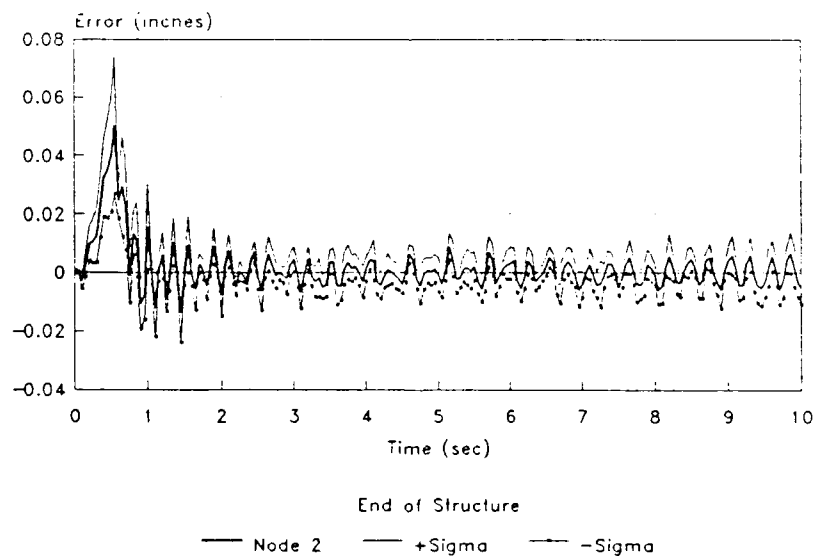


(b)

Figure 5.44. Control Inputs for MMAC with $\lambda = 1.0$. (a) Mid-structure actuator, (b) End of structure and hub of structure actuators.

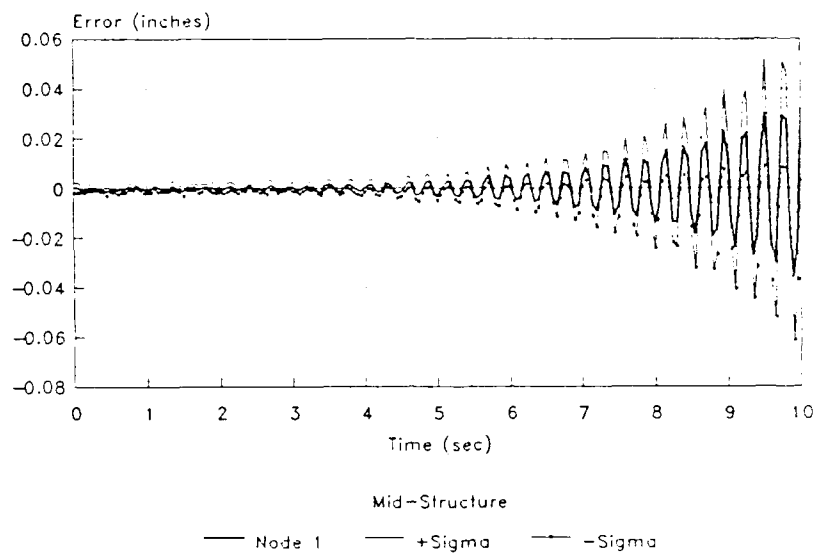


(a)

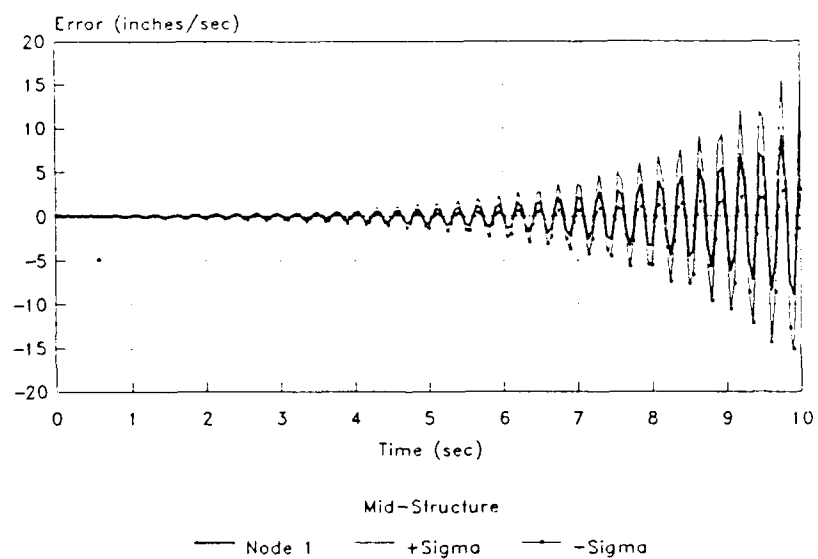


(b)

Figure 5-45. Structure Positions with MMAC and $\lambda = 1.0$. (a) Node 1 position mean and variances and (b) Node 2 position mean and variances.



(a)



(b)

Figure 5.46. "Worst Case" Estimation Errors with Single-LQG-Controller, Node 1 - True Parameter and Filter Mismatch. (a) Position and (b) Velocity Estimation Errors. $\lambda = 0$.

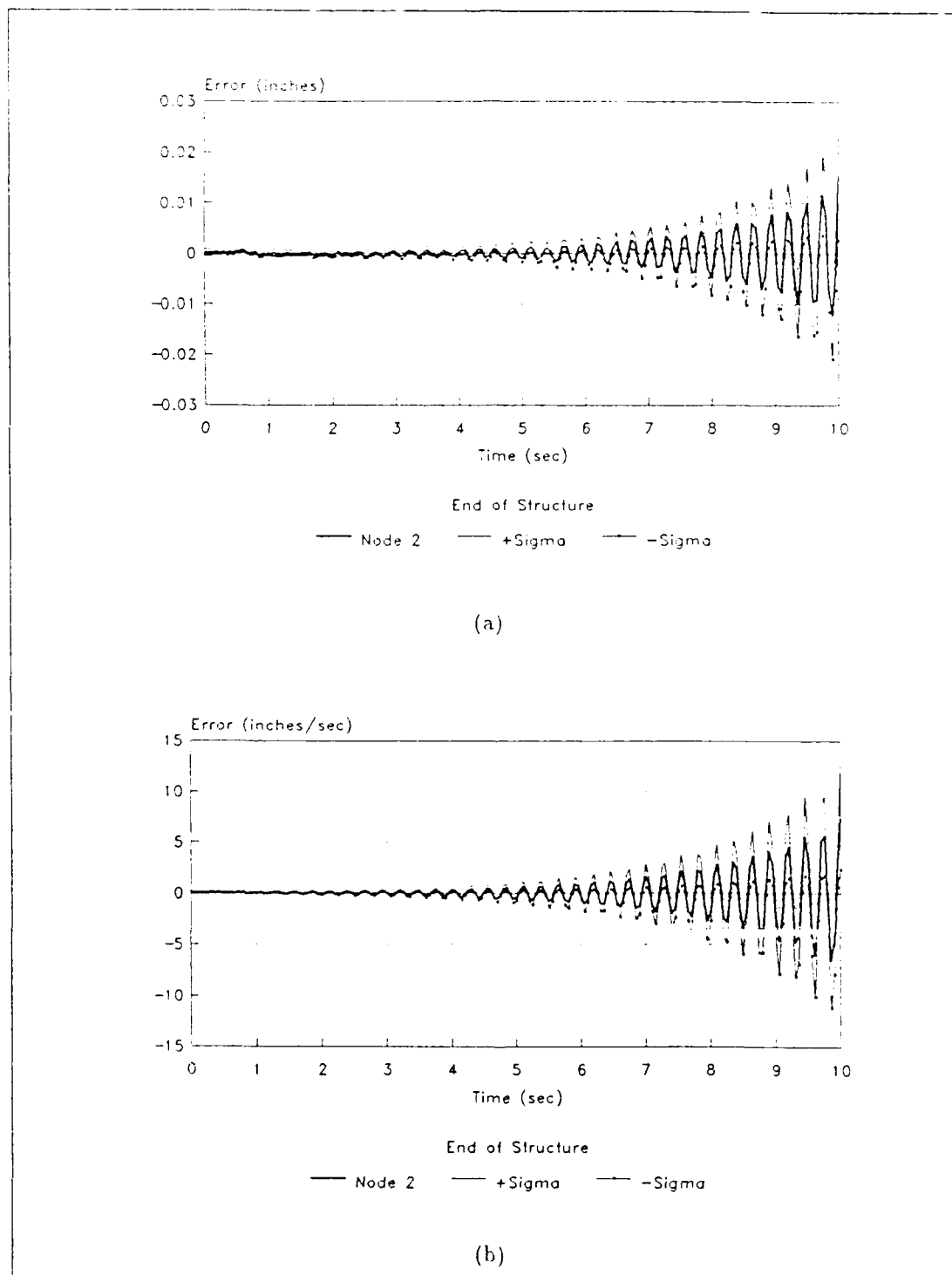


Figure 5.47. "Worst Case" Estimation Errors with Single-LQG-Controller, Node 2 - True Parameter and Filter Mismatch. (a) Position and (b) Velocity Estimation Errors. $\lambda = 0$.

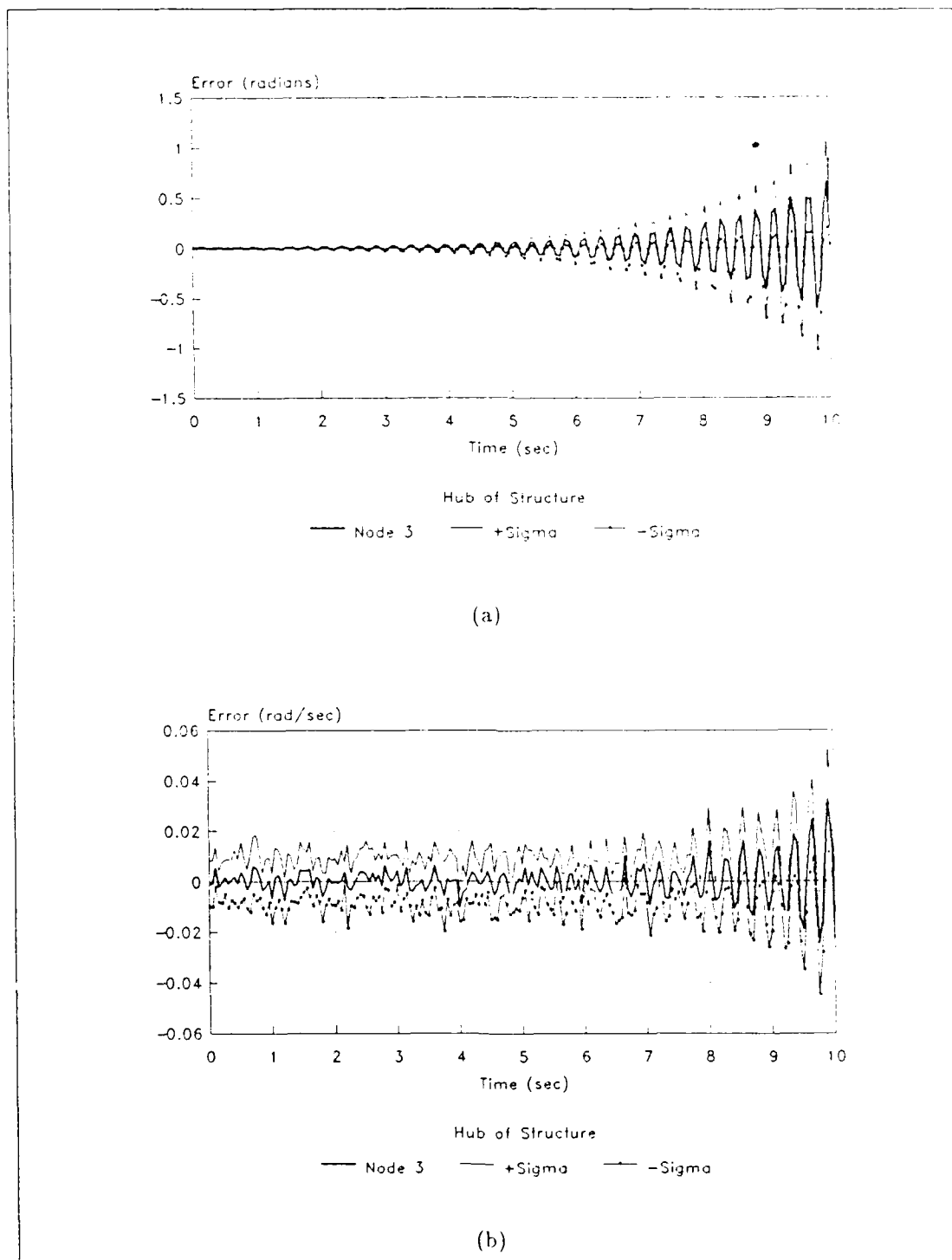
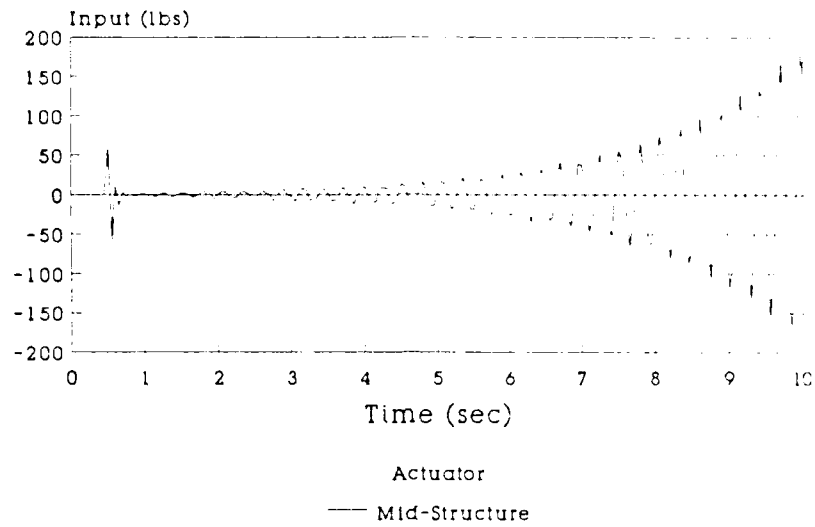
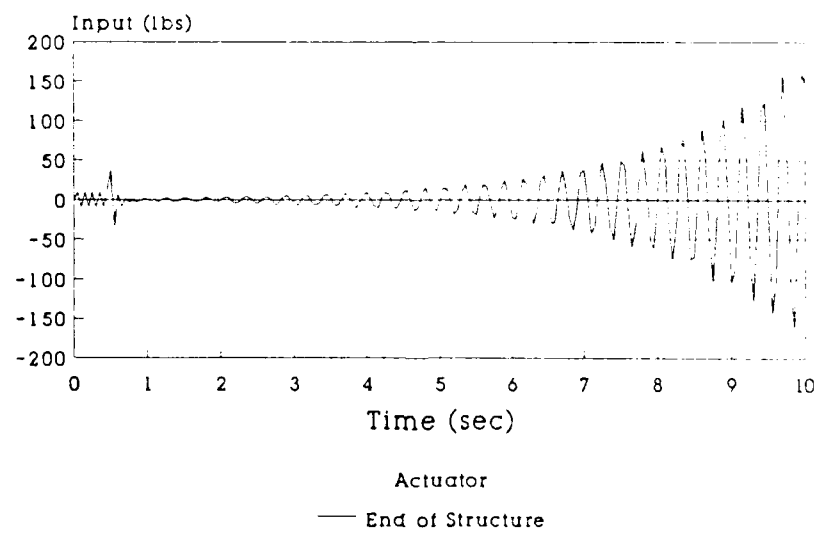


Figure 5.48. "Worst Case" Estimation Errors with Single-LQG-Controller, Node 3 - True Parameter and Filter Mismatch. (a) Position and (b) Velocity Estimation Errors. $\lambda = 0$.



(a)



(b)

Figure 5.49. Control Inputs for "Worst Case" Analysis. (a) Mid-structure actuator. (b) End of structure actuator.

| Node | λ | Mean | σ |
|------|-----------|-------------|----------------|
| 1 | 0.0 | 0.00000650 | 0.001486 (in) |
| 1 | 0.5 | 0.00000443 | 0.001509 |
| 1 | 1.0 | 0.00000539 | 0.001543 |
| 1 | --- | -0.00008770 | 0.004974 |
| 2 | 0.0 | 0.00001241 | 0.000511 |
| 2 | 0.5 | 0.00001153 | 0.000518 |
| 2 | 1.0 | 0.00001280 | 0.000532 |
| 2 | --- | 0.00000210 | 0.001751 |
| 3 | 0.0 | 0.00001405 | 0.002033 (rad) |
| 3 | 0.5 | 0.00004367 | 0.002912 |
| 3 | 1.0 | 0.00004159 | 0.003921 |
| 3 | --- | 0.00385803 | 0.084584 |

Table 5.3. Position Estimation Means and Standard Deviations for MMAC (Single-LQG-Controller)

| Node | λ | Mean | σ |
|------|-----------|-------------|----------------------------|
| 1 | 0.0 | 0.00023811 | 0.023786 $\frac{in}{sec}$ |
| 1 | 0.5 | 0.00022671 | 0.083704 |
| 1 | 1.0 | 0.00001279 | 0.000532 |
| 1 | --- | 0.01290439 | 1.258831 |
| 2 | 0.0 | 0.00502993 | 0.034800 |
| 2 | 0.5 | -0.00028324 | 0.066729 |
| 2 | 1.0 | 0.00031122 | 0.119798 |
| 2 | --- | 0.02472575 | 0.915436 |
| 3 | 0.0 | 0.00034481 | 0.009369 $\frac{rad}{sec}$ |
| 3 | 0.5 | 0.00034629 | 0.009369 |
| 3 | 1.0 | 0.00034503 | 0.009378 |
| 3 | --- | 0.00039543 | 0.010457 |

Table 5.4. Velocity Estimation Means and Standard Deviations for Single-LQG-Controller Case

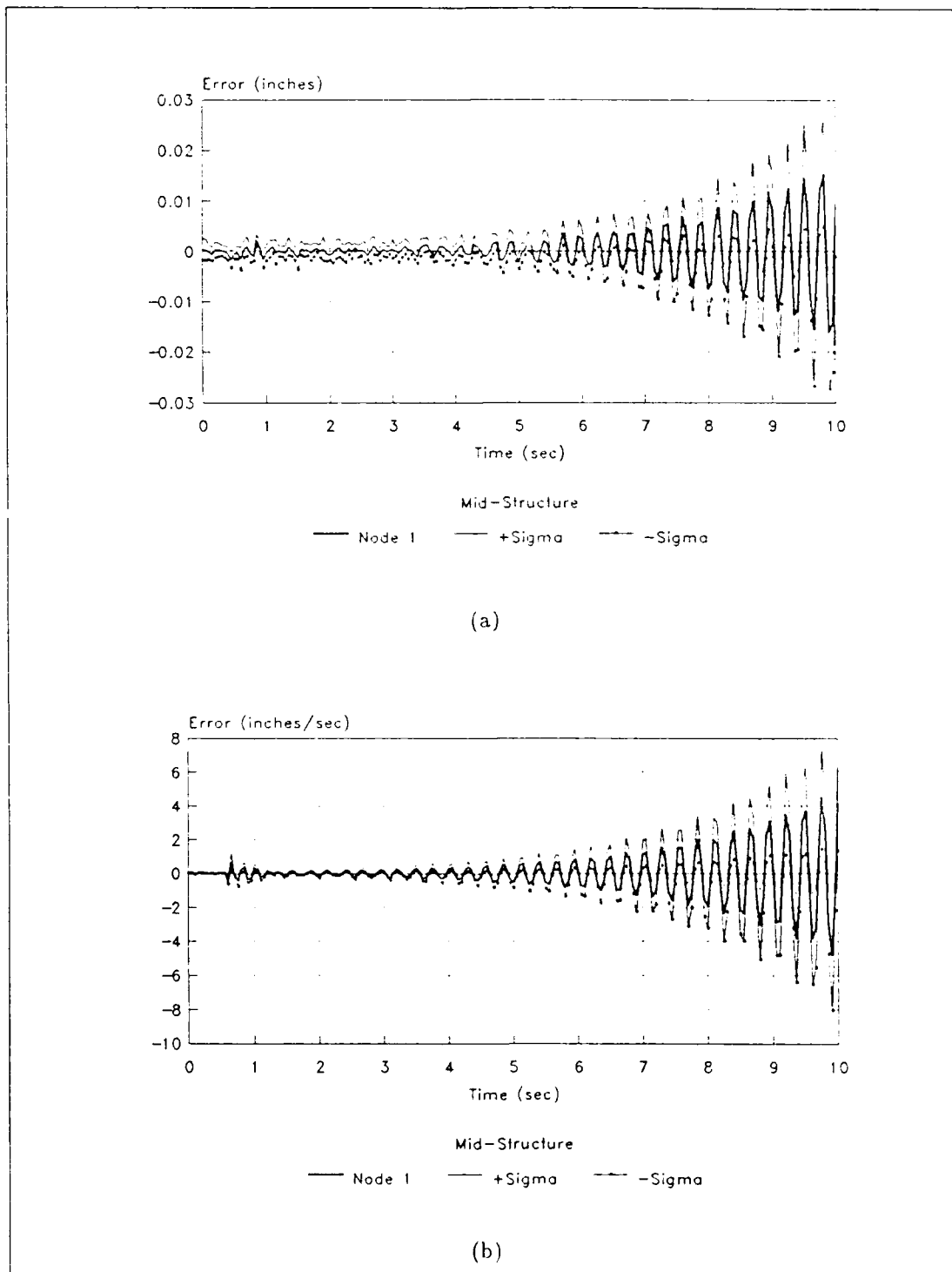


Figure 5.50. "Worst Case" Estimation Errors with Single-LQG-Controller, Node 1 - True Parameter and Filter Mismatch. (a) Position and (b) Velocity Estimation Errors. $\lambda = 0.5$.

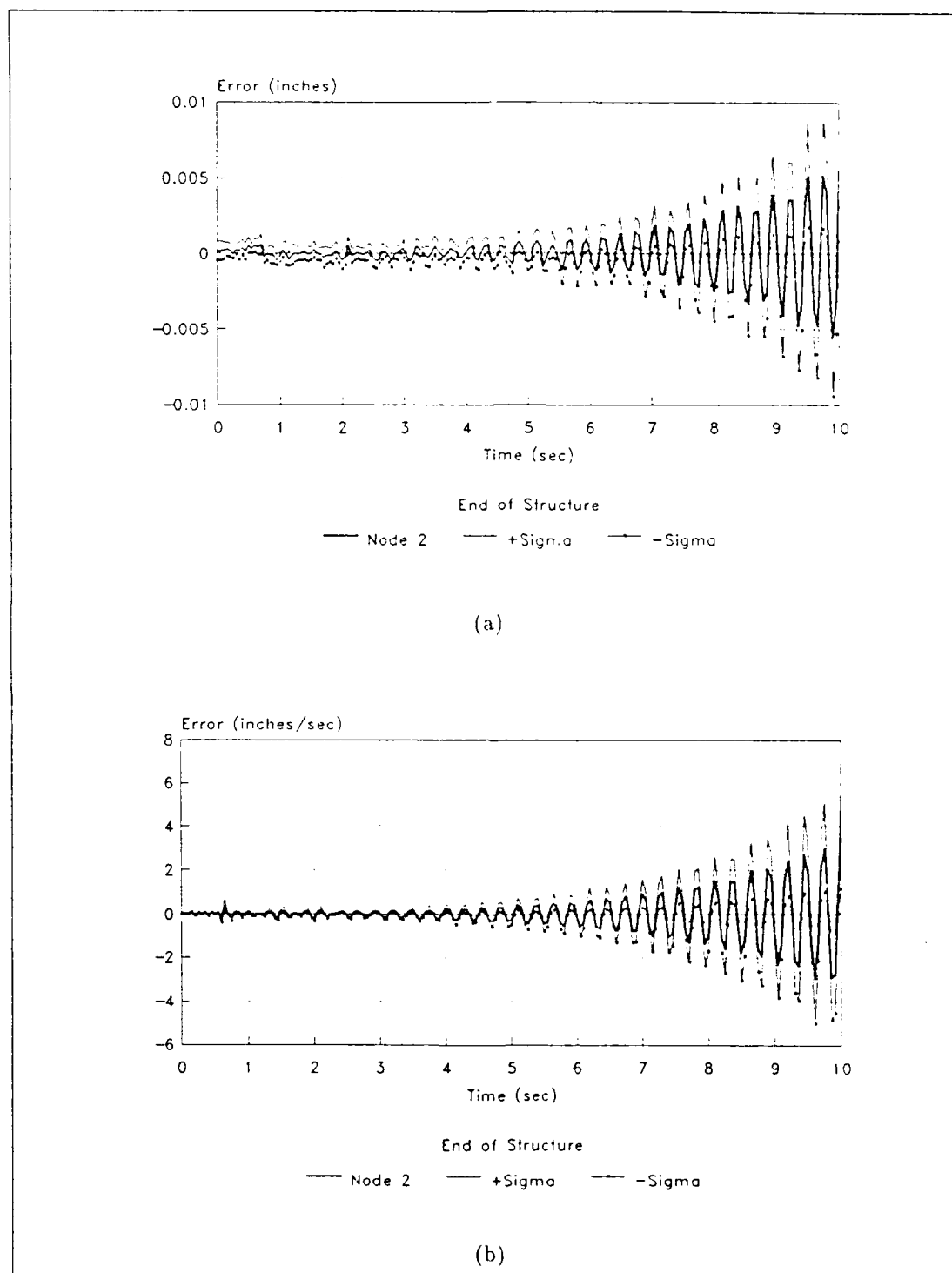
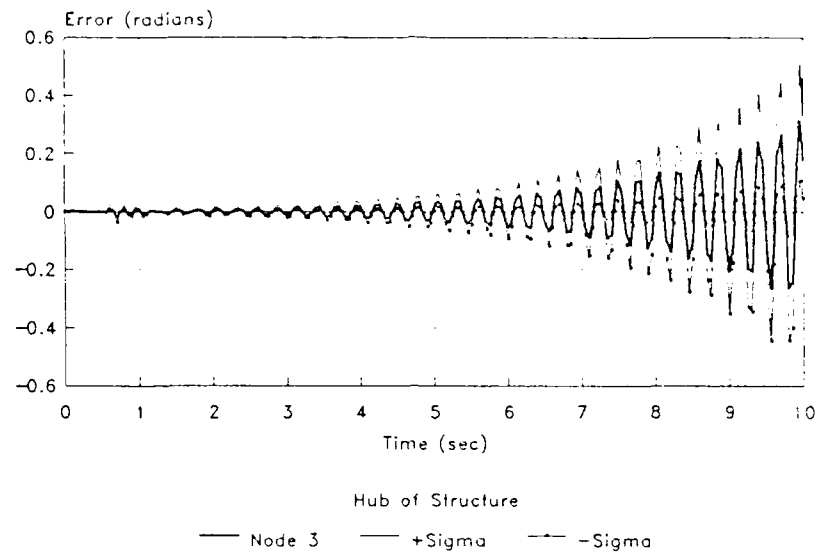
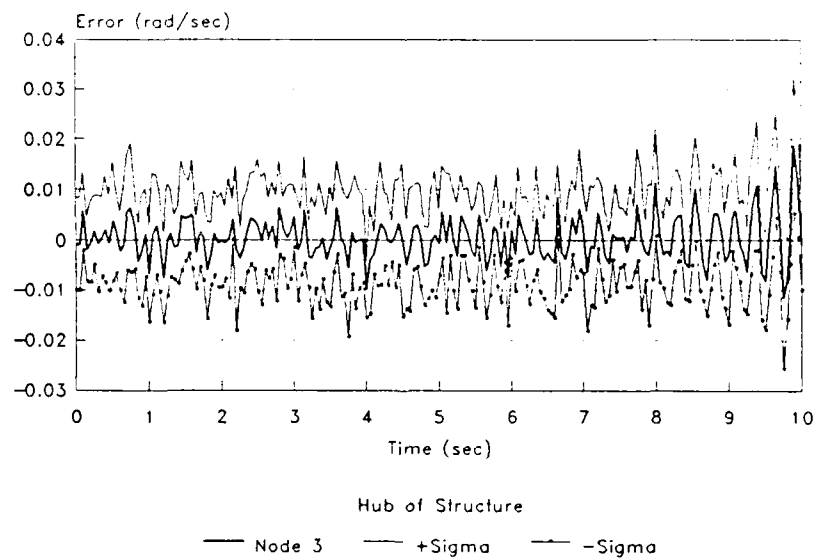


Figure 5.51. "Worst Case" Estimation Errors with Single-LQG-Controller. Node 2 - True Parameter and Filter Mismatch. (a) Position and (b) Velocity Estimation Errors. $\lambda = 0.5$.

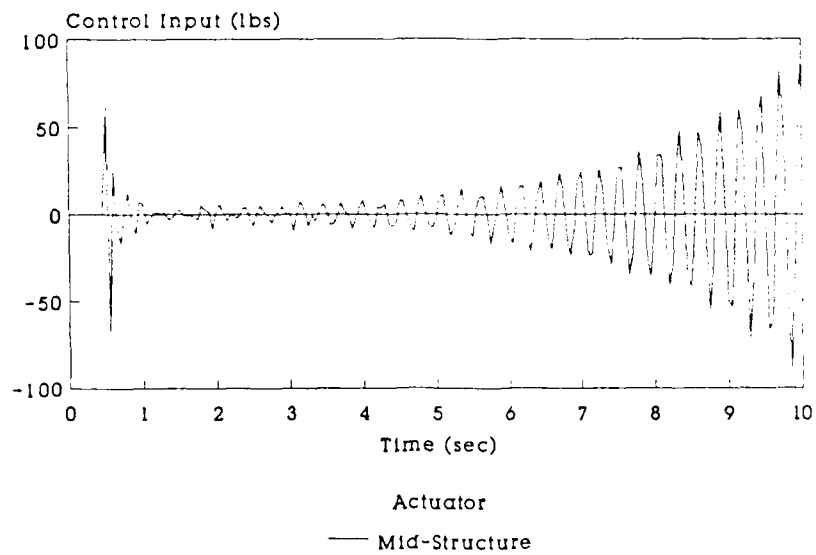


(a)

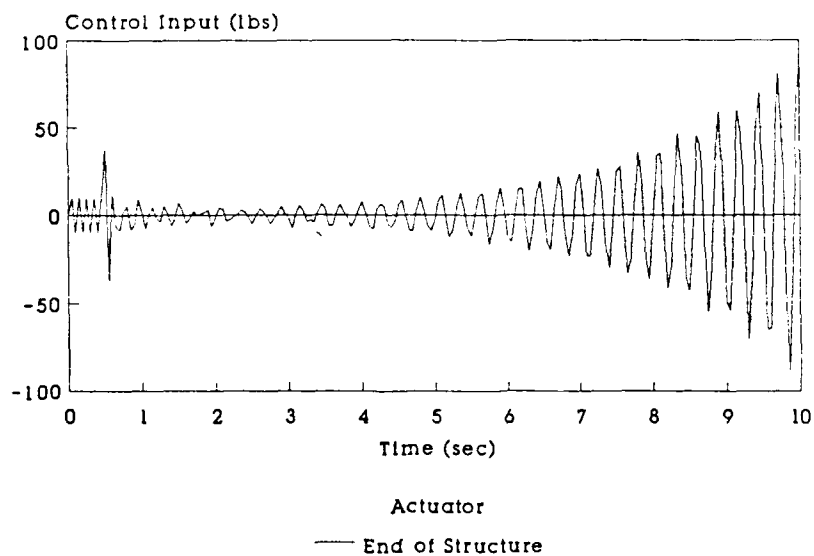


(b)

Figure 5.52. "Worst Case" Estimation Errors with Single-LQG-Controller, Node 1 - True Parameter and Filter Mismatch. (a) Position and (b) Velocity Estimation Errors. $\lambda = 0.5$.

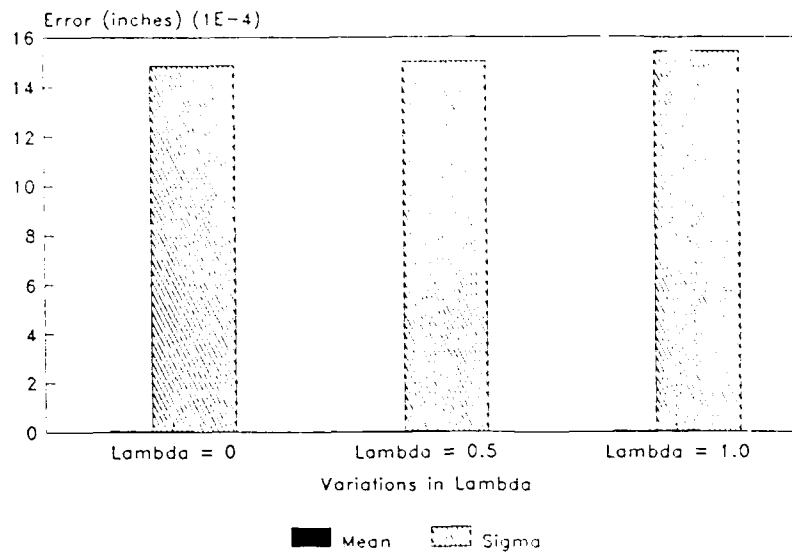


(a)

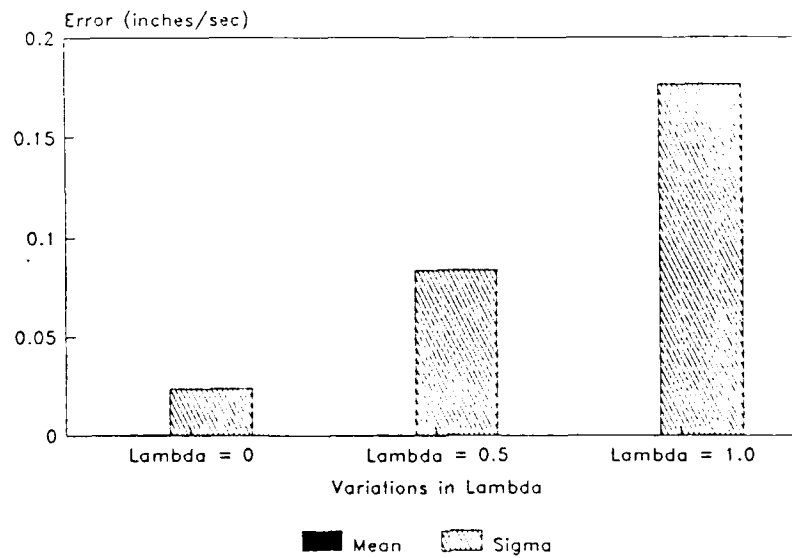


(b)

Figure 5.53. Control Inputs for the MMAC Worst Case Analysis. (a) Mid-structure actuator, (b) end of structure.

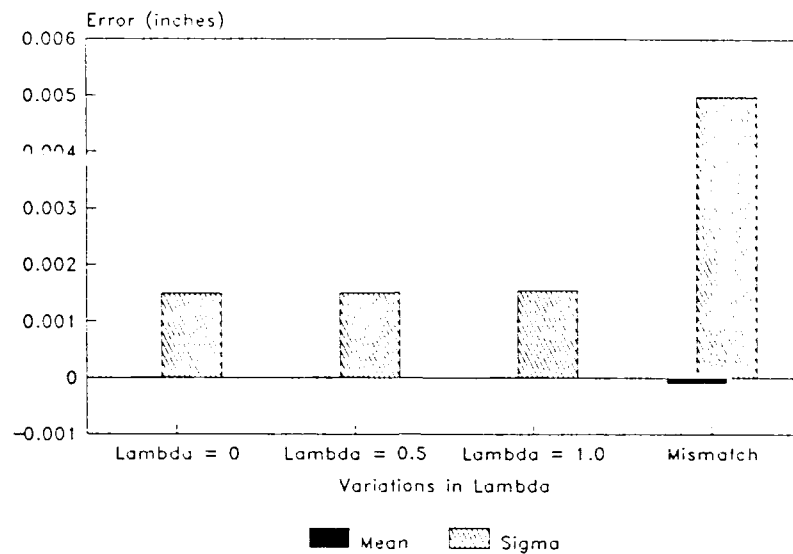


(a)

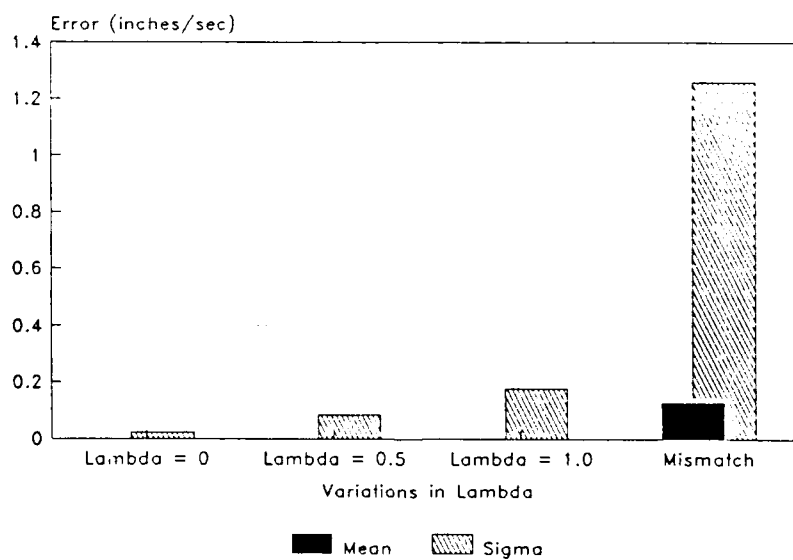


(b)

Figure 5.54. Position Estimation Means and Standard Deviations for Single-LQG-Controller Case, Node 1: (a) Position Estimates and (b) Velocity Estimates.



(a)



(b)

Figure 5.55. Position Estimation Means and Standard Deviations for Single-LQG-Controller Case with "Worst Case" Analysis, Node 1: (a) Position Estimates with Worst Case Analysis and (b) Velocity Estimates with Worst Case Analysis

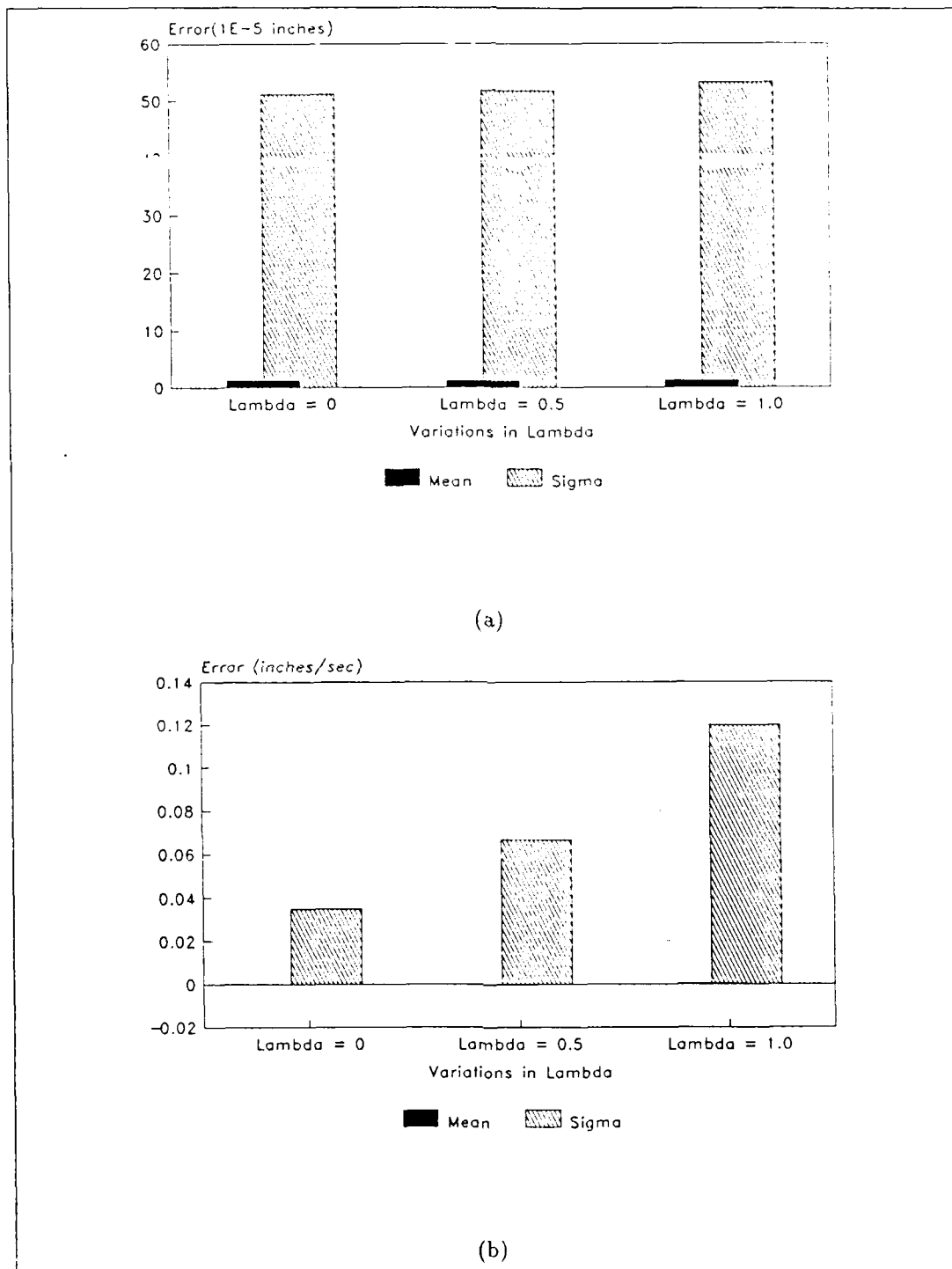


Figure 5.56. Position Estimation Means and Standard Deviations for Single-LQG-Controller Case, Node 2: (a) Position Estimates and (b) Velocity Estimates.

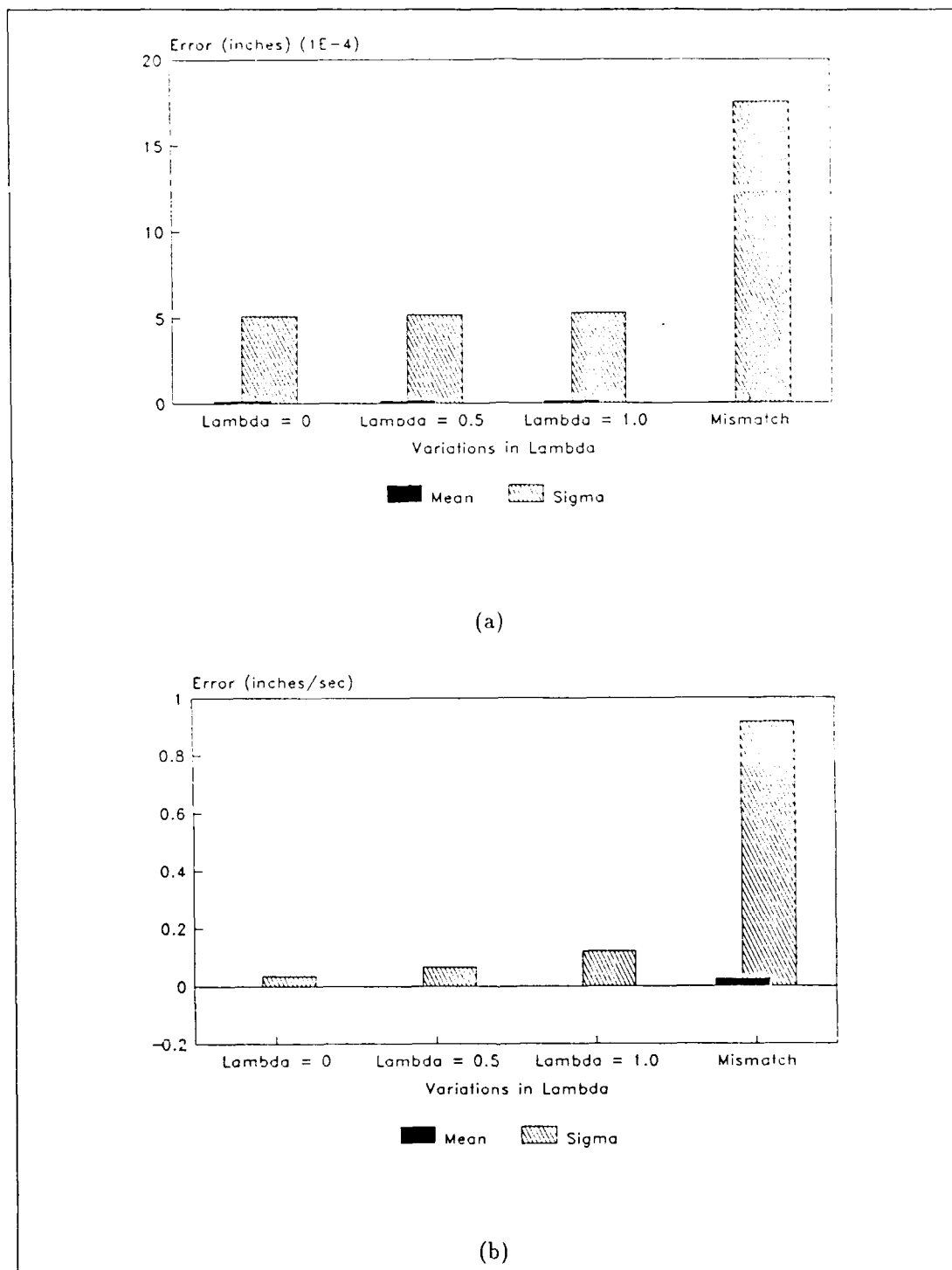


Figure 5.57. Position Estimation Means and Standard Deviations for Single-LQG-Controller Case with "Worst Case" Analysis, Node 2: (a) Position Estimates with Worst Case Analysis and (b) Velocity Estimates with Worst Case Analysis

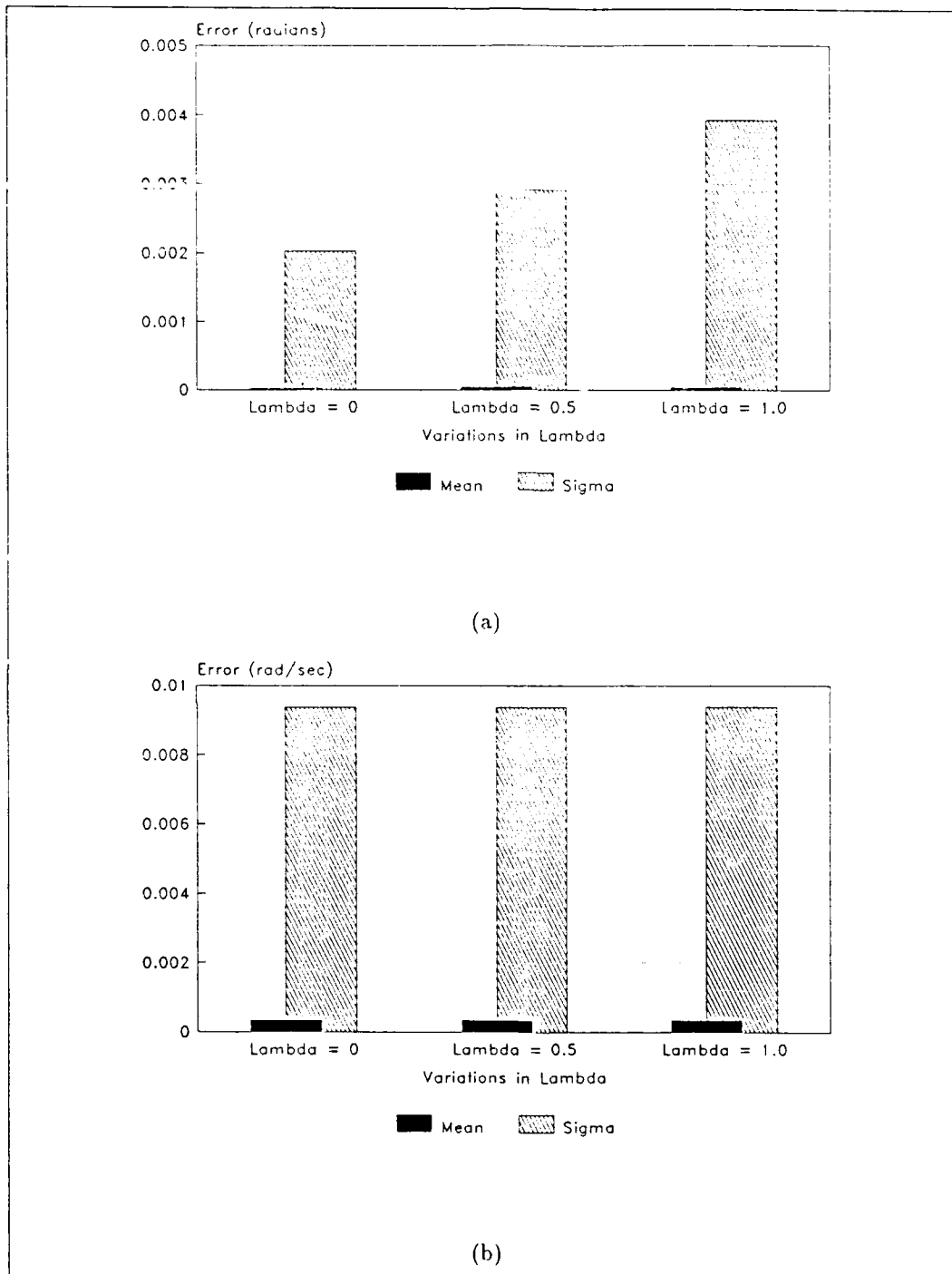


Figure 5.58. Position Estimation Means and Standard Deviations for Single-LQG-Controller Case, Node 3: (a) Position Estimates and (b) Velocity Estimates.

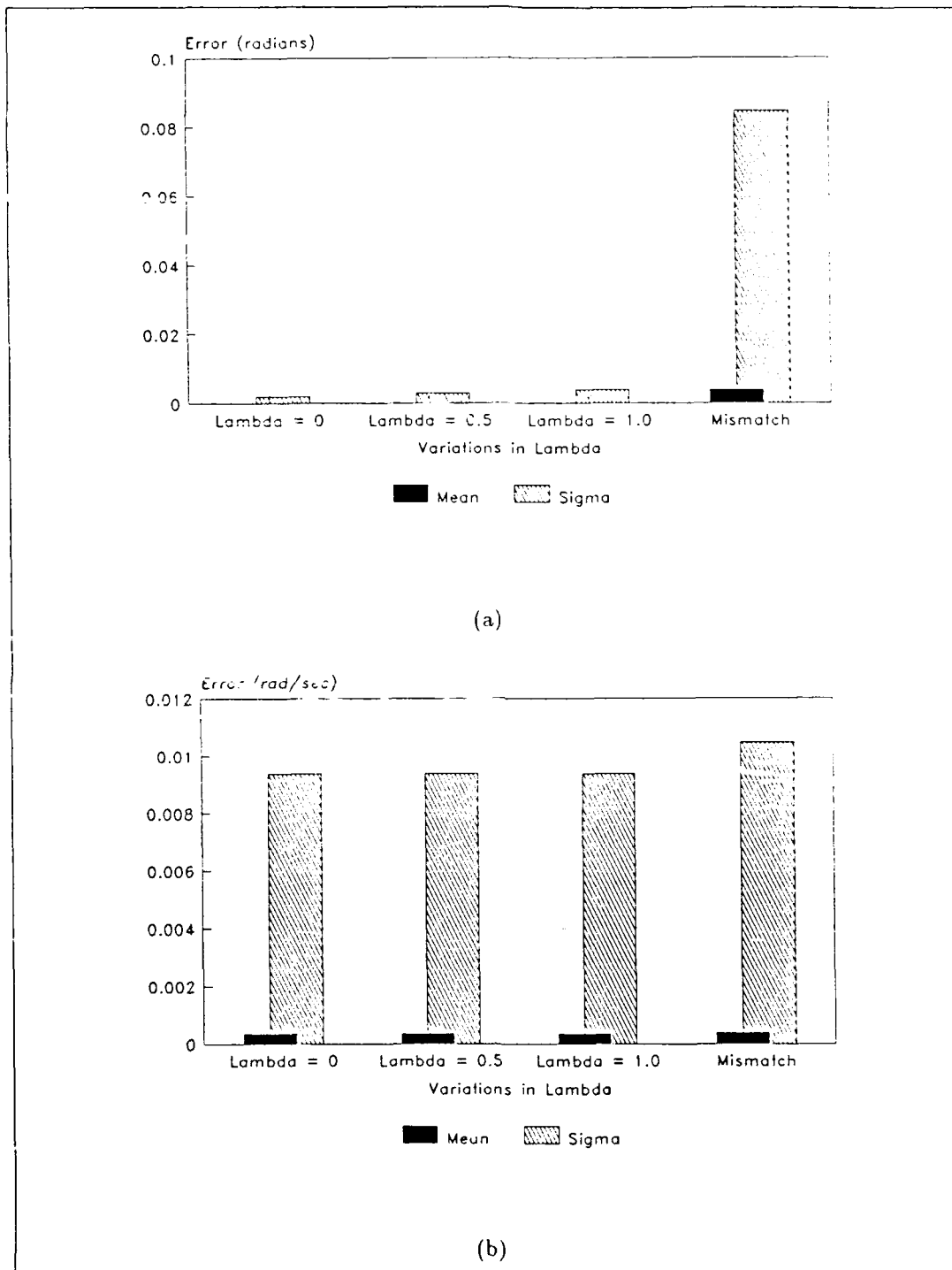
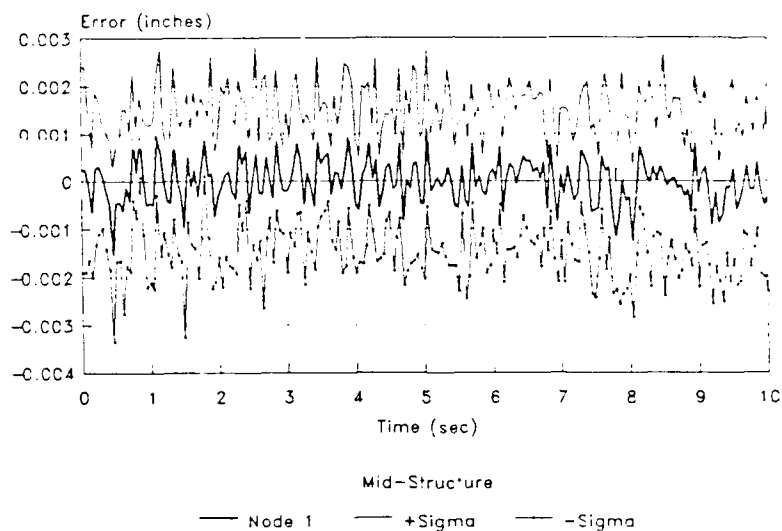
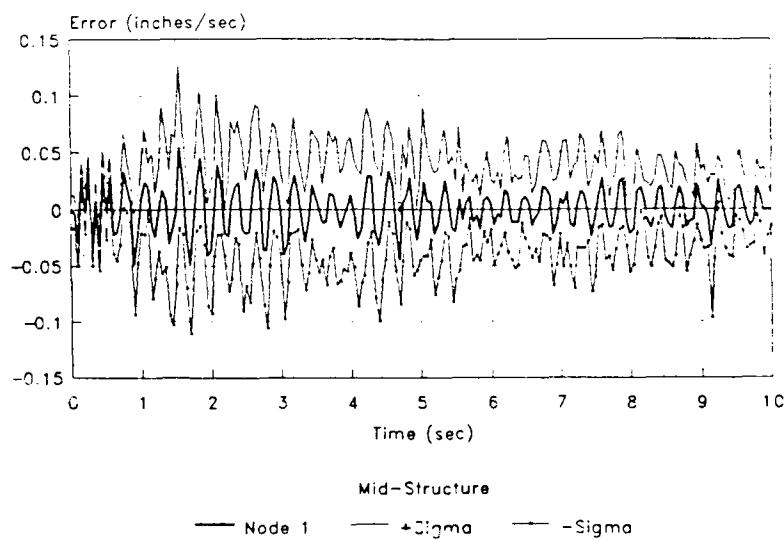


Figure 5.59. Position Estimation Means and Standard Deviations for Single-LQG-Controller Case with "Worst Case" Analysis, Node 3: (a) Position Estimates with Worst Case Analysis and (b) Velocity Estimates with Worst Case Analysis

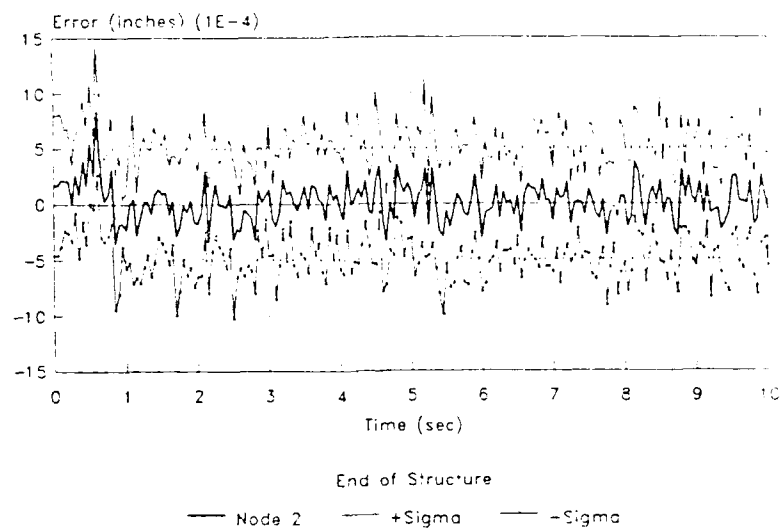


(a)

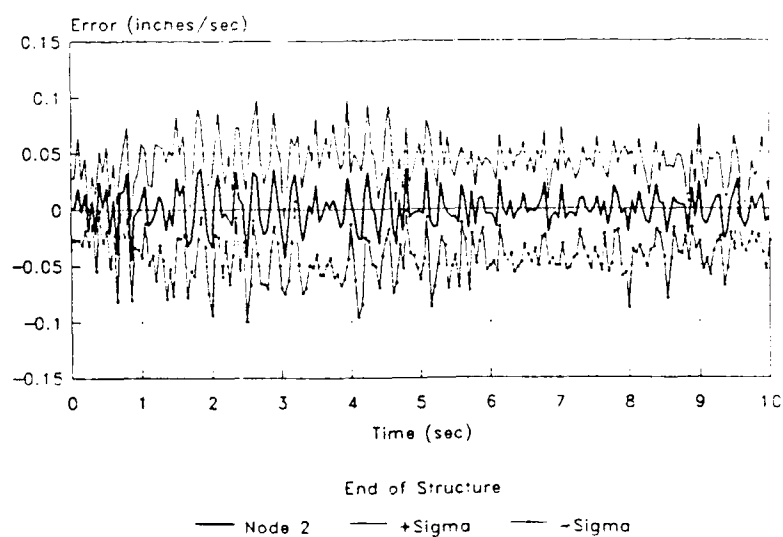


(b)

Figure 5.60. Estimation Errors with Parameter/Filter Location Mismatch and Movement of the Bank with MMAC, Node 1 - True Parameter at (7,6) and Filter Initially at (5,5). (a) Position and (b) Velocity Estimation Errors. $\lambda = 0.0$.

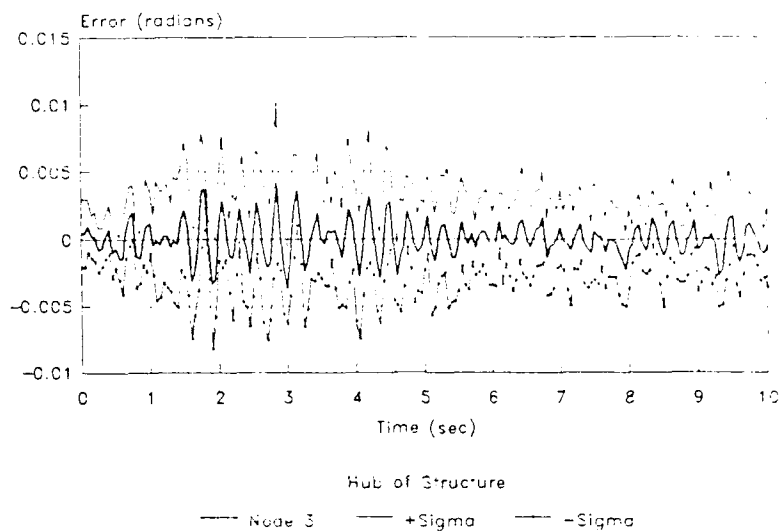


(a)

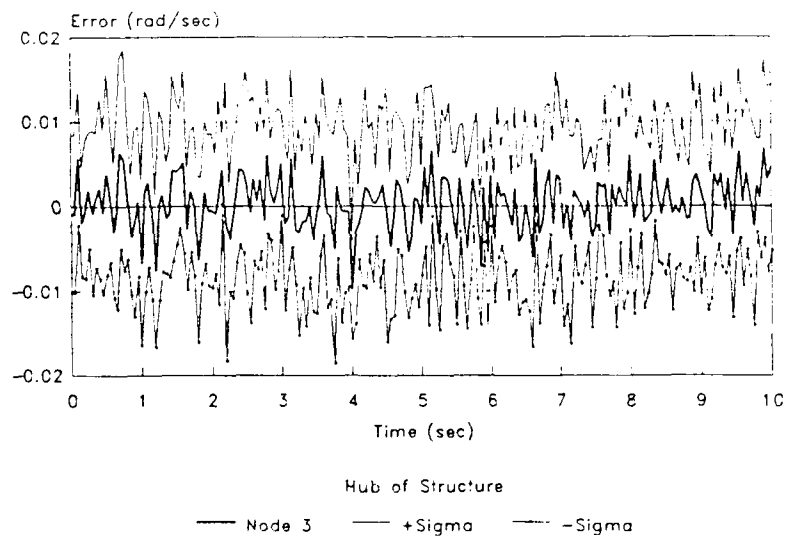


(b)

Figure 5.61. Estimation Errors with Parameter/Filter Location Mismatch and Movement of the Bank with MMAC. Node 2 - True Parameter at (7,6) and Filter Initially at (5,5). (a) Position and (b) Velocity Estimation Errors. $\lambda = 0.0$.

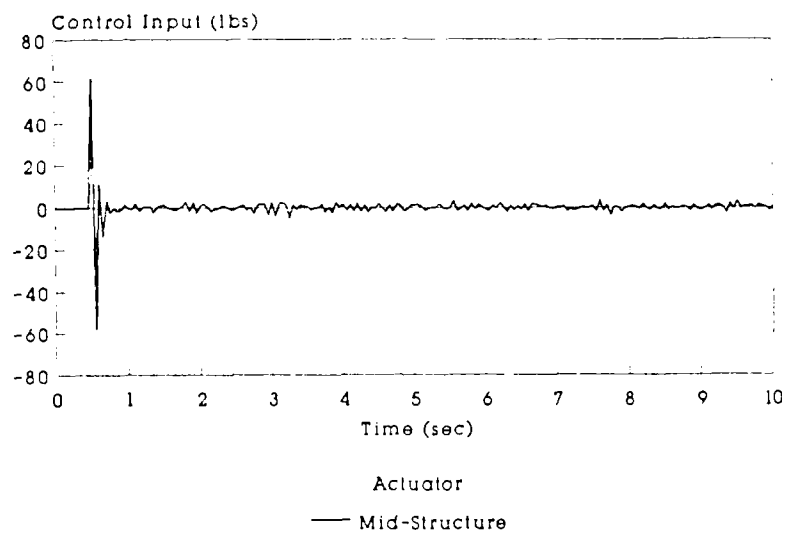


(a)

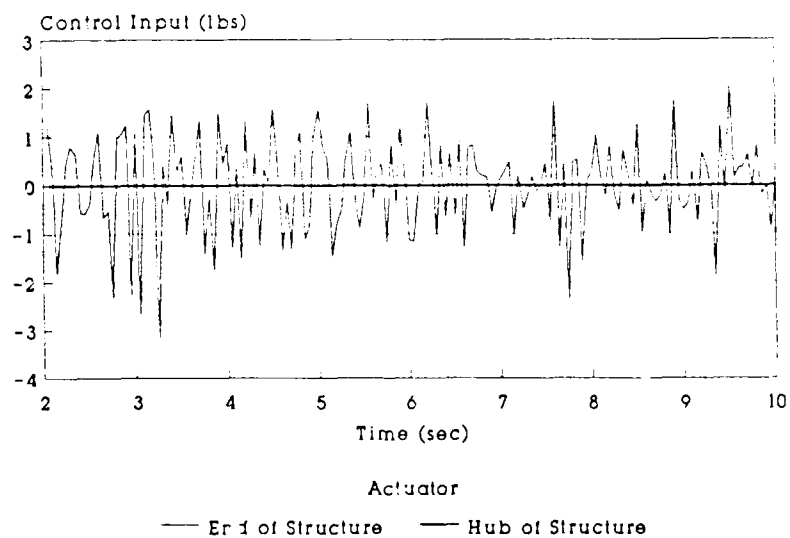


(b)

Figure 5.62. Estimation Errors with Parameter/Filter Location Mismatch and Movement of the Bank with MMAC, Node 3 - True Parameter at (7,6) and Filter Initially at (5,5). (a) Position and (b) Velocity Estimation Errors. $\lambda = 0.0$.



(a)



(b)

Figure 5.63. Control Inputs for the Single-LQG-Controller Case Bank Movement Analysis, $\lambda = 0$
 (a) Mid-structure actuator, (b) End of structure and hub of structure actuators.

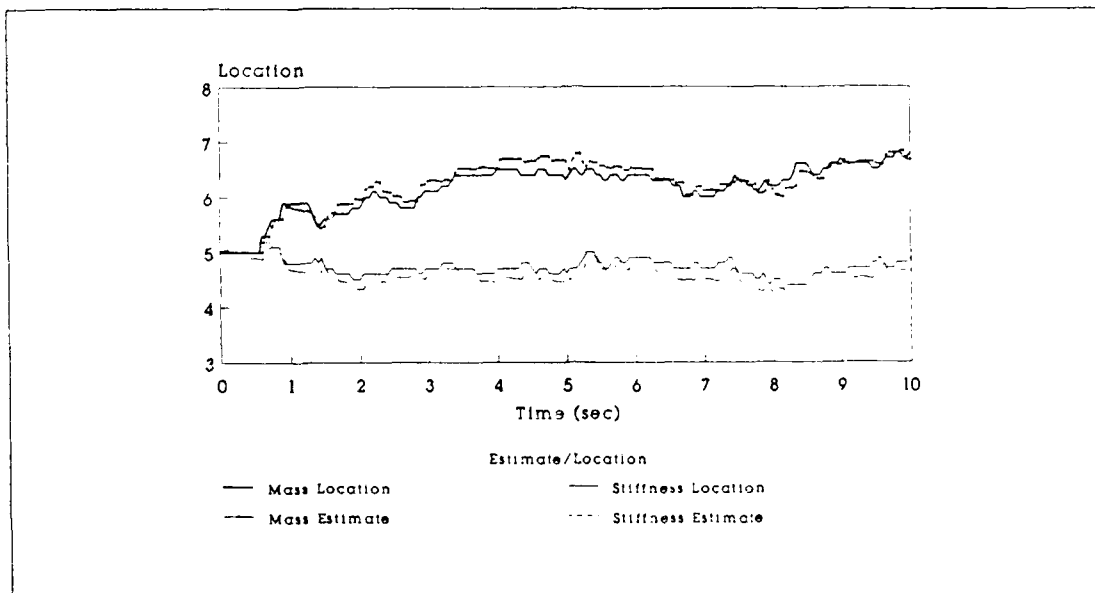


Figure 5.64. Parameter Estimation and Actual Filter Bank Location - True Parameter at (7.6) and Filter at (5.5). $\lambda = 0.0$. Initial Probabilities = $\frac{1}{9}$.

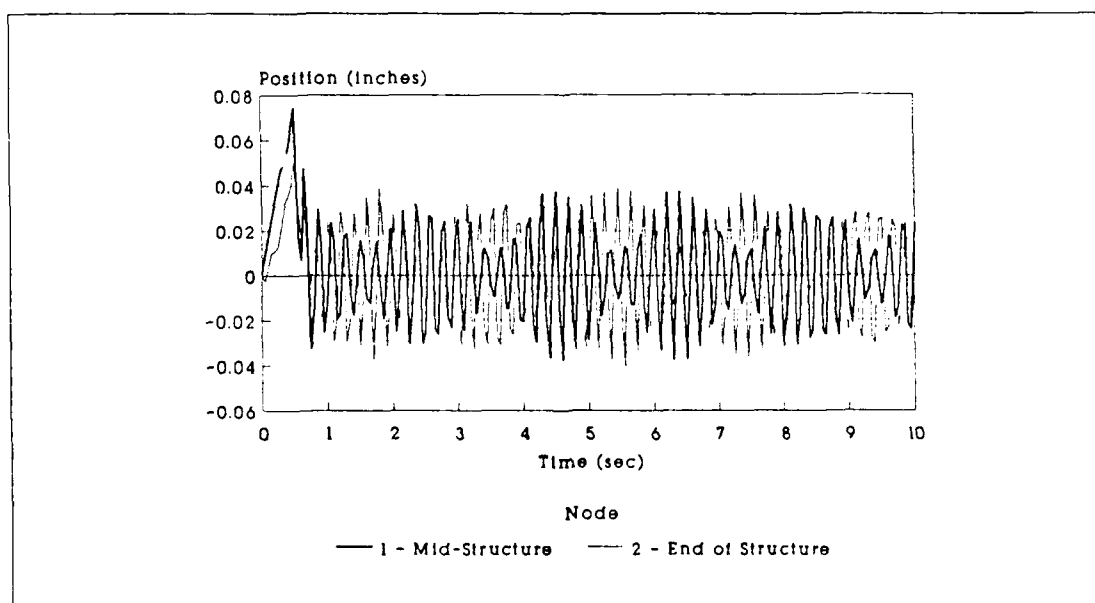
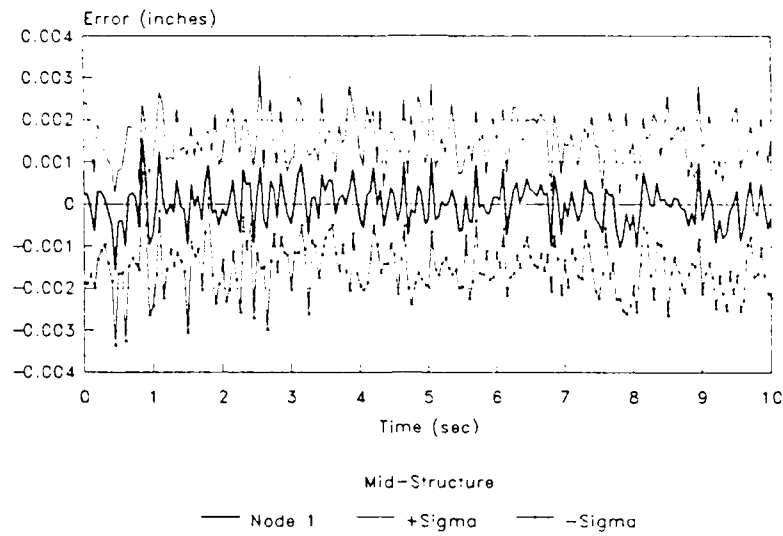
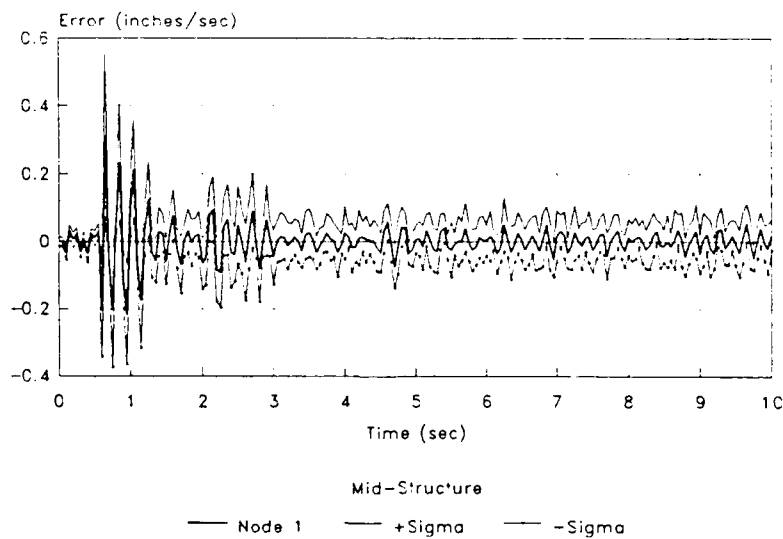


Figure 5.65. Mean Structure Positions

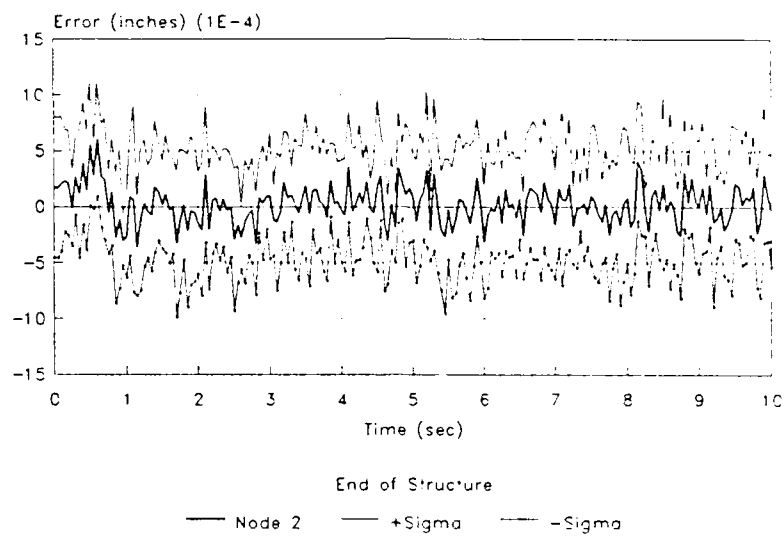


(a)

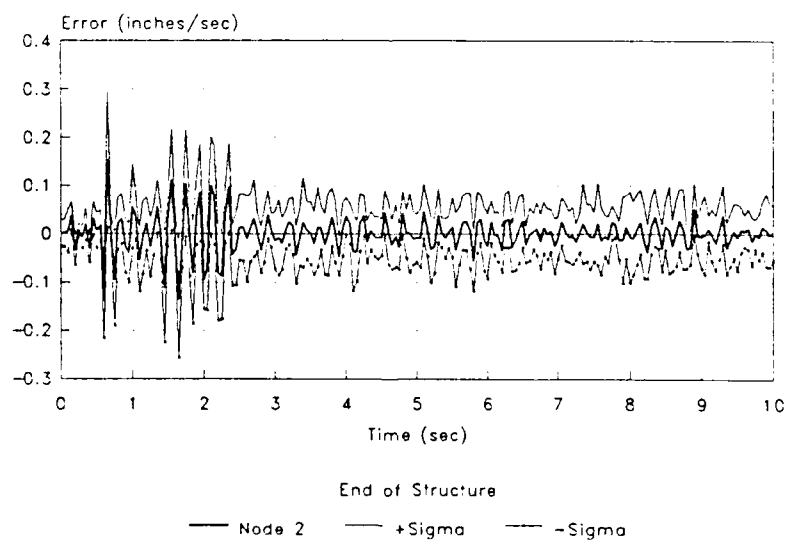


(b)

Figure 5.66. Estimation Errors with Parameter/Filter Location Mismatch and Movement of the Bank with Control, Node 1 - True Parameter at (7,6) and Filter Initially at (5,5). (a) Position and (b) Velocity Estimation Errors. $\lambda = 0.25$.

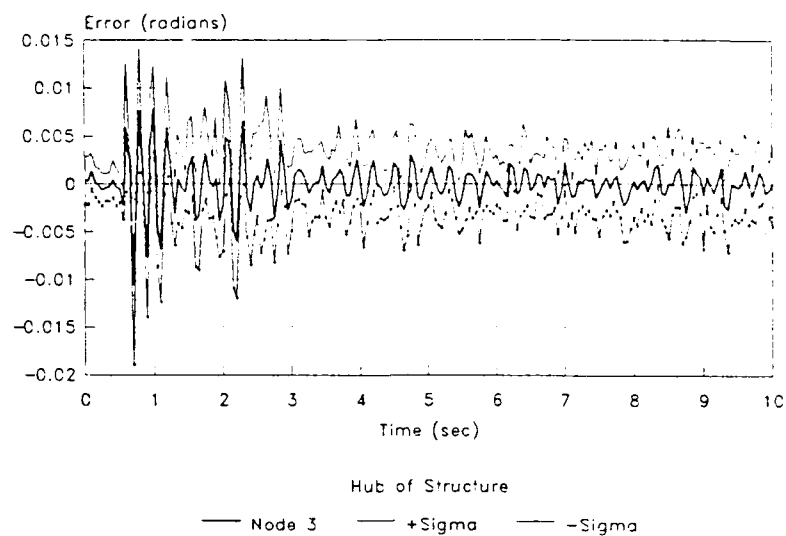


(a)

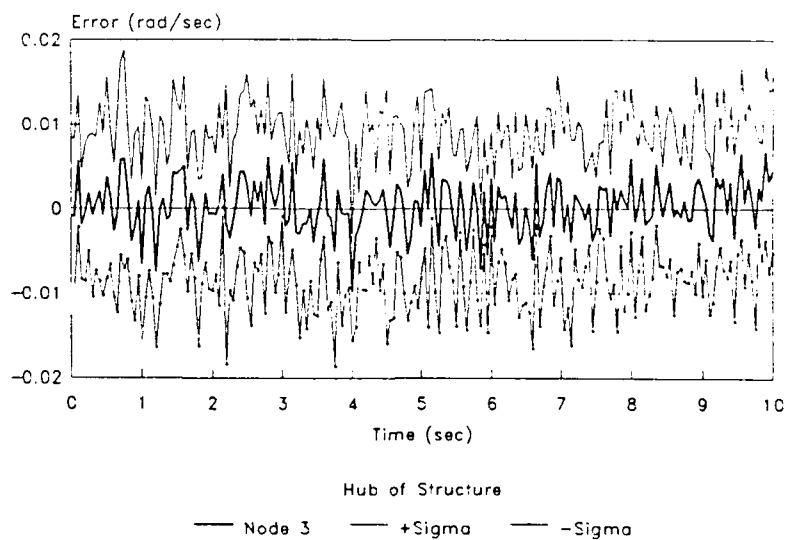


(b)

Figure 5.67. Estimation Errors with Parameter/Filter Location Mismatch and Movement of the Bank with MMAC, Node 2 - True Parameter at (7.6) and Filter Initially at (5.5). (a) Position and (b) Velocity Estimation Errors. $\lambda = 0.25$.

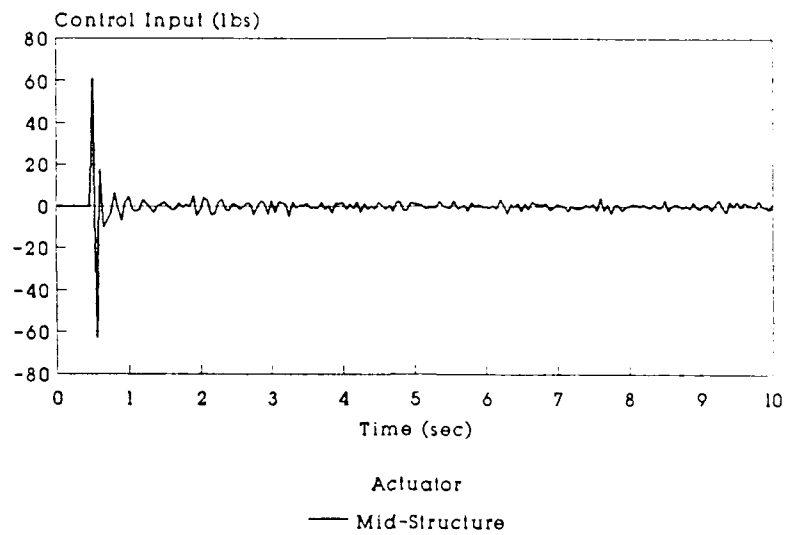


(a)

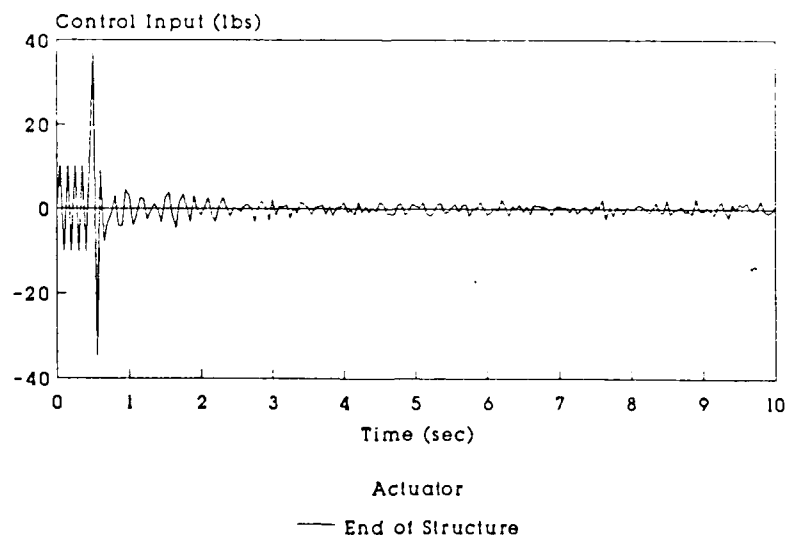


(b)

Figure 5.68. Estimation Errors with Parameter/Filter Location Mismatch and Movement of the Bank with MMAC, Node 3 - True Parameter at (7,6) and Filter Initially at (5,5). (a) Position and (b) Velocity Estimation Errors. $\lambda = 0.25$.



(a)



(b)

Figure 5.69. Control Inputs for the MMAC Bank Movement Analysis, $\lambda = 0.25$. (a) Mid-structure actuator, (b) End of structure and hub of structure actuators.

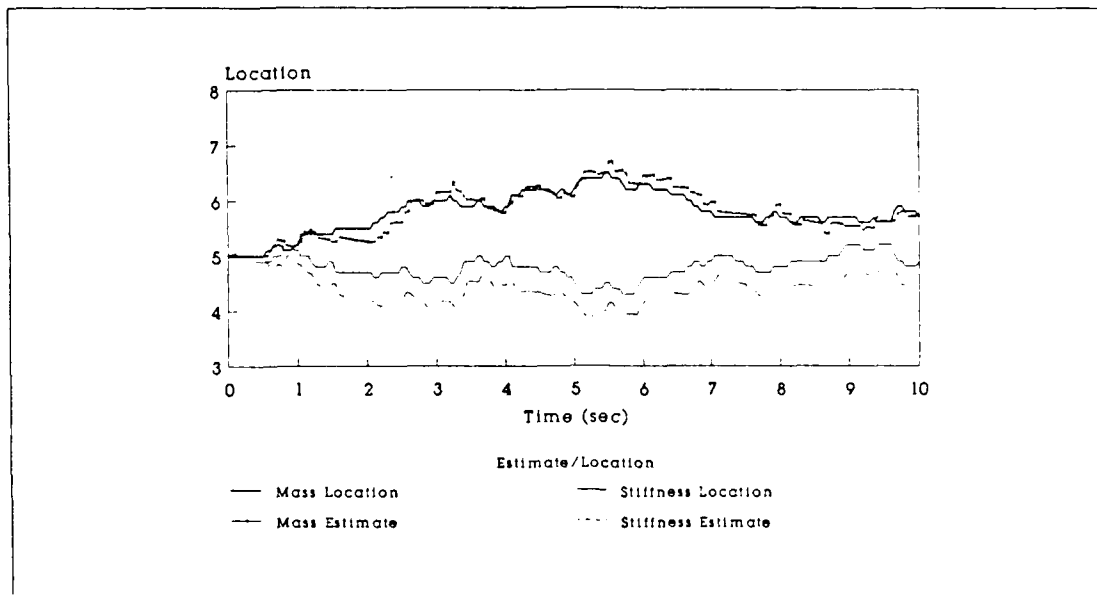


Figure 5.70. Parameter Estimation and Actual Filter Bank Location - True Parameter at (7,6) and Filter Initially at (5,5). $\lambda = 0.25$. Initial Probabilities = $\frac{1}{9}$.

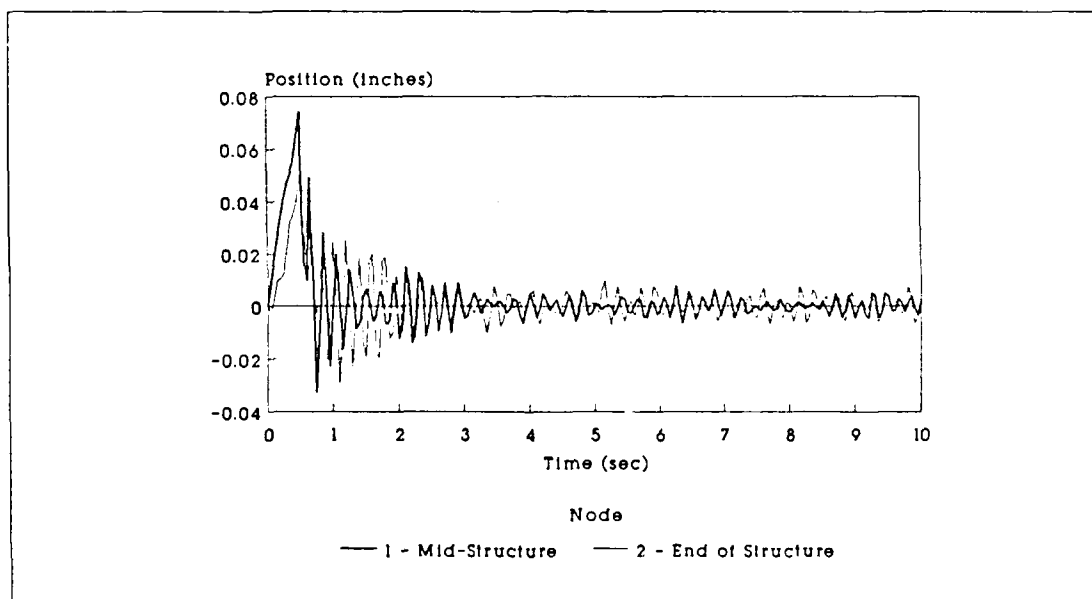
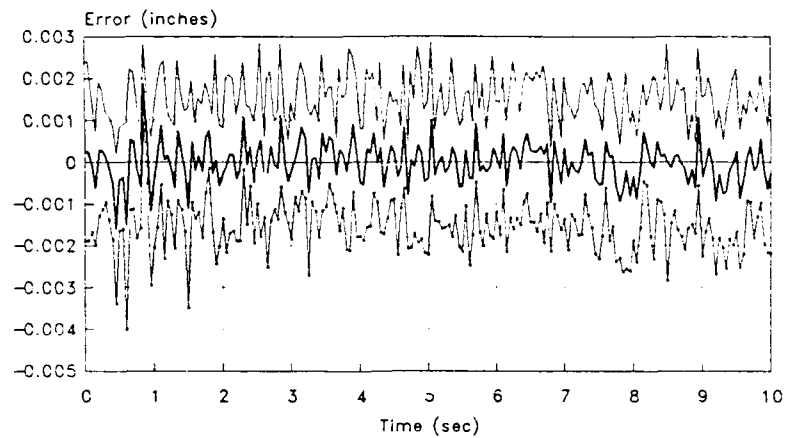


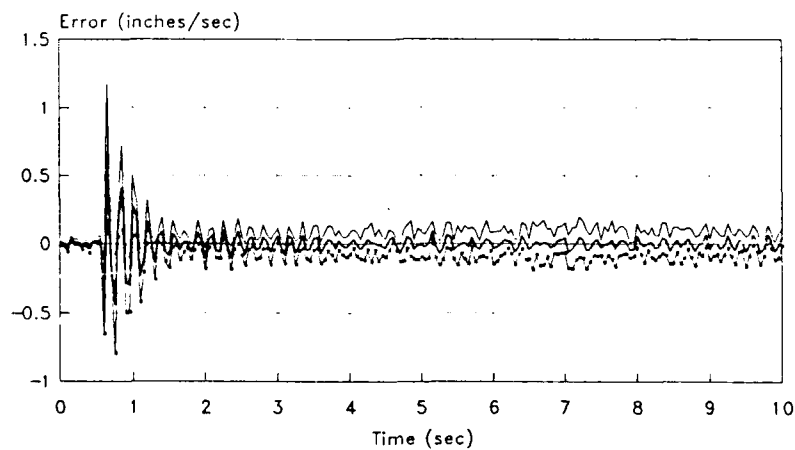
Figure 5.71. Mean Structure Positions



Mid-Structure

— Node 1 - - - +Sigma . . . -Sigma

(a)



Mid-Structure

— Node 1 - - - +Sigma . . . -Sigma

(b)

Figure 5.72. Estimation Errors with Parameter/Filter Location Mismatch and Movement of the Bank with MMAC , Node 1 - True Parameter at (7,6) and Filter Initially at (5,5). (a) Position and (b) Velocity Estimation Errors. $\lambda = 0.5$.

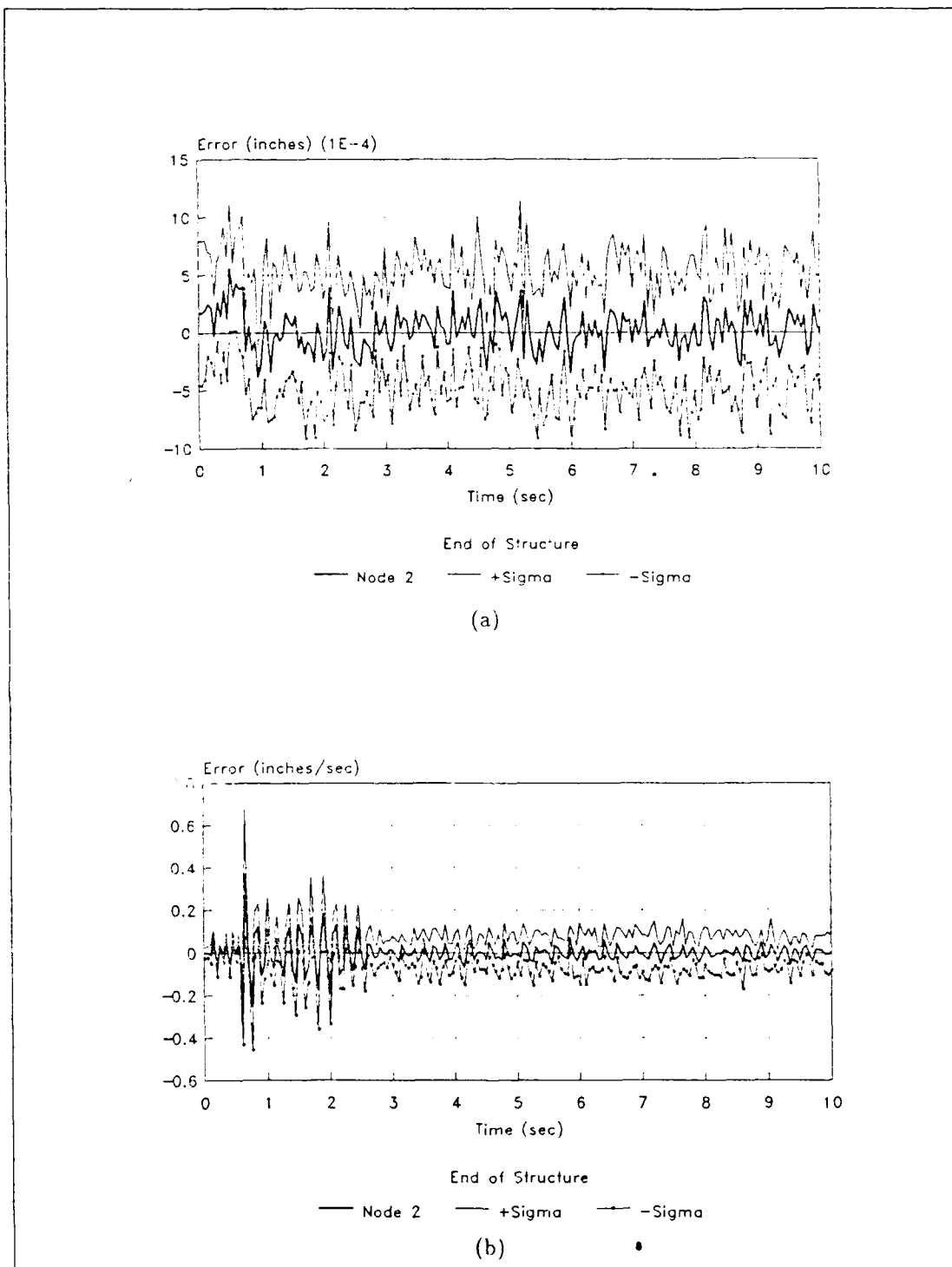


Figure 5.73. Estimation Errors with Parameter/Filter Location Mismatch and Movement of the Bank with MMAC , Node 2 - True Parameter at (7,6) and Filter Initially at (5.5). (a) Position and (b) Velocity Estimation Errors. $\lambda = 0.5$.

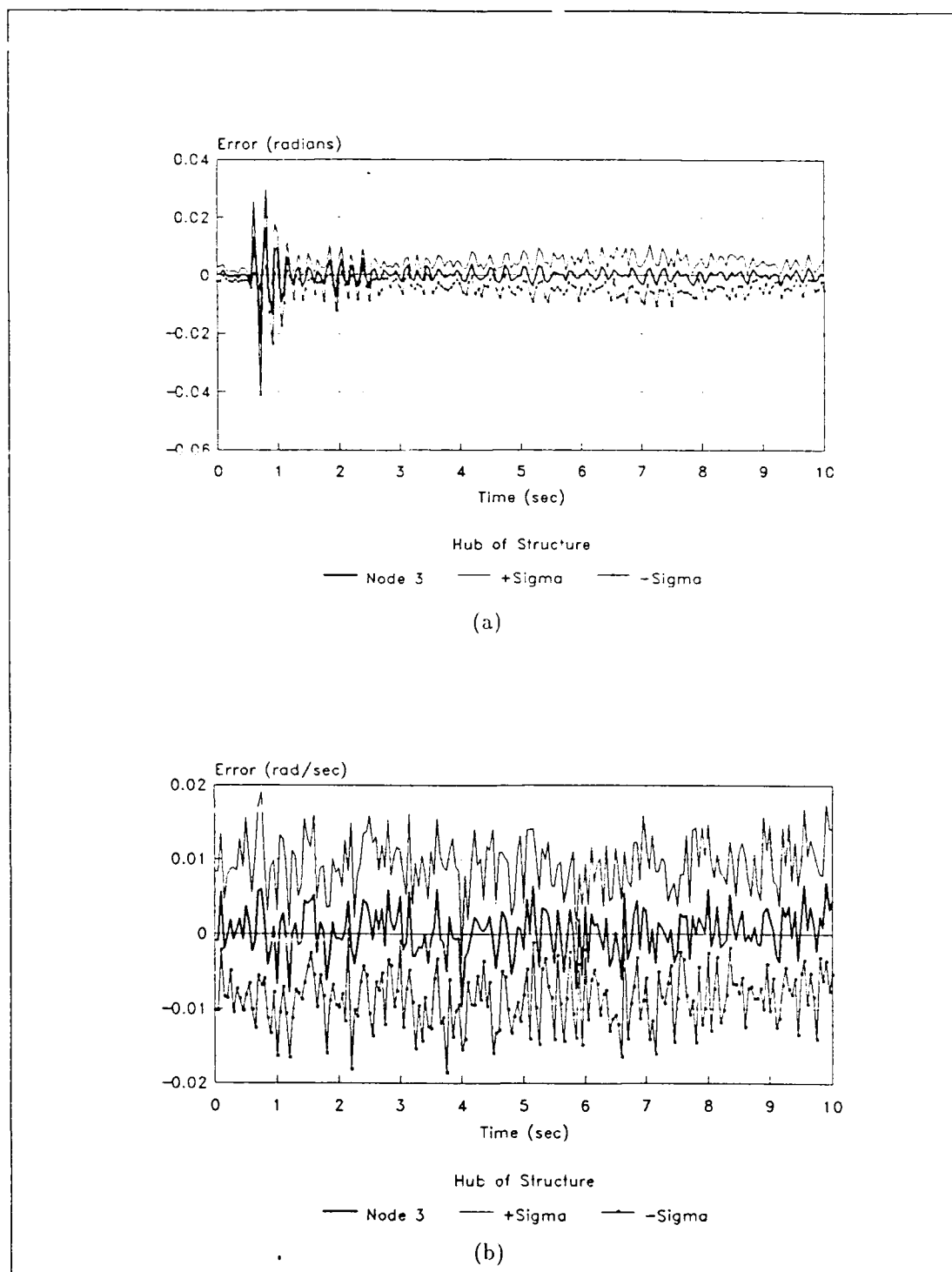
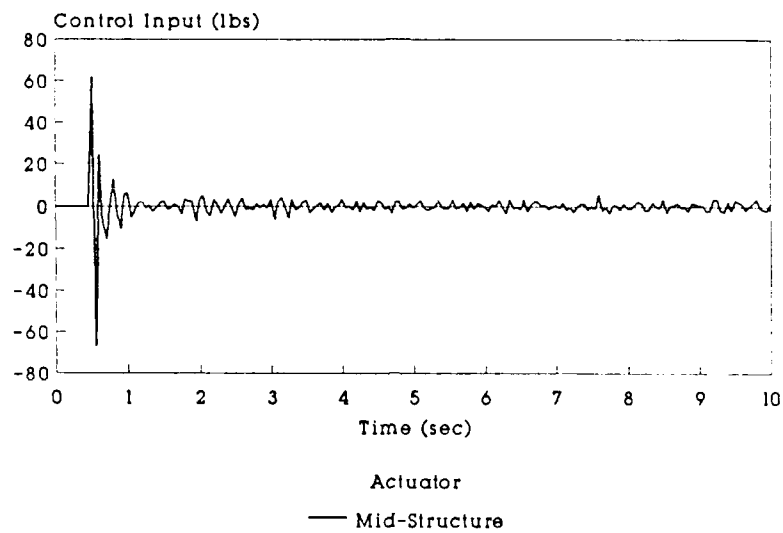
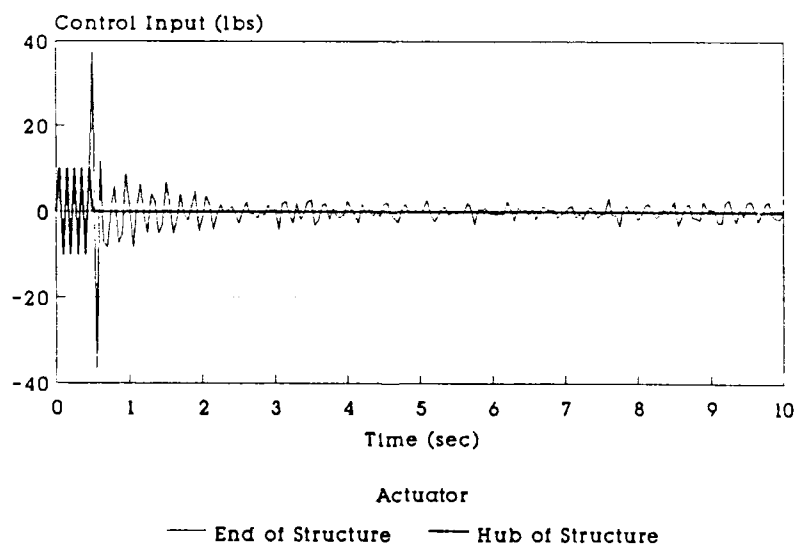


Figure 5.74. Estimation Errors with Parameter Filter Location Mismatch and Movement of the Bank with MMAC, Node 3 - True Parameter at (7,6) and Filter Initially at (5,5). (a) Position and (b) Velocity Estimation Errors. $\lambda = 0.5$.



(a)



(b)

Figure 5.75. Control Inputs for the MMAC Bank Movement Analysis, $\lambda = 0.5$. (a) Mid-structure actuator, (b) End of structure and hub of structure actuators.

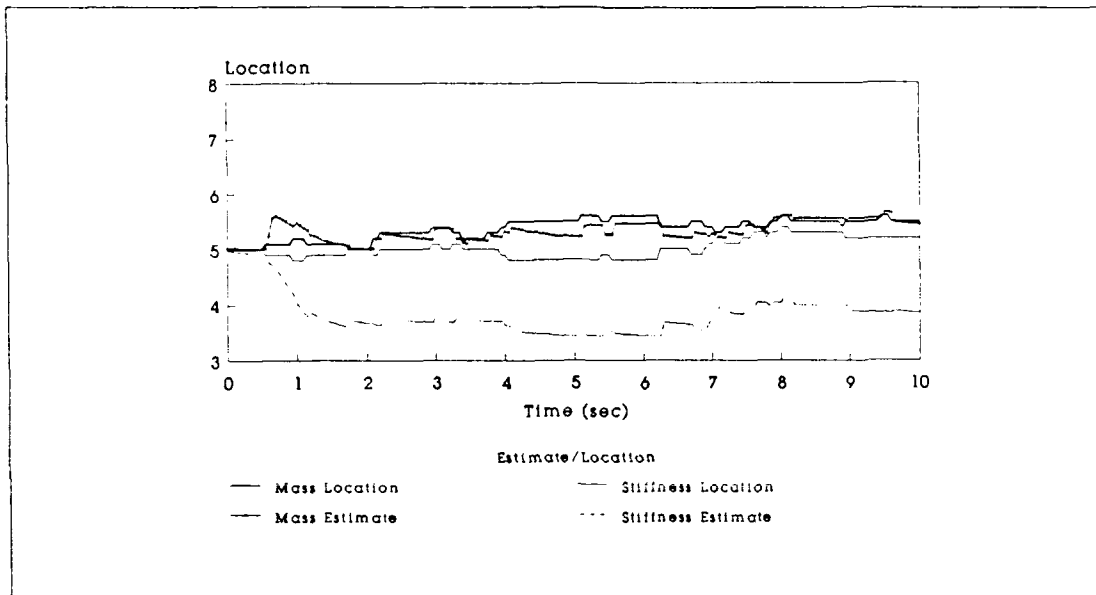


Figure 5.76. Parameter Estimation and Actual Filter Bank Location - True Parameter at (7.0) and Filter Initially at (5.5). $\lambda = 0.5$. Initial Probabilities = $\frac{1}{2}$.

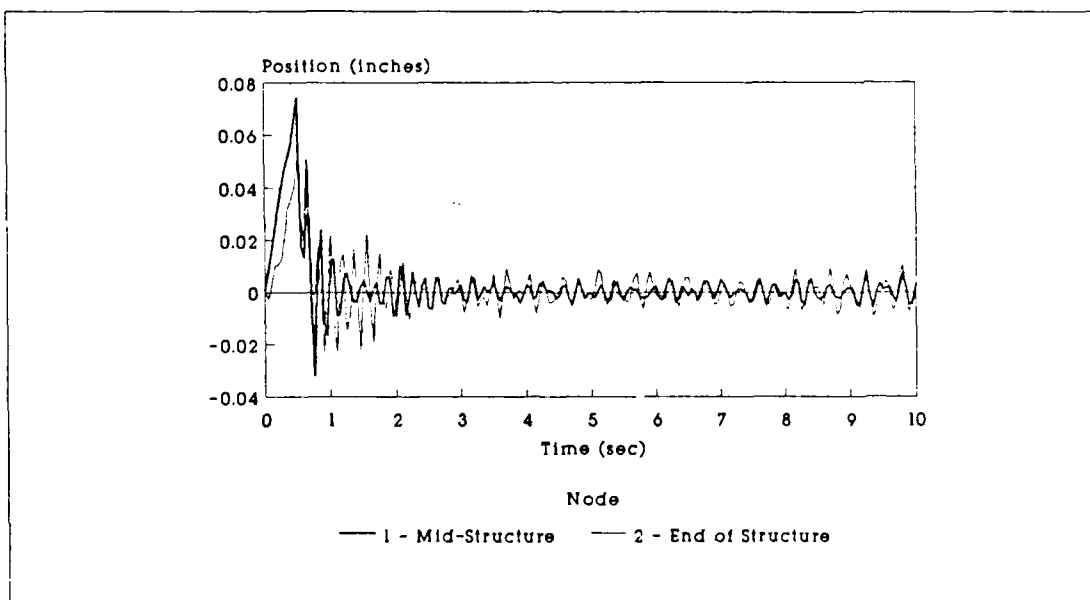


Figure 5.77. Mean Structure Positions

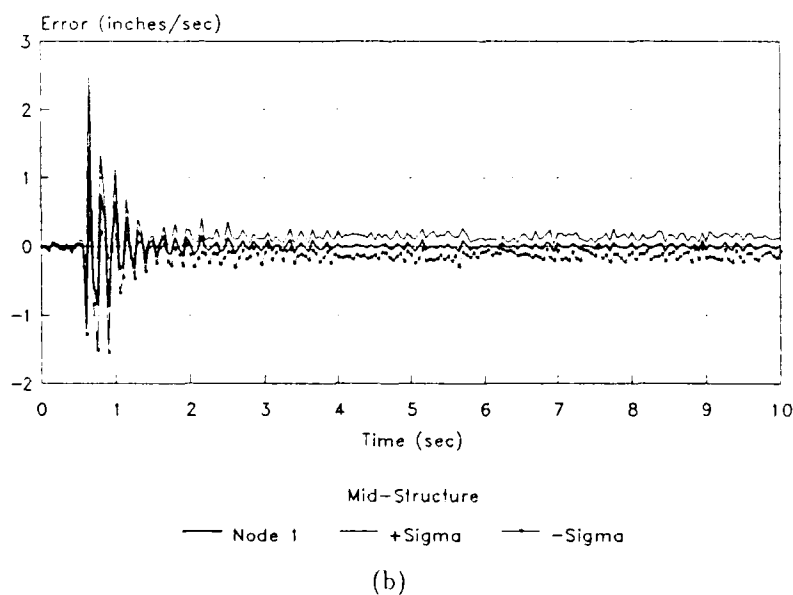
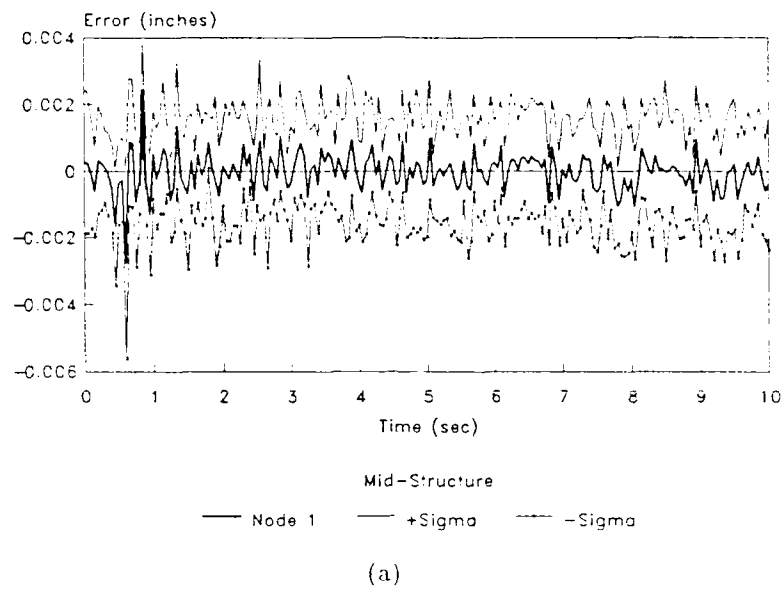


Figure 5.78. Estimation Errors with Parameter/Filter Location Mismatch and Movement of the Bank with Control, Node 1 - True Parameter at (7,6) and Filter Initially at (5.5). (a) Position and (b) Velocity Estimation Errors. $\lambda = 1.0$.

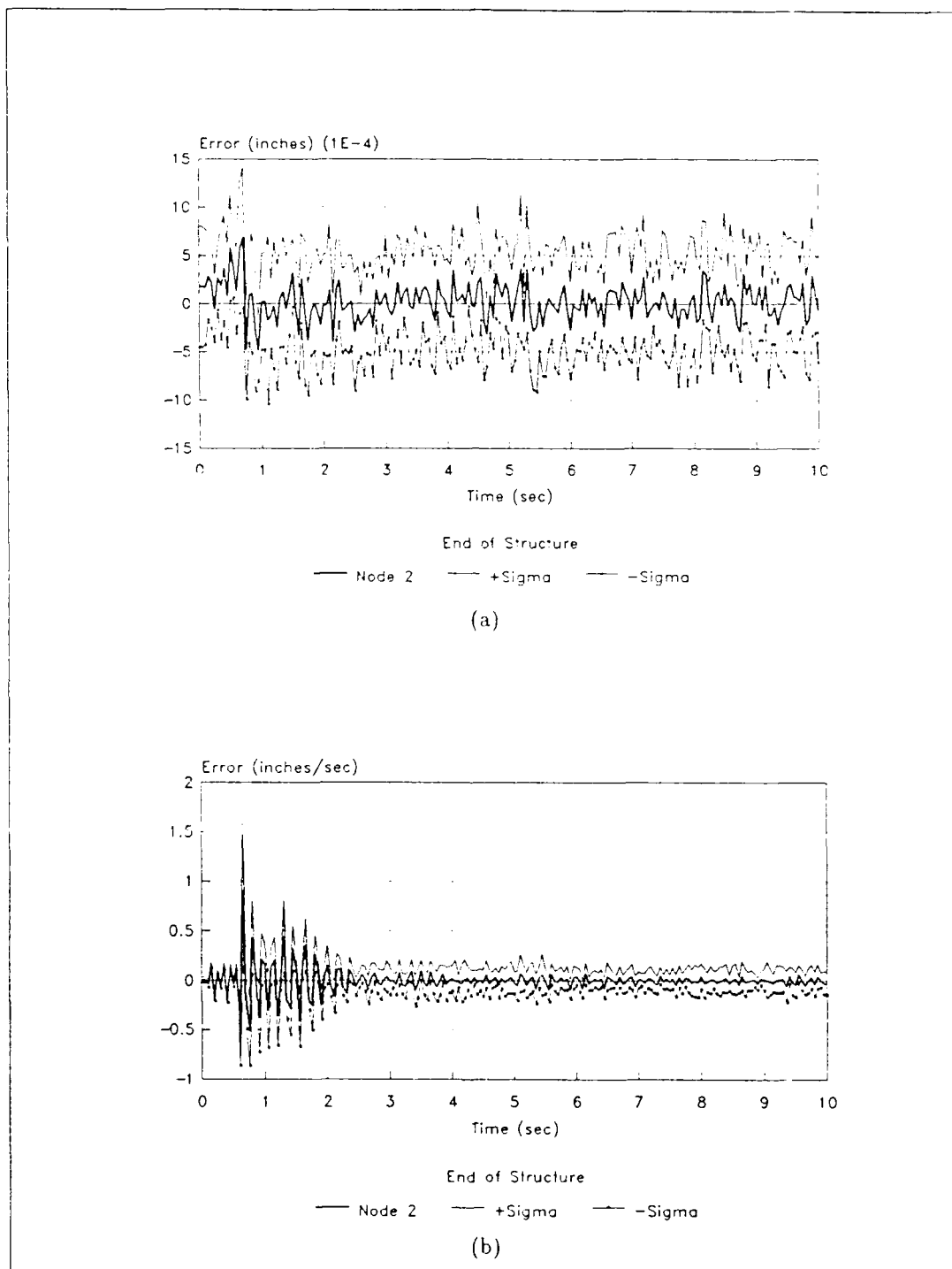


Figure 5.79. Estimation Errors with Parameter/Filter Location Mismatch and Movement of the Bank. Node 2 - True Parameter at (7,6) and Filter Initially at (5,5). (a) Position and (b) Velocity Estimation Errors. $\lambda = 1.0$.

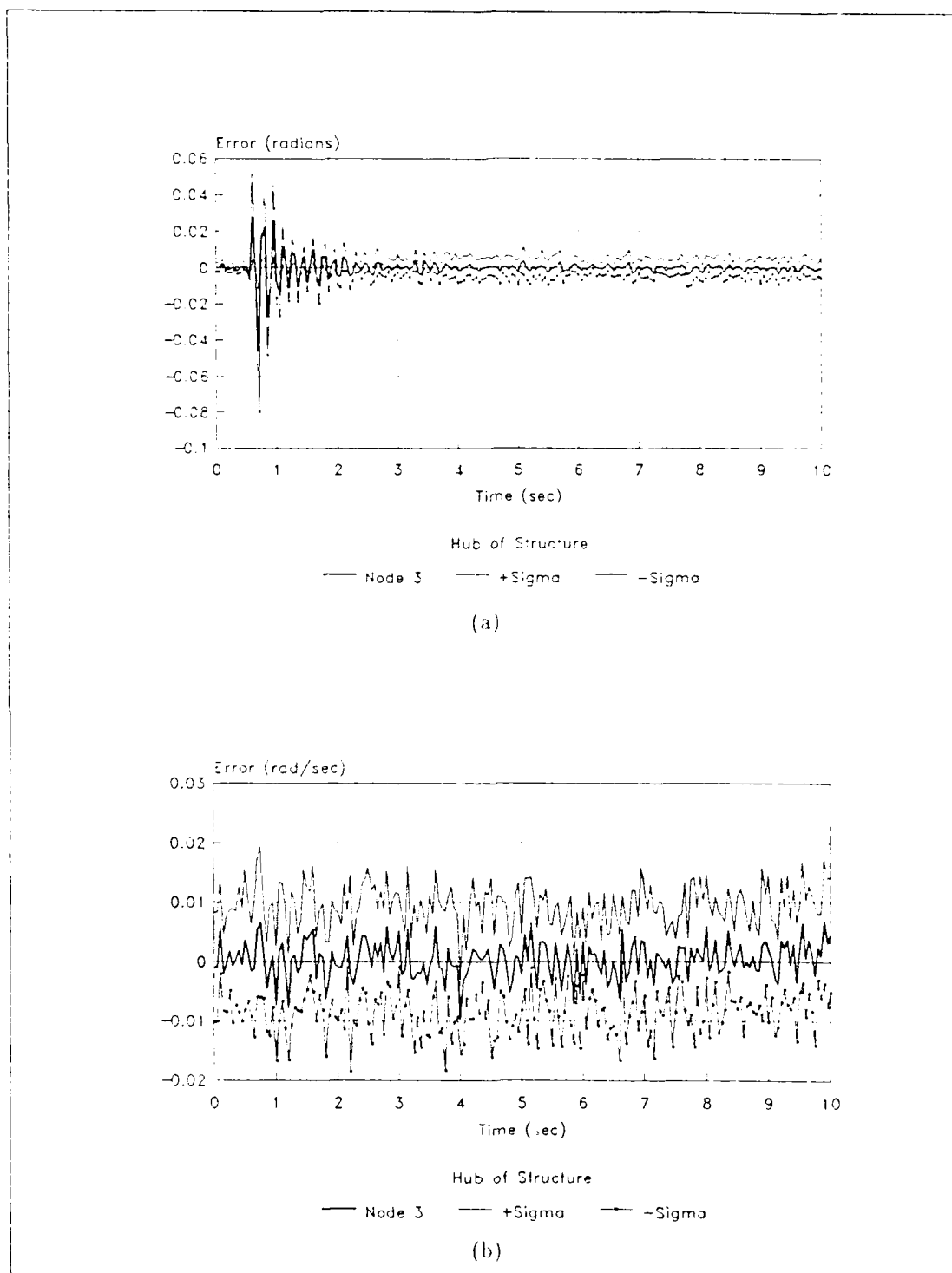
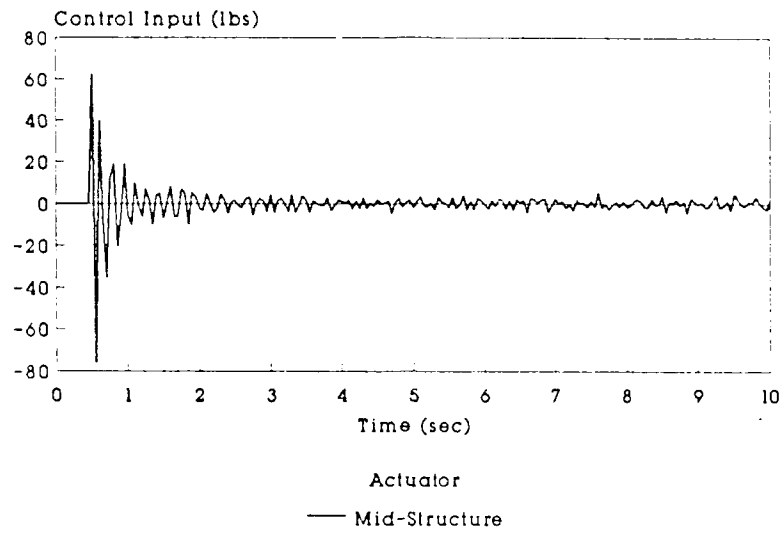
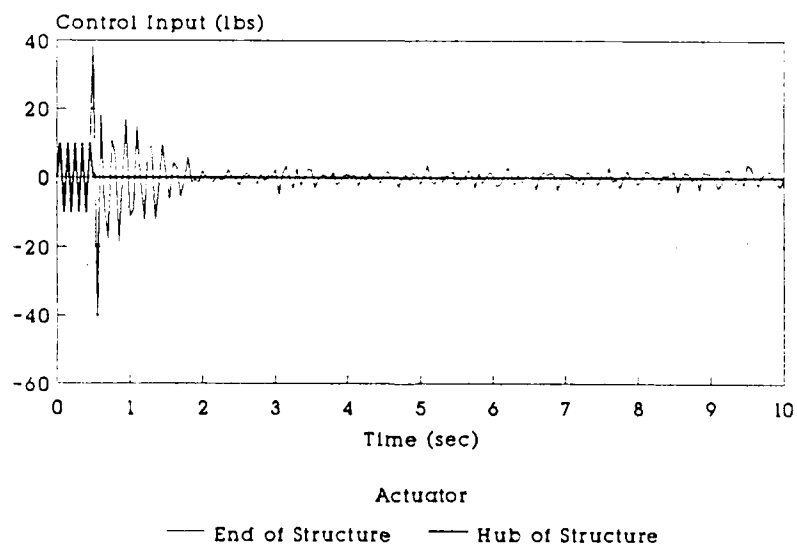


Figure 5.80. Estimation Errors with Parameter/Filter Location Mismatch and Movement of the Bank, Node 3 - True Parameter at (7.6) and Filter Initially at (5.5). (a) Position and (b) Velocity Estimation Errors. $\lambda = 1.0$



(a)



(b)

Figure 5.81. Control Inputs for the MMAC Bank Movement Analysis, $\lambda = 1.0$. (a) Mid-structure actuator. (b) End of structure and hub of structure actuators.

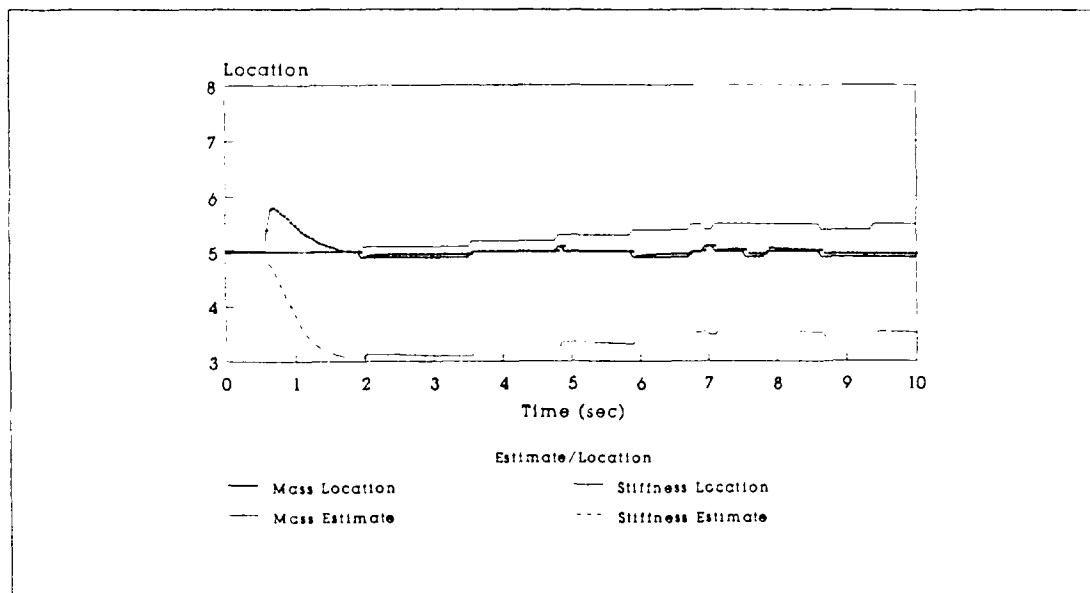


Figure 5.82. Parameter Estimation and Actual Filter Bank Location - True Parameter at (7.0) and Filter Initially at (5.5). $\lambda = 1.0$. Initial Probabilities $= \frac{1}{9}$.

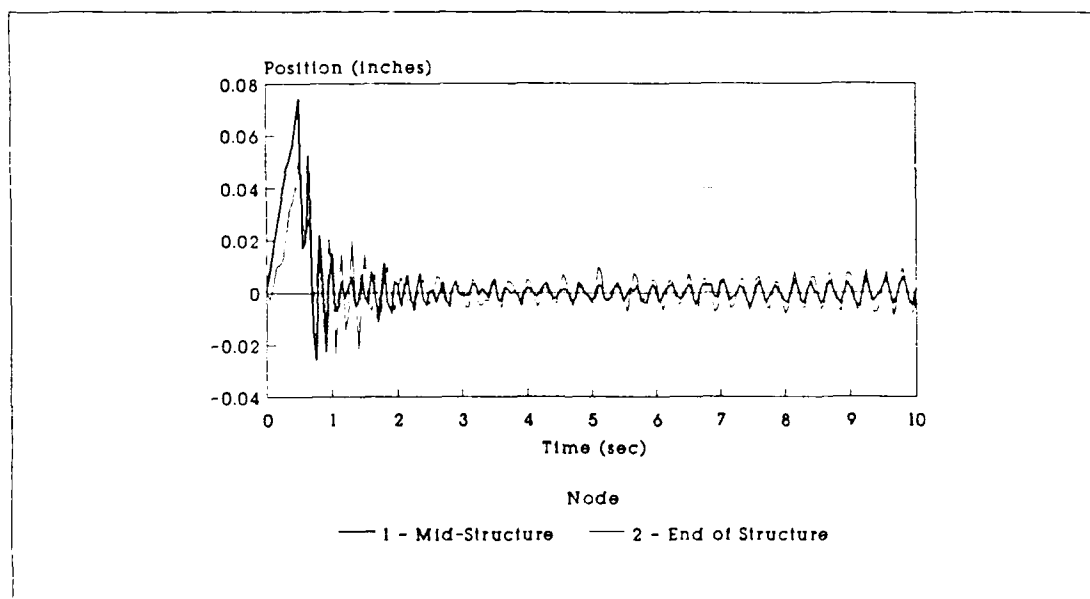
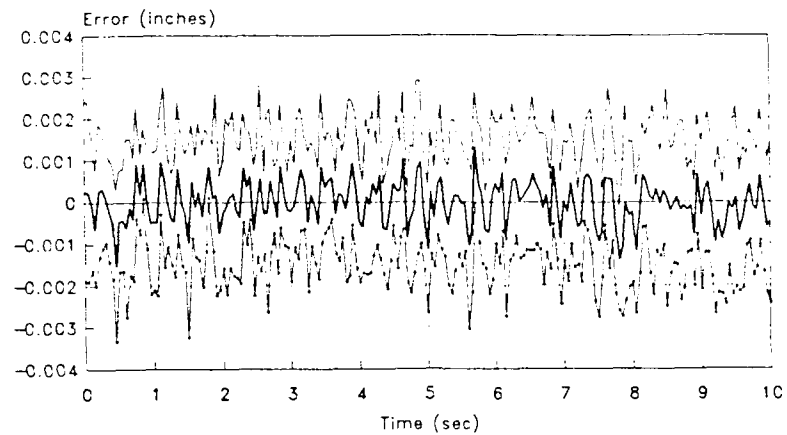


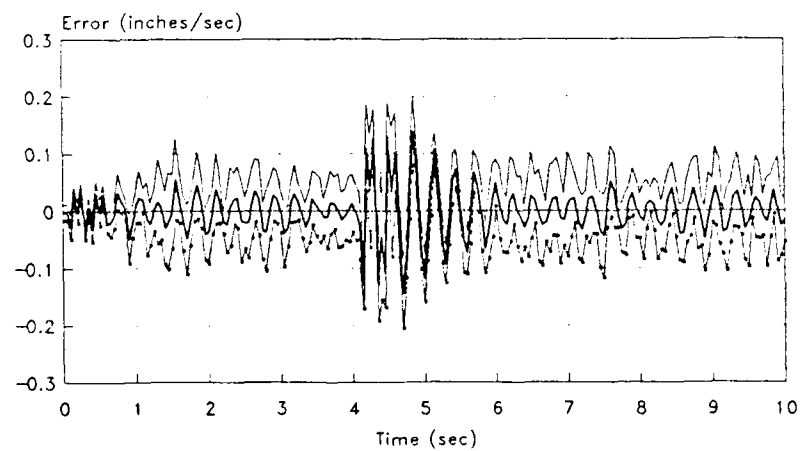
Figure 5.83. Mean Structure Positions



Mid-Structure

— Node 1 - - - +Sigma ···· -Sigma

(a)



Mid-Structure

— Node 1 - - - +Sigma ···· -Sigma

(b)

Figure 5.84. Estimation Errors with Control and Disturbance - True Parameter at (7,6) and Filter Initially at (5,5). (a) Position and (b) Velocity Estimation Errors. $\lambda = 0$. Initial Probabilities $\approx \frac{1}{9}$.

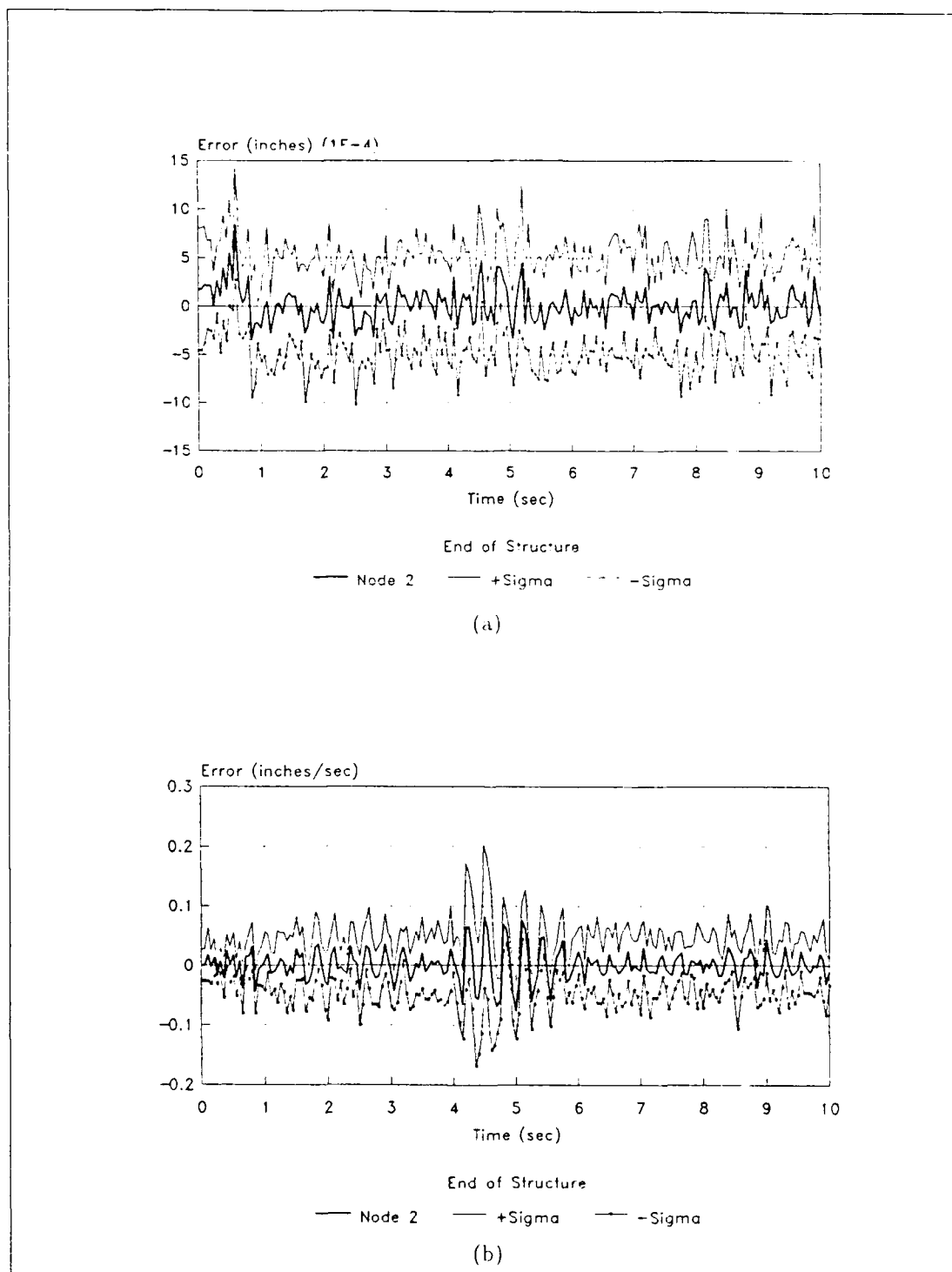


Figure 5.85. Estimation Errors with Control and Disturbance - - True Parameter at (7.6) and Filter Initially at (5.5). (a) Position and (b) Velocity Estimation Errors. $\lambda = 0$. Initial Probabilities = $\frac{1}{9}$.

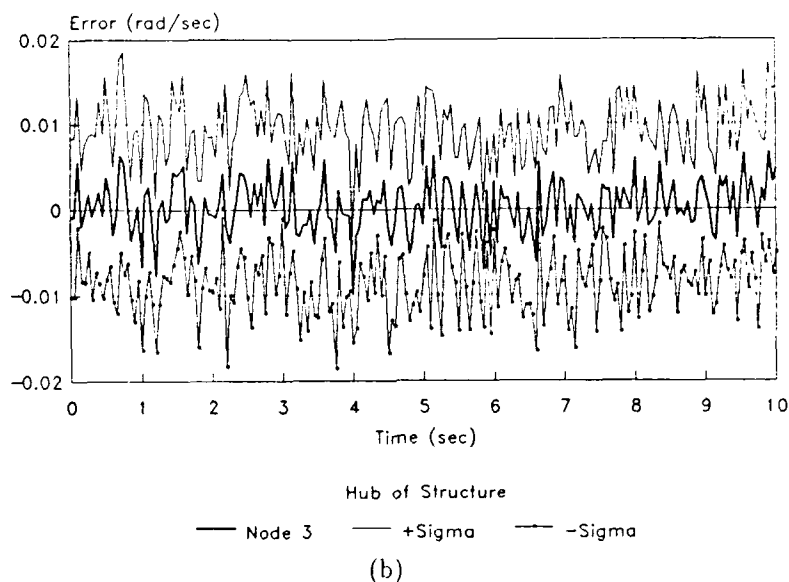
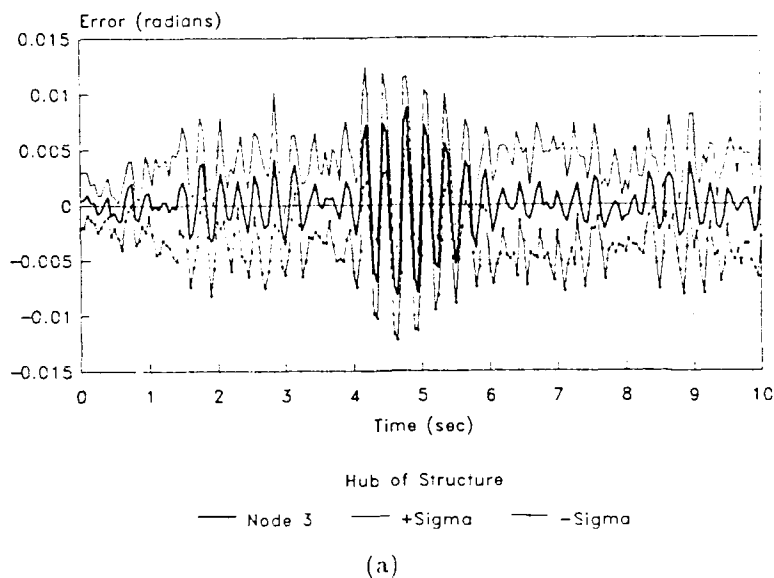
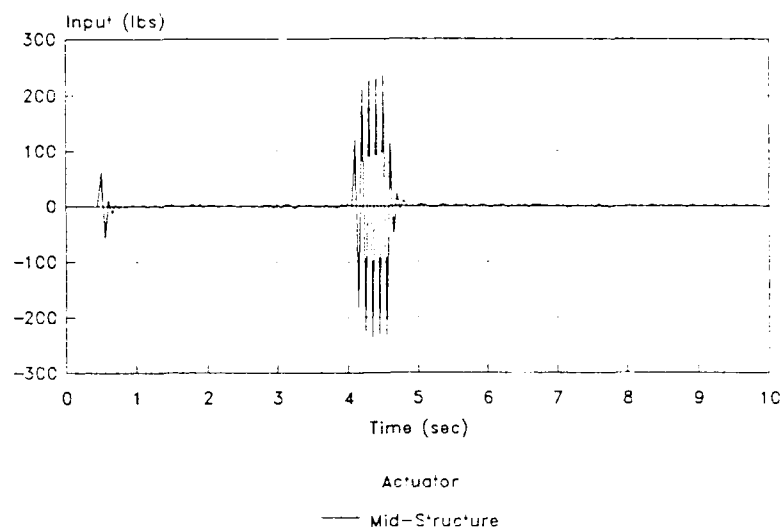
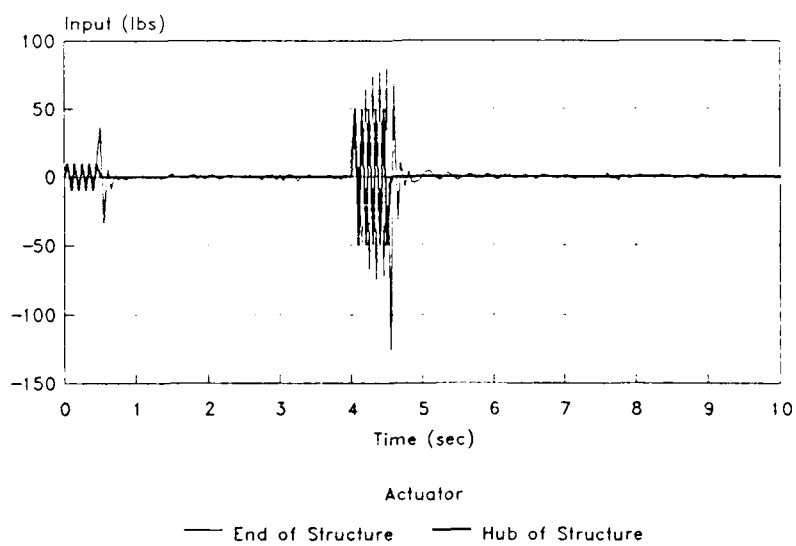


Figure 5.86. Benchmark Estimation Errors with Control and Disturbance - True Parameter at (7,6) and Filter Initially at (5,5). (a) Position and (b) Velocity Estimation Errors. $\lambda = 0$. Initial Probabilities = $\frac{1}{9}$.



(a)



(b)

Figure 5.87. Control Inputs for the MMAC Benchmark. (a) Mid-structure actuator, (b) End of structure and hub of structure actuators.

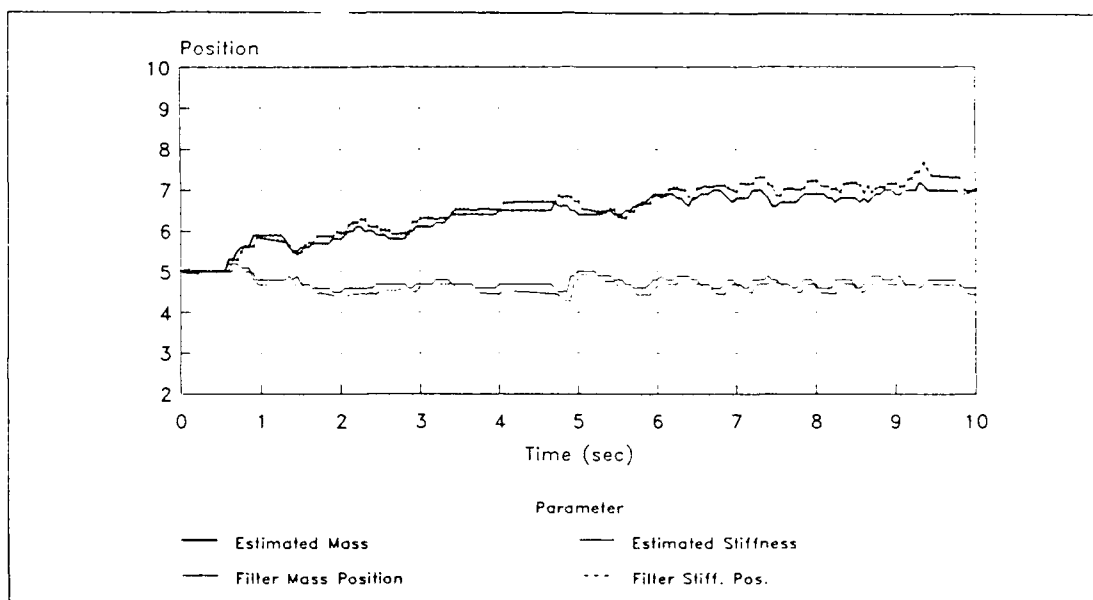
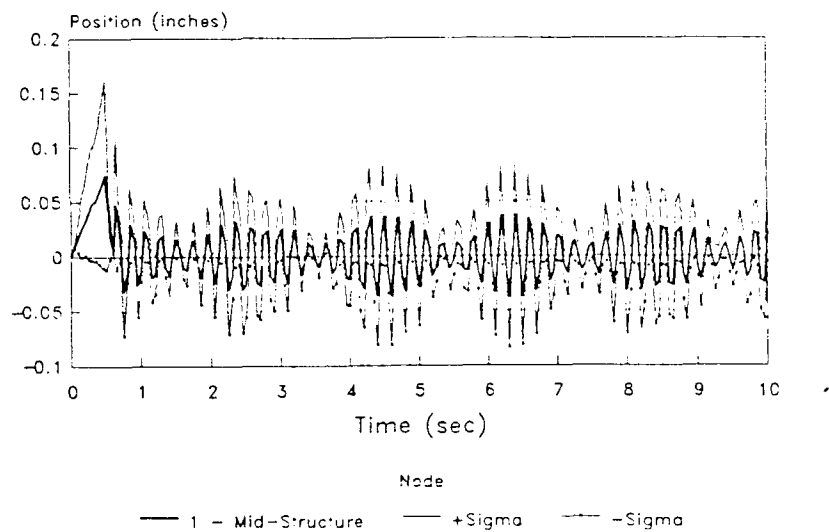
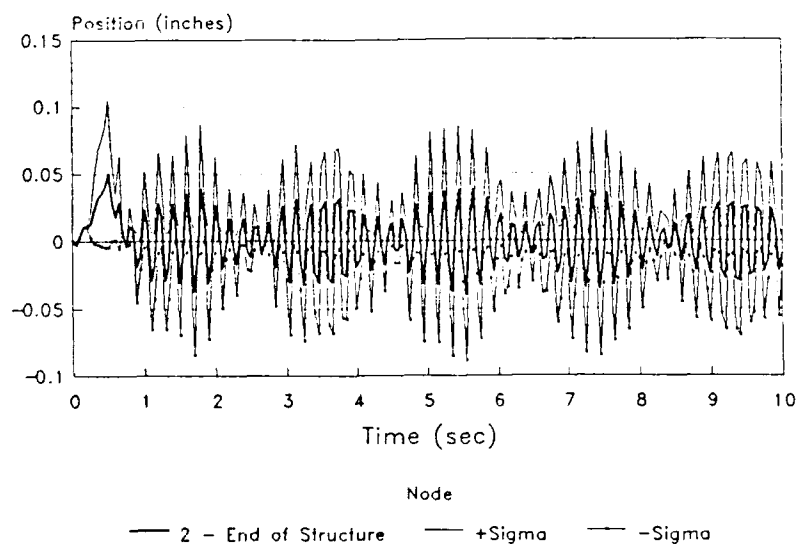


Figure 5.88. Parameter Estimation and Actual Filter Bank Location for Disturbed System - True Parameter and Filter at Mass = 7 and Stiffness = 6. $\lambda = 0$. Initial Probabilities = $\frac{1}{9}$.



(a)



(b)

Figure 5.89. Mean Structure Positions for Disturbed System. (a) Node 1 Mean Position and Variances and (b) Node 2 Mean Position and Variances.

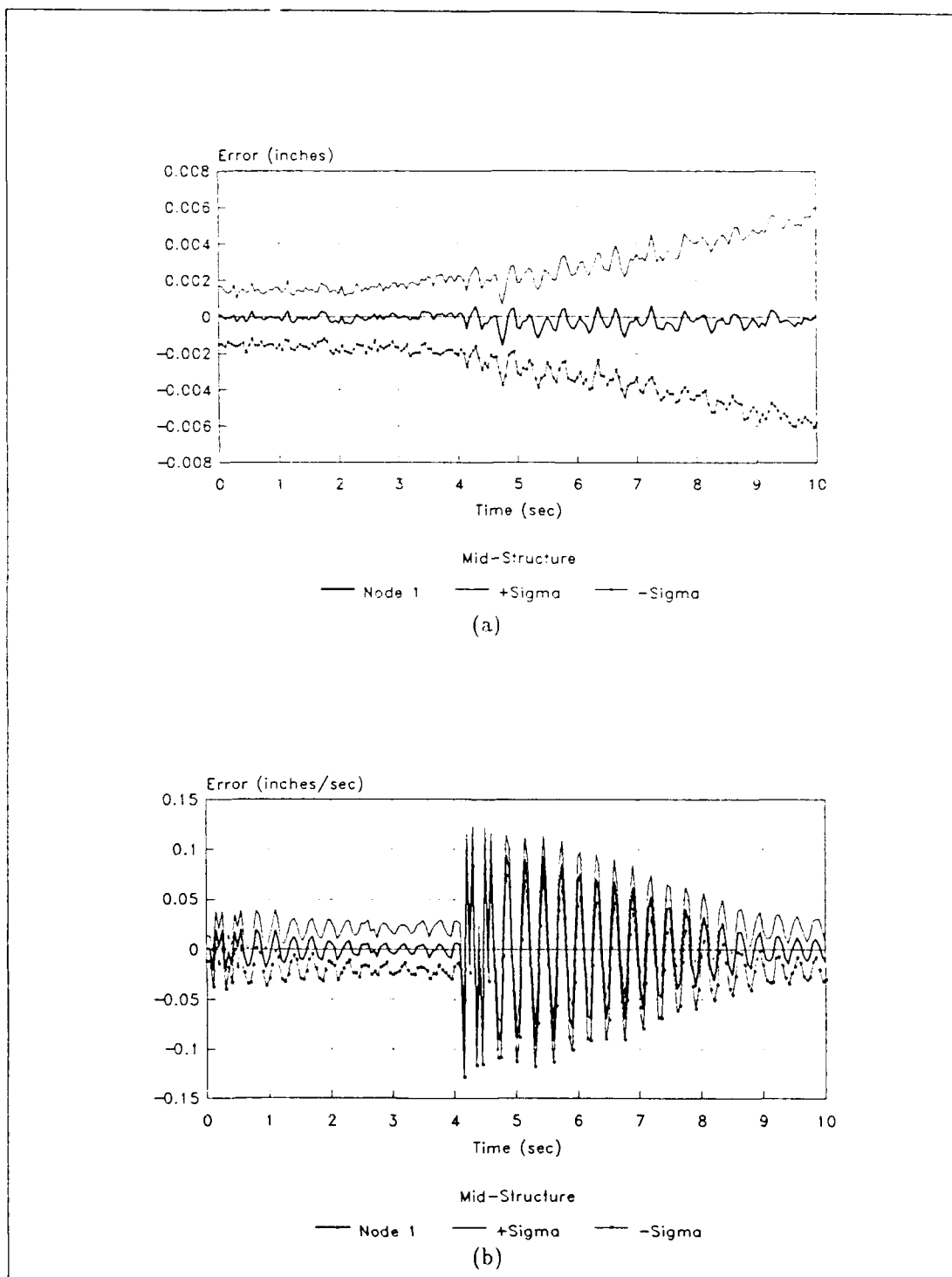


Figure 5.90. 100 Run Monte Carlo Analysis: Estimation Errors with Parameter/Filter Location Mismatch and Movement of the Bank with Control, Node 1 - True Parameter at (7,6) and Filter Initially at (5,5). (a) Position and (b) Velocity Estimation Errors. $\lambda = 0.0$.

VI. Conclusions and Recommendations

6.1 Introduction

The robustness analysis of the MMAE and MMAC algorithms, for the structure evaluated and for the state mismatch between the truth model and filters, indicates that the effects of unmodeled states do not cause serious degradation of the algorithms' performance. The results presented in Chapter 5 clearly indicate that the proposed reduced order models and resulting filter/truth model mismatch could be tolerated by the algorithms and that more research should be performed to provide further understanding of the abilities of these algorithms to control a large space structure.

6.2 Conclusions

The results of the MMAE study showed that, while the estimation process of the algorithm was sensitive to the mismatch between the filter and truth models, the sensitivity was not sufficient to justify increasing the filter model mode content. The computational burden created by going beyond the current 6-state model would be dramatic since it would appear that the addition of several states would be required for a significant improvement in performance. Additionally, the worst case analysis showed that the performance of the mismatched-parameter, nonadaptive filter was very poor. The ability of the bank, in the fine discretization mode, to move within the parameter space was good enough to provide equivalent performance to the artificially informed, non-adaptive filter used for the benchmark.

The results of the MMAC study were even more conclusive in determining that an increase in filter state size is not required when compared to a 24-state truth model. The performance of the benchmark showed a very tight control over the space structure. The worst case analysis showed that the mismatch of the assumed parameter in a single LQG controller could lead to a catastrophic failure of the structure itself. The ability of the bank to move in the parameter space was sufficient to provide adequate control of the large space structure, despite unmodeled effects.

The disturbance rejection study of the MMAC algorithm showed that the controller could respond to a large short duration disturbance and maintain control over the structure.

The moving-bank MMAE/MMAC algorithms used in this thesis provide good control over the two-bay truss structure. There remain several topics of research that should be investigated to refine the performance of the algorithms. The next section outlines recommendations that should be performed in future research.

6.3 Recommendations

The research performed in this thesis was hampered by a number of factors. The scope of the research performed was not sufficient to cover all areas of interest, and research should be continued to address some of the concerns raised in this and previous thesis efforts. Using the same space structure, filter/controller models, and truth model, the following recommendations are made:

1. The values of the dynamics noise strength \mathbf{Q} and the measurement noise covariance \mathbf{R} matrices in the Kalman filter gains should be varied and the effect of these should be investigated in detail. Special attention should be paid in the generation of new filter and truth model matrices because of the numerical instability problem suggested in Chapter 5. The software modifications to allow for tuning \mathbf{Q} and \mathbf{R} should be made as suggested by Van Der Werken [24:210]. The \mathbf{Q} and \mathbf{R} should be scalable in the same manner as the mass and stiffness matrices by inputting base matrices and an array of scalar multipliers. The issue of non-zero off-diagonal terms in the measurement noise matrix should also be investigated [24:210].
2. Verify that the state weighting matrices are tuned for the best possible performance of each elemental LQG controller within the MMAC synthesis.
3. The issue of changing parameters should be researched thoroughly. The parameter should be allowed to vary slowly and perform jump changes, such as would be caused by fuel depletion or structural failure of a truss component, respectively.

4. The parameter space discretization should also be reevaluated, since the capability of the filter bank to move to the area of the true parameter was not optimal. In particular, proper (perhaps coarser) discretization of the stiffness parameter space should receive attention in future research efforts.
5. The use of some variation of residual monitoring might be considered for performing movement of the bank. One possible means may be residual magnitude monitoring, i.e. monitoring the quantity $\mathbf{r}_k(t_i)^T \mathbf{r}_k(t_i)$ as opposed to $\mathbf{r}_k^T(t_i) \mathbf{A}_k^{-1}(t_i) \mathbf{r}_k(t_i)$ as in Equation (1.20) and as accomplished in this research.
6. The software was corrected where appropriate. After being used and modified for five iterations, the software is in need of being overhauled and thoroughly documented (in-code). In addition, several portions of the code, most notably the dither control, has been rewritten in an ad-hoc manner to provide useful information in this thesis. These warrant further study.

Bibliography

1. Asher, Robert B. *et al.* "Bibliography on Adaptive Control Systems." *Proceedings of the IEEE*, 64: 1226-1240 (August 1976).
2. Åström, K.J. "Theory and Applications of Adaptive Control - A Survey." *Automatica*, 19: 471-486 (1983).
3. Brogan, William L. *Modern Control Theory*. Englewood Cliffs, New Jersey: Prentice-Hall, Inc., 1985.
4. Chang, Chaw-Bing, and John A. Tabaczynski. "Application of State Estimation to Target Tracking." *IEEE Transactions on Automatic Control*, AC-29: 98-109 (February 1984).
5. Dasgupta, S., and L.C. Westphal. "Convergence of Partitioned Adaptive Filters for Systems with Unknown Biases." *IEEE Transactions on Automatic Control*, AC-28: 614-615 (May 1983).
6. Filios, Capt Paul G. *Moving-Bank Multiple Model Adaptive Algorithms Applied to Spacecraft Control*. MS Thesis AFIT/GE/ENG/85D-14. School of Engineering, Air Force Institute of Technology (AU), Wright-Patterson AFB, Ohio, December 1985.
7. Hawkes, Robert M., and John B. Moore. "Performance Bounds for Adaptive Estimation." *Proceedings of the IEEE*, 64: 1143-1150 (August 1976).
8. Hentz, Capt Karl P. *Feasibility Analysis of Moving Bank Multiple Model Adaptive Estimation and Control Algorithms*. MS Thesis AFIT/GE/ENG/84D-32. School of Engineering, Air Force Institute of Technology (AU), Wright-Patterson AFB, Ohio, December 1984.
9. Hostetler, Larry D., and Ronald D. Andreas. "Nonlinear Kalman Filtering Techniques for Terrain-Aided Navigation." *IEEE Transactions on Automatic Control*, AC-28: 315-323 (March 1983).
10. FORTRAN Subroutines for Mathematical Applications Software. IMSL, Inc., 1987.
11. Karnick, 2Lt Drew A. *Moving-Bank Multiple Model Adaptive Estimation Applied to Flexible Space-structure Control*. MS Thesis AFIT/GE/ENG/86D-41. School of Engineering, Air Force Institute of Technology (AU), Wright-Patterson AFB, Ohio, December 1986.
12. ——— and Peter S. Maybeck. "Moving Bank Multiple Model Adaptive Estimation Applied to Flexible Spacestructure Control." *Proceedings of the 26th IEEE Conference on Decision and Control*, Los Angeles, California, 1249-1257 (December 1987).
13. Kokotovic, P.V., O'Malley, R.E. Jr., and Sannuti, P. "Singular Perturbations and Order Reduction in Control Theory - An Overview." *Automatica*, 12: 123-132.
14. Lainiotis, Demetrios G. "Partitioning: A Unifying Framework for Adaptive Systems. I: Estimation." *Proceedings of the IEEE*, 64: 1126-1143 (August 1976).
15. Lashlee, Capt Robert W. *Moving-Bank Multiple Model Adaptive Estimation Applied to Flexible Spacestructure Control*. MS Thesis AFIT/GE/ENG/87D-36. School of Engineering, Air Force Institute of Technology (AU), Wright-Patterson AFB, Ohio, December 1987.
16. ——— and Peter S. Maybeck. "Spacestructure Control Using Moving Bank Multiple Model Adaptive Estimation." *Proceedings of the 27th IEEE Conference on Decision and Control*, Austin, Texas (December 1988).

17. Lynch, P.J., and Siva S. Banda. "Active Control for Vibration Damping." *Damping: 1986 Proceedings*, Technical Report, Flight Dynamics Laboratory, Air Force Wright Aeronautical Laboratory, Wright-Patterson AFB, Ohio, 1986 (AFWAL-TR-86-3509).
18. Maybeck, Peter S. *Stochastic Models, Estimation, and Control, Volume 1*. New York: Academic Press, 1979.
19. ———. *Stochastic Models, Estimation, and Control, Volume 2*. New York: Academic Press, 1982.
20. ———. *Stochastic Models, Estimation, and Control, Volume 3*. New York: Academic Press, 1982.
21. ———. Seminar on Multiple Model Adaptive Estimation and Control, April 1989.
22. ——— and Capt Karl P. Hentz. "Investigation of Moving-Bank Multiple Model Adaptive Algorithms." *AIAA Journal of Guidance, Control, and Dynamics*, 10:1 90-96 (Jan-Feb 1987).
23. Proakis, John G. *Digital Communications*. New York: Mcraw-Hill Book Company, 1983.
24. Van Der Werken, Capt Daniel F. Jr. *A Robustness Analysis of Moving-Bank Multiple Model Adaptive Estimation and Control of a Large Flexible Space Structure*. MS Thesis AFIT/GE/ENG/88D-59. School of Engineering, Air Force Institute of Technology (AFIT), Wright-Patterson AFB, Ohio, December 1988.
25. Venkayya, Vipperla B., and Victoria A. Tischler. "Frequency Control and Its Effect on the Dynamic Response of Flexible Structures," *AIAA Journal*, 23: 1768-1774 (November 1984).
26. Venkayya, Vipperla B. *'Analyze' - Analysis of Aerospace Structures with Membrane Elements*. Technical Report, Analysis and Optimization Branch, Structural Mechanics Division, Air Force Flight Dynamics Laboratory, Air Force Wright Aeronautical Laboratories, Wright-Patterson AFB, Ohio, December 1978 (AFFDL-TR-78-170).

Vita

Captain Michael R. Schore was born September 4, 1955 in West Palm Beach, Florida to Roger and Nedra Schore. He graduated from high school in Columbus, New Jersey in 1973. He attended Burlington County Community College from which he recieved an Associate of Applied Science in Medical Laboratory Technology Degree in April 1976. He enlisted in the United States Air Force in May 1977. He bypassed technical training after completion of Basic Training and was assigned to the clinical laboratory at Wilford Hall Medical Center at Lackland Air Force Base. After being selected for the Airmen's Education and Commissioning Program, he attended the University of Texas at Austin. He graduated in December 1983 with a Bachelor of Science Electrical Engineering. After recieving his commission in March 1984, he was assigned to the Foreign Technology Division at Wright-Patterson Air Force Base. He was assigned to the Air Force Institute of Technology in 1988. He has a wife, Sharon, and two children, Elizabeth and Pamela.

Permanent address: 767 So. 78th St.
Tacoma WA 98408

REPORT DOCUMENTATION PAGE

Form Approved
OMB No. 0704-0188

| | | | | |
|---|---|-----------|---|---------------------------------------|
| 1a. REPORT SECURITY CLASSIFICATION Unclassified | | | 1b. RESTRICTIVE MARKINGS | |
| 2a. SECURITY CLASSIFICATION AUTHORITY | | | 3. DISTRIBUTION / AVAILABILITY OF REPORT Approved for public release; Distribution unlimited. | |
| 2b. DECLASSIFICATION / DOWNGRADING SCHEDULE | | | | |
| 4. PERFORMING ORGANIZATION REPORT NUMBER(S) AFIT/GE/ENG/89D-46 | | | 5. MONITORING ORGANIZATION REPORT NUMBER(S) | |
| 6a. NAME OF PERFORMING ORGANIZATION School of Engineering | 6b. OFFICE SYMBOL (If applicable) AFIT/ENG | | 7a. NAME OF MONITORING ORGANIZATION | |
| 6c. ADDRESS (City, State, and ZIP Code) Air Force Institute of Technology Wright-Patterson AFB, OH 45433 | | | 7b. ADDRESS (City, State, and ZIP Code) | |
| 8a. NAME OF FUNDING / SPONSORING ORGANIZATION | 8b. OFFICE SYMBOL (If applicable) | | 9. PROCUREMENT INSTRUMENT IDENTIFICATION NUMBER | |
| 8c. ADDRESS (City, State, and ZIP Code) | | | 10. SOURCE OF FUNDING NUMBERS | |
| | | | PROGRAM ELEMENT NO. | PROJECT NO. |
| | | | TASK NO. | WORK UNIT ACCESSION NO. |
| 11. TITLE (Include Security Classification) Robustness of a Moving-Bank Multiple Model Adaptive Controller for a Large Flexible Space Structure | | | | |
| 12. PERSONAL AUTHOR(S) Michael R. Schore, B.S.E.E., Captain, USAF | | | | |
| 13a. TYPE OF REPORT MS Thesis | 13b. TIME COVERED FROM _____ TO _____ | | 14. DATE OF REPORT (Year, Month, Day) 1989 December | 15. PAGE COUNT 180 |
| 16. SUPPLEMENTARY NOTATION | | | | |
| 17. COSATI CODES | | | 18. SUBJECT TERMS (Continue on reverse if necessary and identify by block number) Adaptive Control Systems, Adaptive Filters, Multiple Model Adaptive Estimation, Multiple Model Adaptive Control | |
| FIELD | GROUP | SUB-GROUP | | |
| | | | | |
| | | | | |
| 19. ABSTRACT (Continue on reverse if necessary and identify by block number) Thesis Chairman: Peter S. Maybeck, Professor of Electrical Engineering | | | | |
| 20. DISTRIBUTION / AVAILABILITY OF ABSTRACT <input type="checkbox"/> UNCLASSIFIED/UNLIMITED <input type="checkbox"/> SAME AS RPT <input type="checkbox"/> DTIC USERS | | | 21. ABSTRACT SECURITY CLASSIFICATION | |
| 22a. NAME OF RESPONSIBLE INDIVIDUAL Peter S. Maybeck, Prof. of Elec. Eng. | | | 22b. TELEPHONE (Include Area Code) (513) 255-2057 | 22c. OFFICE SYMBOL AFIT/ENG |

Block 18: Abstract

The robustness of moving-bank multiple model adaptive estimation (MMAE) and control (MMAC) algorithms is analyzed in this thesis. The mismatch of a 24-state truth model and a 6-state filter model are evaluated on the basis of MMAE/MMAC performance.

A model developed using finite element analysis is used to approximate a large space structure which has a large central hub with appendages radiating out from it. The mass of the hub is considered to be much larger than the mass of the flexible structure. The model is developed in physical coordinates and then transformed into modal coordinates. To obtain a reduced order filter model, the method of singular perturbations is used. The actual positions and velocities of various physical points on the structure are used in the evaluation of the MMAE/MMAC algorithm performance.

The results of this study of model mismatching indicates that the MMAE provides accurate position and velocity estimates even in the face of a 6-state to 24-state model mismatch. When a non-adaptive filter is used with a mismatched parameter location, the performance suffers slightly. The use of an adaptive estimator does provide improved performance in the face of uncertain parameter location. Stable control was obtained with the use of MMAC. For the case of non-adaptive filter and mismatched parameter location, the control algorithm behaved in a possibly destructive manner. By allowing the filter to adapt to the initial parameter location, the MMAC algorithm provided stable control of the structure, even in the face of large disturbances.

END

DATE

FILMED

1-90

DTIC